FREE ACCESS

sponsored by

PICES

North Pacific Marine Science Organization
(www.pices.int)

THEME SECTION

Biophysical coupling of marine hotspots

Editors: E. L. Hazen, R. M. Suryan, S. J. Bograd, Y. Watanuki, R. P. Wilson

Marine Ecology Progress Series Vol. 487, pages 176–304

CONTENTS

Vol. 487: 177–183, 2013
doi: 10.3354/meps10477

MARINE ECOLOGY PROGRESS SERIES
Mar Ecol Prog Ser

Published July 30

Contribution to the Theme Section 'Biophysical coupling of marine hotspots'

FREE ACCESS

INTRODUCTION

Scales and mechanisms of marine hotspot formation

Elliott L. Hazen[1,2,*], Robert M. Suryan[3], Jarrod A. Santora[4,5], Steven J. Bograd[1], Yutaka Watanuki[6], Rory P. Wilson[7]

[1]National Oceanic and Atmospheric Administration, Southwest Fisheries Science Center, Pacific Grove, California 93950, USA
[2]Institute of Marine Sciences, University of California, Santa Cruz, 100 Shaffer Road, Santa Cruz, California 95060, USA
[3]Oregon State University, Hatfield Marine Science Center, 2030 SE Marine Science Dr., Newport, Oregon 97365, USA
[4]Farallon Institute for Advanced Ecosystem Research, 101 H Street, Suite Q, Petaluma, California 94952, USA
[5]Center for Stock Assessment and Research, University of California Santa Cruz, 110 Shaffer Road, Santa Cruz, California 95060, USA
[6]Graduate School of Fisheries, Hokkaido University, Hakodate, Hokkaido 041-8611, Japan
[7]Biosciences, College of Science, Swansea University, Singleton Park, Swansea SA2 8PP, UK

ABSTRACT: Identifying areas of high species diversity and abundance is important for understanding ecological processes and conservation planning. These areas serve as foraging habitat or important breeding or settlement areas for multiple species, and are often termed 'hotspots'. Marine hotspots have distinct biophysical features that lead to their formation, persistence, and recurrence, and that make them important oases in oceanic seascapes. Building upon a session at the North Pacific Marine Science Organization (PICES), this Theme Section explores the scales and mechanisms underlying hotspot formation. Fundamentally, understanding the mechanisms of hotspot formation is important for determining how hotspots may shift relative to ocean features and climate change, which is a prerequisite for determining management priorities.

KEY WORDS: Hotspot · Ocean features · Aggregations · Bottom-up processes · Biodiversity · Marine conservation

What is a biological hotspot?

The term 'hotspot' is used with increased frequency in marine biology and conservation literature. The concept of a hotspot of biodiversity has a longer history in the terrestrial community, with Myers (1988) defining hotspots as areas featuring both high endemism and risk to habitat (Myers et al. 2000). These concepts translate well to more static marine habitats such as coral reefs and kelp forests, but are less easily applied to pelagic systems, where both boundaries and features are dynamic. Here, we build upon previous studies that have defined pelagic hotspots based on bathymetric variation (Dower & Brodeur 2004) and ocean features in the North Pacific (Sydeman et al. 2006), to identify the biophysical mechanisms that result in hotspot formation. This requires defining the concept of a marine hotspot, particularly when it consists of mobile features.

We have taken a biophysical approach to defining marine hotspots, focusing on their ecological rather than their conservation importance. Understanding mechanisms that result in hotspot formation is critical to identify areas of high ecological importance and ultimately conservation concern. Hotspots in marine systems can be defined by (1) important life history areas for a particular species, (2) areas of high biodiversity and abundance of individuals, and (3) areas of important productivity, trophic transfer, and biophysical coupling (Dower & Brodeur 2004, Sydeman et al. 2006, Santora & Veit 2013, this Theme Section). Areas of high trophic transfer are of particular interest, because predictable and recurrent productivity hotspots often serve as the foundation of pelagic food

*Email: elliott.hazen@noaa.gov

webs. Fundamentally, hotspot formation operates across a suite of spatial and temporal scales (discussed in the next section; see Fig. 1).

Life-history hotspots are critical to a large proportion of a species or population, particularly at sensitive life history stages. Examples of life-history hotspots include spawning aggregations, juvenile settling habitat, and areas providing unique foraging resources. For example, bluefin tuna migrate across the Atlantic and regularly use the warm waters in the Gulf of Mexico to spawn (Teo et al. 2007), and grouper species form spawning aggregations in predictable regions (Beets & Friedlander 1999, Sala et al. 2001, De Mitcheson et al. 2008). Current speed, eddy activity, or shelf break habitat within these regions may be important for larval dispersal or retention to maximize survival (Teo et al. 2007, Heyman & Kjerfve 2008). Benthic habitats such as seagrass beds can serve as settlement areas for pelagic fish (Ford et al. 2010) and as foraging habitat for juvenile turtles (McClellan & Read 2007, Casale et al. 2012). Foraging hotspots close to a breeding colony can support a large portion of each species' population while also serving as important areas of trophic energy transfer from the physical environment to phytoplankton to seabirds (Santora et al. 2012a).

At the broadest scales, biodiversity hotspots most frequently occur in upwelling systems, coral reef ecosystems, and along some continental shelves (Tittensor et al. 2010). Where tropical and temperate habitats meet, there are consistent peaks in oceanic predator biodiversity (Worm et al. 2003). The California Current and North Pacific transition zone stand out as particular high biodiversity and high use hotspots (Bograd et al. 2010, Block et al. 2011). Coral reefs often contain high biodiversity, as they provide important structure and habitat near coastlines surrounding tropical and sub-tropical waters (Roberts et al. 2002, Bellwood et al. 2004). High biodiversity allows multiple paths of trophic transfer buffering against wasp-waist dominance of marine food webs (Field et al. 2006, Cury et al. 2008).

Trophic transfer hotspots often translate biophysical processes across multiple trophic levels by supporting a suite of mid-trophic organisms and, in turn, their predators. These areas often have a large ecosystem effect even though they may only support a subset of a predator's population or may not be areas of highest biodiversity. Aggregations of mid-trophic species can be important hotspots for top predators that migrate large distances to optimize foraging opportunities (Cotte & Simard 2005, Bailey et al. 2010). The mechanisms underlying trophic hotspots can include island/seamount wake effects (Johnston & Read 2007, Morato et al. 2010), upwelling shadows (Nur et al. 2011, Wingfield et al. 2011, Pardo et al. 2013, this Theme Section), wind or eddy-driven upwelling (Croll et al. 2005, Atwood et al. 2010, Thorne & Read 2013, this Theme Section), or bathymetric features (Croll et al. 2005, Gende & Sigler 2006). Fundamentally, changes in these hotspots may have indirect consequences on ecosystem functioning that cascade through to top predators.

Scales of hotspots

Inherent to all studies of marine hotspots is the concept of scale — ecological phenomena interact at discrete and often multiple spatial and temporal scales. A Stommel diagram of hotspot mechanisms shows how processes vary across space and time, and for simplicity assumes that the scaling between time and space is linear (Fig. 1). However, meso- and fine-scale studies of aggregative responses among ocean physics, predators and prey have revealed complex non-linear interactions (Hunt & Schneider 1987, Piatt 1990, Fauchald et al. 2000).

Research on the scale of physical and biological hotspots is often dictated by the sampling methodologies and technology employed. For example: (1) Satellite-based observations of ocean conditions offer the greatest flexibility by sampling broadly through space and time at fine to basin scales, but are limited to surface conditions and only sample up to a proxy for primary production in chlorophyll *a* (Palacios et al. 2006). (2) Satellite-tracking of vertebrate predators is dependent on the resolution of tracking devices (e.g. GPS, pop-up archival), the predators' movement, and initial tagging location, but offer exceptional insight into top predator behavior, distribution, and their use of multiple marine ecosystems (e.g. hotspot connectivity, residency: Block et al. 2011, Bailey et al. 2012, Hazen et al. 2012; tagging through the stages: Montevecchi et al. 2012). (3) Shipboard surveys employ a variety of discrete and continuous sampling devices (e.g. nets, acoustics, visual observations) to quantify vertical and horizontal dimensions of seascapes and preyscapes, simultaneously offering insight into hotspot mechanisms and metrics of biodiversity (Santora et al. 2010, 2012a, Sigler et al. 2012), but are expensive and highly influenced by weather conditions. Ultimately, the integration across multiple types of observations should help resolve spatio-temporal mismatches.

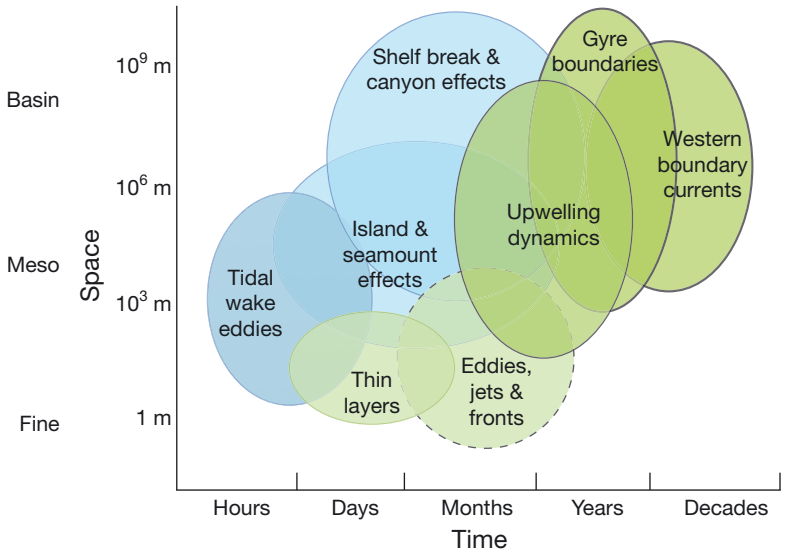

Fig. 1. Stommel diagram. Spatial scale (*y*-axis) plotted against temporal scale, focusing on persistence (*x*-axis). Blue: bathymetric-driven hotspots; green: dynamic features that can move throughout the ocean. For example, upwelling dynamics operate on a temporal scale of days to months while tidally driven mixing lasts for hours. Black outline: features that are persistent throughout time rather than recurrent; dashed outline: features that are ephemeral and neither persistent nor recurrent

Studies of global hotspots, especially diversity/richness hotspots, generally focus on relatively large grid size resolutions (e.g. 10 km; months to decades) and may cover entire marine ecosystems (Tittensor et al. 2010, Block et al. 2011). This approach is useful for comparing biodiversity and risk across ecosystems and identifying important areas warranting fine-scale study (Halpern et al. 2008). Fine-scale research is necessary to elucidate mechanisms of biophysical hotspot formation and persistence and to understand critical species interactions within hotspots. At the global scale, most metrics for physical variability identified as underlying hotspots are proxies for key species interactions (Dawson et al. 2011, Hazen et al. 2013, Mokany et al. 2013).

Mesoscale structure (10 to 1000 km; days to months) underlying physical and biological components of marine ecosystems often determine the strength and recurrence of marine hotspots, and can provide criteria for defining areas of high trophic transfer. Studies at fine spatial scales (1 to 10 km) examining predator–prey–oceanography relationships are critical to describe the mechanisms that determine which mesoscale hotspots are formed and persist. For example, tidal flow and internal waves passing over topographic features in the Gulf of Maine result in dense aggregations of both krill and sand lance, which support seasonal foraging for humpback and fin whales (Stevick et al. 2008, Hazen et al. 2009). Through the integrated assessment of physics, primary productivity, and secondary production, the coupling of fine and mesoscale sampling offers promising directions for studies of marine hotspots (Cury et al. 2008).

Mechanisms of hotspot formation and persistence

Physical processes leading to hotspot formation are varied, ranging from nutrient input to retention or aggregation of subsequent biological production. Mechanisms of nutrient input into the euphotic zone include freshwater run-off (Chase et al. 2007, Planquette et al. 2011), aeolian sources (Fan et al. 2006), and upwelling of deep, nutrient rich water (Meskhidze et al. 2007). Upwelling (or water column mixing) can be seasonal or episodic when wind driven; however, upwelling-enhanced productivity can also be highly persistent, especially when resulting from relatively static or cyclical processes, such as the interaction of the Equatorial Undercurrent meeting the western Galapagos Islands (Palacios et al. 2006) or small scale, tidally driven current interactions with bathymetric features within a bay (Drew et al. 2013, Thorne & Read 2013, both in this Theme Section). Likewise, anticyclonic eddies that form in coastal regions and spin-off into or form in the oceanic domain can entrain or upwell macronutrients, leading to 'traveling' open ocean hotspots of productivity (Crawford et al. 2007) that are often utilized by upper trophic level predators (Ream et al. 2005).

Hotspots can be a function of biophysical aggregation where physical features such as shelf breaks or ocean fronts lead to increased densities of phytoplankton or zooplankton, or bottom-up processes, such as where increased nutrient levels lead to greater primary productivity, greater densities of grazers, and so on up to mid-trophic and top-level predators (Mann & Lazier 1996, Genin 2004). Due to transport mechanisms and temporal lags, a foraging hotspot may not coincide with a region of enhanced primary productivity. In these cases, spatial discordance can result from downstream transport of prey, such as zooplankton for foraging birds (Hunt et al. 1998, Thorne & Read 2013, this Theme Section). There are good examples of bathymetric features

creating important aggregative habitat for species such as krill where they can reduce their exposure to currents while being close to foraging needs (Fiedler et al. 1998, Cotte & Simard 2005, Santora et al. 2010, Santora et al. 2011). These aggregations then become important foraging features for large predators such as baleen whales that require high densities of prey to maximize their foraging efficiency and energetic demands (Cotte & Simard 2005, Sigler et al. 2012). Top-down hotspots are rare, but facilitated foraging, where pelagic predators such as tuna force forage fish towards the surface and make them more available to seabirds, can result in higher biodiversity at pelagic hotspots (Maxwell & Morgan 2013).

The spatial and temporal dynamics of marine hotspot occurrence and persistence is quite important, yet infrequently examined (but see Gende & Sigler 2006, Sigler et al. 2012, Suryan et al. 2012, Santora & Veit 2013, this Theme Section). Many investigations have focused on long-term averages (i.e. spatial climatologies) of physical and biological conditions to map hotspots, but the greatest challenges for research on pelagic hotspots require studies melding space and time to quantify persistence of hotspots. Quantifying their spatio-temporal persistence will require highly replicated observations to establish a baseline scale of variability and measure the frequency of anomalies (Suryan et al. 2012). Due to their ability to sample local to global spatial scales over days to years, satellite-based observations of ocean conditions offer the greatest opportunity to examine the spatio-temporal persistence of many marine hotspots (Palacios et al. 2006). Moored observatories (e.g. Neptune, Diemos, Mars), repeated glider transects, or regular surveys can allow enhanced temporal observations at marine hotspot locations (Bi et al. 2007, Moustahfid et al. 2012).

Contributions to the Theme Section

This Theme Section arose out of a session at the 2011 Annual Meeting of the North Pacific Marine Science Organization (PICES). The session built upon previous efforts to identify hotspots in the North Pacific and examine the biophysical mechanisms that result in their formation (Dower & Brodeur 2004, Sydeman et al. 2006). The session consisted of 19 (total) presentations and posters. This Theme Section contains 8 studies with topics ranging from hotspots of marine snow to migratory top predators.

Prairie et al. (2013) in a laboratory experiment demonstrated mechanisms by which particles can be temporarily retained when encountering density gradients. The density of the aggregate relative to the density of the bottom layer in the gradient is the primary determinant of the extent that marine snow will aggregate, thereby enhancing food web development at the boundary layer.

Boucher et al. (2013) used oceanographic and individual-based movement models to examine larval haddock dynamics in the Gulf of Maine. In good years, increased retention lead to hotspots of larval haddock on the bank but additional factors played a role in the magnitude of haddock recruitment in a given year.

Nishikawa et al. (2013) examined how water column characteristics lead to phytoplankton blooms in the western North Pacific that develop into important spawning habitat for Japanese sardine *Sardinops melanostictus*. A deeper mixed layer and higher phytoplankton density resulted in increased spawning habitat north of the Kuroshio.

Smith et al. (2013) examined how a hurricane passing through the Gulf of Mexico may have temporarily increased foraging hotspots for bottlenose dolphins. The decline in foraging habitat months after Hurricane Katrina suggests some hotspots, such as seagrass beds, may have been lost or disrupted by the hurricane.

Pardo et al. (2013) studied the role of environmental seasonality in a cetacean community within a small bay in the Gulf of California. Different species used the bay as the season progressed; periods of mixing and pycnocline shoaling resulted in increased habitat for blue whales and 2 dolphin species, while other whales were more common during periods of stratification.

Thorne et al. (2013) evaluated the biophysical processes that structure foraging habitat for phalaropes, a surface-feeding, planktivorous seabird in the Bay of Fundy. Their model indicates that copepods are physically upwelled and advected down current, highlighting the potential for spatial mismatch of lower trophic level food web processes and predator foraging.

Drew et al. (2013) used visual transect surveys to examine how foraging strategies of seabirds resulted in differential habitat use in Glacier Bay, Alaska. Bathymetric variability results in differential current speeds and consequently a high diversity of hotspot types in the bay; modeling approaches may help to understand the development of fine scale foraging behavior that has so far been difficult to quantify.

Santora & Veit (2013) examined species richness and abundance in top predators to identify persistent

hotspots near the Antarctic Peninsula. They identified 15 richness hotspots associated with either the Antarctic Circumpolar Current, major breeding colonies, or submarine canyons.

Future directions

To cross spatio-temporal boundaries, more synthetic approaches to hotspot research are necessary, such as combining Eulerian and Lagrangian measurements of hotspot dynamics. Combining tag-based movement data with shipboard surveys can provide information on behavioral ecology and biodiversity to address the suite of physical and ecological processes that result in formation and prolonged use of marine hotspots at multiple trophic levels (see Benoit-Bird et al. 2013). Future studies of biophysical hotspots should explicitly address the scale and scope of their defined hotspot so that syntheses and comparisons can be made across studies of disparate marine ecosystems (Santora et al. 2012b).

One category of marine hotspots that remains under-researched is the deep scattering layers (DSLs) of the open ocean, which are made up of a complex of species including fish, shrimp, jellies, and squid. DSLs have been observed at various depths around the world, yet little is known on their extent or variability (Barham 1963). They serve as a critical prey resource in otherwise oligotrophic ocean basins, so understanding the spatial and temporal distribution of DSL hotspots is critical (Benoit-Bird & Au 2004). Recent studies in Monterey Bay have shown a high degree of temporal variability in distribution, both vertical and horizontal, and abundance seasonally, of DSL organisms (Urmy et al. 2012). Broad scale spatial patterns of deepwater fishes in the southern California Bight were recently described, with low oxygen levels proposed as a primary mechanism determining vertical distributions (Koslow et al. 2011).

An increasing number of studies focus on areas in the ocean that are important for conservation. The Global Ocean Biodiversity Initiative (GOBI) is an international organization working to define Ecological and Biologically Significant Areas (EBSAs) in the world's oceans (Williams et al. 2010). The clear identification of hotspots and the establishment of a 'hotspot repository' would ensure the effective study of hotspot mechanisms and persistence, and subsequently inform management and conservation efforts. Dynamic management has been proposed and even implemented in a few systems, but with ocean use projected to increase in the future, new tools are required to optimize ecological services and ecosystem functioning (Hobday et al. 2010, Dunn et al. 2011, Grantham et al. 2011, Ronconi et al. 2012). Examination of the overlap between human-use hotspots and the temporal persistence of ecological hotspots will enable real-time management approaches to allow human uses when hotspots are absent and protect habitats when hotspots are persistent.

LITERATURE CITED

Atwood E, Duffy-Anderson JT, Horne JK, Ladd C (2010) Influence of mesoscale eddies on ichthyoplankton assemblages in the Gulf of Alaska. Fish Oceanogr 19:493–507

Bailey H, Mate BR, Palacios DM, Irvine L, Bograd SJ, Costa DP (2010) Behavioural estimation of blue whale movements in the Northeast Pacific from state-space model analysis of satellite tracks. Endang Species Res 10:93–106

Bailey H, Benson SR, Shillinger GL, Bograd SJ and others (2012) Identification of distinct movement patterns in Pacific leatherback turtle populations influenced by ocean conditions. Ecol Appl 22:735–747

Barham EG (1963) Siphonophores and the deep scattering layer. Science 140:826–828

Beets J, Friedlander A (1999) Evaluation of a conservation strategy: a spawning aggregation closure for red hind, *Epinephelus guttatus*, in the U.S. Virgin Islands. Environ Biol Fishes 55:91–98

Bellwood DR, Hughes TP, Folke C, Nystrom M (2004) Confronting the coral reef crisis. Nature 429:827–833

Benoit-Bird KJ, Au WWL (2004) Diel migration dynamics of an island-associated sound-scattering layer. Deep-Sea Res I 51:707–719

Benoit-Bird KJ, Battaile BC, Heppell SA, Hoover B and others (2013) Prey patch patterns predict habitat use by top marine predators with diverse foraging strategies. PLoS ONE 8:e53348

Bi HS, Ruppel RE, Peterson WT (2007) Modeling the pelagic habitat of salmon off the Pacific Northwest (USA) coast using logistic regression. Mar Ecol Prog Ser 336:249–265

Block BA, Jonsen ID, Jorgensen SJ, Winship AJ and others (2011) Tracking apex marine predator movements in a dynamic ocean. Nature 475:86–90

Bograd SJ, Block BA, Costa DP, Godley BJ (2010) Biologging technologies: new tools for conservation. Introduction. Endang Species Res 10:1–7

Boucher JM, Chen C, Sun Y, Beardsley RC (2013) Effects of interannual environmental variability on the transport-retention dynamics in haddock *Melanogrammus aeglefinus* larvae on Georges Bank. Mar Ecol Prog Ser 487:201–215

Casale P, Broderick AC, Freggi D, Mencacci R, Fuller WJ, Godley BJ, Luschi P (2012) Long-term residence of juvenile loggerhead turtles to foraging grounds: a potential conservation hotspot in the Mediterranean. Aquat Conserv 22:144–154

Chase Z, Strutton PG, Hales B (2007) Iron links river runoff and shelf width to phytoplankton biomass along the U.S. West Coast. Geophys Res Lett 34LO4607, doi:10.1029/2006GL028069

Cotte C, Simard Y (2005) Formation of dense krill patches under tidal forcing at whale feeding hot spots in the St. Lawrence Estuary. Mar Ecol Prog Ser 288:199–210

Crawford WR, Brickley PJ, Thomas AC (2007) Mesoscale eddies dominate surface phytoplankton in northern Gulf of Alaska. Prog Oceanogr 75:287–303

Croll DA, Marinovic B, Benson S, Chavez FP, Black N, Ternullo R, Tershy BR (2005) From wind to whales: trophic links in a coastal upwelling system. Mar Ecol Prog Ser 289:117–130

Cury PM, Shin YJ, Planque B, Durant JM and others (2008) Ecosystem oceanography for global change in fisheries. Trends Ecol Evol 23:338–346

Dawson TP, Jackson ST, House JI, Prentice IC, Mace GM (2011) Beyond predictions: biodiversity conservation in a changing climate. Science 332:53–58

De Mitcheson YS, Cornish A, Domeier M, Colin PL, Russell M, Lindeman KC (2008) A global baseline for spawning aggregations of reef fishes. Conserv Biol 22:1233–1244

Dower JF, Brodeur RD (2004) The role of biophysical coupling in concentrating marine organisms around shallow topographies. J Mar Syst 50:1–2

Drew GS, Piatt JF, Hill DF (2013) Effects of currents and tides on a fine-scale use of marine bird habitats in a Southeast Alaska hotspot. Mar Ecol Prog Ser 487:275–286

Dunn DC, Boustany AM, Halpin PN (2011) Spatio-temporal management of fisheries to reduce by-catch and increase fishing selectivity. Fish Fish 12:110–119

Fan SM, Moxim WJ, Levy H II (2006) Aeolian input of bioavailable iron to the ocean. Geophys Res Lett 33: L07602, doi:10.1029/2005GL024852

Fauchald P, Erikstad KE, Skarsfjord H (2000) Scale-dependent predator-prey interactions: the hierarchical spatial distribution of seabirds and prey. Ecology 81:773–783

Fiedler PC, Reilly SB, Hewitt RP, Demer D and others (1998) Blue whale habitat and prey in the California Channel Islands. Deep-Sea Res II 45:1781–1801

Field JC, Francis RC, Aydin K (2006) Top-down modeling and bottom-up dynamics: linking a fisheries-based ecosystem model with climate. Prog Oceanogr 68:238–270

Ford JR, Williams RJ, Fowler AM, Cox DR, Suthers IM (2010) Identifying critical estuarine seagrass habitat for settlement of coastally spawned fish. Mar Ecol Prog Ser 408:181–193

Gende SM, Sigler MF (2006) Persistence of forage fish 'hot spots' and its association with foraging Steller sea lions (*Eumetopias jubatus*) in southeast Alaska. Deep-Sea Res II 53:432–441

Genin A (2004) Bio-physical coupling in the formation of zooplankton and fish aggregations over abrupt topographies. J Mar Syst 50:3–20

Grantham HS, Game ET, Lombard AT, Hobday AJ and others (2011) Accommodating dynamic oceanographic processes and pelagic biodiversity in marine conservation planning. PLoS ONE 6:e16552

Halpern BS, Walbridge S, Selkoe KA, Kappel CV and others (2008) A global map of human impact on marine ecosystems. Science 319:948–952

Hazen EL, Friedlaender AS, Thompson MA, Ware CR, Weinrich MT, Halpin PN, Wiley DN (2009) Fine-scale prey aggregations and foraging ecology of humpback whales *Megaptera novaeangliae*. Mar Ecol Prog Ser 395: 75–89

Hazen EL, Maxwell SM, Bailey H, Bograd SJ and others (2012) Ontogeny in marine tagging and tracking science: technologies and data gaps. Mar Ecol Prog Ser 457: 221–240

Hazen EL, Jorgensen S, Rykaczewski RR, Bograd SJ and others (2012) Predicted habitat shifts of Pacific top predators in a changing climate. Nat Clim Change 3:234–238

Heyman WD, Kjerfve B (2008) Characterization of transient multi-species reef fish spawning aggregations at Gladden Spit, Belize. Bull Mar Sci 83:531–551

Hobday AJ, Hartog JR, Timmiss T, Fielding J (2010) Dynamic spatial zoning to manage southern bluefin tuna (*Thunnus maccoyii*) capture in a multi-species longline fishery. Fish Oceanogr 19:243–253

Hunt GL Jr, Schneider DC (1987) Scale-dependent processes in the physical and biological environment of marine birds. In: Croxall JP (ed) Seabirds: feeding ecology and role in marine ecosystems. Cambridge University Press, Cambridge

Hunt GL Jr, Russell RW, Coyle KO, Weingartner T (1998) Comparative foraging ecology of planktivorous auklets in relation to ocean physics and prey availability. Mar Ecol Prog Ser 167:241–259

Johnston DW, Read AJ (2007) Flow-field observations of a tidally driven island wake used by marine mammals in the Bay of Fundy, Canada. Fish Oceanogr 16:422–435

Kobayashi DR, Cheng IJ, Parker DM, Polovina JJ, Kamezaki N, Balazs GH (2011) Loggerhead turtle (*Caretta caretta*) movement off the coast of Taiwan: characterization of a hotspot in the East China Sea and investigation of mesoscale eddies. ICES J Mar Sci 68:707–718

Koslow JA, Goericke R, Lara-Lopez A, Watson W (2011) Impact of declining intermediate-water oxygen on deep-water fishes in the California Current. Mar Ecol Prog Ser 436:207–218

Mann KH, Lazier J (1996) Dynamics of marine ecosystems, Vol 389. Blackwell Science, Cambridge, MA

Maxwell SM, Morgan LE (2013) Foraging of seabirds on pelagic fishes: implications for management of pelagic marine protected areas. Mar Ecol Prog Ser 481:289–303

McClellan CM, Read AJ (2007) Complexity and variation in loggerhead sea turtle life history. Biol Lett 3:592–594

Meskhidze N, Nenes A, Chameides WL, Luo C, Mahowald N (2007) Atlantic Southern Ocean productivity: fertilization from above or below? Global Biogeochem Cycles 21: GB2006, doi:10.1029/2006GB002711

Mokany K, Harwood TD, Ferrier S (2013) Comparing habitat configuration strategies for retaining biodiversity under climate change. J Appl Ecol 50:519–527

Montevecchi WA, Hedd A, Tranquilla LM, Fifield DA and others (2012) Tracking seabirds to identify ecologically important and high risk marine areas in the western North Atlantic. Biol Conserv 156:62–71

Morato T, Hoyle SD, Allain V, Nicol SJ (2010) Seamounts are hotspots of pelagic biodiversity in the open ocean. Proc Natl Acad Sci USA 107:9707–9711

Moustahfid H, Jech MM, Weise MJ, Horne JK, O'Dor R, Alexander C (2012) Advancing 'bio' sensor integration with Ocean Observing Systems to support ecosystem based approaches. Proc Oceans 2012. IEEE, New York, NY

Myers N (1988) Threatened biotas: 'hotspots' in tropical forests. Environmentalist 8:187–208

Myers N, Mittermeier RA, Mittermeier CG, da Fonseca GAB, Kent J (2000) Biodiversity hotspots for conservation priorities. Nature 403:853–858

Nishikawa H, Ichiro Y, Komatsu K, Sasaki H, Sasai Y, Setou T, Shimuzu M (2013) Winter mixed layer depth and spring bloom along the Kuroshio front: implications for the Japanese sardine stock. Mar Ecol Prog Ser 487: 217–229

Nur N, Jahncke J, Herzog MP, Howar J and others (2011) Where the wild things are: predicting hotspots of seabird aggregations in the California Current System. Ecol Appl 21:2241–2257

Palacios DM, Bograd SJ, Foley DG, Schwing FB (2006) Oceanographic characteristics of biological hot spots in the North Pacific: a remote sensing perspective. Deep-Sea Res II 53:250–269

Pardo MA, Silverberg N, Gendron D, Beier E, Palacios DM (2013) Role of environmental seasonality in the turnover of a cetacean community in the southwestern Gulf of California. Mar Ecol Prog Ser 487:245–260

Piatt JF (1990) The aggregative response of common murres and Atlantic puffins to schools of capelin. Stud Avian Biol 14:36–51

Planquette H, Sanders RR, Statham PJ, Morris PJ, Fones GR (2011) Fluxes of particulate iron from the upper ocean around the Crozet Islands: A naturally iron-fertilized environment in the Southern Ocean. Global Biogeochem Cycles 25:GB2011, doi:10.1029/2010GB003789

Prairie JC, Ziervogel K, Arnosti C, Camassa R, Falcon C, Khatri S, McLaughlin RM, White BL, Yu S (2013) Delayed settling of marine snow at sharp density transitions driven by fluid entrainment and diffusion-limited retention. Mar Ecol Prog Ser 487:185–199

Ream RR, Sterling JT, Loughlin TR (2005) Oceanographic features related to northern fur seal migratory movements. Deep-Sea Res II 52:823–843

Roberts CM, McClean CJ, Veron JEN, Hawkins JP and others (2002) Marine biodiversity hotspots and conservation priorities for tropical reefs. Science 295:1280–1284

Ronconi RA, Lascelles BG, Langham GM, Reid JB, Oro D (2012) The role of seabirds in Marine Protected Area identification, delineation, and monitoring: introduction and synthesis. Biol Conserv 156:1–4

Sala E, Ballesteros E, Starr RM (2001) Rapid decline of Nassau grouper spawning aggregations in Belize: fishery management and conservation needs. Fisheries 26: 23–30

Santora JA, Veit RR (2013) Spatio-temporal persistence of top predator hotspots near the Antarctic Peninsula. Mar Ecol Prog Ser 487:287–304

Santora JA, Reiss CS, Loeb VJ, Veit RR (2010) Spatial association between hotspots of baleen whales and demographic patterns of Antarctic krill *Euphausia superba* suggests size-dependent predation. Mar Ecol Prog Ser 405:255–269

Santora JA, Sydeman WJ, Schroeder ID, Wells BK, Field JC (2011) Mesoscale structure and oceanographic determinants of krill hotspots in the California Current: implications for trophic transfer and conservation. Prog Oceanogr 91:397–409

Santora JA, Field JC, Schroeder ID, Sakuma KM, Wells BK, Sydeman WJ (2012a) Spatial ecology of krill, micronekton and top predators in the central California Current: Implications for defining ecologically important areas. Prog Oceanogr 106:154–174

Santora JA, Sydeman WJ, Schroeder ID, Reiss CS and others (2012b) Krill space: a comparative assessment of mesoscale structuring in polar and temperate marine ecosystems. ICES J Mar Sci 69:1317–1327

Sigler MF, Kuletz KJ, Ressler PH, Friday NA, Wilson CD, Zerbini AN (2012) Marine predators and persistent prey in the southeast Bering Sea. Deep-Sea Res II 65–70: 292–303

Smith CE, Hurley BJ, Toms CN, Mackey AD, Solangi M, Kuczaj SA II (2013) Hurricane impacts on the foraging patterns of bottlenose dolphins *Tursiops truncatus* in Mississippi Sound. Mar Ecol Prog Ser 487:231–244

Stevick PT, Incze LS, Kraus SD, Rosen S, Wolff N, Baukus A (2008) Trophic relationships and oceanography on and around a small offshore bank. Mar Ecol Prog Ser 363: 15–28

Suryan RM, Santora JA, Sydeman WJ (2012) New approach for using remotely sensed chlorophyll a to identify seabird hotspots. Mar Ecol Prog Ser 451:213–225

Sydeman WJ, Brodeur RD, Grimes CB, Bychkov AS, McKinnell S (2006) Marine habitat 'hotspots' and their use by migratory species and top predators in the North Pacific Ocean: Introduction. Deep-Sea Res II 53:247–249

Teo SH, Boustany A, Block B (2007) Oceanographic preferences of Atlantic bluefin tuna, *Thunnus thynnus*, on their Gulf of Mexico breeding grounds. Mar Biol 152: 1105–1119

Thorne LH, Read AJ (2013) Fine-scale biophysical interactions drive prey availability at a migratory stopover site for *Phalaropus* spp. in the Bay of Fundy, Canada. Mar Ecol Prog Ser 487:261–273

Tittensor DP, Mora C, Jetz W, Lotze HK, Ricard D, Vanden Berghe E, Worm B (2010) Global patterns and predictors of marine biodiversity across taxa. Nature 466: 1098–1107

Urmy SS, Horne JK, Barbee DH (2012) Measuring the vertical distributional variability of pelagic fauna in Monterey Bay. ICES J Mar Sci 69:184–196

Williams MJ, Ausubel J, Poiner I, Garcia SM and others (2010) Making marine life count: a new baseline for policy. PLoS Biol 8:e1000531

Wingfield DK, Peckham SH, Foley DG, Palacios DM and others (2011) The making of a productivity hotspot in the coastal ocean. PLoS ONE 6:e27874

Worm B, Lotze HK, Myers RA (2003) Predator diversity hotspots in the blue ocean. Proc Natl Acad Sci USA 100: 9884–9888

Submitted: February 24, 2012; Accepted: May 23, 2012

Proofs received from author(s): July 20, 2013

Vol. 487: 185–200, 2013
doi: 10.3354/meps10387

MARINE ECOLOGY PROGRESS SERIES
Mar Ecol Prog Ser

Published July 30

Contribution to the Theme Section 'Biophysical coupling of marine hotspots'

FREE ACCESS

Delayed settling of marine snow at sharp density transitions driven by fluid entrainment and diffusion-limited retention

Jennifer C. Prairie[1,2,3,*], Kai Ziervogel[1], Carol Arnosti[1], Roberto Camassa[2,3], Claudia Falcon[2,3], Shilpa Khatri[2,3], Richard M. McLaughlin[2,3], Brian L. White[1,3], Sungduk Yu[1,3]

[1]Department of Marine Sciences, [2]Carolina Center for Interdisciplinary Applied Mathematics, Department of Mathematics, and [3]Joint Fluids Lab, University of North Carolina at Chapel Hill, Chapel Hill, North Carolina 27599, USA

ABSTRACT: Marine snow is central to the marine carbon cycle, and quantifying its small-scale settling dynamics in different physical environments is essential to understanding its role in biogeochemical cycles. Previous field observations of marine aggregate thin layers associated with sharp density gradients have led to the hypothesis that these layers may be caused by a decrease in aggregate settling speed at density interfaces. Here, we present experimental data on aggregate settling behavior, showing that these particles can dramatically decrease their settling velocity when passing through sharp density transitions. This delayed settling can be caused by 2 potential mechanisms: (1) entrainment of lighter fluid from above as the particle passes through the density gradient, and (2) retention at the transition driven by changes in the density of the particle due to its porosity. The aggregates observed in this study exhibited 2 distinct settling behaviors when passing through the density transition. Quantitatively comparing these different behaviors with predictions from 2 models allow us to infer that the delayed settling of the first group of aggregates was primarily driven by diffusion-limited retention, whereas entrainment of lighter fluid was the dominant mechanism for the second group. Coupled with theory, our experimental results demonstrate that both entrainment and diffusion-limited retention can play an important role in determining particle settling dynamics through density transitions. This study thus provides insight into ways that delayed settling can lead to the formation of aggregate thin layers, important biological hotspots that affect trophic dynamics, and biogeochemical cycling in the ocean.

KEY WORDS: Aggregation · Thin layer · Accumulation · Biophysical coupling · Hotspots

INTRODUCTION

Marine snow plays a critical role in the marine carbon cycle, as a dominant component of carbon flux from the surface ocean, a site of enhanced bacterial activity, and often an important food source for zooplankton (Alldredge & Silver 1988, Smith et al. 1992, Simon et al. 2002, Kiørboe 2011). Knowledge of the vertical distribution of marine aggregates in the water column, as well as of the factors that underlie these distributions, are critical to understanding the functions of aggregates in the ocean.

Recent studies have observed that thin layers of aggregates—with concentrations several times back-

*Email: jprairie@email.unc.edu

ground levels—are common in coastal waters (MacIntyre et al. 1995, Alldredge et al. 2002, Prairie et al. 2010), and are often associated with sharp density transitions (MacIntyre et al. 1995, Dekshenieks et al. 2001, Prairie et al. 2010). These layers can have significant consequences for local carbon cycling, since aggregates may act as hot spots for bacterial activity or foraging zooplankton (Green & Dagg 1997, Kiørboe 2000, Ziervogel & Arnosti 2008, Ziervogel et al. 2010). Some studies have suggested that a possible explanation for the formation of these layers is locally decreased settling speeds as particles pass through these regions of sharp stratification (Derenbach et al. 1979, Alldredge & Crocker 1995, MacIntyre et al. 1995).

Previous theoretical and experimental studies have investigated the effect of sharp stratification on settling particles, and have shown that there are 2 potential mechanisms that could explain a decrease in settling velocity for a particle falling through a density transition. Studies with solid spheres have demonstrated that a sphere passing through a density transition will entrain lighter fluid from above in a thin boundary layer shell around the particle, and the additional buoyancy can decrease its settling velocity—in some cases even cause it to temporarily reverse direction (Srdi -Mitrovi et al. 1999, Abaid et al. 2004, Camassa et al. 2009, 2010, Yick et al. 2009). This delayed settling due to entrainment of lighter fluid can be seen in Fig. 1A, a sequence of previously published images from experiments with solid spheres along with matching theory (Camassa et al. 2010). However, marine aggregates are extremely porous (usually containing >99.5% water by volume; Ploug & Passow 2007), providing for another potential mechanism for delayed settling. The density of a porous particle will change depending on the fluid surrounding it. Thus, a porous particle may encounter a sharp density transition such that the particle is initially too light to sink through the density transition; however, after denser fluid diffuses into the particle, its density may increase sufficiently such that it can continue to sink. This diffusion-limited retention of porous particles, depicted schematically in Fig. 1B, has been investigated theoretically (MacIntyre et al. 1995, Alldredge & Crocker 1995, Kindler et al. 2010) and experimentally using agarose spheres (Kindler et al. 2010).

This recent work with both solid and porous spheres has provided important insight into the potential for sharp density gradients to lead to accumulations of aggregates through delayed settling. However, there is a lack of experimental work investigating whether natural aggregates will exhibit the same behavior as artificial particles, since natural aggregates differ from artificial spheres in important aspects including composition, shape, density, and size. In addition, it remains unclear which of the proposed mechanisms for delayed settling (i.e. entrainment of lighter fluid or diffusion-limited retention) dominates aggregate settling behavior for different types of aggregates in different environments.

Here, we present experimental results demonstrating that natural aggregates formed in the laboratory can significantly decrease their settling velocity as they pass through sharp density transitions. Our results demonstrate 2 distinct settling behaviors; one suggestive of diffusion-limited retention, and one suggestive of entrainment of lighter fluid. Although our experimental conditions are directly comparable only to a subset of field conditions, the general dynamics underlying the observed behavior is applicable to a wide range of aggregates settling through sharp density gradients. By comparing our results with those of previously developed models, we determined the mechanism that plays a dominant role depends on aggregate size, settling velocity, and the vertical density gradient. Lastly, we discuss the implications for the delayed settling of aggregates by each mechanism to form a layer that can act as a hot spot for foraging zooplankton and carbon remineralization.

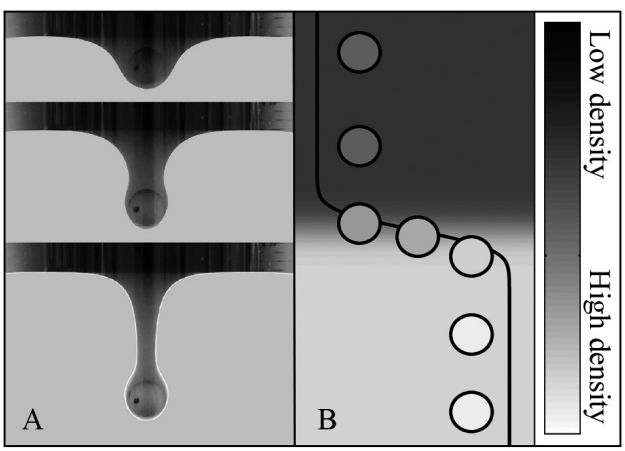

Fig. 1. Two mechanisms for decreased settling velocity of aggregates as they pass through sharp density transitions. (A) Lighter fluid is entrained around the sinking particle causing it to slow as shown in a time series of 3 experimental images (along with comparisons to theory). Figure from Camassa et al. (2010). (B) The aggregate pauses at the density transition until diffusion of denser fluid into the porous aggregate increases its density allowing it to continue sinking. Schematic adapted from figure in Kindler et al. (2010)

MATERIALS AND METHODS

Formation of aggregates

Aggregates were formed in a rotating acrylic cylindrical tank (total volume ~4 l) filled with either river water or seawater and placed on a roller table. This approach is widely used for aggregate formation in the lab (Shanks & Edmondson 1989, Jackson 1994, Ziervogel & Forster 2005, Ploug et al. 2008, Ziervogel & Arnosti 2008, Ziervogel et al. 2010). We chose to use aggregates formed from both fresh water and seawater to observe the settling behavior of a wider range of aggregate types with different densities and compositions. Aggregates are derived from natural organic matter present in the source water, and riverine and marine dissolved and particulate organic matter differ in their sources and composition (Hedges & Oades 1997, Cauwet 2002), although the specific composition of the organic matter in the source water was not measured in this study.

River water was collected in October 2011 at the mouth of the Tar River, North Caroline (NC) USA. Seawater was collected in December 2011 from the pier at the University of North Carolina Institute of Marine Sciences, located in Morehead City, NC. Particles were visible in both water samples prior to roller table experiments, which were started in the laboratory at room temperature shortly after sample collection. Rotation speed of the tank was set to 3.5 rpm, which proved suitable for forming aggregates useable in settling experiments. Macroscopic aggregates formed within the first day of both experiments. Aggregates were incubated in roller tanks for 7 d (seawater) and 17 d (river water); the time of incubation reflected the length of time required to form aggregates that were stable enough to use in settling experiments. At the end of the incubation, roller tanks were placed upright, and single aggregates that settled to the bottom of the tank were individually removed via volumetric pipette from the tank water (hereafter referred to as aggregate ambient water), and analyzed separately for their settling behavior. Four settling experiments were conducted in total—one with freshwater aggregates (Expt 1) and 3 with seawater aggregates (Expts 2, 3, and 4).

Measuring aggregate size

Aggregates used for calculation of aggregate densities as well as aggregates used in the 2-layer settling experiments were first measured by microscopy. Individual aggregates were placed on top of a millimeter square grid in a Petri dish with water of density approximately equal to that of their ambient water. Aggregates were then photographed with a digital microscope (Model 26700-300, Aven), producing images of the 2-dimensional projection of the aggregate (Fig. 2A). Images were processed using MATLAB to determine the cross-sectional area (Fig. 2B), which was used to calculate the equivalent spherical diameter for each aggregate, i.e. the cross sectional area was assumed to represent that of a sphere with an equivalent cross-sectional area (see Table 2). Since the aggregates are irregularly shaped and are most likely to lie such that their largest cross-section is the area imaged, the estimates of equivalent spherical diameter for each aggregate are likely overestimated. In addition, the irregular shape of the aggregates has consequences for their surface area to volume ratio, which would be much larger than an equivalently sized sphere. The implications of these factors on the delayed settling behavior of the aggregates are discussed below when comparing the experimental delayed settling behavior to models.

Calculating aggregate densities

Aggregate densities were calculated by measuring the sinking velocity of 5 to 12 representative aggregates per experiment in water of homogenous density (given in Table 1) approximately equal to that of their ambient water (~0.998 g cm^{-3} for freshwater aggregates and ~1.025 g cm^{-3} for marine aggregates). All water densities were measured using a DMA 35 Portable Density Meter (Anton Paar). After measuring their sizes as described above, individual aggregates were gently transferred by pipette to a rectangular tank with a base 18 × 18 cm and a height of 32 cm. The path of the aggregate as it settled in the tank was recorded using a Pike F-100B camera

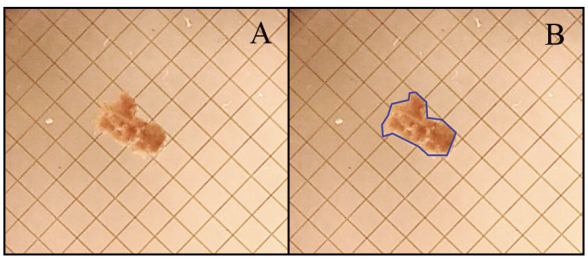

Fig. 2. (A) Microscope image of the aggregate shown on a 1 mm^2 grid. (B) Same image as (A) with perimeter outlined to illustrate how cross-sectional area is approximated to derive equivalent spherical diameter of aggregates

Table 1. Aggregate sinking experiments. Aggregate density was calculated using Eq. (1). Average aggregate density is shown over n aggregates along with the standard deviation. The subsequent columns provide the density of the homogenous water used to calculate aggregate densities, the densities of the top and bottom layer of the 2-layer settling experiments, and the number of aggregates observed in the 2-layer settling experiments. Aggregate excess density in bottom layer gives the difference between the average aggregate density and the density of the bottom layer

Expt no.	Average aggregate density (g cm^{-3})	Density of water for aggregate density measurement (g cm^{-3})	Density of top layer (g cm^{-3})	Density of bottom layer (g cm^{-3})	No. of aggregates	Aggregate excess density (g cm^{-3})
1	1.0098 ± 0.0064 (n = 12)	0.9985	0.9985	1.0401	5	–0.0303
2	1.0598 ± 0.0102 (n = 5)	1.0261	1.0248	1.0404	7	0.0194
3	1.0606 ± 0.0145 (n = 10)	1.0256	1.0249	1.0352	12	0.0254
4	1.0599 ± 0.0112 (n = 10)	1.0253	1.0250	1.0460	15	0.0139

(Allied Vision Technologies) recording at a rate between 25 and 33 frames s^{-1} (but that remained constant within an experiment). Sinking velocity was calculated from the vertical displacement (captured at the recording rate of the camera) and then an average sinking velocity (U) was calculated over at least 3 continuous seconds. This was used to estimate aggregate density (ρ_a) using the following equation (Batchelor 1967, Ploug et al. 2008):

$$U = \sqrt{\frac{4g(\rho_a - \rho_f)d}{3\rho_f C_D}} \quad (1)$$

where g is the acceleration due to gravity, ρ_f is the density of the fluid, C_D is the drag coefficient, and d is the equivalent spherical diameter as measured from the microscope images. The drag coefficient was calculated using the following empirical drag law (White 1974):

$$C_D = \frac{24}{Re} + \frac{6}{1+Re^{0.5}} + 0.4 \quad (2)$$

for Re > 0.5 where Re is the Reynolds number calculated as:

$$Re = \frac{dU}{\nu} \quad (3)$$

where ν is the kinematic viscosity of water (1.19 × 10^{-2} cm^2 s^{-1} at 15°C; Ploug et al. 2008). Since the above equations assume spherical particles, aggregates used to estimate aggregate density were chosen to be as spherical as possible. Individual densities for all aggregates measured were then averaged to obtain an average ρ_a for each experiment (Table 1). Since aggregates are porous, their densities depend on the fluid in which they are measured; the aggregate densities reported here are estimated in water approximately the density of the ambient water in which they were originally formed (see Table 1).

Two-layer aggregate settling experiments

After an average aggregate density was calculated, different aggregates from the same roller table batch were observed as they settled through a 2-layer water column with a sharp density transition in the middle. The tank used in these experiments had a square base (30 × 30 cm) and had a height of 61 cm. The tank was filled to approximately 20 cm with salt water. This salt water, hereafter defined as the bottom layer fluid, varied in density from experiment to experiment but was always more dense than the water in which the aggregates were formed (Table 1). After the bottom layer fluid was still, water with density approximately equal to that of the aggregates' ambient water—defined as the top layer fluid—was carefully poured on top of the bottom layer fluid through a diffuser initially soaked with top layer fluid. The diffuser floats at the surface of the water column; it is ~2 cm thick and is constructed of foam and sponge to slow down the flow of top layer fluid as it is introduced into the tank in order to create a sharp density transition between the top layer and bottom layer fluid. The thickness of the density transition was not measured for these experiments but is estimated from previous application of this stratification method (Abaid et al. 2004, Camassa et al. 2009) to be between 1 and 2 cm thick. Variations in this thickness will affect the sharpness of the density gradient, which is likely to affect aggregate settling behavior, although future work investigating this dependence is needed to determine the exact effect. The vertical density difference is calculated as the difference between the density of the bottom layer fluid (ρ_{BL}) and the density of the top layer fluid (ρ_{TL}) and ranged between 0.0103 and 0.0416 g cm^{-3}. For each experiment, the initial excess density of the aggregates in the bottom layer was calculated as $\rho_a - \rho_{BL}$ and is given in Table 1.

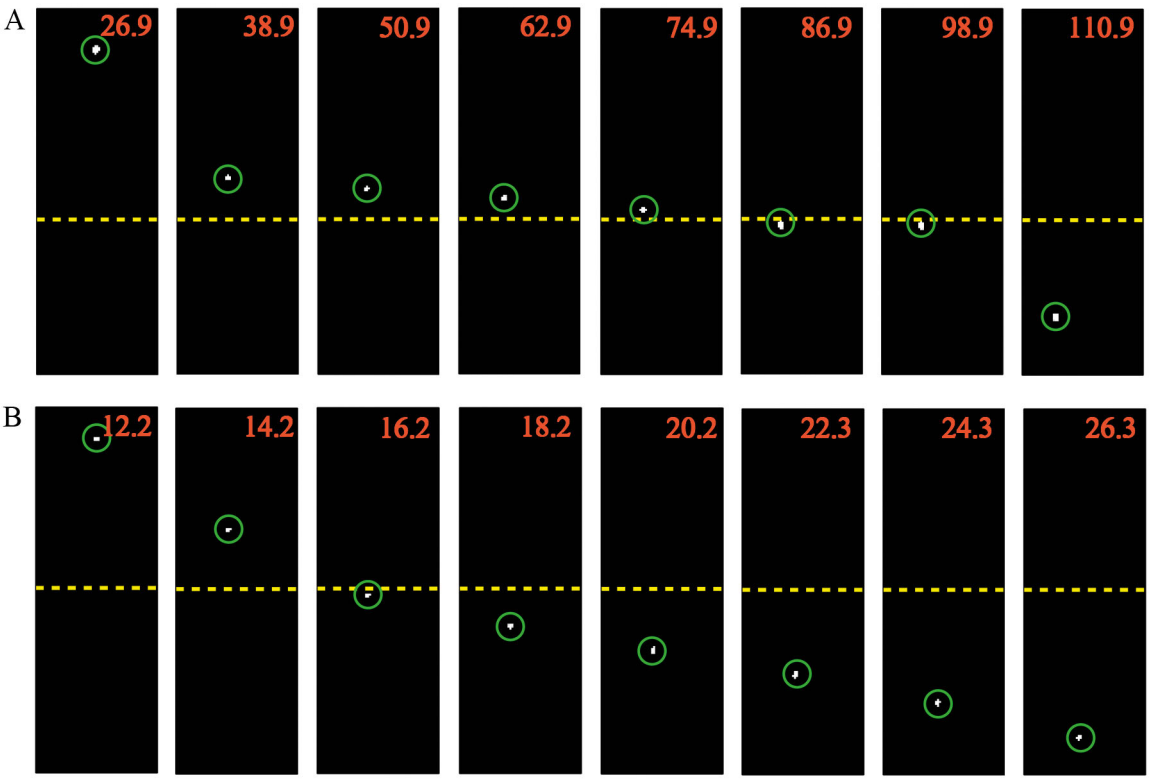

Fig. 3. Sequential panels show a region of images from (A) Expt 1 (Aggregate 4) and (B) Expt 4 (Aggregate 7) as the aggregate passes through the density transition (dotted yellow line). Time between images is ~12 s for (A) and ~2 s for (B). Time stamps are shown in orange in seconds. The region shown is ~2 cm × 6 cm. The aggregate in (A) demonstrates a smaller minimum settling velocity and a much longer delayed settling time than the aggregate in (B)

Aggregates were transferred gently by pipette into the 2-layer water column one at a time to observe their settling behavior. Aggregate settling behavior was recorded using the Pike camera, recording at a frame rate that was constant within runs, but varied among runs between 12 and 25 frames s^{-1}. Recordings were conducted with the room dark and the tank lit from the sides, using light-emitting diode (LED) strips attached to 2 panels that spanned the height and width of the tank. Although the LED panels did introduce some heat laterally into the tank, measurements indicate that the rise in temperature was slight (<1°C over the course of an experiment) and any convective motion was negligible in comparison to aggregate settling velocities. The square field of view of the images had dimensions which ranged among experiments between 31.5 cm × 31.5 cm and 37.2 cm × 37.2 cm. The top of the field of view was positioned between ~11.5 and 17 cm above the density transition (varied between experiments but kept constant within each experiment). The size of the field of view was chosen to maximize the vertical distance that the aggregate could be tracked while retaining adequate resolution of the aggregate.

Data analysis

All images (Fig. 3) were processed in MATLAB to determine the location of the aggregate (defined as the location of its centroid) over time. Position data was linearly corrected from pixels to cms using the measured dimensions of the field of view of the camera. The settling velocity was calculated by dividing the aggregate's vertical displacement between sequential images by the time between images; the settling velocity was then smoothed using a moving average over approximately a 1 s span.

The settling velocity in the top layer was calculated by averaging the smoothed settling velocity in a region above the density transition where the velocity was relatively constant for a period of at least 2 s. The settling velocity in the bottom layer was calculated by averaging the smoothed settling velocity in the very last part of the settling velocity time record (for a period of at least 2 s), representing the point at which the aggregate had reached its terminal velocity after passing through the density transition. The aggregates in Expt 1 did not appear to fully reach their terminal velocity in the bottom layer; in these

cases, settling velocity in the bottom layer was likely underestimated. Measured settling velocities for each aggregate are reported in Table 2; it is important to note that these measured values are not expected to match theoretical sinking velocity values (as calculated from Eq. 1) given the wide range of aggregate shapes observed in these experiments, and that an average aggregate density was used for each experiment.

Two metrics were calculated to determine the extent to which the aggregate's settling velocity decreased within the density transition. The normalized minimum settling velocity (NMSV) was calculated as the minimum value of the smoothed settling velocity (MSV) divided by the settling velocity in the bottom layer. The delayed settling time (DST) was calculated as the length of time that the aggregate's smoothed settling velocity was less than 90% of the settling velocity in the bottom layer. This definition for DST was chosen because it quantified the time of delayed settling of the aggregate independent of its settling velocity; the threshold of 90% was chosen to obtain a

Table 2. For each aggregate from the four 2-layer sinking experiments, experimental results are reported, including equivalent spherical diameter, settling velocity in the top and bottom layer, normalized minimum settling velocity (NMSV), delayed settling time (DST), and Reynolds number (Re) in the top layer

Expt no.	Aggregate no.	Aggregate equivalent spherical diameter (cm)	Settling velocity in top layer (cm s^{-1})	Settling velocity in bottom layer (cm s^{-1})	NMSV	DST (s)	Re in top layer
1	1	0.206	0.62	0.42	−0.01	244.2	10.7
	2	0.658	0.75	0.48	−0.15	600.6	41.3
	3	0.144	0.73	0.47	−0.01	191.4	8.8
	4	0.101	0.51	0.40	0	104.6	4.3
	5	0.137	0.52	0.41	0	149.8	5.9
2	1	0.089	1.48	0.87	0.65	6.6	11.0
	2	0.150	1.39	1.09	0.62	6.9	17.4
	3	0.122	1.23	0.89	0.57	11.2	12.6
	4	0.138	1.01	0.83	0.45	12.5	11.7
	5	0.071	0.97	0.79	0.67	6.6	5.8
	6	0.064	0.89	0.55	0.54	13.0	4.8
	7	0.096	1.22	0.81	0.58	9.5	9.9
3	1	0.077	0.50	0.50	0.30	18.9	3.2
	2	0.051	0.39	0.38	0.51	9.2	1.7
	3	0.062	0.55	0.53	0.54	9.9	2.8
	4	0.056	0.44	0.43	0.40	13.4	2.1
	5	0.112	0.88	0.82	0.63	8.5	8.3
	6	0.108	0.70	0.66	0.48	15.0	6.4
	7	0.098	1.09	0.98	0.79	3.5	9.0
	8	0.138	1.06	0.95	0.74	1.0	12.3
	9	0.105	0.85	0.77	0.67	7.9	7.5
	10	0.166	1.56	1.34	0.89	1.1	21.6
	11	0.116	0.86	0.80	0.64	9.2	8.4
	12	0.110	0.92	0.85	0.71	7.5	8.5
4	1	0.100	0.57	0.54	0.08	45.4	4.8
	2	0.136	1.28	1.07	0.52	9.3	14.6
	3	0.083	0.73	0.66	0.35	23.2	5.1
	4	0.088	0.94	0.74	0.58	8.9	7.0
	5	0.131	1.06	0.86	0.32	13.6	11.6
	6	0.111	1.45	0.82	0.75	8.6	13.5
	7	0.098	0.76	0.65	0.23	25.1	6.3
	8	0.110	1.22	1.06	0.58	7.2	11.3
	9	0.083	0.65	0.60	0.31	18.4	4.5
	10	0.084	0.92	0.59	0.23	24.0	6.5
	11	0.131	1.42	0.96	0.59	9.3	15.6
	12	0.105	1.09	0.96	0.46	10.2	9.6
	13	0.104	0.92	0.83	0.47	14.6	8.1
	14	0.102	1.36	1.16	0.66	6.7	11.6
	15	0.096	1.07	0.90	0.55	9.4	8.6

positive time scale even for aggregates that decreased their velocity only slightly while limiting the effect of noise. These metrics were calculated for each aggregate individually and compared to aggregate size and vertical density difference.

RESULTS

Experimental results

Data of settling behavior for all 39 aggregates observed in the 2-layer aggregate settling experiments are given in Table 2. It is important to note that aggregates that form in roller tanks are generally denser than those formed in nature, and thus typically exhibit much higher settling velocities than aggregates observed *in situ* (Shanks 2002). Thus, aggregates used in this study may be more representative of dense nearshore aggregates (which contain more mineral material) rather than offshore aggregates formed from phytoplankton blooms.

All aggregates demonstrated a settling velocity minimum when passing through the density transition (Table 2). However, the extent to which the aggregates decreased their velocity varied between aggregates, as well as among experiments.

The most striking differences in settling behavior occurred between aggregates in Expt 1 and aggregates in the other 3 experiments (Fig. 4). The 5 aggregates in Expt 1 all demonstrated a VMSV less than or equal to 0 (within the resolution of our images) when passing through the density transition. Although some of the aggregates had a negative NMSV, all except for Aggregate 2 were within the error (due to video recording noise) of having a 0 minimum settling velocity. By contrast, the NMSV of the aggregates in Expts 2, 3, and 4 ranged from 0.08 to 0.89, with a mean value of 0.53 (Fig. 4A). This difference between Expt 1 and the other 3 experiments is also evident in the DST, which ranged between 104.6 and 600.6 s for Expt 1 (mean of 258.1 s), and between 1.0 and 45.4 s for Expts 2, 3, and 4 (mean of 11.9 s) (Fig. 4B). The large spread in DSTs observed within a given experiment is expected because of the wide range of aggregate shapes and sizes used in the experiments. Although aggregates from each of the 4 experiments represent a range of sizes, it is important to note that the largest aggregate in Expt 1 was more than 3 times larger (by equivalent spherical diameter) than any of the other aggregates, and likewise its delayed settling time was much longer and not representative of the rest of the aggregates tested. The different settling behaviors are exemplified in plots of aggregate vertical location and settling velocity over time for an aggregate from Expt 1 (Fig. 5A,B) and for an aggregate from Expt 4 (Fig. 5C,D).

Differences also occurred in the manner in which DST varied with aggregate equivalent spherical diameter, which ranged between 0.051 cm and 0.658 cm for all experiments (mean of 0.121 cm) (Table 2). DST for aggregates in Expt 1 showed a strong positive linear relationship with equivalent spherical diameter ($r^2 = 0.988$, $p < 0.001$; Fig 6A). However, the other 3 experiments—when grouped together—showed a negative but not significant relationship between DST and aggregate equivalent spherical diameter (Fig. 6B). When Expts 2, 3, and 4 were considered separately, only Expt 3 showed a significant relationship at the $p = 0.05$ level ($r^2 = 0.398$, $p = 0.028$).

Although many experimental parameters differed among the experiments, one particularly notable difference between Expt 1 and the other 3 experiments was the initial excess density of the aggregates in

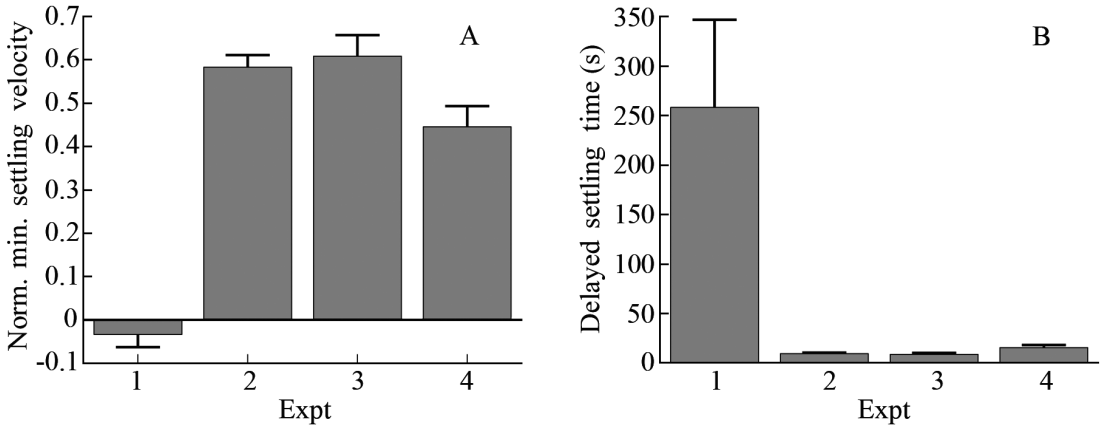

Fig. 4. Mean (A) normalized minimum settling velocity and (B) delayed settling time for aggregates in each experiment. Error bars = standard error

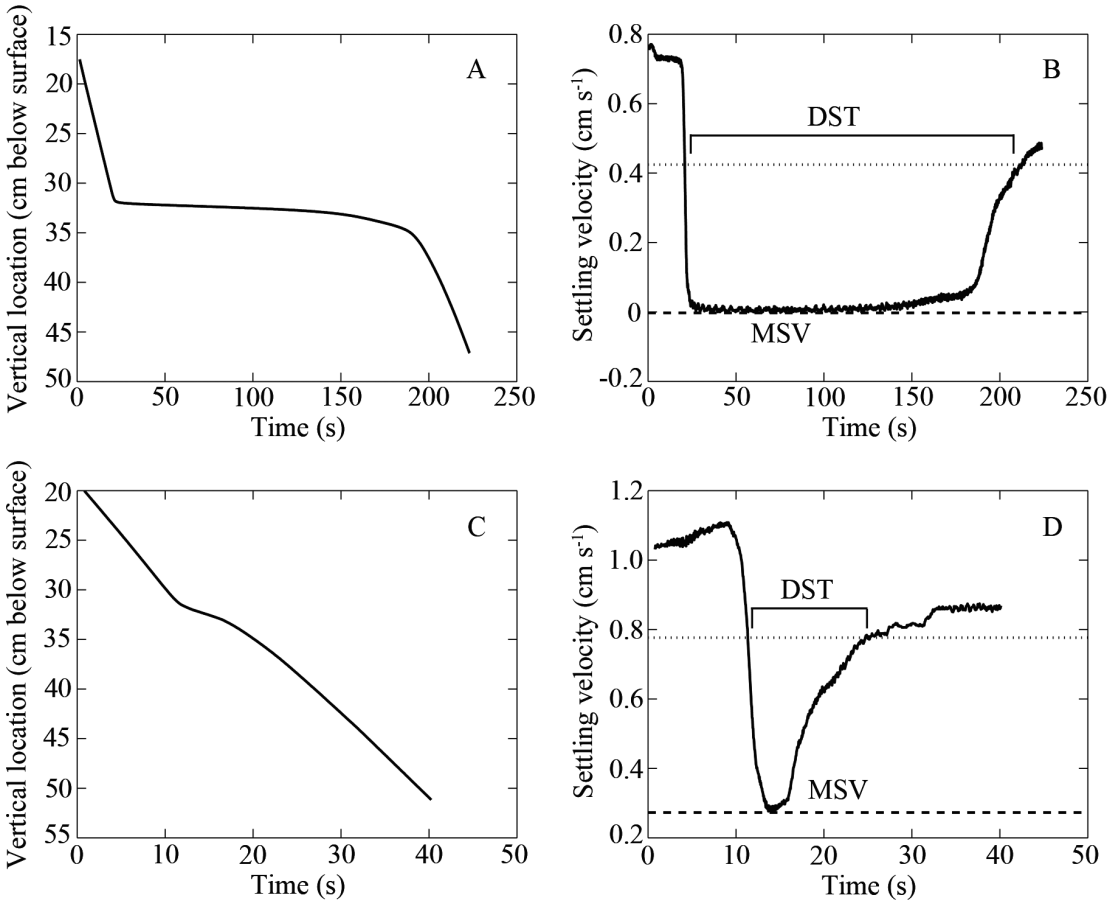

Fig. 5. Settling behavior of 2 aggregates through a sharp density transition. (A) Aggregate vertical location over time for Aggregate 3 from Expt 1. (B) Smoothed aggregate settling velocity over time for the same aggregate as in (A). (C) Aggregate vertical location over time for Aggregate 5 from Expt 4. (D) Smoothed aggregate settling velocity over time for same aggregate as in (C). In plots (B) and (D), the dashed line shows the minimum settling velocity (MSV, not normalized) and the dotted line represents 90% of the terminal velocity in the bottom layer, which was used to find delayed settling time (DST, shown with brackets)

the bottom layer (Table 1). The aggregates in Expt 1 were less dense than the bottom layer fluid initially (a negative excess density) while the aggregates in Expts 2, 3, and 4 were more dense than the bottom layer fluid (a positive excess density).

Comparison of experimental results to models

The observed relationships between aggregate size and DST (Fig. 6A & B) can be used to determine the dominant mechanism of delayed settling for each experiment by comparing the relationships with theoretical predictions of particle settling behavior from 2 different models. The first model—hereafter referred to as the porous particle model—illustrates the settling behavior of a porous particle as it passes through a sharp density transition. A brief description of the model is given here, but specific details of this model—ongoing in development—will be published elsewhere (R. Camassa, S. Khatri, R. M. McLaughlin, J. C. Prairie, B. L. White, S. Yu unpubl. data). The settling behavior in this model does not include any entrainment of fluid around the particle; thus, any decrease in particle settling velocity at the density transition is strictly due to diffusion-limited retention. The model assumes: (1) the Re is much smaller than 1, (2) a spherical particle whose size is not changing in time, (3) a density gradient formulated as an error function, (4) the ambient density gradient does not diffuse during the total time that it takes the sphere to settle through the transition region, (5) the radius of the sphere is small compared to variations in the ambient density profile, and (6) the time scale of diffusion into the sphere is small relative to the particle settling time scale. Under these assumptions, the model can be formulated as a force balance between the drag forces acting on the particle and buoyancy forces exerted by the fluid on the particle. The diffusion equation is solved dependent upon the location

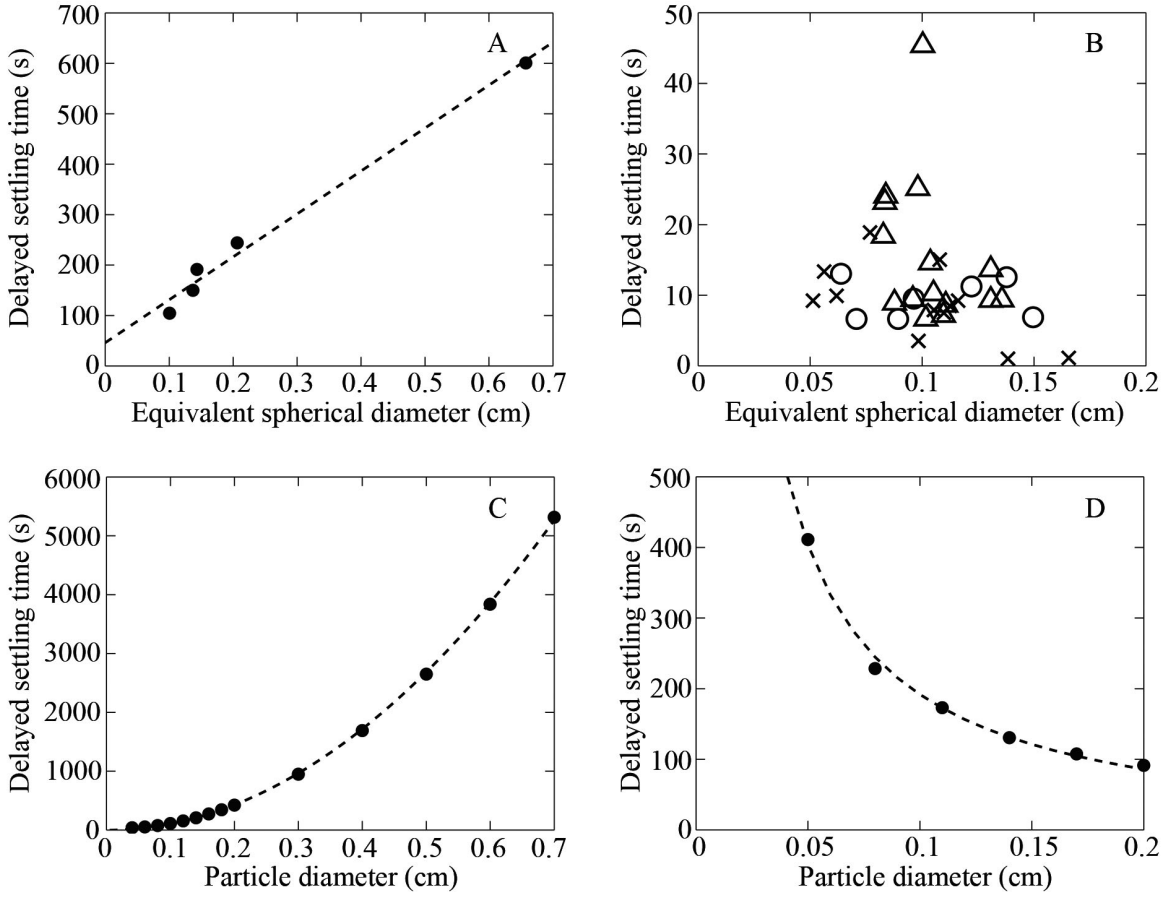

Fig. 6. (A) Aggregate equivalent spherical diameter vs. delayed settling time (DST) for all aggregates from Expt 1. Linear regression shown as dotted line ($y = 851.1x + 46.2$; $p < 0.001$, $r^2 = 0.988$). (B) Aggregate equivalent spherical diameter vs. DST for all aggregates from Expts 2 (○), 3 (×), and 4 (△). Linear regression was not significant when all data was grouped together at $p = 0.05$. For each experiment calculated separately, only Expt 3 had a significant linear regression ($y = -99.2x + 18.7$; $p = 0.028$, $r^2 = 0.398$). (C) DST for different particle diameters from the porous particle model. Model was run with parameters: density of the top layer (ρ_{TL}) = 0.998 g cm^{-3}, density of the bottom layer (ρ_{BL}) = 1.04 g cm^{-3}, particle porosity (P) = 0.98, density of the solid fraction of the particle (ρ_{solid}) = 1.3 g cm^{-3}, and diffusivity coefficient for salt (κ_S) = 1.5×10^{-5} cm^2 s^{-1}. Dashed line shows quadratic fit ($y = 10747x^2 - 2.4$; $p < 0.001$, $r^2 > 0.999$). (D) DST for different particle diameters from the solid particle entrainment model. Model was run with parameters: ρ_{TL} = 1.36 g cm^{-3}, ρ_{BL} = 1.38 g cm^{-3}, and particle density ($\rho_{particle}$) = 1.48 g cm^{-3}. Dashed line shows a fit of the form $y = 1/x$ ($y = 21.2(1/x) - 19.9$; $p < 0.001$, $r^2 = 0.995$). The different curves shown in (C) and (D) demonstrate that delayed settling due to diffusion limited retention results in a positive (quadratic) relationship between DST and aggregate size while entrainment of lighter fluid results in a negative relationship between DST and aggregate size

of the sphere to determine how much salt has diffused into the fluid within the sphere and therefore determines the weight of the sphere. Also, the buoyancy force is dependent upon the ambient fluid density surrounding the particle. By solving the diffusion equation analytically, we have developed a nonlinear integro-differential equation for the position of the particle as a function of time, which is then solved using numerical methods. Parameters in the model include density of the top layer (ρ_{TL}), density of the bottom layer (ρ_{BL}), diffusivity coefficient for salt (κ_S), the particle porosity (P), and the density of the solid fraction of the particle (ρ_{solid}).

This model was run for particle diameters ranging from 0.04 to 0.7 cm and the DST was calculated for each particle diameter in the same way as for the experimental results. These preliminary simulations demonstrate a positive correlation between particle diameter and DST that was fit with a quadratic polynomial ($r^2 > 0.999$; Fig. 6C). The model was formulated at low Re (the Stokes flow regime) since there is an analytical formula for the drag force in this case (Batchelor 1967). However, simulations using an empirical drag law for larger Re numbers, the White drag law (White 1974), showed no significant differences in the observed trends presented here while

having a minor decrease in the magnitude of the DST (<10 % for all particle diameters tested).

The second model—hereafter referred to as the solid particle entrainment model—gives the settling behavior of a solid particle as it passes through a sharp density transition (Camassa et al. 2009, 2010). This previously developed model illustrates decreased settling velocity at the density transition due to entrainment of lighter fluid; diffusion plays no role in the delayed settling of the particle since the particle is not porous. The model assumes: (1) the Re is much smaller than 1, (2) a spherical particle, (3) a density profile represented by a step function, and (4) neglects the effects of molecular diffusion. Parameters include ρ_{TL}, ρ_{BL}, and the particle density ($\rho_{particle}$). A full description of the formulation and assumptions of the model can be found in Camassa et al. (2009). The model was run for particle diameters ranging from 0.05 to 0.2 cm, and the DST was calculated for each particle diameter. This model predicts a negative correlation between particle diameter and delayed settling time that was fit with a curve of the form $y = 1/x$ ($r^2 = 0.995$; Fig 6D).

The predictions from the models presented in Fig. 6C & D provide insight into the relationship between particle size and DST for each of the 2 mechanisms for delayed settling. The formulation of these models allows us to consider each mechanism—entrainment and diffusion-limited retention—separately. Although such a perspective does not reflect real conditions for the experiments in which both mechanisms play a role and are likely interacting, it helps us gain an understanding of the conditions under which one mechanism may be more important than the other. Other important differences between the experiments and the models include particle shape (which is assumed to be spherical in the models) and Re (which is assumed to be less than 1 in the models). For these reasons, we do not attempt to directly compare the experimental and theoretical results, but instead compare trends between particle size and delayed settling time that might provide information about the underlying mechanisms.

The porous particle model predicts a positive quadratic relationship between particle diameter and DST. This relationship is expected since the mechanism that controls the retention time of the particle at the density transition is diffusion, and the time scale of diffusion is proportional to particle radius squared. By contrast, the solid particle entrainment model predicts a negative hyperbolic relationship between particle diameter and DST. This relationship can also be explained by the underlying mechanism, since the decrease in particle settling speed should be regulated by the volume of the entrained lighter fluid (proportional to the surface area) relative to the volume of the particle. We therefore may expect that the DST is proportional to the surface area to volume ratio, which for a sphere scales as $1/R$, where R is the particle radius.

The strong positive correlation between aggregate size and DST for Expt 1 (Fig. 6A) suggests that the settling behavior of these aggregates was driven primarily by diffusion-limited retention. The relationship observed between aggregate size and DST was linear rather than the quadratic relationship predicted by the porous particle model (Fig. 6C). The discrepancies observed between the model and experiments—both in the magnitude of the DST and the shape of the relationship between particle size and DST—are most likely due to the assumption of a spherical particle, lack of entrainment in the model, and the parameterization of the model used here. Although the model assumes the particles are spherical, the aggregates used in the experiments often had irregular shapes, particularly the larger particles; this will increase particle surface area at which diffusion takes place, resulting in lowered DSTs relative to equivalently-sized spherical particles. Additionally, although the porous particle model only includes delayed settling due to diffusion-limited retention, both diffusion-limited retention and entrainment played a role (likely interacting) in the delayed settling of each of the aggregates in the experiments, even if one mechanism dominated the observed behavior. Lastly, the parameter values for P and ρ_{solid} used in the model simulations presented here represent estimates from literature and other experiments (Alldredge & Gotschalk 1988, Ploug et al. 2008); however, these may not reflect the actual properties of the aggregates used in the experiments.

Other characteristics of aggregate settling behavior from Expt 1 also suggest that diffusion-limited retention was the dominant mechanism. For example, all aggregates in Expt 1 had a settling velocity of zero at the density transition, as expected for particles exhibiting diffusion-limited retention. In addition, the DSTs for the aggregates in Expt 1 were on average more than an order of magnitude larger than for the other 3 experiments.

The weak negative relationship between aggregate size and DST for Expts 2, 3, and 4 (although significant only for Expt 3) suggests that the settling behavior for these experiments may be dominated primarily by entrainment of lighter fluid. The non-significant relationships between aggregate size and

DST in Fig. 6B are likely due to the large range in aggregate shapes observed in these experiments. However, the non-zero minimum settling velocities for all aggregates in Expts 2, 3, and 4 and the relatively short DSTs (as compared to Expt 1) further suggest that entrainment of lighter fluid is more important than diffusion in these cases. As for Expt 1, the discrepancies in DST values between the solid particle entrainment model and Expts 2, 3, and 4 can be explained by the model assumption of a spherical particle, lack of diffusion in the model, and the model parameterization.

DISCUSSION

Predicting the dominant mechanism for delayed settling at density transitions

The sinking behavior of aggregates through sharp density transitions observed in both the experimental data and model simulations provides insight into the circumstances under which the decreased settling velocity at the transition is primarily driven by diffusion-limited retention (Fig. 1B) or entrainment of lighter fluid (Fig. 1A). When the density of the aggregate in the top layer fluid is less than the density of the bottom layer fluid, the aggregate will have to stop at the density transition until sufficient diffusion into the particle allows it to continue to sink. However, when the density of the aggregate in the top layer fluid is greater than the density of the bottom layer fluid, the aggregate can continue settling through the density transition but experiences a decrease in settling velocity because of fluid entrained from the top layer. Thus, the curve

$$\rho_{BL} = \rho_a \quad (4)$$

divides 2 broad regimes: above this curve, diffusion-limited retention controls the particle's delayed setting at the density transition, although there may be important interactions with the effects due to entrainment; below this curve, diffusion is no longer important and the dominant mechanism for delayed settling is entrainment of lighter fluid.

The 2 regimes described by Eq. (4) are shown in Fig. 7A. For the 4 experiments conducted, the settling behavior regime can be identified easily from the initial excess density of the aggregate in the bottom layer (Table 1). When this excess density is positive, the density of the aggregate is greater than the density of the bottom layer fluid, thus placing it in the entrainment regime. Likewise, when this excess density is negative, the aggregates fall in the diffusion-limited retention regime. It is important to note that the regimes represented in Fig. 7 simply depict relative effects of one mechanism compared to the other, rather than an absolute trend. For example, in the entrainment regime, moving further away from the dividing line indicates that the effect of entrainment becomes stronger relative to the effect of diffusion-limited retention; it does not indicate that the effect of entrainment becomes stronger in an absolute sense. In fact, in a study of solid spheres settling

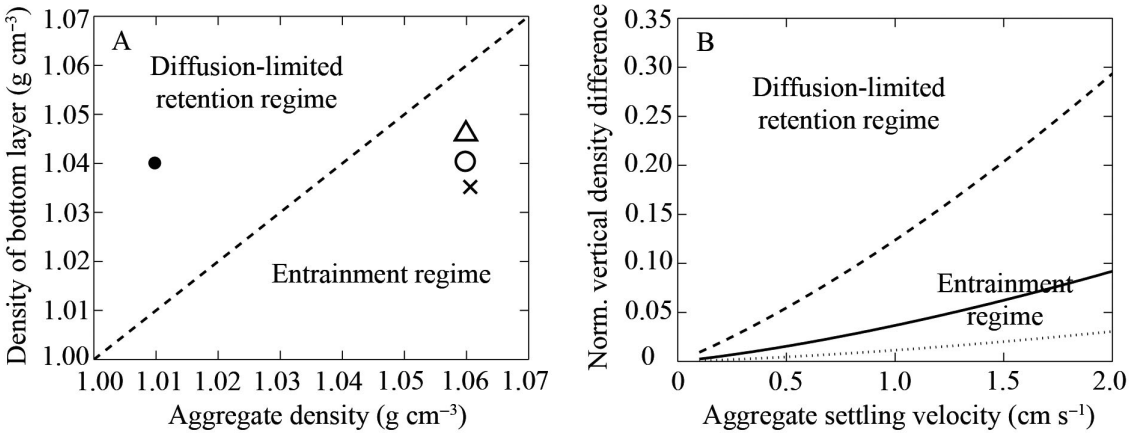

Fig. 7. Two aggregate sinking behavior regimes for an aggregate passing through a sharp density transition. (A) Aggregate density vs. bottom layer density. The curve (Eq. 4) separates the regime dominated by diffusion-limited retention (above the curve) and the regime dominated by entrainment of lighter fluid (below the curve). (●) Expt 1, (○) Expt 2, (×) Expt 3, and (△) Expt 4. (B) Aggregate sinking velocity vs. normalized layer density. Several curves of Eq. (6) are shown for different values of aggregate radius (R): R = 0.025 cm (dashed line), R = 0.05 cm (solid line), and R = 0.1 cm (dotted line). For each curve, the region above the curve represents the regime dominated by diffusion-limited retention and the region below the curve represents the regime dominated by entrainment of lighter fluid

through density transitions, the effect of entrainment was observed to become stronger as the density of the sphere became closer to the density of the bottom layer fluid (R. Camassa, R. M. McLaughlin, A. Vaidya unpubl. data).

Moreover, although one mechanism can be dominant in certain cases, both mechanisms are always at work to some extent, and interactions between them can alter the delayed settling behavior. Particularly for the diffusion-limited retention regime, although diffusion is necessary for the particle to increase its density and thus continue to sink, the effects of entrainment have been shown to be important in many cases, particularly in accurately predicting delayed settling times (R. Camassa, S. Khatri, R. M. McLaughlin, J. C. Prairie, B. L. White, S. Yu unpubl. data).

The 2 regimes can also be described as a function of settling velocity, which is more easily measured in the field than aggregate density. By combining Eq. (4) with Eq. (1) — which provides an estimate of aggregate density (in top layer fluid) as a function of settling velocity and aggregate size — the following curve is obtained:

$$\rho_{BL} = \frac{3U^2\rho_{TL}C_D}{8gR} + \rho_{TL} \quad (5)$$

Eq. (5) can be rewritten so that a normalized measure of the vertical density difference $(\rho_{BL} - \rho_{TL})/\rho_{TL}$ is expressed in terms of aggregate settling velocity and radius:

$$\frac{\rho_{BL} - \rho_{TL}}{\rho_{TL}} = \frac{3U^2C_D}{8gR} \quad (6)$$

For given aggregate radii, a curve of this normalized vertical density difference vs. settling velocity can be calculated; in the same way as for Eq. (4), above the curve represents delayed settling primarily driven by diffusion-limited retention while below the curve represents delayed settling primarily driven by entrainment of lighter fluid. Fig. 7B illustrates several curves of the normalized vertical density difference vs. aggregate settling velocity for different aggregate radii. As before, both mechanisms can act to delay settling and interact with each other.

Implications of delayed settling for aggregate thin layer formation

The results of this study have shown that aggregates derived from natural waters can exhibit significantly decreased settling velocities when passing through sharp density transitions because of 2 different mechanisms: diffusion-limited retention and entrainment of lighter fluid. In some cases, aggregates demonstrated only a modest decrease in settling velocity (with a minimum settling velocity as large as ~89% of the settling velocity in bottom layer), while in other cases, aggregates came to a complete stop. The DST reached up to ~600 s in the most dramatic case observed; however, in the majority of cases the decrease in settling velocity was on the order of ~10 s, representing a relatively short-term event given the total time required for an aggregate to sink out of the surface ocean. However, the importance of this phenomenon is not the delay experienced by a single aggregate in its journey to depth, but rather, the resulting accumulation of aggregates at the depth of the density transition.

Even modest decreases in aggregate settling speed at sharp density transitions can result in significant local increases in aggregate abundance. Using a rough approximation — only considering the effects of settling speed — the local increase in aggregate abundance will equal the inverse of the NMSV. For example, a NMSV of 0.5 would result in a doubling in local aggregate concentration, even if the delayed settling time of an individual aggregate is only ~10 s. This model is overly simplistic, since it suggests that in cases where the NMSV equals 0, there would be an infinite buildup of aggregates. Including the effects of vertical diffusivity, as done in previous models of plankton thin layer formation (Stacey et al. 2007, Birch et al. 2008, Prairie et al. 2011), will provide a balance between the accumulation caused by the delayed settling and the dissipating effects of mixing, thus presenting a more realistic idea of how these mechanisms can affect vertical aggregate distributions.

The intensity of the resulting aggregate layer will depend strongly on whether the delay in aggregate settling is driven primarily by diffusion-limited retention or entrainment of lighter fluid. As demonstrated by this study, the decrease in settling velocity is more pronounced as well as longer-lasting for aggregates undergoing diffusion-limited retention. Thus, layers formed by this mechanism will demonstrate higher increases in aggregate concentrations compared to layers formed by entrainment of lighter fluid. However, even in the case where entrainment dominates, aggregate layers can form.

The persistence of aggregate layers would largely be determined by the persistence of the density transition that originally caused the decrease in settling velocity. If the sharp density gradient is transient, then the aggregate layer would also be expected to

be ephemeral. However, in many cases sharp density gradients can persist for days or significantly longer in the ocean (Dekshenieks et al. 2001), thus allowing long-lived aggregate layers to form.

Aggregate layers have important effects on food web dynamics, acting as hot spots for zooplankton foraging. Studies have demonstrated that marine snow can be an important food source for a diverse variety of zooplankton, including protists, copepods, other mesozooplankton, and larval invertebrates (Alldredge 1972, Lampitt et al. 1993, Steinberg 1995, Shanks & Walters 1996, 1997, Green & Dagg 1997, Artolozaga et al. 2002). Aggregate layers formed through delayed settling may further enhance local zooplankton abundance and grazing, explaining the finding that up to 70% of aggregate carbon can be degraded by invertebrate grazers before an aggregate sinks out of the surface ocean (Kiørboe 2000). Laboratory experiments have shown that several taxa of zooplankton are able to seek out and remain in regions of high food concentration (Jakobsen & Johnsen 1987, Tiselius 1992, Menden-Deuer & Grünbaum 2006). For marine snow, zooplankton may be able to use chemical sensing to detect sinking particles (Jackson & Kiørboe 2004, Kiørboe 2011). Field observations have demonstrated that the distributions and grazing rates of zooplankton and perhaps higher trophic levels such as small fish are often associated with planktonic layers (McManus et al. 2003, Benoit-Bird et al. 2009, 2010, Menden-Deuer & Fredrickson 2010). However, there is still a need for studies of trophic interactions in aggregate layers in the field, since most studies of zooplankton grazing on aggregates have focused on zooplankton associations with single particles (Green & Dagg 1997, Shanks & Walters 1997, Jackson & Kiørboe 2004). Continuing advances in optical and acoustic technology may allow for *in situ* measurements of the settling behavior and vertical distributions of aggregates concurrent with grazing rates and distributions of zooplankton and fish, providing a better mechanistic understanding of the role of delayed settling in aggregate layer formation and its impact on trophic interactions.

Aggregate layers may also be a hotspot for bacterial activity and organic matter remineralization. Experimental and theoretical studies have suggested that bacteria may preferentially find and colonize sinking aggregates (Kiørboe et al. 2001, 2002, Kiørboe & Jackson 2001, Stocker et al. 2008). In addition, bacterial activity and enzymatic hydrolysis rates on aggregates can be several orders of magnitude higher than that of aggregate-free water (Grossart et al. 2007, Ziervogel & Arnosti 2008, Ziervogel et al. 2010), demonstrating that aggregates not only represent regions of enhanced bacterial abundance but also active carbon remineralization. In aggregate layers formed by delayed aggregate sinking, the effect of aggregates as remineralization hot spots may be further strengthened. Given the potential for aggregate layers as hotspots for zooplankton foraging and bacterial activity, the presence of these layers may act to reduce local carbon flux, with implications for larger-scale carbon cycling.

Applicability to aquatic ecosystems

The experimental results presented here represent a small fraction of natural conditions found in aquatic ecosystems; however, the basic observation of delayed aggregate settling at sharp density transitions may be widely applicable to many regions of the world's oceans since the general dynamics underlying the delayed settling behavior will remain the same. The vertical density differences tested in the current study (with density differences of ~1.025 to ~1.046 g cm^{-3} for the marine aggregates tested) are much greater and over shorter vertical distances than would be observed in most coastal regions or the open ocean (density for the entire water column will typically range from ~1.02 to ~1.029 g cm^{-3}). However, similar aggregate settling behavior may be observed at much weaker density gradients since the effect of density gradients on aggregate settling behavior is controlled not only by the sharpness of the gradient but also by the density of the aggregate. Since aggregates used in this study were formed in roller tanks, they are likely much denser than aggregates found in the open ocean and other regions outside of very nearshore environments (Alldredge & Gotschalk 1988, Shanks 2002). For example, for natural marine aggregates from the San Pedro and Santa Barbara Basins, Alldredge & Gotschalk (1988) measured a median aggregate density of 1.02502 g cm^{-3} (equal to 0.00014 g cm^{-3} higher than the ambient seawater). Thus, natural, less-dense aggregates in these systems are likely to exhibit significantly decreased settling velocities even with weaker density gradients than those tested in this study.

In some stratified aquatic environments, the density differences tested in this study are representative of naturally occurring gradients. In estuaries, for example, the transition from fresh water to seawater can occur over a relatively small vertical distance which can retain particles for extended periods of

time, resulting in estuarine turbidity maxima, as has been observed in the Columbia River, USA, estuary (Crump et al. 1999). Under these conditions, carbon remineralization can be enhanced by particle-attached bacteria (Crump et al. 1999). Furthermore, deep hypersaline basins, such as those in the Gulf of Mexico, the Red Sea, and the Mediterranean Sea, can exhibit up to an order of magnitude vertical change in salinity over very short depth scales (Polymenakou et al. 2007, Tribovillard et al. 2009). In these extreme environments, trapped particles at the halocline can affect the distribution, composition, and abundance of both organic matter and the microbial community (LaRock et al. 1979, Polymenakou et al. 2007, Tribovillard et al. 2009). In estuaries as well as hypersaline basins, the intense vertical density differences would make delayed settling by aggregates more likely to be driven by diffusion-limited retention, resulting in minimum settling velocities close to zero and resulting in very long particle residence times. These settling behavior attributes explain the intense particle accumulations often observed at these sites (Crump et al. 1999, Tribovillard et al. 2009).

Finally, it is important to consider whether the density gradients in question are driven by changes in salinity or temperature. In some parts of the ocean, vertical salinity variations can cause sharp pycnoclines (most notably in estuaries and hypersaline basins as discussed previously), thus mimicking the experiments presented here. However, most often in the upper ocean, temperature gradients are responsible for vertical changes in density. Since the molecular diffusion of heat occurs at a rate nearly 2 orders of magnitude faster than that of salt (Gargett et al. 2003), aggregates settling through temperature-driven density gradients will likely exhibit decreases in settling velocity that are much more short-lived than those observed in this study.

CONCLUSIONS

These experimental results demonstrate that delayed settling of natural aggregates at density transitions can occur by 2 different mechanisms — entrainment of lighter fluid and diffusion-limited retention. The time scale and extent to which an aggregate decreases its velocity at the density transition depends on the dominant mechanism at work. A first-order prediction of the conditions in which entrainment vs. diffusion-limited retention will dominate shows that the governing mechanism depends on the aggregate size, settling speed, and strength of the density gradient. However, since in many intermediate cases both mechanisms are important, future work exploring the interactions between these 2 mechanisms is needed. In addition, although we demonstrate decreased settling velocity across a range of aggregate sizes and conditions, further experimental work is needed to understand how settling behavior of natural aggregates varies with changing aggregate and environmental parameters, including porosity, aggregate density, aggregate size, and density gradient. Lastly, investigation on whether the settling behavior of aggregates (especially in highly concentrated regions) is affected by fluid interactions with other aggregates will provide a more complete understanding of aggregate settling dynamics.

The mechanisms for delayed settling of aggregates across density transitions illustrated here have important implications for both trophic dynamics and carbon cycling. Even modest decreases in aggregate settling velocities can result in significant accumulations of aggregates in layers that can act as hot spots for foraging by zooplankton (and subsequently higher trophic levels) in addition to bacterial remineralization. For both zooplankton grazing and bacterial activity, overlooking the impact of hot spots such as aggregate layers may cause total water column rates of these important processes to be significantly underestimated.

Acknowledgements. We thank A. Brandt, J. Dresser and A. Horne for their help with experimental work. Thanks to E. Monbureau for her technical help. We thank 3 anonymous reviewers whose comments greatly improved this manuscript. This work is funded primarily by NSF CMG ARC-1025523 and additionally by NSF DMS-1009750, NSF RTG DMS-0943851, NSF RAPID CBET-1045653, NSF OCE-0848703, and NSF GRFP DGE-0646083.

LITERATURE CITED

Abaid N, Adalsteinsson D, Agyapong A, McLaughlin RM (2004) An internal splash: levitation of falling spheres in stratified fluids. Phys Fluids 16:1567–1580

Alldredge AL (1972) Abandoned larvacean houses: a unique food source in the pelagic environment. Science 177: 885–887

Alldredge AL, Crocker KM (1995) Why do sinking mucilage aggregates accumulate in the water column? Sci Total Environ 165:15–22

Alldredge AL, Gotschalk C (1988) In situ settling behavior of marine snow. Limnol Oceanogr 33:339–351

Alldredge AL, Silver MW (1988) Characteristics, dynamics, and significance of marine snow. Prog Oceanogr 20: 41–82

Alldredge AL, Cowles TJ, MacIntyre S, Rines JEB and others (2002) Occurrence and mechanisms of formation

of a dramatic thin layer of marine snow in a shallow Pacific fjord. Mar Ecol Prog Ser 233:1–12

Artolozaga I, Valcárcel M, Ayo B, Latatu A, Iriberri J (2002) Grazing rates of bacterivorous protists inhabiting diverse marine planktonic microenvironments. Limnol Oceanogr 47:142–150

Batchelor GK (1967) An introduction to fluid dynamics. Cambridge University Press, Cambridge

Benoit-Bird KJ, Cowles TJ, Wingard CE (2009) Edge gradients provide evidence of ecological interactions in planktonic thin layers. Limnol Oceanogr 54:1382–1392

Benoit-Bird KJ, Moline MA, Waluk CM, Robbins IC (2010) Integrated measurements of acoustical and optical thin layers I: vertical scales of association. Cont Shelf Res 30: 17–28

Birch DA, Young WR, Franks PJS (2008) Thin layers of plankton: formation by shear and death by diffusion. Deep-Sea Res I 55:277–295

Camassa R, Falcon C, Lin J, McLaughlin RM, Parker R (2009) Prolonged residence times for particles settling through stratified miscible fluids in the Stokes regime. Phys Fluids 21:031702

Camassa R, Falcon C, Lin J, McLaughlin RM, Mykins N (2010) A first-principle predictive theory for a sphere falling through sharply stratified fluid at low Reynolds number. J Fluid Mech 664:436–465, doi:10.1017/S0022112010003800

Cauwet G (2002) DOM in the coastal zone. In: Hansell DA, Carlson CA (eds) Biogeochemistry of marine dissolved organic matter. Academic Press, New York, NY

Crump BC, Armbrust EV, Baross JA (1999) Phylogenetic analysis of particle-attached and free-living bacterial communities in the Columbia River, its estuary, and the adjacent coastal ocean. Appl Environ Microbiol 65:3192–3204

Dekshenieks MM, Donaghay PL, Sullivan JM, Rines JEB, Osborn TR, Twardowski MS (2001) Temporal and spatial occurrence of thin phytoplankton layers in relation to physical processes. Mar Ecol Prog Ser 223:61–71

Derenbach JB, Astheimer H, Hansen HP, Leach H (1979) Vertical microscale distribution of phytoplankton in relation to the thermocline. Mar Ecol Prog Ser 1:187–193

Gargett AE, Merryfield WJ, Holloway G (2003) Direct numerical simulation of differential scalar diffusion in three-dimensional stratified turbulence. J Phys Oceanogr 33:1758–1782

Green EP, Dagg MJ (1997) Mesozooplankton associations with medium to large marine snow aggregates in the northern Gulf of Mexico. J Plankton Res 19:435–447

Grossart HP, Tang KW, Kiørboe T, Ploug H (2007) Comparison of cell-specific activity between free-living and attached bacteria using isolates and natural assemblages. FEMS Microbiol Lett 266:194–200

Hedges JI, Oades JM (1997) Comparative organic geochemistries of soils and marine sediments. Org Geochem 27:319–361

Jackson GA (1994) Particle trajectories in a rotating cylinder: implications for aggregation incubations. Deep-Sea Res I 41:429–437

Jackson GA, Kiørboe T (2004) Zooplankton use of chemodetection to find and eat particles. Mar Ecol Prog Ser 269: 153–162

Jakobsen PJ, Johnsen GH (1987) Behavioural response of the water flea *Daphnia pulex* to a gradient in food concentration. Anim Behav 35:1891–1895

Kindler K, Khalili A, Stocker R (2010) Diffusion-limited retention of porous particles at density interfaces. Proc Natl Acad Sci USA 107:22163–22168

Kiørboe T (2000) Colonization of marine snow aggregates by invertebrate zooplankton: abundance, scaling, and possible role. Limnol Oceanogr 45:479–484

Kiørboe T (2011) How zooplankton feed: mechanisms, traits and trade-offs. Biol Rev Camb Philos Soc 86:311–339

Kiørboe T, Jackson GA (2001) Marine snow, organic solute plumes, and optimal sensory behavior of bacteria. Limnol Oceanogr 46:1309–1318

Kiørboe T, Ploug H, Thygesen UH (2001) Fluid motion and solute distribution around sinking aggregates. I. Small-scale fluxes and heterogeneity of nutrients in the pelagic environment. Mar Ecol Prog Ser 211:1–13

Kiørboe T, Grossart HP, Ploug H, Tang K (2002) Mechanisms and rates of bacterial colonization of sinking aggregates. Appl Environ Microbiol 68:3996–4006

Lampitt RS, Wishner KF, Turley CM, Angel MV (1993) Marine snow studies in the Northeast Atlantic Ocean: distribution, composition and role as a food source for migrating plankton. Mar Biol 116:689–702

LaRock PA, Lauer RD, Schwarz JR, Watanabe KK, Wiesenburg DA (1979) Microbial biomass and activity distribution in an anoxic, hypersaline basin. Appl Environ Microbiol 37:466–470

MacIntyre S, Alldredge AL, Gotschalk CC (1995) Accumulation of marine snow at density discontinuities in the water column. Limnol Oceanogr 40:449–468

McManus MA, Alldredge AL, Barnard AH, Boss E and others (2003) Characteristics, distributions, and persistence of thin layers over a 48 hour period. Mar Ecol Prog Ser 261:1–19

Menden-Deuer S, Fredrickson K (2010) Structure-dependent, protistan grazing and its implication for the formation, maintenance and decline of phytoplankton patches. Mar Ecol Prog Ser 420:57–71

Menden-Deuer S, Grünbaum D (2006) Individual foraging behaviors and population distributions of a planktonic predator aggregating to phytoplankton thin layers. Limnol Oceanogr 51:109–116

Ploug H, Passow U (2007) Direct measurement of diffusivity within diatom aggregates containing transparent exopolymer particles. Limnol Oceanogr 52:1–6

Ploug H, Iversen MH, Fischer G (2008) Ballast, sinking velocity, and apparent diffusivity within marine snow and zooplankton fecal pellets: implications for substrate turnover by attached bacteria. Limnol Oceanogr 53: 1878–1886

Polymenakou PN, Stephanou EG, Tselepides A, Bertilsson S (2007) Organic matter preservation and microbial community accumulations in deep-hypersaline anoxic basins. Geomicrobiol J 24:19–29

Prairie JC, Franks PJS, Jaffe JS (2010) Cryptic peaks: invisible vertical structure in fluorescent particles revealed using a planar laser imaging fluorometer. Limnol Oceanogr 55:1943–1958

Prairie JC, Franks PJS, Jaffe JS, Doubell MJ, Yamazaki H (2011) Physical and biological controls of vertical gradients in phytoplankton. Limnol Oceanogr Fluids Environ 1:75–90

Shanks AL (2002) The abundance, vertical flux, and still-water and apparent sinking rates of marine snow in a shallow coastal water column. Cont Shelf Res 22: 2045–2064

Shanks AL, Edmondson EW (1989) Laboratory-made artifi-

cial marine snow: a biological model of the real thing. Mar Biol 101:463–470

Shanks AL, Walters K (1996) Feeding by a heterotrophic dinoflagellate (*Noctiluca scintillans*) in marine snow. Limnol Oceanogr 41:177–181

Shanks AL, Walters K (1997) Holoplankton, meroplankton, and meiofauna associated with marine snow. Mar Ecol Prog Ser 156:75–86

Simon M, Grossart HP, Schweitzer B, Ploug H (2002) Microbial ecology of organic aggregates in aquatic ecosystems. Aquat Microb Ecol 28:175–211

Smith DC, Simon M, Alldredge AL, Azam F (1992) Intense hydrolytic enzyme activity on marine aggregates and implications for rapid particle dissolution. Nature 359: 139–142

Srdi -Mitrovi AN, Mohamed NA, Fernando HJS (1999) Gravitational settling of particles through density interfaces. J Fluid Mech 381:175–198

Stacey MT, McManus MA, Steinbuck JV (2007) Convergences and divergences and thin layer formation and maintenance. Limnol Oceanogr 52:1523–1532

Steinberg DK (1995) Diet of copepods (*Scopalatum vorax*) associated with mesopelagic detritus (giant larvacean houses) in Monterey Bay, California. Mar Biol 122: 571–584

Stocker R, Seymour JR, Samadani A, Hunt DE, Polz MF (2008) Rapid chemotactic response enables marine bacteria to exploit ephemeral microscale nutrient patches. Proc Natl Acad Sci USA 105:4209–4214

Tiselius P (1992) Behavior of *Acartia tonsa* in patchy food environments. Limnol Oceanogr 37:1640–1651

Tribovillard N, Bout-Roumazeilles V, Sionneau T, Serrano JCM, Riboulleau A, Baudin F (2009) Does a strong pycnocline impact organic-matter preservation and accumulation in an anoxic settling? The case of the Orca Basin, Gulf of Mexico. CR Geoscience 341:1–9

White FM (1974) Viscous fluid flow. McGraw-Hill, New York, NY

Yick KY, Torres CR, Peacock T, Stocker R (2009) Enhanced drag of a sphere settling in a stratified fluid at small Reynolds numbers. J Fluid Mech 632:49–68

Ziervogel K, Arnosti C (2008) Polysaccharide hydrolysis in aggregates and free enzyme activity in aggregate-free seawater from the north-eastern Gulf of Mexico. Environ Microbiol 10:289–299

Ziervogel K, Forster S (2005) Aggregation and sinking behaviour of resuspended fluffy layer material. Cont Shelf Res 25:1853–1863

Ziervogel K, Steen AD, Arnosti C (2010) Changes in the spectrum and rates of extracellular enzyme activities in seawater following aggregate formation. Biogeosciences 7:1007–1015

Submitted: July 2, 2012; Accepted: April 29, 2013

Proofs received from author(s): May 30, 2013

Vol. 487: 201–215, 2013
doi: 10.3354/meps10462

MARINE ECOLOGY PROGRESS SERIES
Mar Ecol Prog Ser

Published July 30

Contribution to the Theme Section 'Biophysical coupling of marine hotspots'

FREE ACCESS

Effects of interannual environmental variability on the transport-retention dynamics in haddock *Melanogrammus aeglefinus* larvae on Georges Bank

Jason M. Boucher[1,*], Changsheng Chen[1], Yunfang Sun[1], Robert. C. Beardsley[2]

[1]School for Marine Science and Technology, University of Massachusetts-Dartmouth, New Bedford, Massachussetts 02742, USA
[2]Department of Physical Oceanography, Woods Hole Oceanographic Institution, Woods Hole, Massachussetts 02543, USA

ABSTRACT: Georges Bank is a region of high biological productivity characterized by a well-defined clockwise tidal rectified circulation gyre. Fluctuations in the year-class strength of haddock *Melanogrammus aeglefinus* on Georges Bank have been attributed to mortality during the highly vulnerable larval stages. While predation and starvation greatly impact on survival, advection to unfavorable regions may result in greatly reduced numbers of individuals. For successful self-recruitment to occur, individuals must remain within the shoal region of Georges Bank until settlement. An individual-based model (IBM) was utilized to estimate the retention of haddock eggs and larvae on Georges Bank annually for 1995 through 2009. The IBM was driven by the Finite-Volume Community Ocean Model (FVCOM) for the Gulf of Maine domain. Biological components of haddock larvae were omitted to restrict analyses to the impact of circulation on passive transport. Inflow over the Scotian Shelf and tidal interaction patterns were identified as the major drivers of variability in interannual transport-retention dynamics. The simulations indicated that retention rates were highest in 2000 and 2003, and lowest in 1997. The above-average retention in 2000 and 2003 with anomalously large recruitment only in 2003 indicates that high retention appears to be necessary but not sufficient to explain large recruitment events of haddock on Georges Bank.

KEY WORDS: Larval retention · Haddock · Modeling · Georges Bank · Bio-physical coupling · Fish early life history stages · Fish larvae

INTRODUCTION

Biological hotspots are ecologically important areas characterized by high biodiversity (species richness, abundance, and biomass) and high chlorophyll concentration (Hughes et al. 2002, Valavanis et al. 2004, Reese & Brodeur 2006). Georges Bank exhibits both characteristics, with annual primary productivity in the tidally mixed shoals approaching 3 times the global mean value for continental shelves (O'Reilly et al. 1987). The high productivity on Georges Bank is caused by (1) the nutrient-rich deep waters surrounding the bank, (2) tidal mixing on the shoals incorporating the deep water nutrients into the tidal-mixing front zones, and (3) insignificant light limitation (Riley 1941, Horne et al. 1989, Franks & Chen 1996, Townsend & Pettigrew 1997).

Circulation in the Gulf of Maine-Georges Bank region is driven by a combination of local forcing (winds, heat flux, precipitation/evaporation, tides, and freshwater discharge from coastal rivers and groundwater) and remote forcing from upstream inflow and intrusion of Gulf Stream warm-core rings (Loder 1980, Smith et al. 2001, Hu 2009). Tidal currents over Georges Bank can exceed 100 cm s^{-1} and tidal rectification (interactions of tidal currents with steep bottom topography and tidal mixing) generates a permanent clockwise gyre around the bank (Fig. 1) (Loder 1980). Tidal-mixing fronts on Georges Bank are located around the 40 m isobaths on the northern flank and intensified by the shelf-break front on the

*Email: jboucher1@umassd.edu

southern flank at the 100 m isobath in winter and the 40–50 m isobaths in summer. As a result of seasonal intensification of tidal-mixing fronts, the clockwise gyre is strengthened by increasing stratification in late spring through summer (Chen et al. 1995) and varies on monthly, seasonal, and interannual time scales due to the fluctuation in river discharge and winds (Brink et al. 1987, Limeburner & Beardsley 1996, Chen et al. 2001). The circulation system is directly controlled by southward transport on the Scotian Shelf and slope, which originates upstream from the Labrador Sea and Arctic Ocean (Chapman & Beardsley 1989). The interaction of the Gulf Stream-associated warm and salty water and the cooler, fresher Labrador slope water is a driver of the interannual variability in the circulation in the Gulf of Maine-Georges Bank region (Drinkwater & Gilbert 2004).

Recruitment of highly fecund marine fishes is dependent on mortality through the egg and larval stages, mediated by starvation, predation, and advection away from the nursery area (Hjort 1914, Cushing 1974, Lasker 1975). Environmental variability in the key physical mechanisms that retain plankton, eggs, and larvae (Townsend & Pettigrew 1996, Chen et al. 2001) has a pronounced influence on fish recruitment during the early larval stages (Bartsch & Coombs 2001, 2004). Circulation, water temperature, and mixing can directly affect survival by impacting the spatio-temporal interaction of prey, predators, and settlement (Cushing 1974, Lasker 1975, Sale 1978).

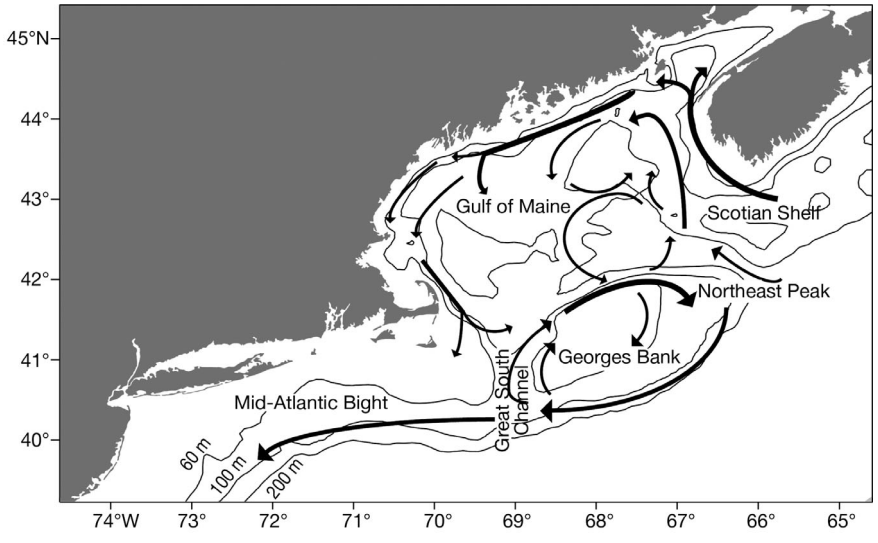

Fig. 1. General circulation patterns in the Gulf of Maine. The prominent gyre circulation on Georges Bank, enhanced by stratification and tidal interaction, produces enhanced chlorophyll concentration and biological productivity

Haddock *Melanogrammus aeglefinus* on Georges Bank spawn in the spring, from February through May (Smith & Morse 1985), releasing eggs near the bottom (Hardy 1978, Page et al. 1989). Hatching occurs after 15 to 21 d and exogenous feeding begins 5 to 7 d later (Hardy 1978, Page & Frank 1989). The clockwise gyre around Georges Bank retains haddock larvae within their nursery area, with losses transported towards the Mid-Atlantic Bight or entrained in the Gulf Stream warm core rings (Flierl & Wroblewski 1985, Smith & Morse 1985, Polacheck et al. 1992).

Recruitment into the Georges Bank haddock stock averaged 87 million fish annually between 1994 and 2002, with the 2003 year-class (the largest on record) exceeding 789 million age-1 recruits (Brodziak et al. 2006). Recruitment success, the ratio of the number of year-1 recruits to the previous year's spawning stock biomass (Churchill et al. 2011), fluctuates widely between years (Fig. 2) and is dependent on starvation, predation, and advective transport on Georges Bank. Strong year-classes of haddock are associated with circulation and retention on Georges Bank (Colton & Temple 1961, Polacheck et al. 1992), with shoalward transport to the nursery region increasing with depth in the water column (Lough & Bolz 1989, Werner et al. 1993). Wind stress enhances circulation off-bank, reducing recruitment as wind speed increases (Chase 1955, Lough et al. 1994, 2006, Mountain et al. 2008).

Individual-based models (IBMs) incorporate physical dynamics of the environment (circulation, advection, stratification, and turbulent mixing) with individual- and cohort-level processes during the early life stages to infer relationships resolved in the model to observed patterns in the field (Bartsch & Coombs 2004, Tian et al. 2009). IBMs of cod and haddock larvae in the Gulf of Maine have relied primarily on climatological circulation models, with variability in flow fields incorporated through the addition of monthly-averaged wind-driven forcing (Werner et al. 1993, Brickman & Frank 2000). However, circulation driven by climatological mean surface forcing is not representative of observed conditions in the Gulf of Maine-Georges Bank region, as wind stress and freshwater input change dramatically on short time scales (Miller

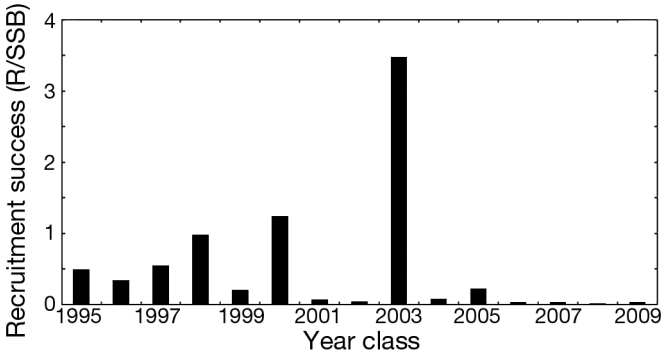

Fig. 2. Estimates of recruitment success of the Georges Bank haddock stock. Recruitment success (R/SSB) is the ratio of age-1 recruits (R, ind.) for a given year to the spawning stock biomass (SSB, kg) of the previous year

1946, Hopkins & Raman 1987, Beardsley et al. 2003, Hu 2009). With the availability of circulation models capable of resolving interannual patterns, it is now possible to assess bio-physical interactions within and between years with increased accuracy.

Observational field ecology and modeling studies indicate the importance of interannual variation in circulation on the retention and survival of haddock on Georges Bank or on transport to the Mid-Atlantic Bight (Chase 1955, Polacheck et al. 1992, Lough et al. 1994). The purpose of the present study was to examine how interannual variation in the circulation of Georges Bank impacted on the distribution and retention of haddock larvae spawned on the Northeast Peak annually from 1995 through 2009. Our work follows an earlier study of larval haddock transport on Georges Bank (Werner et al. 1993) where particles were released on the Northeast Peak to determine the impact of advective transport on retention and settlement under climatological flow fields. Here we extend that analysis to include multiple years and investigate the impact of vertical turbulence in the water column with an advanced circulation model.

METHODS

Circulation model

The physical environment was represented using the prognostic free-surface, 3-dimensional (3D) primitive equation unstructured-grid, Finite-Volume Community Ocean Model (FVCOM) (Chen et al. 2006, 2007, 2011). The structure of this model is described in detail in Chen et al. (2011), and key components related to the current study are briefly provided. As a finite-volume model, FVCOM solves the governing equations in unstructured triangular volumes with a second-order accurate discrete flux scheme, resulting in more accurate representations of mass, momentum, heat, and salinity conservation (Chen et al. 2011). An unstructured triangular grid is used in the horizontal dimension, with terrain-following coordinates in the vertical. Vertical viscosity was computed using the Mellor and Yamada level-2.5 turbulence closure model (Mellor & Yamada 1982) and the horizontal diffusion coefficient was determined using the Smagorinsky turbulent closure scheme (Smagorinsky 1963).

Two versions of the Gulf of Maine-FVCOM (GoM-FVCOM) are utilized in this study. The GoM1-FVCOM was configured for the Gulf of Maine with a cutoff at a depth of 300 m off the shelf break. This model was driven by local forcing including: (1) tides (constructed at the open boundary using 5 tidal constituents: M_2, S_2, N_2, K_1, and O_1), (2) sea surface interactions (wind stress, net heat flux plus shortwave irradiance, atmospheric pressure gradient, and precipitation/evaporation), and (3) freshwater discharges from the major coastal rivers of the Gulf of Maine. The computational domain encompasses the Gulf of Maine-Georges Bank region, bounded by the Scotian Shelf to the northeast and the New England Shelf to the southwest (Fig. 3). The domain was arranged by an unstructured triangular grid with a horizontal resolution varying from ~0.5–1.0 km in the tidal-mixing front on Georges Bank to ~10 km near the open boundary. Vertical resolution was divided into 31 levels, providing a variable depth per layer ranging from ~1.5 m over the top of the Bank to 10 m offshore of the continental shelf where the bathymetry was truncated to 300 m. The second version, GoM3-FVCOM, was configured as a global-regional nested model system with the same local forcing as GoM1-FVCOM, but the open boundary is specified using the output of the global FVCOM hindcast model simulation (Sun et al. 2013). This nested model system uses the real ocean bathymetry without a depth cutoff at the shelf break. The computational domain is extended to the south with coverage to Cape Hatteras, North Carolina, a horizontal resolution up to 0.3–0.5 km at the shelf break of Georges Bank and a total of 41 levels in the vertical.

Both GoM1-FVCOM and GoM3-FVCOM predicted 3D fields of water temperature, currents, and vertical viscosity, which were used to drive the IBM. The GoM1-FVCOM output provided physical forcing for simulations of interannual variability in retention caused primarily by local drivers of circulation for

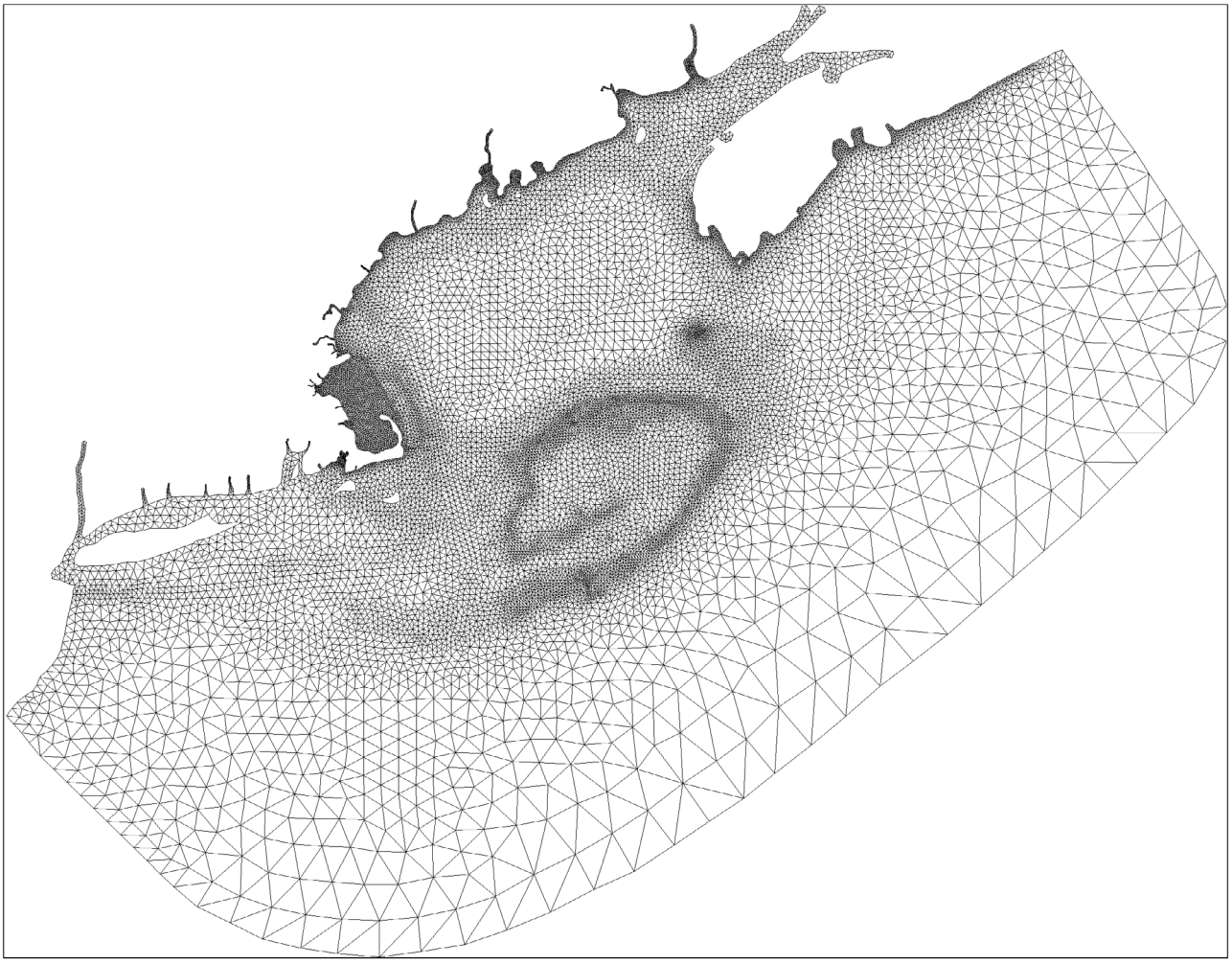

Fig. 3. Domain and mesh grid of the first Gulf of Maine Finite Volume Community Ocean Model (GoM1-FVCOM). The high resolution on Georges Bank enables greater replication of local dynamics

1995–2009. GoM3-FVCOM simulated the combined influence of local and remote drivers, but model output was only available for the 1997 and 1998 forcing fields. Use of the 2 circulation models enabled comparison of local and remote forcing on the transport-retention dynamics of haddock eggs and larvae on Georges Bank.

Individual-based model

The IBM is described following the 'Overview, Design Concepts, and Details' (ODD) protocol of Grimm et al. (2006).

Purpose: A spatially-explicit individual-based model was developed to simulate the passive transport-retention dynamics experienced by haddock eggs and larvae from spawning until juvenile settlement on Georges Bank. The IBM was designed to track the impacts of the dynamic physical environment in the absence of larval behavior.

State variables & scales: No biological state variables were included for the tracking of passive particles. We assumed that all individuals have no swimming ability or biological attributes, which may be appropriate only for the first 30 d (Auditore et al. 1994).

Process overview & scheduling: Individuals were advected throughout the domain by the 3D circulation fields from FVCOM and tracked by the Lagrangian particle tracking algorithm. No foraging, growth, behavior or mortality processes were included.

Design concepts: Individual haddock eggs were released on the spawning grounds and tracked for the 90 d duration of their pelagic phases. Passive individuals were transported by a 3D Lagrangian

flow. Passive individuals were utilized to elucidate the impact of interannual variability in circulation on transport in the absence of biological mediation.

Model data: For each time step (1 h), the particle position and depth, as well as temperature, salinity, and density at each particle location were updated. The recorded information for all individuals was combined to derive properties and characteristics at the population level.

Initialization: The IBM was initialized at the spawning of haddock on Georges Bank. Spawning events were simulated to occur over a 7 d period, released with a normal distribution in time. The normal distribution function of Tian et al. (2009) is used:

$$e_i(t) = NS_e \int_{t_0}^{t} \frac{1}{\sqrt{2\pi\sigma}} e^{-\frac{1}{2}\left(\frac{t-t_M}{\sigma}\right)} dt \quad (1)$$

where $e_i(t)$ is the number of eggs spawned by the ith individual female adult at the time t, N is the total number of females, S_e is the total numbers of eggs spawned by each individual adult in a spawning season, t_0 is the start time of spawning, t_M is the maximum spawning time, and σ is the standard deviation.

Spawning location was based on a prior modeling study (Werner et al. 1993), with spawning period inferred from analyses of large-scale sampling programs (Smith & Morse 1985, Sibunka et al. 2006). The median spawning date was set to March 29 for each year, with particles released from a grid on the Northeast Peak of Georges Bank. Particles were released at 1, 10, 30, and 50 m depths and tracked for 90 d, to account for the egg and larval stages of haddock up to settlement (Werner et al. 1993, Brickman 2003). Successful retention and settlement occurred if individuals remained within the 100 m isobaths and east of the Great South Channel (68.86° W) by the end of the simulation.

Input: The 3D flow fields, water temperature, vertical eddy viscosity, horizontal mixing coefficients, and upwelling index were generated by the GoM-FVCOM models.

Model assumptions: It was necessary to make some assumptions in order to use the physical model output and the biological data. It was assumed that no behavior capable of altering the position of the larvae was possible. While this may not be valid over the entire period of development, it was necessary to assume this to determine the variability that the environment alone can impart to the retention of eggs and larvae. It was also assumed that circulation on Georges Bank was accurately represented by the offline model velocity fields produced by FVCOM (see Chen et al. 2011 for details).

Submodels

The movement of individuals was controlled by a 3D Lagrangian flow, with the option to include vertical shear turbulence through the random walk formulation of Visser (1997) (adapted from Li et al. unpubl.):

$$P_n(\vec{x},t) = \int_{t-\Delta t}^{t} \vec{v} dt + R(K_m) + P(\vec{x}_{t-\Delta t}, t-\Delta t) \quad (2)$$

where $P_n(\vec{x},t)$ and $P(\vec{x}_{t-\Delta t}, t-\Delta t)$ are the locations of the nth individual at times t and $t-\Delta t$; $\vec{v}$ is the 3D velocity vector; R is a random process with mean (R^2 = 0) and standard deviation (R^2 = r), K_m is the maximum diffusivity during the time interval, and $R(K_m)$ is the vertical random walk distance moved during the time interval (Δt). The advective distance was calculated by a modified 4th-order Runge-Kutta time-stepping scheme (Chen et al. 2003). A vertical random walk was simulated following the Visser (1997) differential equation with a time step of δt. Where $\hat{n}$ is the random walk time step at time $t-\Delta t$, the vertical location of the nth individual caused by the random walk after δt is computed by:

$$z_{\hat{n}+1} = z_{\hat{n}} + K'_m \delta t + r[2\sigma_z^{-1} K_m(z_{\hat{n}} + 0.5K'_m \delta t)\delta t]^{1/2} \quad (3)$$

where $K'_m \delta t = \delta K_m / \delta z$, r is a random process with mean = 0, and σ_z is the standard deviation. Assuming that r represents a uniform distribution between +1 and −1, σ_z = 1/3. The random walk generator requires δt to be much smaller than Δt (the Lagrangian integral time scale) to prevent an unrealistic aggregation of individuals (Chen et al. 2003). In the present study, Δt = 120 s, and δt = 6 s, so that $R(K_m) = z_{\hat{n}+20} - z_{\hat{n}}$, where $z_{\hat{n}}$ is the vertical location of the nth individual at $t-\Delta t$.

Simulation experiments

An experiment was conducted to examine how spatial and temporal variability of the environment affects transport and potential settlement of larvae interannually, as an extension to the climatological results of Werner et al. (1993), who suggested that interannual variability in larval distributions and circulation would produce variable losses from Georges Bank. Individuals were simulated to drift for 90 d after spawning in each experiment. A 2-dimensional (2D) model was utilized to determine the impact of fixed depth on the advection of larvae around Georges Bank. Next, a 3D tracking simulation was performed to simulate vertical dispersal in the water

column due to bio-physical interactions. Persistence at depth will alter particle dispersal patterns and retention, requiring 3D advection of individuals. Two physical conditions were compared: (1) advection from the FVCOM circulation fields and (2) advection with the inclusion of vertical turbulence. Physical dynamics of a high and a low retention year were then compared to elucidate the components of the environment that may contribute to successful year-classes of haddock on Georges Bank. The importance of remote forcing on retention was tested using the GoM3-FVCOM forcing for 1997 and 1998 as test cases with (1) 2D, (2) 3D, and (3) 3D with vertical turbulence, scenarios.

Recruitment is a complex process involving spawning dynamics (spawning stock biomass, fecundity, and nutritional state) as well as losses of the early life history stages (Hjort 1914, Cushing 1974, Lasker 1975). Small, almost imperceptible changes in larval growth or mortality rates can drastically alter recruitment, making prediction difficult and unreliable (Rothschild 1986, Beyer 1989). In an attempt to relate retention rates to prediction of recruitment, model retention rates were compared to recruitment success of the Georges Bank haddock stock (Churchill et al. 2011, NFSC 2012).

RESULTS

Interannual variability in larval haddock retention occurred in the 2D, 3D, and 3D with vertical turbulence, simulations (Fig. 4). Similar trends were obtained from the 3 scenarios, with lowest retention in 1997 and 1998 and highest retention in 2000, 2003, and 2004. Mean retention between the 3 scenarios exhibited high variability within a year, ranging from a 24% difference in 2008 to 4% in 2009 (Fig. 4).

2D tracking

A pattern of increased retention with increasing release depth was observed for all years in this study. Highest retention occurred for individuals constrained to the 50 m depth, and lowest for individuals at 1 m. After 30 d, retention of individuals released at 1 m ranged from 0.25% in 1997 to 92.97% in 1995; while retention exceeded 90% for all years when individuals were retained at 50 m. By Day 90, retention at 1 m was less than 1% in 8 of the years and had decreased to 21.88% in 1995. In contrast, the lowest retention at 50 m was 18.03% in 1998 and the highest was 96.32% in 2000. These results are consistent with climatological modeling studies (Werner et al. 1993, Lough et al. 1994), where higher retention occurred when particles were released at 30 m or deeper.

3D tracking

The pattern of increased retention for individuals released at 30 m or deeper was also observed in the 3D simulations, with dispersal throughout the water column impacting transport speed and direction. Retention of individuals released at 1 m after 90 d ranged from 0.00% (1997) to 24.60% (1995), while

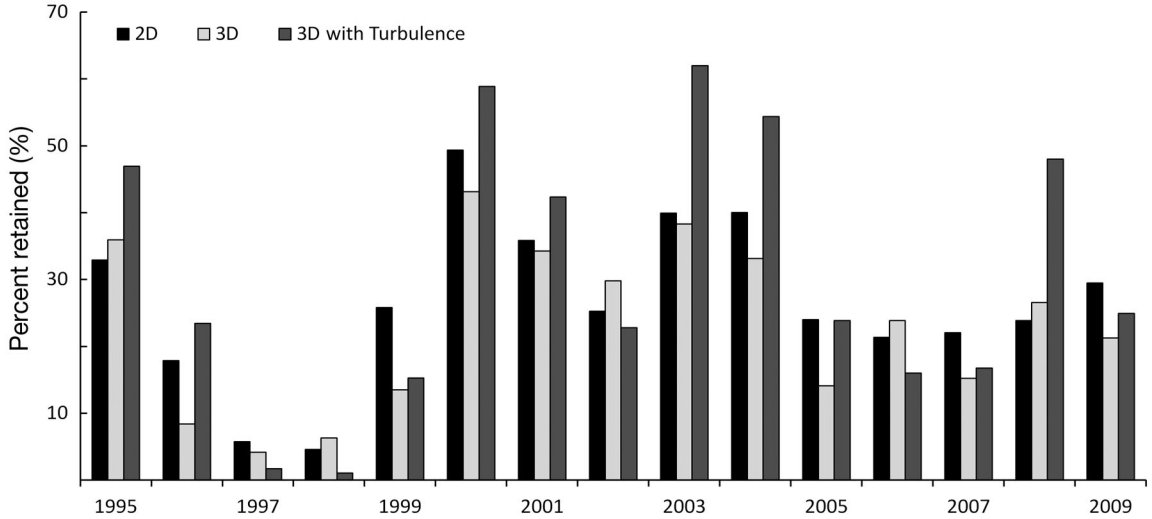

Fig. 4. Comparison of depth-averaged annual retention rates on Georges Bank after 90 d determined from GoM1-FVCOM simulations of 2-dimensional (2D) advection, 3-dimensional (3D) advection, and 3D advection with vertical turbulence

retention of individuals released at the 50 m depth ranged from 16.61% (1997) to 76.28% (2000).

3D tracking with vertical turbulence

The highly energetic environment and substantial vertical mixing of Georges Bank necessitated the inclusion of an artificial turbulence formulation to approximate non-linearity in the vertical dispersion of the system. When turbulence was included, the release depth had a negligible impact on retention compared to the 2D or 3D simulations. After 90 d, retention was lowest in 1997, ranging from 1.98% for individuals released at 1 m to 1.41% for individuals released at 50 m. Highest retention occurred in 2003, ranging from 61.26% at 1 m to 61.75% at 50 m.

Utilizing the 3D tracking with vertical turbulence, substantial interannual variability in the spatial distribution and retention of haddock eggs and larvae occurred on Georges Bank from 1995 to 2009 (Fig. 5). Highest retention within the 100 m isobath occurred in 1995, 2000, 2003, 2004 and 2008. During these years, decreased velocity of the gyre resulted in reduced transport off of Georges Bank. The reduced circulation increased transport to the shoals in these years as well, with greater than 40% occurring within the 60 m isobath (shoals) after 90 d. The depth-distribution of individuals indicated that 43 to 54% of all individuals retained on Georges Bank occurred in the upper 20 m of the water column at the end of the simulation.

Depth-dependent transport (2D/3D) in 2003 produced high retention of individuals released at the 30 and 50 m depths, with a primary loss route to the Mid-Atlantic Bight. Additional losses off the edges of the Bank were due to the 'leaky' gyre in 2003 (Fig. S1 in the Supplement at www.int-res.com/articles/suppl/m487p201_supp.pdf). With vertical turbulence, a greater number of individuals are recirculated around the bank and advected toward the shoals. Lowest retention occurred in 1997, with less than 2% of individuals retained on Georges Bank. Spawning at 50 m and persistence in water 50 m or deeper increased the potential for individuals to be retained (Fig. S2 in the Supplement).

Local and remote forcing

The IBM was updated with GoM3-FVCOM physical forcing for 1997 and 1998 to provide a comparison of the contribution of local and remote forcing on retention. Both years produced low retention estimates with GoM1-FVCOM, which increased with the addition of remote forcing. Retention from the 3D tracking with vertical turbulence simulations increased from 1.72 to 15.45% for 1997 (Fig. S3 in the Supplement), while retention in 1998 increased from 1.08% with GoM1-FVCOM to over 31.02% with GoM3-FVCOM (Fig. 6). Greater retention in 1998 with GoM3-FVCOM physical forcing occurred at all depths as a result of changes in current direction and speed compared to GoM1-FVCOM (Fig. S4 in the Supplement).

Comparison to recruitment

Increased recruitment success appeared weakly related to increased retention over the period 1995 to 2009 (Table 1). The 2003 recruitment event for Georges Bank haddock exhibited the highest recruitment success and model retention rates. Although retention in 2003 exceeded all other years in this study, comparable estimates were obtained for 2000 and 2004, which did not exhibit comparably large recruitment events. The 4 yr with highest retention were 2003, 2000, 2004, and 2008 (61.97, 58.89, 54.37, and 47.99%, respectively), while the highest recruitment success occurred in 2003, 2000, 1998, and 1997 (3.46, 1.23, 0.97, and 0.54, respectively). The 2 yr with highest recruitment success also exhibited high model retention, but there is a disconnection between retention rate and recruitment success in most years.

DISCUSSION

IBMs of haddock larvae on Georges Bank have not reexamined the impact of currents and advection on the retention of individuals since the study of Werner et al. (1993), even though substantial progress in circulation models has occurred. The general pattern of increased retention with increasing depth established by Werner et al. (1993) was reproduced in the present study with both the GoM1-FVCOM and GoM3-FVCOM physical models. Although their results indicate that a directional swimming capability significantly enhanced shoalward displacement of larvae, the model-predicted circulation processes on Georges Bank produced a similar response for passive larvae, which varied substantially between years (Fig. 5).

The use of a turbulent formulation has become standard practice for IBMs simulating foraging of fish larvae (see Werner et al. 1996, 2001, Vikebo et al.

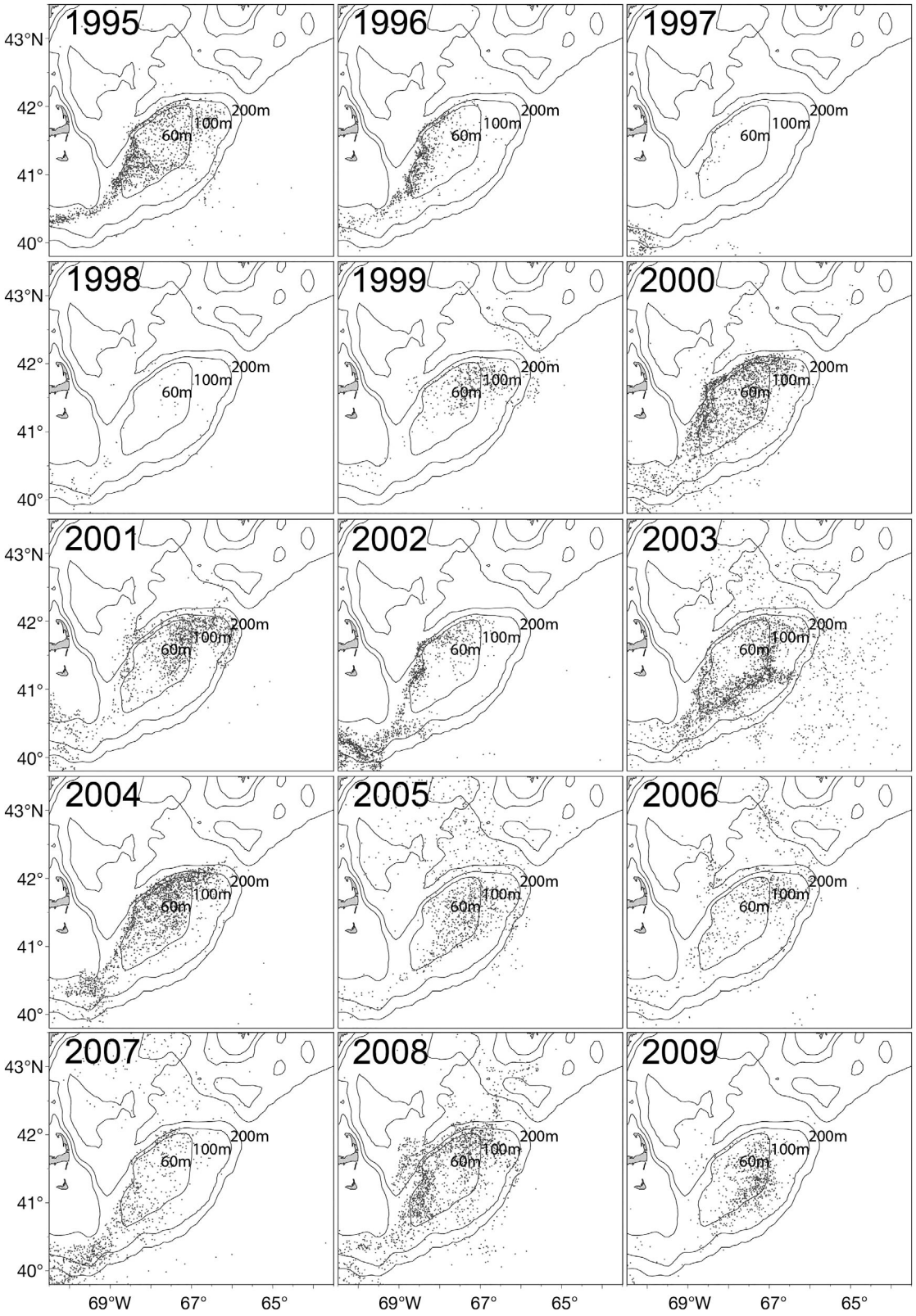

Fig. 5. Simulated depth-averaged distribution of particles 90 d after release during March on the Northeast Peak of Georges Bank, from 1995 through 2009, with GoM1-FVCOM physical forcing. Slower gyre circulation in 1995, 2000, 2003, and 2004 results in increased particle retention on Georges Bank and settlement to the shoals

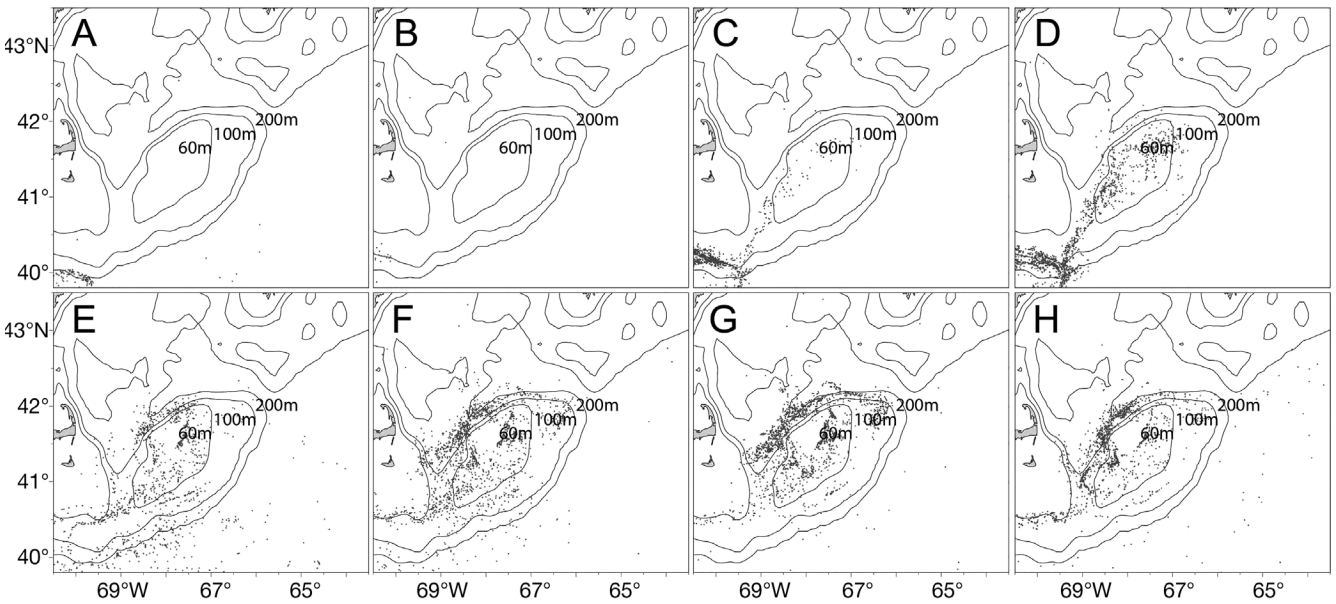

Fig. 6. Comparison of the retention of haddock larvae on Georges Bank in 1998 after 90 d, with (A–D) local forcing (GoM1-FVCOM) and (E–H) combined local and remote forcing (GoM3-FVCOM) at (A,E) 1 m, (B,F) 10 m, (C,G) 30 m, and (D,H) 50 m release depths simulated with vertical turbulence

Table 1. Comparison of age-1 recruitment success of the Georges Bank haddock stock with model-generated retention rate (%) estimates for 1995 through 2009. Highest recruitment success and retention occurred in 2003

	Retention rates (%)	Recruitment success
1995	46.92	0.47
1996	23.45	0.33
1997	15.45	0.54
1998	31.02	0.97
1999	15.24	0.20
2000	58.89	1.23
2001	42.36	0.06
2002	22.77	0.03
2003	61.97	3.46
2004	54.37	0.07
2005	23.86	0.23
2006	16.01	0.03
2007	16.76	0.04
2008	47.99	0.02
2009	24.91	0.04

2005, Kristiansen et al. 2007), but the impact of vertical diffusion on depth-dependent transport has not been analyzed in detail for Georges Bank, where displacement may be out of the control of small, pelagic organisms. The potential for buoyancy and vertical behavior to alter the vertical displacement of individuals on Georges Bank was not included in this study and requires additional investigation.

Anatomy of high versus low retention years

The 3 general pathways for the transport of larvae around Georges Bank consist of transport from the Northeast Peak: (1) recirculated around the Bank, (2) advected over the Great South Channel and onto the Mid-Atlantic Bight, or (3) advected into the North Atlantic or interior Gulf of Maine region due to a 'leaky' gyre. Interannual variability in the circulation of the Gulf of Maine-Georges Bank region caused retention rates and distributions to differ substantially between years, with patterns common to high and low retention years emerging. One year of high (2003) and low (1997) retention are compared here.

The disparity in retention between 1997 and 2003 is a result of the advective dynamics in the environment. The physical processes of 1997 and 2003 differed substantially in circulation patterns and velocity, frontal system dynamics, and stratification. In 1997, surface currents exhibited increased velocities recirculating around the gyre at the shelf break and southwest over the Great South Channel (Fig. 7A–C). Currents on the southwest of the gyre were insufficient to recirculate eggs and larvae around Georges Bank, resulting in increased advective losses. In comparison, the surface currents in 2003 were reduced, decreasing the transport speed of individuals around the gyre (Fig. 7D–F). The slow meandering of the current reduced advective losses to the Mid-Atlantic Bight, and increased transport to the shoals.

Tidal-mixing and shelf-break fronts serve as barriers, entraining eggs and larvae within the Georges Bank gyre and reducing advective losses, but vary in intensity and location on seasonal and interannual scales (Townsend & Pettigrew 1996, Chen et al. 2003). The gyre functions as a corral to retain individuals on Georges Bank in most years, but variability in water mass density, current speed, and wind intensity impact the dynamics of the shelf-break and tidal-mixing fronts.

Spatially and temporally reduced intensity of the fronts around Georges Bank produces a 'leaky' gyre with substantial losses, caused by currents and wind events. In 1997, the frontal dynamics exhibited extensive spatial and temporal distributions around Georges Bank, creating a persistent horseshoe-shaped barrier open to the southwest (Fig. 8). The fronts corralled individuals within the gyre, limiting losses off the edges; however, reduced frontal distribution and intensity at the Great South Channel enabled advection of larvae onto the Mid-Atlantic Bight. Diminished frontal dynamics in 2003 created a 'leaky' gyre, with losses off the edges of Georges Bank to the North Atlantic and interior Gulf of Maine, but increased intensity of the fronts in the Great South Channel provided greater recirculation than in 1997.

Variability in the fronts between years is directly impacted by gyre circulation. Current speed and direction on Georges Bank are influenced by winds, runoff, and flow from the Arctic, but locally the clockwise gyre around Georges Bank is enhanced by stratification and tidal rectification (Loder & Wright 1985, Chen et al. 1995). Onset and intensification of stratification in 1997 and 2003 differed substantially (Fig. 9). In 1997 stratification developed by May, intensifying gyre circulation; while in 2003 stratification was delayed until June. Increased intensities of the gyre velocities, tidal rectification, and tidal-mixing fronts in 1997 generated a pathway to quickly transport individuals onto the Mid-Atlantic Bight. Slower currents, increased frontal formation in the Great South Channel, and delayed onset of stratification resulted in a meandering, leaky gyre with increased retention of larval haddock on Georges Bank during the spring of 2003.

The inability of the retention estimates to reflect large recruitment events can be attributed to the dynamic nature of recruitment. Retention estimates in 2000 and 2003 were the highest obtained from the

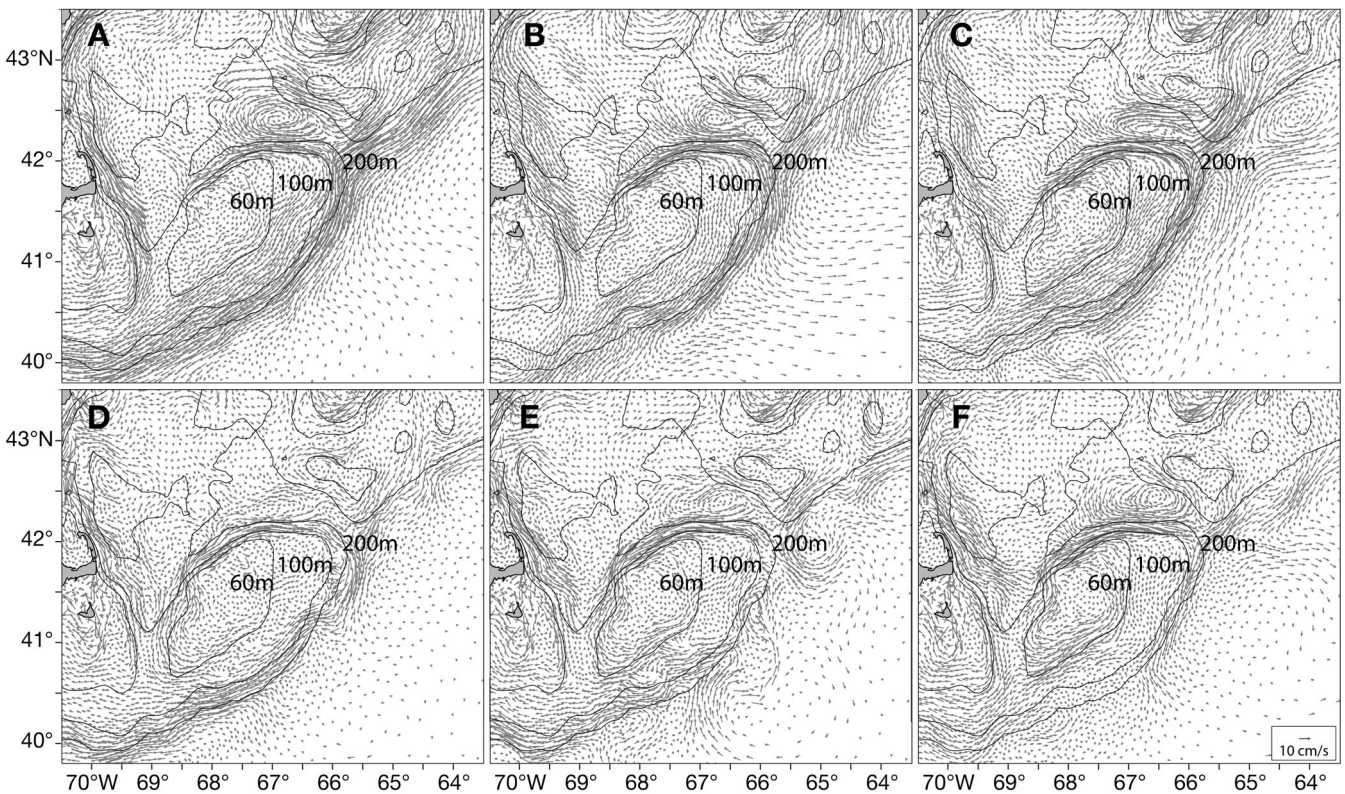

Fig. 7. Comparison of monthly-averaged surface currents on Georges Bank in (A–C) 1997 and (D–F) 2003 in (A,D) April, (B,E) May, and (C,F) June with GoM1-FVCOM physical forcing

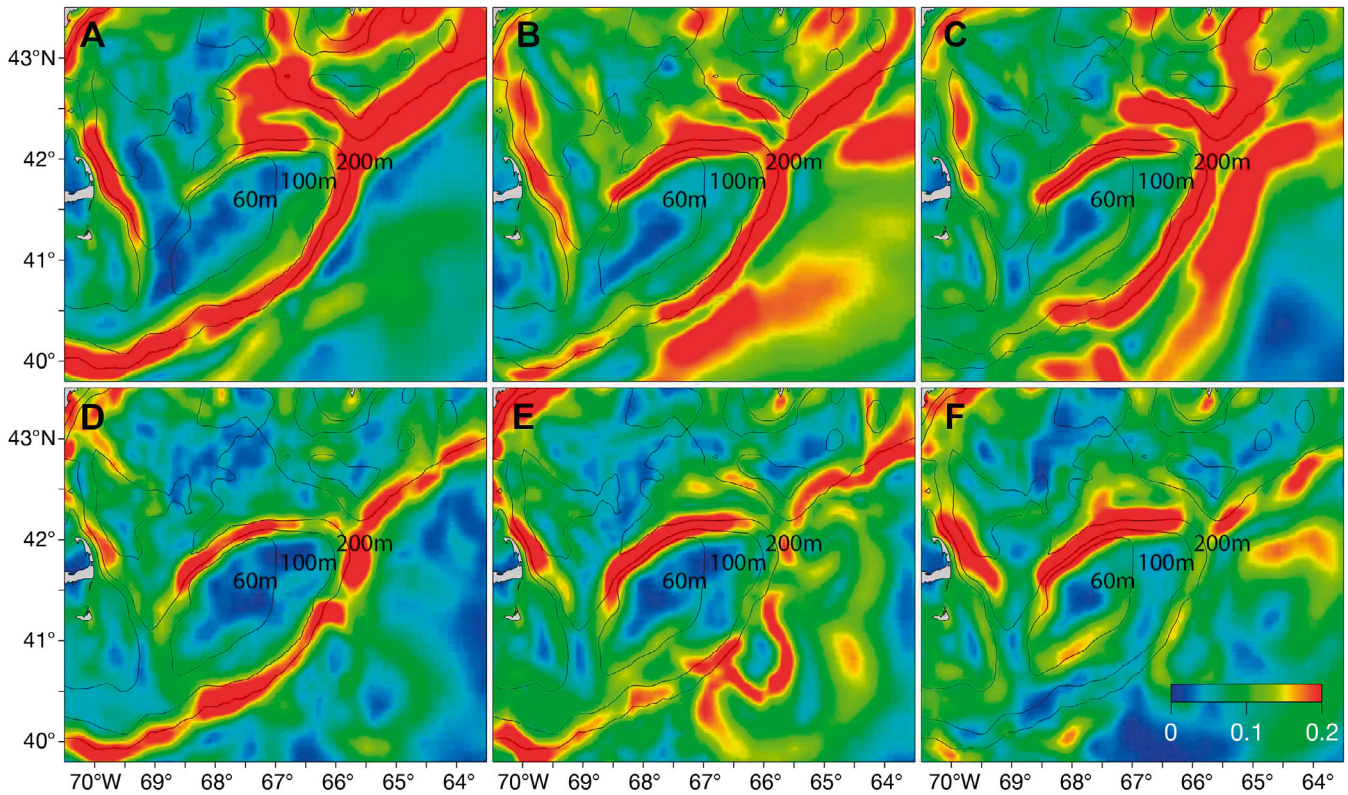

Fig. 8. Comparison of monthly-averaged frontal systems on Georges Bank in (A–C) 1997 and (D–F) 2003, in (A,D) April, (B,E) May, and (C,F) June, with GoM1-FVCOM physical forcing. Frontal systems are determined as the ratio (color scale) of shear dispersion in the surface layer and bottom layer of the circulation model

simulations and coincided with the 2 highest recruitment success values. Retention in 2004 was only 4.52% lower than in 2000, but had low recruitment success. The larger recruitment events may be attributed in part to circulation patterns allowing the larvae and their prey to remain on Georges Bank, but reduced predation or enhanced foraging and growth may provide the key mechanism to understanding survival rates of anomalously large events.

From spawning until juvenile settlement, haddock on Georges Bank experience a highly dynamic environment with limited control over dispersal or transport to nursery areas (Lough & Bolz 1989). The primary factor influencing retention was the circulation speed of the gyre. Retention was low in years with high flow rates throughout the Gulf of Maine and around Georges Bank, increasing as circulation intensity decreased. Inflow over the Scotian Shelf and slope increased flow rates throughout the coastal Gulf of Maine and intensified recirculation around Georges Bank. The dominance of large-scale processes persists over the 15 yr period, with tidal interaction, stratification, and tidal rectification further altering the intensity of the gyre. A combination of circulation, vertical mixing, and the onset of stratification created an 'optimal environmental window' (Cury & Roy 1989) for retention, with the timing and duration highly variable between years.

Influence of remote forcing

The flow fields generated by the GoM1-FVCOM for 1998 do not accurately reflect observations from the region. The lack of association between our retention estimates and haddock recruitment in this year is consistent with results for a lower trophic level from a food web model by Tian et al. (unpubl.), who reported that the model-predicted chlorophyll *a* concentration showed a significant bias to observed values on Georges Bank.

The GoM1-FVCOM is an early version of FVCOM for the Gulf of Maine, which did not include transport input from the upstream shelf and slope regions connected to the Labrador Sea and Arctic Ocean. The Gulf of Maine exhibited a large salinity anomaly

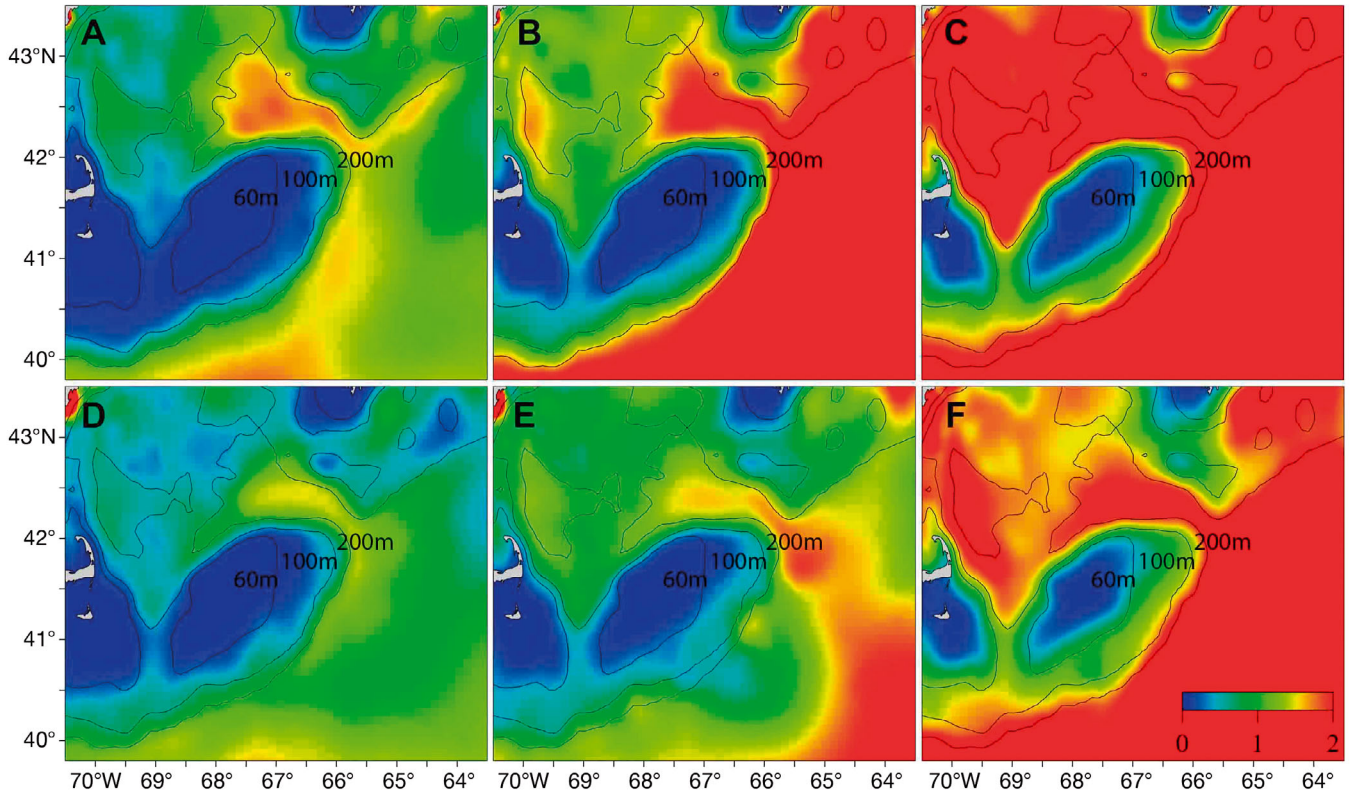

Fig. 9. Comparison of monthly-averaged stratification on Georges Bank in (A–C) 1997 and (D–F) 2003, in (A,D) April, (B,E) May, and (C,F) June, with GoM1-FVCOM physical forcing. Stratification is determined as the ratio (color scale) of water density in the sur-face layer and bottom layer of the circulation model

in 1998, with significant influence by water transport from the upstream region. Failure of the GoM1-FVCOM to produce a retention estimate comparable to recruitment in 1998 was assumed to be due to the exclusion of remote forcing. The GoM1-FVCOM circulation exhibited strong currents flowing from the northeast, enhancing the gyre around the bank and flowing over the Great South Channel, while the GoM3-FVCOM circulation exhibited decreased flow over the Scotian Shelf, reduced current speed over the Northeast Channel, and increased recirculation of the gyre around the shoal region of Georges Bank (Fig. S4 in the Supplement). We hypothesized that the low retention estimate for 1997 would not increase substantially with the addition of remote forcing, as recruitment estimates for that year were the lowest of the study period (NFSC 2012). It was assumed that the GoM1-FVCOM circulation accurately represented the dynamics for 1997, while remote forcing was inaccurately represented for 1998.

The low retention estimates obtained for 1997 and 1998 with the GoM1-FVCOM were increased when the GoM3-FVCOM forcing was implemented (Figs. S1 & S3 in the Supplement). The influence of remote forcing on transport to the shoals of Georges Bank appears to vary by year, increasing by 13.73% in 1997 and 29.94% in 1998. Interannual variability in the model occurs through 2 primary components: (1) local (winds, precipitation/evaporation, heat flux, freshwater discharge) and (2) remote (inflow from the boundaries). GoM1-FVCOM includes local forcing and limited remote forcing over the Scotian Shelf, but lacks flow over the slope. The increased retention estimates for both 1997 and 1998 indicate that inclusion of remote forcing in the Gulf of Maine is necessary for interpreting transport-retention dynamics, with slope water interaction essential in some years. The dynamic nature of remote forcing may have a positive effect on haddock retention, but further study is necessary to determine if this trend persists between additional years. Circulation models that rely primarily on local forcing may neglect important sources of variability for the Gulf of Maine-Georges Bank region, making them insufficient for studies involving large-scale dynamics such as climate change.

CONCLUSIONS

The retention of a cohort is altered by dynamic interactions with the physical environment on multiple spatial and temporal scales, with eggs and larvae subjected to highly variable winds, currents, temperatures, and resulting transport velocities. Individuals residing lower in the water column, where the influence of wind-driven transport declines, were more likely to be retained on Georges Bank. However, the depth of spawning does not have a substantial influence on vertical distribution over the entire pelagic duration, when individuals encounter intense vertical mixing on Georges Bank. Development of swimming behaviors by larvae over ontogeny may not be necessary for substantial shoalward transport in all years, but provides an essential mechanism when strong off-bank transport exists in the upper water column.

In all years the majority of advective losses from the nursery area occurred over the Great South Channel, with retention dependent upon recirculation around the southern flank of Georges Bank. The intensity and distribution of the tidal-mixing and shelf-break fronts comprised the primary regulating factor for retention. Increased retention occurred in years when the fronts formed earlier in the Great South Channel and recirculating currents persisted on the southern flank. Greater advection off-bank was predominant when fronts were absent or minimal in the Great South Channel and strong advective currents off of the southern flank occurred.

Inflow of colder, fresher waters from the Arctic over the Scotian Shelf and slope influence current velocity and water mass density in the Gulf of Maine, directly impacting the onset of stratification and formation of frontal systems around Georges Bank. Circulation models capable of resolving time-varying remote forcing in the Gulf of Maine region are essential for studies of transport-retention dynamics on Georges Bank and should be considered for future studies involving IBMs.

Acknowledgements. This research is supported by the U.S. GLOBEC Northwest Atlantic/Georges Bank Program NSF (OCE-0234545, 0227679, 0606928, 0726851 and 0814505. The GoM3-FVCOM product was built with support from the NOAA NERACOOS and Massachusetts Ocean Partnership (MOP) (renamed SeaPlan in 2012) programs. C.C. was also supported by the Shanghai Ocean University International Cooperation Program (No. A-2302-11-0003), the Program of Science and Technology Commission of Shanghai Municipality (No. 09320503700) and the Leading Academic Discipline Project of Shanghai Municipal Education Commission (Project number J50702). The authors thank Rucheng Tian and Pengfei Xue for their assistance in developing the IBM; and also Brian Rothschild, Steven X. Cadrin, Jon Hare, and Rubao Ji for their valuable comments and suggestions throughout this project.

LITERATURE CITED

Auditore PJ, Lough RG, Broughton EA (1994) A review of the comparative development of Atlantic cod (*Gadus morhua*) and haddock (*Melanogrammus aeglefinus*) based on an illustrated series of larvae and juveniles from Georges Bank. J Northwest Atl Fish Sci 20:7–18

Bartsch J, Coombs SH (2001) An individual-based growth and transport model of the early life history stages of mackerel (*Scomber scombrus*) in the eastern North Atlantic. Ecol Model 138:127–141

Bartsch J, Coombs SH (2004) An individual-based model of the early life history of mackerel (*Scomber scombrus*) in the eastern North Atlantic, simulating transport, growth and mortality. Fish Oceanogr 13:365–379

Beardsley RC, Lentz SJ, Weller RA, Limeburner R, Irish JD, Edson JB (2003) Surface forcing on the southern flank of Georges Bank, February–August 1995. J Geophys Res 108:8007, doi:10.1029/2002JC001359

Beyer JE (1989) Recruitment stability and survival — simple size-specific theory with examples from the early life dynamics of marine fish. Dana 7:45–47

Brickman D (2003) Controls on the distribution of Browns Bank juvenile haddock. Mar Ecol Prog Ser 263:235–246

Brickman D, Frank K (2000) Modelling the dispersal and mortality of Browns Bank egg and larval haddock (*Melanogrammus aeglefinus*). Can J Fish Aquat Sci 57: 2519–2535

Brink KH, Chapman DC, Halliwell GR Jr (1987) A stochastic model for wind-driven currents over the continental shelf. J Geophys Res 92:1783–1797, doi:10.1029/JC092iC02p01783

Brodziak J, Traver M, Col L, Sutherland S (2006) Stock assessment of Georges Bank haddock, 1931–2004. Northeast Fisheries Science Center, Ref Doc 06-11. NEFSC, Woods Hole, MA

Chapman DC, Beardsley RC (1989) On the origin of shelf water in the Middle Atlantic Bight. J Phys Oceanogr 19: 384–391

Chase J (1955) Winds and temperatures in relation to the brood-strength of Georges Bank haddock. J Cons Int Explor Mer 21:17–24

Chen C, Beardsley RC, Limeburner D (1995) A numerical study of stratified tidal rectification over finite-amplitude banks. II. Georges Bank. J Phys Oceanogr 25:2111–2128

Chen C, Beardsley RC, Franks PJS (2001) A 3-D prognostic model study of the ecosystem over Georges Bank and adjacent coastal regions. I. Physical model. Deep-Sea Res 48:419–456

Chen C, Schlitz R, Lough C, Smith K, Beardsley R, Manning J (2003) Wind-induced cross-frontal water transport on the southern flank of Georges Bank: a physical mechanism for the cross-frontal fish larval transport in early summer. J Geophys Res 108:8011, doi:10.1029/2002JC001358

Chen C, Beardsley RC, Cowles GW (2006) An unstructured-grid, Finite-Volume Coastal Ocean Model (FVCOM) system. Oceanography 19:78–89

Chen C, Huang H, Beardsley RC, Liu H, Xu Q, Cowles GW (2007) A finite volume numerical approach for coastal ocean circulation studies: comparisons with finite difference models. J Geophys Res 112:C03018, doi:10.1029/2006JC003485

Chen C, Haung H, Beardsley RC, Xu Q and others (2011) Tidal dynamics in the Gulf of Maine and New England Shelf: an application of FVCOM. J Geophys Res 116: C12010, doi:10.1029/2011JC007054

Churchill JH, Runge J, Chen C (2011) Processes controlling retention of spring-spawned Atlantic cod (G*adus morhua*) in the western Gulf of Maine and their relationship to an index of recruitment success. Fish Oceanogr 20:32–46

Colton JB Jr, Temple RF (1961) The enigma of Georges Bank spawning. Limnol Oceanogr 6:280–291

Cury P, Roy C (1989) Optimal environmental window and pelagic fish recruitment success in upwelling areas. Can J Fish Aquat Sci 46:670–680

Cushing DH (1974) The possible density-dependence of larval mortality and adult mortality in fishes. In: Blaxter JHS (ed) The early life history of fish. Springer-Verlag, Berlin, p 103–111

Drinkwater KF, Gilbert D (2004) Hydrographic variability in the waters of the Gulf of St. Lawrence, the Scotian Shelf and the Eastern Gulf of Maine (NAFO Subarea 4) during 1991–2000. J Northwest Atl Fish Sci 34:85–101

Flierl GR, Wroblewski JS (1985) The possible influence of warm core Gulf Stream rings upon shelf water larval fish distribution. Fish Bull 83:313–330

Franks PJS, Chen C (1996) Plankton production in tidal fronts: a model of Georges Bank in summer. J Mar Res 54:631–651

Grimm V, Berger U, Bastiansen F, Eliassen S and others (2006) A standard protocol for describing individual-based and agent-based models. Ecol Model 198:115–126

Hardy JD (1978) Development of fishes of the Mid-Atlantic Bight: an atlas of egg, larval and juvenile stages. Vol. 2: Anguillidae through Syngnathidae. US Fish Wildl Serv Biol Serv Program FWS/OBS-78/12

Hjort J (1914) Fluctuations in the great fisheries of northern Europe viewed in the light of biological research. Rapp Cons Int Explor Mer 20:1–228

Hopkins TS, Raman S (1987) Atmospheric variables and patterns. In: Backus RH (ed) Georges Bank. MIT Press, Cambridge, MA, p 66–73

Horne EPW, Loder JW, Harrison WG, Mohn R, Lewis MR, Irwin B, Platt T (1989) Nitrate supply and demand at the Georges Bank tidal front. Sci Mar 53:145–158

Hu S (2009) Variability of physical forcing and its impacts on nutrient supplies and fall phytoplankton blooms in the Gulf of Maine-Georges Bank region. PhD dissertation, University of Massachusetts, North Dartmouth, MA

Hughes TP, Bellwood DR, Connolly SR (2002) Biodiversity hotspots, centres of endemicity, and the conservation of coral reefs. Ecol Lett 5:775–784

Kristiansen T, Fiksen O, Folkvord A (2007) Modelling feeding, growth, and habitat selection in larval Atlantic cod (*Gadus morhua*): observations and model predictions in a macrocosm environment. Can J Fish Aquat Sci 64: 136–151

Lasker R (1975) Field criteria for survival of anchovy larvae: the relation between inshore chlorophyll maximum layers and successful first feeding. Fish Bull 73:453–462

Limeburner R, Beardsley RC (1996) Near-surface recirculation over Georges Bank. Deep-Sea Res II 43:1547–1574

Loder J (1980) Topographic rectification of tidal currents on the sides of Georges Bank. J Phys Oceanogr 10:1399–1416

Loder JW, Wright DG (1985) Tidal rectification and frontal circulation on the sides of Georges Bank. J Mar Res 43: 581–604

Lough RG, Bolz GR (1989) The movement of cod and haddock larvae onto the shoals of Georges Bank. J Fish Biol 35(Suppl A):71–79

Lough RG, Smith WG, Werner FE, Loder JW and others (1994) Influence of wind-driven advection on the interannual variability in cod egg and larval distributions on Georges Bank: 1982 vs 1985. ICES Mar Sci Symp 198: 356–378

Lough RG, Hannah CG, Berrien P, Brickman D, Loder JW, Quinlan JA (2006) Spawning pattern variability and its effect on retention, larval growth and recruitment in Georges Bank cod and haddock. Mar Ecol Prog Ser 310: 193–212

Mellor GL, Yamada T (1982) Development of a turbulence closure model for geophysical fluid problems. Rev Geophys 20:851–875, doi:10.1029/RG020i004p00851

Miller JE (1946) Cyclogenesis in the Atlantic coastal region of the United States. J Atmos Sci 2:31–44

Mountain D, Green J, Sibunka J, Johnson D (2008) Growth and mortality of Atlantic cod *Gadus morhua* and haddock *Melanogrammus aeglefinus* eggs and larvae on Georges Bank, 1995 to 1999. Mar Ecol Prog Ser 353:225–242

NFSC (Northeast Fisheries Science Center) (2012) Assessment or data updates of 13 Northeast groundfish stocks through 2010. NFSC Ref Doc. 12-06

O'Reilly JE, Evans-Zetlin CE, Busch DA (1987) Primary production. In: Backus RH (ed) Georges Bank. MIT Press, Cambridge, MA

Page FH, Frank KT (1989) Spawning time and egg stage duration in Northwest Atlantic haddock (*Melanogrammus aeglefinus*) stocks with emphasis on Georges and Browns Bank. Can J Fish Aquat Sci 46(Suppl. 1):68–81

Page FH, Frank KT, Thompson KR (1989) Stage dependent vertical distribution of haddock (*Melanogrammus aeglefinus*) eggs in a stratified water column: observations and model. Can J Fish Aquat Sci 46(Suppl. 1):55–67

Polacheck T, Mountain D, McMillan D, Smith W, Berrien P (1992) Recruitment of the 1987 year class of Georges Bank haddock (*Melanogrammus aeglefinus*): the influence of unusual larval transport. Can J Fish Aquat Sci 49: 484–496

Reese DC, Brodeur RD (2006) Identifying and characterizing biological hotspots in the northern California Current. Deep-Sea Res II 53:291–314

Riley GA (1941) Plankton studies. III. Long Island Sound. Bull Bingham Oceanogr Collect Yale Univ 7:1–93

Rothschild BJ (1986) Dynamics of marine fish populations. Harvard University Press, Cambridge, MA

Sale P (1978) Coexistence of coral reef fishes—a lottery for living space. Environ Biol Fishes 3:85–102

Sibunka JD, Johnson DL, Berrien PL (2006) Distribution and abundance of fish eggs collected during the GLOBEC broad-scale Georges Bank surveys, 1995–1999. NOAA Tech Memo NMFS-NE-199

Smagorinsky J (1963) General circulation experiments with the primitive equations: I. The basic experiment. Mon Weather Rev 91:99–164

Smith WG, Morse WW (1985) Retention of larval haddock *Melanogrammus aeglefinus* in the Georges Bank region,

a gyre-influenced spawning area. Mar Ecol Prog Ser 24: 1–13

Smith P, Houghton RW, Fairbanks RG, Mountain DG (2001) Interannual variability of boundary fluxes and water mass properties in the Gulf of Maine and on Georges Bank. Deep-Sea Res II 48:37–70

Sun Y, Chen C, Beardsley RC, Xu Q, Qi J, Lin H (2013) Impact of current-wave interaction on storm surge simulation: a case study for Hurricane Bob. J Geophys Res Oceans 118, doi:10.1002/jgrc.20207

Tian RC, Chen C, Stokesbury KDE, Rothschild BJ and others (2009) Dispersal and settlement of sea scallop larvae spawned in the fishery closed areas on Georges Bank. ICES J Mar Sci 66:2155–2164

Townsend DW, Pettigrew NR (1996) The role of frontal currents in larval fish transport on Georges Bank. Deep-Sea Res II 43:1773–1792

Townsend DW, Pettigrew NR (1997) Nitrogen limitation of secondary production on Georges Bank. J Plankton Res 19:221–235

Valavanis VD, Dapantagakis A, Katara I, Palialexis A (2004) Critical regions: a GIS-based model of marine productivity hotspots. Aquat Sci 66:139–148

Vikebo F, Sundby S, Adlandsvik B (2005) The combined effect of transport and temperature on distribution and growth of larvae and pelagic juveniles of Arcto-Norwegian cod. ICES J Mar Sci 62:1375–1386

Visser AW (1997) Using random walk models to simulate the vertical distribution of particles in a turbulent water column. Mar Ecol Prog Ser 158:275–281

Werner FE, Page FH, Lynch DR, Loder JW and others (1993) Influences of mean advection and simple behavior on the distribution of cod and haddock early life stages on Georges Bank. Fish Oceanogr 2:43–64

Werner FE, Perry RI, Lough RG, Naimie CE (1996) Trophodynamic and advective influences on Georges Bank larval cod and haddock. Deep-Sea Res II 43:1793–1822

Werner FE, MacKenzie BR, Perry RI, Lough RG, Naimie CE, Blanton BO, Quinlan JA (2001) Larval trophodynamics, turbulence, and drift on Georges Bank: a sensitivity analysis of cod and haddock. Sci Mar 65(Suppl. 1): 99–115

Submitted: July 7, 2012; Accepted: June 28, 2013

Proofs received from author(s): July 19, 2013

Vol. 487: 217–229, 2013
doi: 10.3354/meps10201

MARINE ECOLOGY PROGRESS SERIES
Mar Ecol Prog Ser

Published July 30

Contribution to the Theme Section 'Biophysical coupling of marine hotspots'

FREE ACCESS

Winter mixed layer depth and spring bloom along the Kuroshio front: implications for the Japanese sardine stock

Haruka Nishikawa[1,4,*], Ichiro Yasuda[1], Kosei Komatsu[1], Hideharu Sasaki[2], Yoshikazu Sasai[2], Takashi Setou[3], Manabu Shimizu[3]

[1]Atmosphere and Ocean Research Institute, The University of Tokyo, 5-1-5, Kashiwanoha, Kashiwa-shi, Chiba 277-8568, Japan
[2]Japan Agency for Marine-Earth Science and Technology, 3173-25, Showa-machi, Kanazawa-ku, Yokohama 236-0001, Japan
[3]National Research Institute of Fisheries Science, Fisheries Research Agency, 2-12-4, Fukuura, Kanazawa-ku, Yokohama 236-8648, Japan
[4]*Present address:* Japan Agency for Marine-Earth Science and Technology, 3173-25, Showa-machi, Kanazawa-ku, Yokohama 236-0001, Japan

ABSTRACT: Recruitment of Japanese sardine *Sardinops melanostictus* is related to interannual variability in the winter mixed layer depth (MLD) near the Kuroshio axis (line of maximum current), possible because MLD may influence the feeding environment of sardine larvae through phytoplankton productivity. However, a relationship between the winter MLD and phytoplankton productivity has not been shown. Particle release experiments with quasi-observed current fields from ocean reanalysis products and satellite-observed phytoplankton (chlorophyll *a*) density from 1998 to 2006 showed that deeper waters of the winter mixed layer flowing 0° to 0.5° north of the Kuroshio axis led to a greater bloom in the subsequent spring, although such a relationship was not detected south of the Kuroshio axis. By using the output of a 3-dimensional, high-resolution lower trophic level ecosystem model that reproduced the MLD–phytoplankton relationship, we found that entrainment of deeper nutrient-rich subsurface water leads to abundant nutrients in the early spring and enhances the subsequent spring bloom along the northern side of the Kuroshio axis. On the southern side, where mode water develops in winter, the deeper winter mixed layer does not necessarily contain higher nutrient contents, because nutrient vertical profiles often have inversions. These results support the hypothesis that sardine larvae that are distributed in the deeper winter mixed layer north of the Kuroshio axis (called the Kuroshio frontal zone) encounter a higher phytoplankton density, which yields favorable feeding conditions, resulting in recruitment success.

KEY WORDS: Mixed layer depth · Bloom · Kuroshio · Ecosystem model · Japanese sardine

INTRODUCTION

Japanese sardine *Sardinops melanostictus* are known to undergo drastic and multi-decadal stock fluctuations (e.g. Ito 1961, Yasuda et al. 1999). The largest landing of sardine in Japan was 4.49 million tons in 1988; in contrast, the catch in recent years has been <1% of this amount. Watanabe et al. (1995) attributed this drastic fluctuation in stock to large recruitment variability, especially with regards to the survival rate from the end of first-feeding larvae to age-1.

Recruitment variability has been attributed to differences in the physical environment and associated ecosystem in the Kuroshio system, where sardines spawn and their larvae are distributed. Noto & Yasuda (1999, 2003) reported a relationship between sardine mortality and winter/spring sea-surface

*Email: harukan@jamstec.go.jp

temperature (SST) in the Kuroshio Extension (KE) and its southern recirculation area (KESA; 30° to 35° N, 145° to 180° E). Takasuka et al. (2007) reported an optimal temperature of 16.2°C for the growth rates of sardine larvae, suggesting the importance of environmental temperature. Nishikawa & Yasuda (2008) reported significant negative correlations between mortality and the winter mixed layer depth (MLD) in regions of the KE and suggested the importance of spring feeding conditions, which may be controlled by the wintertime entrainment of subsurface nutrients. Takahashi et al. (2008, 2009) reported that interannual variations in the growth rates of early stage juveniles corresponded to recruitment variability in the low-stock period of 1996 to 2003.

More recently, Nishikawa et al. (2011) pointed out that sardine recruitment variability is related to the winter MLD and winter/spring SST near the Kuroshio axis ('axis' being defined as the positions representing the maximum current speed at each degree longitude), where sardine eggs were mainly spawned in the high-stock period of 1980 to 1994. Winter SST and MLD variability near the Kuroshio axis are caused by variability in the velocity of the Kuroshio jet and local atmospheric cooling, and are well correlated with SST in the KESA (Nishikawa & Yasuda 2011). By performing numerical analyses of egg release based on spawning data from observations, Nishikawa et al. (2013) confirmed the dense distribution of sardine larvae near the Kuroshio axis and suggested that the environmental factors and transport routes critical to recruitment variability are the winter MLD and winter/spring SST from 0.5° south to 1° north of the Kuroshio axis, in both the high- and low-stock periods from 1978 to 2004. The winter MLD–recruitment relationship near the Kuroshio axis (Nishikawa & Yasuda 2008, Nishikawa et al. 2011, 2013) needs further study because no evidence exists to show that the relationship between the winter MLD and phytoplankton density influences the feeding environment of sardine larvae. Nishikawa & Yasuda (2008) have, however, hypothesized, based on a simplified ecosystem model, that the spring bloom may be enhanced by entrainment of deeper subsurface water.

Nutrient, phytoplankton and zooplankton distributions and hydrography are considerably different north and south of the Kuroshio axis (Kawai 1972, Nakata et al. 1995, 2004, Sukigara et al. 2011). For example, satellite data show a high density of chlorophyll *a* (chl *a*) along the northern side of the Kuroshio axis (Fig. 1), indicating its potential importance for sardine recruitment. On the northern side (or coastal side south of Japan) of the Kuroshio axis, the pycnocline and nutricline are shallow, at a depth of about 100 m, and wintertime convective mixing entrains abundant subsurface nutrients. In contrast, on the southern (offshore) side of the Kuroshio axis, the pycnocline and nutricline are much deeper, down to 400 m depth, and the vertically uniform North Pacific Subtropical Mode Water (e.g. Masuzawa 1969) is distributed here. Along the southern edge of the Kuroshio axis, a narrow band of the warmest and least dense water in the area exists (referred to as the maximum temperature band; Kawai 1972). Thus, since the hydrographic structure is more complicated on the southern side of the Kuroshio axis than on the northern side, nutrient vertical profiles may also be more complicated. With respect to the processes of nutrient supply along the Kuroshio, Chu & Kuo (2010) examined the pumping and advection of nutrients due to eddies associated with propagating Rossby waves in the KE. Yamazaki et al. (2009) suggested that enhanced vertical mixing along the Kuroshio over the Izu Ridge is a possible source of summertime nutrients in the KE.

Temporal variability in the winter/spring MLD and phytoplankton density around the Kuroshio, which we are also interested in, has previously been re-

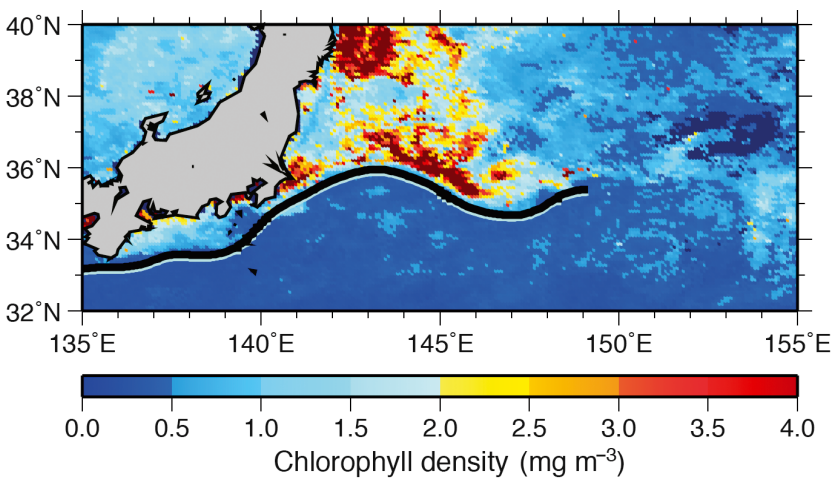

Fig. 1. Chlorophyll *a* density off the coast of Japan in April 2004 (SeaWiFS data). The black curve represents the Kuroshio axis (Marine Information Research Center 2007), based on observed sea-surface temperature (SST), sea-surface height (SSH) and surface velocity

ported for the interannual variability of the MLD in the KESA (Yasuda et al. 2000) and for the relation between the winter MLD and spring chl *a* on the southern side of the Kuroshio axis south of Japan (Limsakul et al. 2001) and in the KESA (Nishikawa & Yasuda 2008). A MLD and chl *a* time-series in the KESA has been recorded using a float that drifted in the surface mixed layer for 1.5 yr (Yasuda & Watanabe 2007). However, these studies were not sufficient to resolve the cross-frontal structure of the Kuroshio.

In the present study, we examined the relationship between the winter MLD and phytoplankton density by using hydrographic reanalysis data and satellite observations of chl *a*, and compared the winter MLD and chl *a* density in winter and spring along the transport routes of sardine eggs and larvae from the Kuroshio south of Japan in winter to the KE area. We then also performed similar MLD–phytoplankton analyses with an ecosystem model, confirming that the model captured the observed relationship between MLD and phytoplankton density. We then tried to establish the specific processes and underlying mechanisms behind the relationship by using the model's output data.

MATERIALS AND METHODS

MLD and chl *a* observations

We used chl *a* data gathered by a SeaWiFS (sea-viewing wide field-of-view sensor, NASA) satellite between 1998 and 2006 (the period when satellite-derived chl *a* data were available), to examine the relationship between winter MLD and winter/spring phytoplankton density. The data used were standard mapped image products (Level-3), with 9 km horizontal and monthly resolutions. For quasi-observational environmental data of the MLD and ocean currents, FRA-JCOPE (Miyazawa et al. 2008) velocity and temperature data were used. FRA-JCOPE is an ocean general circulation model (OGCM) based on JCOPE (Japan Coastal Ocean Predictability Experiment, operated by the Frontier Research Center for Global Change of JAMSTEC), which is operated by the Fisheries Research Agency (FRA). FRA-JCOPE assimilates satellite sea-surface height (SSH), SST and hydrographic data from the Global Temperature–Salinity Profile Program (GTSPP) and has 1/12° × 1/12° horizontal and daily resolutions. The FRA-JCOPE model output best represents conditions near Japan. We define MLD as the depth at which temperature is 0.5°C lower than at the surface.

Eddy-resolving coupled physical–biological model

To determine the underlying processes behind the MLD–phytoplankton relationship, we used the output of an eddy-resolving coupled physical–biological model (Sasai et al. 2006, 2010) for the period from 2001 to 2007. The physical model is the ocean general circulation model for the earth simulator (OFES) (Masumoto et al. 2004, Sasaki et al. 2008), which is based on the Geophysical Fluid Dynamics Laboratory's modular ocean model (MOM3) (Pacanowski & Griffies 2000). The horizontal resolution is 0.1°. There are 54 vertical levels with varying distances between the levels, from 5 m at the surface to 330 m at the maximum depth of 6065 m. After the physical fields have been spun up for 50 yr under monthly mean climatological data from NCEP/NCAR (National Centers for Atmospheric Prediction/National Center for Atmospheric Research), OFES is forced by the daily mean NCEP/NCAR reanalysis data (Kalnay et al. 1996) for 48 yr from 1950 to 1998. The last day of 1998 is used for the initial physical fields in this simulation.

The marine ecosystem model is a simple nitrogen-based NPZD (nitrogen, phytoplankton, zooplankton and detritus) pelagic model (Oschlies 2001). The evolution of any biological tracer concentration is governed by an advection–diffusion equation with source and sink terms. The source and sink terms represent the ecosystem dynamics (Sasai et al. 2006, 2010). The phytoplankton growth rate depends on the light intensity, nitrate concentration and temperature (Eppley 1972). The light intensity is given by the NCEP/NCAR shortwave radiation. The initial nitrate field is taken from the climatological dataset (WOA98). The coupled physical–biological model is forced by the daily mean surface wind stress data of Quick Scatterometer (QSCAT) and the atmospheric daily mean data (heat and salinity fluxes) of the NCEP/NCAR reanalysis data (1999 to 2007): these are initialized from a 5 yr spin up of the biological model under the monthly mean climatological forcing of NCEP, following a 98 yr integration of the physical model.

We used 3 d snapshot output of the coupled physical–biological model. The 3 d interval data were interpolated into 20 min intervals for particle tracking. The simulated phytoplankton density (mmol m^{-3}) was converted to chl *a* density using a ratio of 1.59 g chl *a* mol^{-1} nitrogen (e.g. Oschlies 2001).

In this physical–biological model, the Kuroshio path variability was not necessarily realistic, because no oceanic observational data were assimi-

lated. Since the MLD and its variability near the Kuroshio axis are strongly influenced by velocity and local atmospheric forcing (Nishikawa & Yasuda 2011), model reproduction of year-to-year MLD variability near the Kuroshio axis is not complete due to the unrealistic Kuroshio path variability in this model. This might cause the winter MLD difference between the model and observations. However, we believe that it is worthwhile to further explore the relationship between the winter MLD and spring phytoplankton in the model, because the model enables us to examine specific processes connecting winter MLD and spring phytoplankton by providing time-series data on nutrients, whereas observational field data are quite limited.

Another issue is that the phytoplankton in this model tends to be overestimated in comparison to the observed values near the Kuroshio axis. Since hydrography, nutrients and, thus, phytoplankton change considerably across the Kuroshio axis and are influenced by various complicated processes, such as horizontal and vertical advections and mixing as well as nitrate fixation, nitrification and atmospheric deposition, accurate determinations of nutrients and phytoplankton are quite difficult to achieve. Furthermore, since this global coupled physical–biological model considers each bio-geochemical parameter as spatially uniform rather than spatially variable depending on the location in the Kuroshio region (Sasai et al. 2006, 2010), it is difficult to accurately reproduce all of the variables in this complicated region.

Particle tracking experiment

We released particles to simulate sardine eggs and larvae on the FRA-JCOPE and coupled physical–biological model velocity fields. Particles were released in sardine spawning grounds in the Kuroshio, south of Japan, in the areas from 130° to 140° E and from the coast to 1.5° south of the Kuroshio axis, at 0.2° latitude and longitude intervals. Since the spawning of the Japanese sardine *Sardinops melanostictus* is greatest in February (Nishikawa et al. 2013), particles were released on 15 February in each year from 1998 to 2006 for the FRA-JCOPE and from 2001 to 2007 for the coupled physical–biological model. For the FRA-JCOPE, MLD and chl *a* were recorded along particle trajectories from Days 0 to 75. For the coupled physical–biological model, nitrate concentrations were also recorded to better understand phytoplankton variation.

Particles were released at the shallow depth of 2.5 m, because particle distribution is not sensitive to release depth (Nishikawa et al. 2013) in a range from the surface to 50 m, where sardine eggs and larvae are mainly observed (Konishi 1980). Since correlations between sardine recruitment and transport environment were found for larvae that were distributed near the Kuroshio axis and transported to the KE east of 142° E (Nishikawa et al. 2013), we selected particles that were distributed within the area from 1.5° south to 1.5° north of the Kuroshio axis and reaching east of 142° E by Day 75. These particles were divided into 2 groups (GR1 and GR2, to the north and south of the Kuroshio axis, respectively; Fig. 2) and further subdivided into 6 subgroups at 0.5° intervals (GR1a to GR1c and GR2a to GR2c; Table 1). Correlation analyses were performed among mean environmental parameters (MLD and nitrate) and chl *a*/phytoplankton density for each transport route.

Fig. 3 shows an example of particle tracking in the FRA-JCOPE case for particles along the GR1c route (Table 1) that were released on 15 February 2005 and were transported along the route 0° to 0.5° north of the Kuroshio axis and to the KE east of 142° E. We show 3 snapshots of particle locations on 15 February, 15 March and 15 April. Almost all the particles appeared in the KE east of 142° E by 15 April.

Phytoplankton and nitrate balance analysis in the ecosystem model

The temporal variation in phytoplankton density and source–sink terms in the surface mixed layer were evaluated by following particle drift in the surface current. The time change rate of vertically uni-

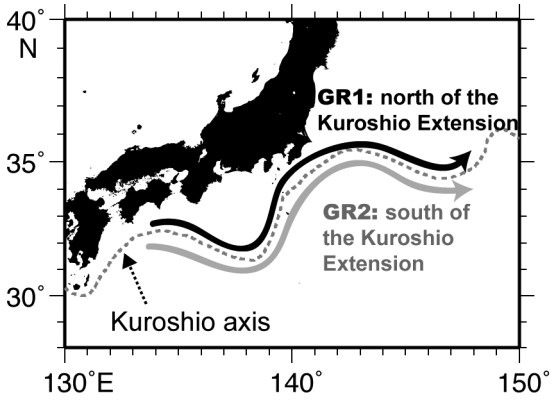

Fig. 2. Representative sardine transport routes: GR1 and GR2. Each route is further subdivided across the Kuroshio axis in 0.5° intervals of latitudinal distance relative to the Kuroshio axis

Table 1. Pearson correlations among winter (15 February to 31 March) mixed layer depth (wMLD), spring (1 to 30 April) chl *a* density (sCHL) or phytoplankton density (sPHY), winter nitrate concentration (wNTR) and winter chl *a* density (wCHL) or phytoplankton density (wPHY) for 9 yr of observed data (1998 to 2006) and for 7 yr of model data (2001 to 2007) along 6 transport routes (GR1a to GR1c and GR2a to GR2c) from 1.5° north to 1.5° south of the Kuroshio axis (at 0.5° intervals). GR1 and GR2 are north and south of the Kuroshio axis, respectively. p-values given in parentheses. See Figs. 4 & 5 for details on observed and modeled data, respectively, for routes GR1c and GR2a. $^{*}0.05 < p < 0.1$, $^{**}p \leq 0.05$

		FRA-JCOPE (1998–2006)		OFES (2001–2007)			
		wMLD/sCHL	wMLD/wCHL	wMLD/sPHY	wMLD/wNTR	wNTR/sPHY	wMLD/wPHY
GR1a	1.0–1.5°	0.22 (0.60)[a]	−0.54 (0.17)[a]	0.13 (0.78)	0.51 (0.24)	0.84 (0.02)**	−0.89 (<0.01)**
GR1b	0.5–1.0°	0.45 (0.22)	−0.33 (0.39)	0.31 (0.50)	−0.12 (0.65)	0.61 (0.15)	−0.88 (<0.01)**
GR1c	0.0–0.5°	0.67 (0.05)**	−0.19 (0.63)	0.73 (0.06)*	0.66 (0.11)	0.72 (0.07)*	0.23 (0.62)
GR2a	0.0–0.5°	−0.13 (0.75)[a]	0.21 (0.62)[a]	−0.60 (0.15)	−0.44 (0.32)	0.94 (<0.01)**	−0.77 (0.04)**
GR2b	0.5–1.0°	0.17 (0.66)	−0.38 (0.31)	−0.28 (0.54)	−0.19 (0.68)	0.98 (<0.01)**	−0.49 (0.26)
GR2c	1.0–1.5°	−0.22 (0.57)	−0.31 (0.42)	−0.54 (0.21)	−0.35 (0.44)	0.80 (0.03)**	−0.73 (0.06)*

[a]No particle was detected on the route in 2002

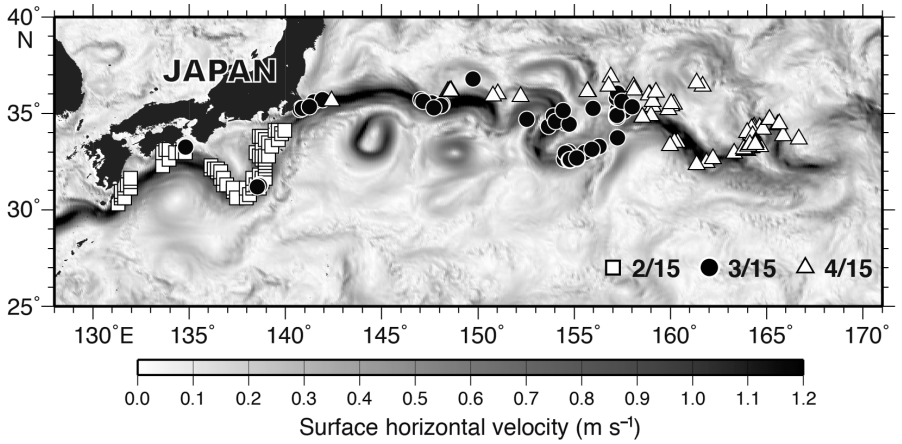

Fig. 3. Location of particles that were released on 15 February 2005 and transported along the route 0° to 0.5° north of the Kuroshio axis and to the Kuroshio Extension east of 142° E (corresponding to GR1c in Table 1) superimposed on FRA-JCOPE velocity field data for 15 April (shading). (□) Locations on 15 February (denoting starting spawning grounds along the GR1c route); (●) 15 March; and (△) on 15 April

form phytoplankton in the surface mixed layer was approximated as:

$$\frac{dP}{dt} = \text{photosynthesis–grazing–natural mortality–entrainment} \quad (1)$$

where P is the phytoplankton averaged in the mixed layer and d/dt is the Lagrangian time derivative following the particle surface velocity. The natural mortality term consists of the specific mortality (or recycling) rate (from phytoplankton to nitrate) and the quadratic mortality rate (from phytoplankton to detritus) (Sasai et al. 2006, 2010). Underestimation of primary production in the standard NPZD model is resolved by adding a rapid recycling path from simulated phytoplankton back to the nitrate compartment. To restrict the overestimation of primary production in oligotrophic regions, phytoplankton loss to the detritus compartment was changed from a linear function of phytoplankton concentration to a quadratic function (Oschlies 2001).

The temporal change of MLD-integrated nitrate per unit area is determined by the 4 following factors in the model. First is the entrainment of subsurface water with a generally higher nitrate concentration. This depends on vertical mixing and mixed layer deepening and is here referred to as 'EN'. Although entrainment decreases phytoplankton density (fourth term of right hand side in Eq. 1), due to the dilution of entrained water with less phytoplankton, entrainment increases nitrate concentration. Second is the decomposition of organic matter: detritus, zooplankton and phytoplankton. This is independent of the MLD and is referred to as 'DN'. The third factor in the model is the consumption of nitrate due to uptake during photosynthesis. The fourth factor is the loss of nitrate in the period of mixed layer shoaling, although nitrate concentration in the mixed layer is unchanged.

RESULTS

Relationship between MLD and chl *a*/phytoplankton near the Kuroshio axis

Results of the correlation analysis for winter (defined in the present study as 15 February to 31 March)

MLD, spring (1 to 30 April) chl *a*/phytoplankton density, winter nitrate concentration and winter phytoplankton density, along the 6 larval transport routes, are summarized in Table 1.

Significant positive correlation (r = 0.67, p = 0.05, n = 9) was only detected for the route 0° to 0.5° north of the Kuroshio axis (GR1c) between mean winter MLD and mean spring chl *a* (Table 1). Correlation for the transport route 0.5° to 1.0° north of the Kuroshio axis (GR1b) (r = 0.45, p = 0.22, n = 9) was positive. A scatter plot between winter MLD and spring chl *a* is depicted in Fig. 4a for the GR1c route. For the MLD of 80 to 120 m, chl *a* ranged from ~0.45 to 0.65 mg m^{-3}.

For the routes south of the Kuroshio axis, no significant correlations were detected between observed winter MLD and spring chl *a*. A scatter plot between observed winter MLD and spring chl *a* for the GR2a route (0° to 0.5° south of the Kuroshio axis) is depicted in Fig. 4c; MLD and chl *a* ranged from 120 to 140 m and 0.35 to 0.56 mg m^{-3}, respectively.

For the observed winter MLD and winter chl *a*, correlations were mostly negative, except along the GR2a route (Table 1, Fig. 4d); in years with a deeper winter mixed layer, winter chl *a* tended to be lower. The scatter plots for GR1c (Fig. 4b) indicate that winter chl *a* ranged from 0.24 to 0.31 mg m^{-3} for the winter MLD of 80 to 120 m. For GR2a (Fig. 4d), winter chl *a* ranged from 0.23 to 0.32 mg m^{-3} for the winter MLD of 120 to 140 m.

In the model, a positive correlation between winter MLD and spring phytoplankton density was detected along routes GR1b (r = 0.31, p = 0.5, n = 7) and GR1c (r = 0.73, p = 0.06, n = 7) (Table 1). For GR1c, both observations and the model indicated that spring chl *a*/phytoplankton tends to be higher in years of large winter MLD. The scatter plot for the GR1c model (Fig. 5a) indicated that, for an MLD of 60 to 110 m, phytoplankton ranged from 0.55 to 0.85 mg m^{-3}. The phytoplankton in the model was greater than that observed (Fig. 4a). In the model route GR1c, positive correlations were detected between winter MLD and winter nitrate concentration (r = 0.66, p = 0.1, n = 7; Fig. 5b) and between winter nitrate concentration and spring phytoplankton (r = 0.72, p = 0.07, n = 7; Fig. 5c).

Along the routes south of the Kuroshio axis (GR2), correlations were negative between model winter MLD and spring phytoplankton (Table 1, Fig. 5e), in contrast with the GR1c route. This is because while the spring phytoplankton depends on the winter nitrate (Fig. 5g), the deep mixed layer does not necessarily entrain more nitrate in winter (Fig. 5f). For the model relationship between winter MLD and winter phytoplankton, negative correlations were mostly significant, except for GR1c, because of light limitation due to a deeper mixed layer in winter.

Although the year of large winter MLD and high spring chl *a*/phytoplankton did not completely agree for the GR1c between observations and the model, positive correlations were detected between winter MLD and spring chl *a*/phytoplankton in both the observations (r = 0.67; Table 1) and the model (r = 0.73). The top 4 years in terms of MLD (i.e. the years with the largest MLD) were 2004, 2001, 2000 and 2005 in the observations, while the top years in the model were 2005, 2003, 2004 and 2002 (Figs. 4a & 5a). This discrepancy in MLDs between the observations and model may also have caused the spring chl *a*/phytoplankton density difference; the 4 years of greatest spring chl *a*/phytoplankton density were 2004, 2005, 2000 and 2002 in the observations,

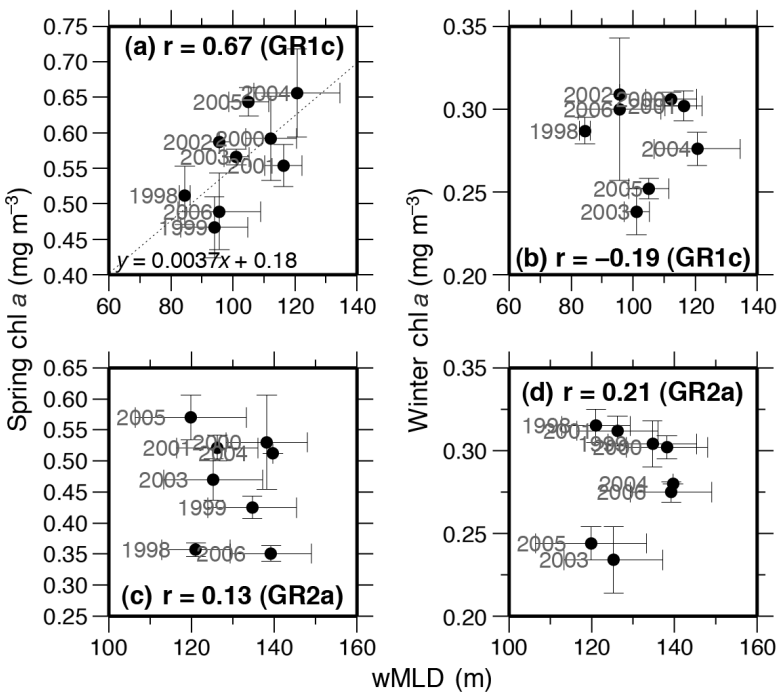

Fig. 4. Observed data (1998 to 2006) on (a) winter mixed layer depth (wMLD; m) versus spring chl *a* density (mg m^{-3}), with the regression line shown, and (b) wMLD versus winter chl *a* density, both for the GR1c route (0° to 0.5° north of the Kuroshio axis); and (c) wMLD versus spring chl *a* density and (d) wMLD versus winter chl *a* density, both for the GR2a route (0° to 0.5° south of the Kuroshio axis). Numerals denote years; error bars: 95% confidence intervals (1.96 × standard error)

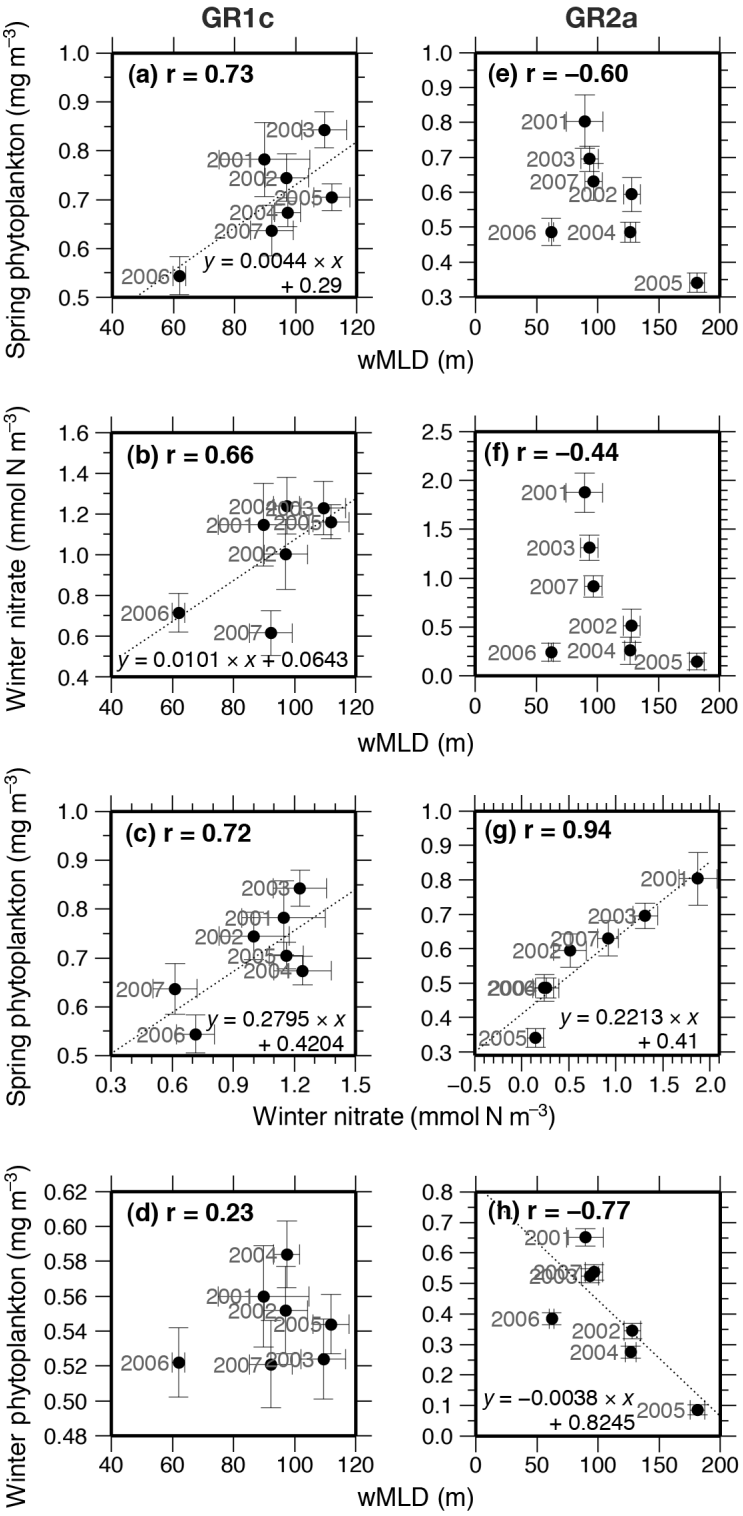

Fig. 5. Modeled data (2001 to 2007) for (a–d) the GR1c route (0° to 0.5° north of the Kuroshio axis) and (e–h) the GR2a route (0 to 0.5° south of the Kuroshio axis). (a,e) Winter mixed layer depth (wMLD; m) and spring phytoplankton (mg m^{-3}), (b,f) wMLD and winter nitrate concentration (mmol N m^{-3}), (c,g) winter nitrate and spring phytoplankton, and (d,h) wMLD and winter phytoplankton. Regression lines are displayed in Panels a–c, g and h, with correlations of >90% confidence

whereas they were 2003, 2001, 2002 and 2005 in the model.

Processes north of the Kuroshio axis

Here we examined time-series of physical and biological properties to better understand the processes behind the relationships among the MLD, nitrate and phytoplankton along the GR1c route, with a positive correlation between winter MLD and spring chl *a*/phytoplankton (Figs. 4a & 5a). We examined the 2 contrasting years of 2005 and 2006. The year 2005 represented a large winter MLD and a high spring phytoplankton density, and the year 2006 showed the opposite trend.

Winter MLDs averaged from 15 February to 31 March were 112.5 m in 2005 and 62.1 m in 2006 (Fig. 6a). Spring (from 1 to 30 April) MLDs were 76.2 m in 2005 and 85.2 m in 2006. Fig. 6b shows time-series of phytoplankton averaged for the mixed layer.

While spring-averaged phytoplankton in 2005 (0.71 mg m^{-3}) was higher than that in 2006 (0.54 mg m^{-3}) (Fig. 6b), the phytoplankton values on 12 March in 2005 and 2006 were almost the same—0.46 mg m^{-3} in 2005 and 0.48 mg m^{-3} in 2006. The increase of phytoplankton due to photosynthesis from 12 March to 30 April (time-integration of the first term on the right hand side of Eq. 1) was estimated at 8.02 mg m^{-3} in 2005 and 5.81 mg m^{-3} in 2006. The decrease in phytoplankton from 12 March to 30 April by grazing was 4.63 mg m^{-3} in 2005 and 3.35 mg m^{-3} in 2006, the decrease by natural mortality was 2.30 and 1.76 mg m^{-3}, and the decrease by entrainment was 0.96 and 0.69 mg m^{-3}, respectively. Because all terms on the right hand side of Eq. 1 in Eq. (1) in 2005 were higher than those in 2006, photosynthesis was the only component that yielded a higher phytoplankton density in 2005.

Photosynthesis in the mixed layer depends on nitrate concentration and light intensity in the mixed layer. Because spring mean MLDs were almost the same in 2005 and 2006 (76.2 m in 2005 and 85.2 m in 2006), spring MLD was not a primary cause of the photosynthesis difference. Instead, the greater winter MLD in 2005 than in 2006 caused a higher nitrate level (Fig. 7a) and more active photosynthesis (Fig. 6b) in 2005.

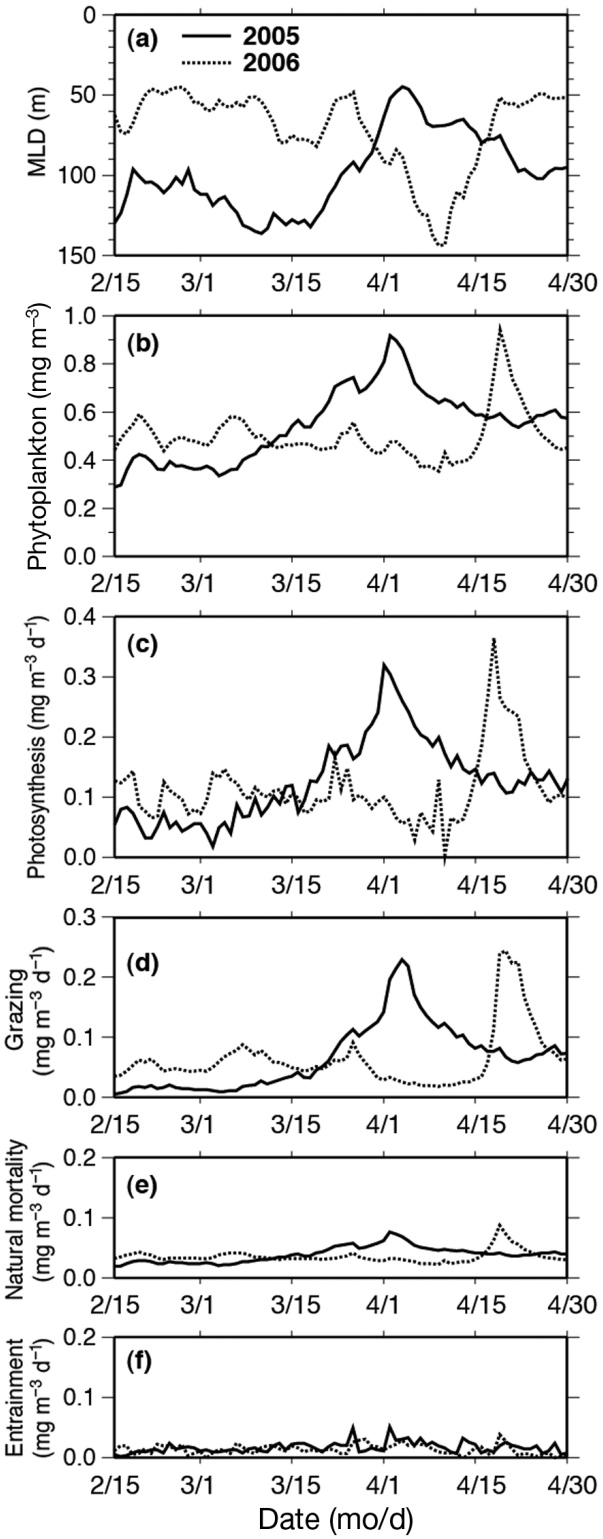

Fig. 6. (a) Mixed layer depth (MLD), (b) phytoplankton averaged in the mixed layer for the GR1c route, and (c–f) source or sink terms for phytoplankton in Eq. (1): (c) phytoplankton growth rate by photosynthesis, (d) grazing rate by zooplankton, (e) natural mortality rate and (f) dilution rate by vertical entrainment. Each rate is estimated on a chl *a* basis (mg m^{-3} d^{-1})

The next question was why the nitrate concentration was higher in 2005 than in 2006. The nitrate balance from winter to spring in both years is shown in Table 2. At the beginning of particle tracking on 15 February, there was little difference between the nitrate inventory (nitrate integrated in the mixed layer per unit area) in 2005 and in 2006 (Table 2a). During the winter (15 February to 31 March) of 2005, the total supply of nitrate was twice as high as that during the winter of 2006 (Table 2b). This difference was mainly caused not by decomposition of organic matter (DN) but by the nitrate supplied by mixed layer deepening (EN). EN was several times larger than DN and was the main source of the nitrate supply (Fig. 7b,c). Since EN depended on the MLD, wintertime entrainment of nitrate in 2005 was greater than in 2006, corresponding to a greater winter MLD (112.5 m) in 2005 than in 2006 (62.1 m) (Fig. 6a).

Nitrate consumed during photosynthesis in winter (Table 2c) and nitrate loss by mixed layer shoaling in winter (Table 2d) were higher in 2005 than in 2006; however, the residual nitrate concentration was higher by 116.6 mmol N m^{-2} in 2005, because of a more abundant nitrate supply during winter due to the deeper mixed layer in 2005. Differences in nitrate between 2005 and 2006, in the mixed layer on 15 February (Table 2a), and in the nitrate supplies by entrainment (Table 2b) and decomposition (Table 2c) during winter were 24.7, 190.2 and 31.7 mmol N m^{-2}, respectively. Thus, most of the difference in the residual nitrate at the end of the winter was explained by the nitrate supply due to entrainment, that is, due to the winter MLD.

There was little difference between nitrate supply in spring (1 to 30 April) in 2005 and in 2006 (Table 2f). Also, loss of nitrate by mixed layer shoaling in spring in both years was similar (Table 2h). The nitrate that can be used for spring photosynthesis was residual nitrate at the end of the winter + spring nitrate supply – loss of nitrate by mixed layer shoaling in spring: 321.6 mmol N m^{-2} in 2005 and 199.8 mmol N m^{-2} in 2006 (Table 2i). Because the difference between 2005 and 2006 in spring nitrate supply was relatively minor, the total difference (121.8 mmol N m^{-2}) between 2005 and 2006 was predominantly caused by the difference in residual nitrate at the end of the winter in each year (116.6 mmol N m^{-2}; Table 2e).

Nitrate consumed by spring photosynthesis was 270.9 mmol N m^{-2} in 2005 and 196.0 mmol N m^{-2} in 2006 (Table 2g). Thus, the winter nitrate supply, especially the nitrate supply caused by the deepening of the winter mixed layer, determined the spring

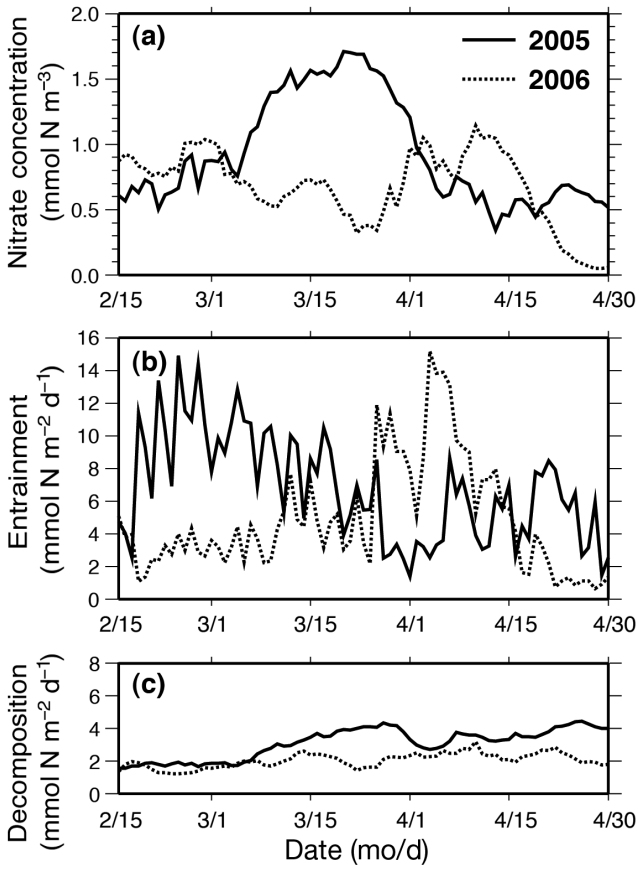

Fig. 7. (a) Nitrate concentration averaged in the surface mixed layer and the rate of nitrate supply (in mmol N m^{-2} d^{-1}) to the mixed layer for the GR1c route by (b) entrainment and (c) decomposition of organic matter in the ecosystem model

nitrate concentration and phytoplankton abundance in the model. A similar relationship between the winter nitrate supply through mixed layer deepening and spring photosynthesis was also seen for other years (Table 2b,g). The 3 years of the most winter entrainment were 2002, 2003 and 2005; these corresponded to the 3 years of greatest spring consumption during photosynthesis (Table 2b,g). These were also deep winter mixed layer years (Fig. 5a).

When we compared mean nitrate distributions in the model on the northern side of the Kuroshio axis between February and April (Fig. 8), the nitrate concentration in the mixed layer was much higher in February than in April; this is because phytoplankton consumes nitrate in the mixed layer in spring.

Processes south of the Kuroshio axis

In the GR2 routes, where particles are transported on the southern side of the Kuroshio axis, spring

Table 2. Balance of nitrate in the mixed layer (mmol N m^{-2}, nitrate density × mixed layer depth) from 2001 to 2007. Inventory: total nitrate in the mixed layer on a specific date; EN: nitrate supply by mixed layer deepening; DN: nitrate supply by decomposition of organic matter (detritus, zooplankton and phytoplankton); photosynthesis: consumed nitrate during photosynthesis; loss by ML shoaling: nitrate decrease by mixed layer shoaling; available nitrate: (i) = (e) + (f) – (h)

	Winter (15 Feb–31 Mar)					Spring (1–30 Apr)					
	(a) Inventory on 15 Feb	(b) Nitrate supply EN	DN	EN + DN	(c) Photosynthesis	(d) Loss by ML shoaling	(e) Inventory on 1 Apr	(f) Nitrate supply EN	DN	EN + DN	(g) Photosynthesis	(h) Loss by ML shoaling	(i) Available nitrate
2001	37.9	224.5	83.2	307.7	222.4	57.7	65.5	114.0	95.2	209.2	234.0	27.9	246.8
2002	41.0	275.4	92.6	368.0	196.4	10.9	201.7	219.0	137.3	356.3	325.5	225.6	332.4
2003	24.9	333.4	93.5	426.9	207.5	37.9	206.4	214.4	111.4	325.8	304.0	224.0	308.2
2004	132.4	233.1	97.4	330.5	217.4	146.7	98.8	219.8	96.3	316.1	230.8	183.5	231.4
2005	79.2	346.8	102.9	449.7	247.9	132.7	148.3	162.1	127.6	289.7	270.9	116.4	321.6
2006	54.5	156.6	71.2	227.8	160.3	90.3	31.7	209.3	81.5	290.8	196.0	122.7	199.8
2007	35.9	223.9	86.9	310.8	175.5	50.5	120.7	209.6	115.7	325.3	257.2	185.5	260.5

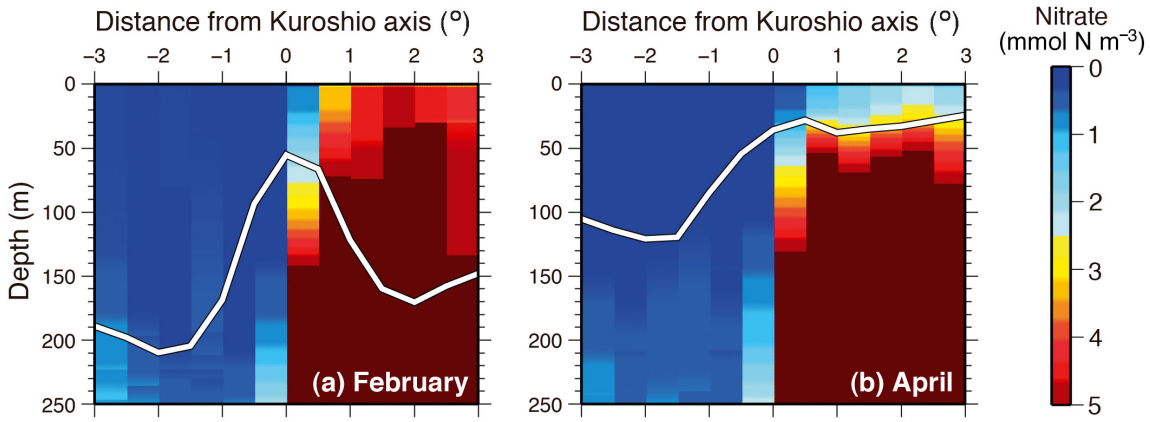

Fig. 8. Mean vertical sections of nitrate across the Kuroshio axis along 142° E in (a) February and (b) April, according to the ecosystem model. Average distance (°) from the Kuroshio axis is given for 2001 to 2007; the positive (negative) numbers denote north (south) of the axis. White line: mixed layer depth

phytoplankton densities were not necessarily high in years of a deep winter mixed layer (Table 1). On the other hand, significant positive correlations were detected between winter nitrate and spring chl *a*/phytoplankton (Table 1). Along the GR2 routes, a deeper winter mixed layer did not always lead to a higher winter nitrate concentration.

Fig. 9 represents the time-series of MLD and nitrate concentration along the GR2a route (0° to 0.5° south of the Kuroshio axis) in 2005 and 2006. 2005 (2006) is the year when the winter mixed layer was deep (shallow). Although the winter mean MLD in 2005 (181 m) was much greater than in 2006 (76 m) (Fig. 9a), the winter mean nitrate concentration in 2005 (0.25 mmol N m^{-3}) was not as high as in 2006 (0.44 mmol N m^{-3}) (Fig. 9b); this was unlike the situation along route GR1c on the northern side of the Kuroshio axis (Fig. 7a).

The independence of nitrate concentration from MLD is shown in the area where nitrate-poor water was distributed below the surface mixed layer. Fig. 10a depicts the modeled vertical cross-section of nitrate in February 2005. A vertical inversion of nitrate concentration was seen at the depth of 130 to 170 m at 31.4° N on the southern side of the Kuroshio axis. During such an inversion, mixed layer deepening is expected to entrain nitrate-poor water and to reduce the nitrate concentration in the surface mixed layer.

Such vertical inversions of nitrate concentration (represented by the occurrence rate of a nitrate minimum layer just below the surface mixed layer, based on the eddy-resolving coupled physical–biological model) frequently occur on the southern side of the Kuroshio axis, whereas they rarely occur on the northern side (Fig. 11). While the rate was <10% in the waters 0 to 3° north of the Kuroshio axis (GR1), the rate was 15 to 20% on the southern side (GR2). Thus, a deeper winter mixed layer did not always lead to higher nitrate concentrations in the surface mixed layer along the GR2 in the model.

Nitrate vertical inversions were actually observed on the southern side of the Kuroshio axis. A nitrate inversion was seen at around 100 m depth from 29.5° to 32.5° N (Fig. 10b). As for the modeled data, obser-

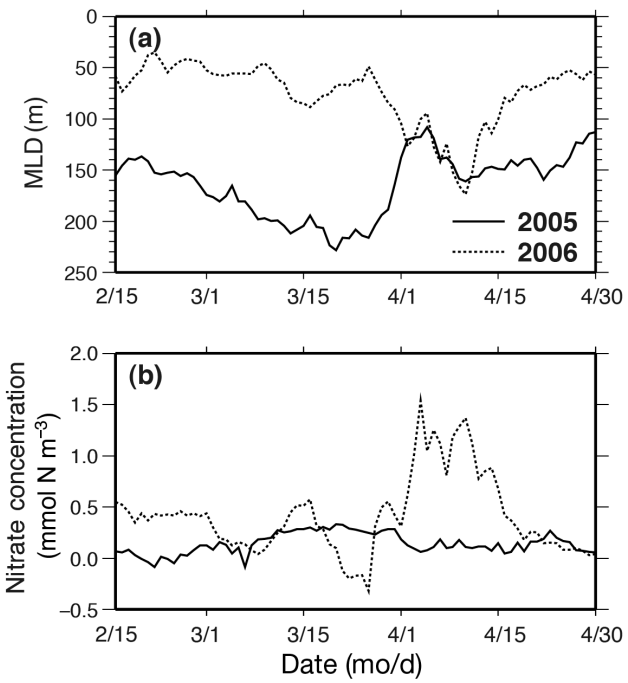

Fig. 9. (a) Mixed layer depth (MLD; m) and (b) nitrate concentration averaged in the surface mixed layer, and the rate of nitrate supply (in mmol N m^{-2} d^{-1}) to the mixed layer for the GR2a route (0° to 0.5° south of the Kuroshio axis)

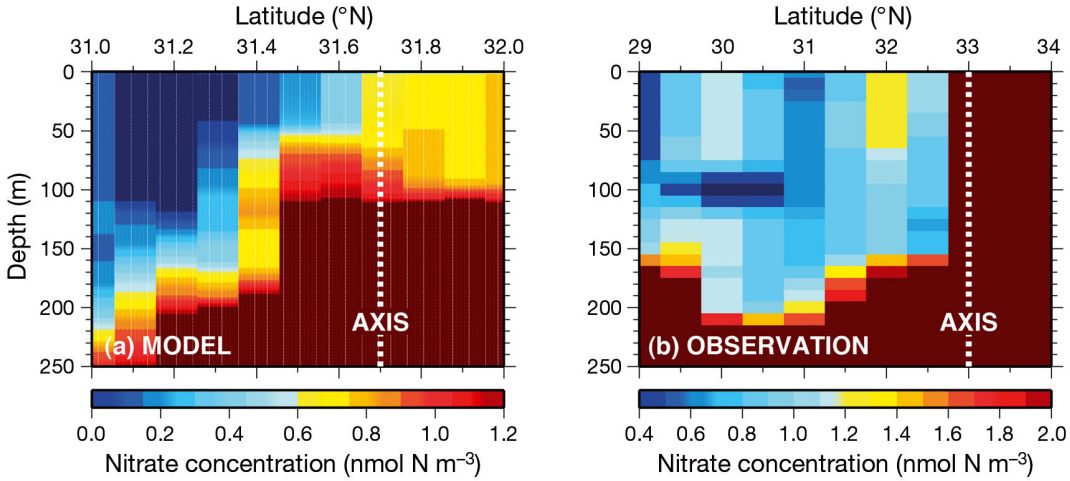

Fig. 10. Vertical cross-sections of nitrate according to the (a) ecosystem model from 31° to 32° N along 133° E on 20 February 2005 and for (b) observations from 29° to 34° N along 137° E in winter 2010 during the Ryofu Maru cruise (Japan Meteorological Agency 2010). Broken lines denote the Kuroshio axis. Since the grid interval is different between the model (0.1°) and observations (0.5°), the latitudinal ranges differ between (a) and (b)

vational data analysis did not detect correlations between spring phytoplankton and winter MLD along the GR2 either (Table 1).

DISCUSSION

Positive correlations were detected between winter MLD and spring phytoplankton density in the water mass that is transported by the Kuroshio along the route 0° to 0.5° north of the Kuroshio axis in both the observations from 1998 to 2006 and the ecosystem model for 2001 to 2007, where the deeper winter mixed layer entrains higher nitrate concentrations, resulting in enhancement of the spring phytoplankton bloom. The route 0° to 0.5° north of the Kuroshio axis and to the KE was a main transport route of sardine larvae, and there were significant positive correlations between MLD and sardine recruitment during the period from 1978 to 1994 (Nishikawa et al. 2013). Especially, the regime shift of the mixed layer from deep to shallow in 1988 might have caused the sudden decrease of sardine stock (Yasuda et al. 2000, Nishikawa & Yasuda 2008, 2011, Nishikawa et al. 2011, 2013). Combination of the these previous studies and our results, and the positive correlation between MLD and phytoplankton density give an important implication for sardine stock variation. Since copepod eggs and nauplii are the main food source of sardine larvae (Nakata et al. 1995), low spring chl *a*, corresponding to a shallow winter mixed layer, might worsen the feeding conditions for sardine larvae; this is because the relationship between chl *a* and nauplius density is not linear (Dr. Tohru Ikeya pers. comm. in 2010), and egg production stops at a chl *a* density lower than a certain threshold value; in the case of *Calanus sinicus*, for example, eggs are produced when the chl *a* density is >0.5 mg m^{-3} (Uye & Murase 1997). Along the route 0° to 0.5° north of the Kuroshio axis, the mean (from 1998 to 2006) observed spring chl *a* density was 0.56 mg m^{-3}. But the density was <0.5 mg m^{-3} in shallow mixed layer years, 1999 and 2006 (Fig. 4a), when sardine recruitment was also low (Fisheries Agency and Fisheries Research Agency of Japan 2007). The shallow winter mixed layer (<100 m) 0° to 0.5° north of the Kuroshio axis may thus have caused unfavorable feeding conditions for sardine larvae and decreased recruitment from 1988 to 1990. Nishikawa

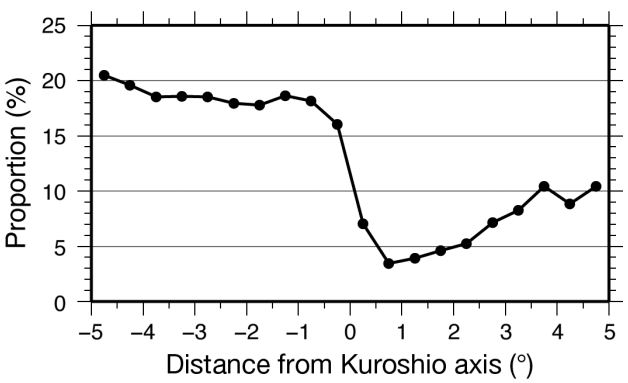

Fig. 11. Frequency (in percent) of the model grids with the nitrate minimum layer just below the surface mixed layer from 130° to 160°E around the Kuroshio axis in March. The positive (negative) numbers denote north (south) of the Kuroshio axis

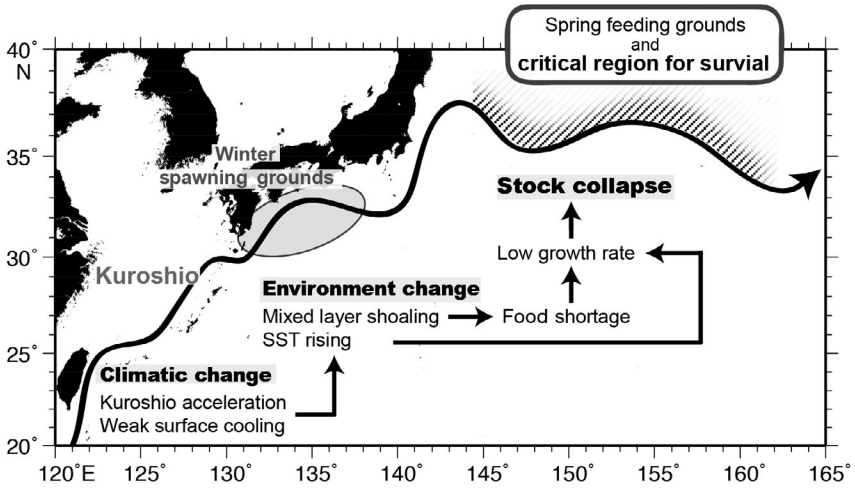

Fig. 12. Hypothesis of how climate change may have led to the collapse of the sardine *Sardinops melanostictus* stock off Japan

et al. (2011) showed that the mean February MLD 0° to 0.5° north of the Kuroshio axis and from 130° to 160°E from 1988 to 1990 was 77 m, whereas it was 109 m from 1980 to 1987 according to OFES data.

In observations, positive correlations were also seen between winter MLD and spring chl *a* of the water mass along the transport route 0.5° to 1° north of the Kuroshio axis. Since MLDs that larvae experience along this route are positively correlated with sardine recruitment (Nishikawa et al. 2011, 2013), MLD variation on this route might also affect the survival of sardine larvae through feeding conditions. These 2 areas 0° to 1° north of the Kuroshio axis with positive correlations between winter MLD and spring chl *a* are the main larval transport routes. More than 15% of total larvae are distributed here (Nishikawa et al. 2013). These large proportions of the larval distribution suggest the importance of the winter MLD along these 2 routes for sardine recruitment.

Considering our findings that winter MLD variations do not necessarily lead to spring phytoplankton variability, winter MLD variations south of the Kuroshio axis may not be a dominant factor contributing to recruitment variability, although Nishikawa et al. (2011, 2013) reported significant positive correlations just south of the Kuroshio axis, where a significant amount of larvae are transported.

The shallow mixed layer near the Kuroshio axis at the end of the 1980s was caused primarily by acceleration of the Kuroshio jet and the reduction of surface cooling (Nishikawa & Yasuda 2011). The strong current velocity reduces the time during which the mixed layer is exposed to wintertime cooling. As a result, the winter mixed layer does not deepen. These climate changes also cause a high SST (Nishikawa & Yasuda 2011). High SST in 1988 co-occurring with a shallow mixed layer could have a negative influence on larvae and recruitment. Larval growth rate is highest at 16.2°C (Takasuka et al. 2007). However, the SST that larvae experienced along the GR1c route from 1988 to 1992 was 17 to 18°C, 0.5°C higher than in the early 1980s (Nishikawa et al. 2012).

The synergetic effects of feeding and environmental temperature changes could affect larval survival. Fig. 12 illustrates our hypothesis that climatic variability induces sardine stock collapse. Sardine spawning grounds are formed from the coasts south of Japan to the Kuroshio axis. Eggs and larvae are transported by the Kuroshio near the Kuroshio axis, and, as observed, large portions are transported to the Kuroshio Extension (Sugisaki 1996, Kinoshita 1998). Here we hypothesize that important factors affecting sardine recruitment variability through feeding conditions may be limited by winter MLD variability 0° to 1° north of the Kuroshio axis, the area usually regarded as Kuroshio frontal zone. The winter MLD variability is caused by variability of local wind cooling and the Kuroshio jet velocity.

Acknowledgements. The present paper is part of a PhD thesis by H.N. at the Graduate School of Science, University of Tokyo. The authors thank Profs. E. Oka, Y. Watanabe, H. Nakamura and M. Uematsu for their useful comments. This study was partially supported by KAKENHI#20221002 and SUPRFISH.

LITERATURE CITED

Chu PC, Kuo YH (2010) Nutrient pumping/advection by propagating Rossby waves in the Kuroshio extension. Deep-Sea Res II 57:1809–1819

Eppley RW (1972) Temperature and phytoplankton growth in the sea. Fish Bull 70:1063–1085

Fisheries Agency and Fisheries Research Agency of Japan (2007) Marine fisheries stock assessment and evaluation for Japanese waters (details for fiscal year 2007). Fisheries Agency and Fisheries Research Agency of Japan, Tokyo, p 11–44 (in Japanese). Also available at: http://abchan.job.affrc.go.jp/digests19/details/1901.pdf

Ito S (1961) Fisheries biology of the sardine, *Sardinops melanostictus* (T. & S.), in the waters around Japan. Bull Jpn Sea Natl Fish Res Inst 9:1–227 (in Japanese with English abstract)

Japan Meteorological Agency (2010) Oceanographic and marine meteorological observations by research vessels, Ryofu Maru 1001 cruise. Available at: www.data.kishou.go.jp/kaiyou/db/vessel_obs/data-report/html/ship/cruise

data_e.php?id=RF1001 (accessed on 30 July 2010)
Kalnay E, Kanamitsu M, Kistler R, Collins W and others (1996) The NCEP/NCAR 40-year reanalysis project. Bull Am Meteorol Soc 77:437–471
Kawai H (1972) Hydrography of the Kuroshio Extension. In: Stommel H, Yoshida K (eds) Kuroshio, its physical aspects. University of Tokyo Press, Tokyo, p 235–352
Kinoshita T (1998) Northward migrating juveniles in the Kuroshio Extension area. In: Watanabe Y, Wada T (eds) Stock fluctuations and ecological changes of the Japanese sardine. Koseisha-Koseikaku, Tokyo, p 84–92 (in Japanese)
Konishi Y (1980) Vertical distribution of eggs and larvae of sardine, *Sardinops melanosticta* (T. et S.), and round herring, *Etrumeus micropus* (T. et S.). Bull Nansei Reg Fish Res Inst 12:93–103
Limsakul A, Saino T, Midorikawa T, Goes JI (2001) Temporal variations in lower trophic level biological environments in the northwestern North Pacific subtropical gyre from 1950 to 1997. Prog Oceanogr 49:129–149
Marine Information Research Center, Japan Hydrographic Association (2007) Data sets of the axis of the Kuroshio from 1955 to 2006. CD-ROM. Japan Hydrographic Association, Tokyo
Masumoto Y, Sasaki H, Kagimoto T, Komori N and others (2004) A fifty-year eddy-resolving simulation of the world ocean—preliminary outcomes of OFES (OGCM for the Earth Simulator). J Earth Sim 1:35–56
Masuzawa J (1969) Subtropical mode water. Deep-Sea Res 16:463–472
Miyazawa Y, Komatsu K, Setou T (2008) Nowcast skill of the JCOPE2 ocean forecast system in the Kuroshio-Oyashio mixed water region. J Mar Meteorol Soc (Umi to Sora) 84:85–91 (in Japanese with English abstract)
Nakata K, Zenitani H, Inagake D (1995) Differences in food availability for Japanese sardine larvae between the frontal region and the waters on the offshore side of Kuroshio. Fish Oceanogr 4:68–79
Nakata K, Itoh H, Ichikawa T, Sasaki K (2004) Seasonal changes in the reproduction of three oncaeid copepods in the surface layer of the Kuroshio Extension. Fish Oceanogr 13:21–33
Nishikawa H, Yasuda I (2008) Japanese sardine (*Sardinops melanostictus*) mortality in relation to the winter mixed layer depth in the Kuroshio Extension region. Fish Oceanogr 17:411–420
Nishikawa H, Yasuda I (2011) Long-term variability of winter mixed layer depth and temperature along the Kuroshio jet in a high-resolution ocean general circulation model. J Oceanogr 67:503–518
Nishikawa H, Yasuda I, Itoh S (2011) Impact of winter-to-spring environmental variability along the Kuroshio jet on the recruitment of Japanese sardine (*Sardinops melanostictus*). Fish Oceanogr 20:570–582
Nishikawa H, Yasuda I, Itoh S, Komatsu K, Sasaki H, Sasai Y, Oozeki Y (2013) Transport and survival of Japanese sardine (*Sardinops melanostictus*) eggs and larvae via particle tracking experiments. Fish Oceanogr (in press)
Noto M, Yasuda I (1999) Population decline of the Japanese sardine, *Sardinops melanostictus*, in relation to sea surface temperature in the Kuroshio Extension. Can J Fish Aquat Sci 56:973–983
Noto M, Yasuda I (2003) Empirical biomass model for the Japanese sardine, *Sardinops melanostictus*, with sea surface temperature in the Kuroshio Extension. Fish Oceanogr 12:1–9
Oschlies A (2001) Model-derived estimates of new production: New results point towards lower values. Deep-Sea Res II 48:2173–2197
Pacanowski RC, Griffies SM (2000) MOM 3.0 manual. Geophysical Fluid Dynamics Laboratory/National Oceanic and Atmospheric Administration, Princeton, NJ
Sasai Y, Ishida A, Sasaki H, Kawahara S, Uehara H, Yamanaka Y (2006) A global eddy-resolving coupled physical–biological model: physical influences on a marine ecosystem in the North Pacific. Simul-T Soc Mod Sim 82: 467–474
Sasai Y, Richards KJ, Ishida A, Sasaki H (2010) Effects of cyclonic mesoscale eddies on the marine ecosystem in the Kuroshio extension region using an eddy-resolving coupled physical–biological model. Ocean Dyn 60:693–704
Sasaki H, Nonaka M, Masumoto Y, Sasai Y, Uehara H, Sakuma H (2008) An eddy-resolving hindcast simulation of the quasiglobal ocean from 1950 to 2003 on the Earth Simulator. In: Ohfuchi W, Hamilton K (eds) High resolution numerical modelling of the atmosphere and ocean. Springer, New York, NY, p 157–186
Sugisaki H (1996) Distribution of larval and juvenile Japanese sardine (*Sardinops melanostictus*) in the western North Pacific and its relevance to predation on these stages. In: Watanabe Y, Yamashita Y, Oozeki Y (eds) Survival strategies in early life stages of marine resources. A.A. Balkema, Rotterdam, p 261–270
Sukigara C, Suga T, Saino T, Toyama K, Yanagimoto D, Hanawa K, Shikama N (2011) Biogeochemical evidence of large diapycnal diffusivity associated with the subtropical mode water of the North Pacific. J Oceanogr 67:77–85
Takahashi M, Nishida H, Yatsu A, Watanabe Y (2008) Year-class strength and growth rates after metamorphosis of Japanese sardine (*Sardinops melanostictus*) in the western North Pacific ocean during 1996–2003. Can J Fish Aquat Sci 65:1425–1434
Takahashi M, Watanabe Y, Yatsu A, Nishida H (2009) Contrasting responses in larval and juvenile growth to a climate–ocean regime shift between anchovy and sardine. Can J Fish Aquat Sci 66:972–982
Takasuka A, Oozeki Y, Aoki I (2007) Optimal growth temperature hypothesis: Why do anchovy flourish and sardine collapse or vice versa under the same ocean regime? Can J Fish Aquat Sci 64:768–776
Uye S, Murase A (1997) Relationship of egg production rates of the planktonic copepod *Calanus sinicus* to phytoplankton availability in the Inland Sea of Japan. Plankton Biol Ecol 44:3–11
Watanabe Y, Zenitani H, Kimura R (1995) Population decline of the Japanese sardine *Sardinops melanostictus* owing to recruitment failures. Can J Fish Aquat Sci 52:1609–1616
Yamazaki H, Iwamatsu I, Hasegawa D, Nagai T (2009) Chlorophyll patches observed during summer in the main stream of the Kuroshio. Atmos-ocean 47:299–307
Yasuda I, Watanabe T (2007) Chlorophyll *a* variation in the Kuroshio extension revealed with a mixed-layer tracking float: implication on the long-term change of Pacific saury (*Cololabis saira*). Fish Oceanogr 16:482–488
Yasuda I, Sugisaki H, Watanabe Y, Minobe SS, Oozeki Y (1999) Interdecadal variations in Japanese sardine and ocean/climate. Fish Oceanogr 8:18–24
Yasuda I, Tozuka T, Noto M, Kouketsu S (2000) Heat balance and regime shifts of the mixed layer in the Kuroshio extension. Prog Oceanogr 47:257–278

Submitted: February 9, 2012; Accepted: November 19, 2012 *Proofs received from author(s): April 8, 2013*

Vol. 487: 231–244, 2013
doi: 10.3354/meps10372

MARINE ECOLOGY PROGRESS SERIES
Mar Ecol Prog Ser

Published July 30

Contribution to the Theme Section 'Biophysical coupling of marine hotspots'

FREE ACCESS

Hurricane impacts on the foraging patterns of bottlenose dolphins *Tursiops truncatus* in Mississippi Sound

Courtney E. Smith[1,*], Brendan J. Hurley[2], Christina N. Toms[1], Angela D. Mackey[1], Moby Solangi[3], Stan A. Kuczaj II[1]

[1]Department of Psychology, University of Southern Mississippi, Hattiesburg, Mississippi 39406, USA
[2]Department of Geography and GeoInformation Science, George Mason University, Fairfax, Virginia 22030, USA
[3]Institute for Marine Mammal Studies, Gulfport, Mississippi 39502, USA

ABSTRACT: Acute catastrophic events, such as hurricanes, have various degrees of impact on marine mammal populations. Although changes in environmental conditions of affected areas have been examined for many storms, little attention has been given to the ecological effects on top-level predators. A longitudinal study on bottlenose dolphin *Tursiops truncatus* behavior and distribution in Mississippi Sound has been ongoing since 2003, allowing the unique opportunity to examine the impacts of the passage of Hurricane Katrina on this coastal dolphin population. Previous research showed an increase in reproductive rates within this population following Hurricane Katrina, most likely due to an increase in prey density following the sharp decline in commercial fishing efforts. In this paper, the frequency and distribution of dolphin foraging encounters in Mississippi Sound were examined from 2003 to 2009, revealing both short- and potentially long-term effects on dolphin foraging patterns following the hurricane. A pulse in dolphin foraging encounters was observed, which increased by ~15% in the 2 yr following the hurricane before returning to pre-Katrina levels. Statistically significant hot spots were identified through the use of the Getis-Ord Gi* hot spot analysis and revealed spatial shifts in foraging habitat consistent with prey selectivity. The results of this study support previous findings that coastal bottlenose dolphins in the southeastern United States are selective feeders, preferring to forage in deeper water known for soniferous prey species. Furthermore, this study presents important baseline information for future studies investigating other acute catastrophic events in Mississippi Sound, such as cumulative impacts following the Deepwater Horizon oil spill.

KEY WORDS: *Tursiops truncatus* · Hurricane impacts · Getis-Ord Gi* · Foraging ecology · Mississippi Sound

INTRODUCTION

Hurricanes cause catastrophic changes to coastal marine ecosystems. Strong winds, large amounts of precipitation, and storm surge can greatly alter the physical structure of existing shorelines and barrier islands. Water chemistry can be dramatically altered for weeks following a storm due to changes in salinity, resuspension of large volumes of sediments and nutrients (Allison et al. 2005, Dreyer et al. 2005), and large increases in contaminant input (e.g. chemicals, sewage, fuels, and pesticides; Burkholder et al. 2004, Bassos-Hull & Wells 2007). Subsequent increases in total nitrogen and phosphorus from contaminant loadings can lead to hypoxic environments (Burkholder et al. 2004, Bassos-Hull & Wells 2007), causing short-term changes in prey distribution and availability (Stevens et al. 2006, Tomasko et al. 2006) and,

*Email: courtney.e.smith@eagles.usm.edu

in some cases, massive fish kills (Burkholder et al. 2004).

The effects of such natural disasters on wildlife populations are poorly understood and difficult to assess due to the limited predictability of storm occurrence, course, strength, and location of impact. This is particularly true for wide-ranging and long-lived marine megafauna, such as marine mammals, which require multi-year studies to be in place prior to a disaster to adequately measure effects. Some immediate and direct effects of hurricanes on marine mammals have been documented, such as the temporary displacement or stranding of individuals (e.g. dugongs *Dugong dugon:* Marsh 1989; pygmy killer whales *Feresa attenuata:* Mignucci-Giannoni et al. 1999; bottlenose dolphins *Tursiops truncatus*: Rosel & Watts 2008). Other effects may manifest on a longer time scale, particularly if food resources are depleted or unavailable. For example, tropical storms have destroyed seagrass beds (a primary food source for dugongs), which has subsequently been related to increases in dugong mortality (Heinsohn & Spain 1974, Preen & Marsh 1995). Likewise, habitat destruction in important foraging areas following severe tropical systems is thought to have indirectly increased mortality in Florida manatees *Trichechus manatus latirostris* (Langtimm et al. 2006). Studies assessing hurricane impacts on the foraging ecology of cetaceans are greatly lacking, and to the best of our knowledge none has been reported in the literature. Given that the distribution patterns and behavior of cetacean species appear to be dependent on foraging habitat (see Würsig 1986, Hastie et al. 2004, Ashe et al. 2010), it is important to identify these areas and the mechanisms that shape them to better understand potential impacts of hurricanes and other catastrophic events.

Hurricane Katrina devastated the coastlines of Louisiana, Mississippi and Alabama on 29 August 2005. With storm surge as high as 24 to 28 feet (7.3 to 8.3 m) along the Mississippi coast, Katrina is ranked the third most deadly and intense (ranked by pressure) tropical cyclone to make landfall in the period 1851–2006 (Blake et al. 2007). A project aimed at understanding the behavior and distribution of bottlenose dolphins in Mississippi Sound has been underway since 2003, showing regular use of this habitat by individuals on both a seasonal and year-round basis (Mackey 2010), thus providing a unique opportunity to examine the impacts of a major hurricane on this coastal dolphin population. In a previous study, Miller et al. (2010a) investigated the effects of Hurricane Katrina on bottlenose dolphin reproduction, reporting an increase in the rate of calf sightings (calves km^{-1} effort), and in the percentage of calves to non-calves per group. The authors attributed this increase in reproduction, in part, to a potential increase in prey abundance in the area following a widespread reduction in the purchase of commercial and residential fishing licenses, as well as large decreases in annual fisheries landings in Gulfport-Biloxi, Mississippi, in the year of the storm (7.4 million kg of fish reported in 2004 compared to 3.9 and 4.4 million kg in 2005 and 2006, respectively; National Marine Fisheries Service 2007).

To complement the work of Miller et al. (2010a) and further explore the potential effects of hurricanes on bottlenose dolphin populations, the goals of this study were to (1) examine indirect evidence for an increase in fish abundance (i.e. dolphin prey) following Hurricane Katrina by means of foraging behaviors and comparison to reported fisheries landings, and (2) identify habitat usage related to dolphin foraging activities (dolphin foraging hot spots) before and after Hurricane Katrina.

MATERIALS AND METHODS

Study area

Mississippi Sound, hereafter referred to as 'the Sound,' is a relatively shallow (~3.0 m average water depth) coastal system that extends from Louisiana to Alabama, and is separated from the Gulf of Mexico by a series of 5 barrier islands located 15 to 20 km from the main coastline: Cat, Ship, Horn, Petit Bois and Dauphin Islands, which comprise the National Park Service's Gulf Islands National Seashore (Fig. 1). These barrier islands exhibit various levels of erosion, as they are prone to absorbing storm surge and flooding from tropical systems. Ship Island was split into 2 islands (East Ship and West Ship) following Hurricane Camille in 1969; however, because the newly created pass (Camille Cut) was too shallow to survey, Ship Island was treated as a single barrier island for the present study. Aside from several patches of oyster beds, the topography of the Sound mainly consists of soft bottom substrates ranging from fine grain sand to mud (Moncreiff 2007). These latter areas are ideal for supporting dense seagrass habitats, which are important foraging areas for numerous fish, seabird, and marine mammal species. Multiple mainland watershed sources from the north, combined with tidal exchange with the Gulf of Mexico contribute to a wide range of salinities across

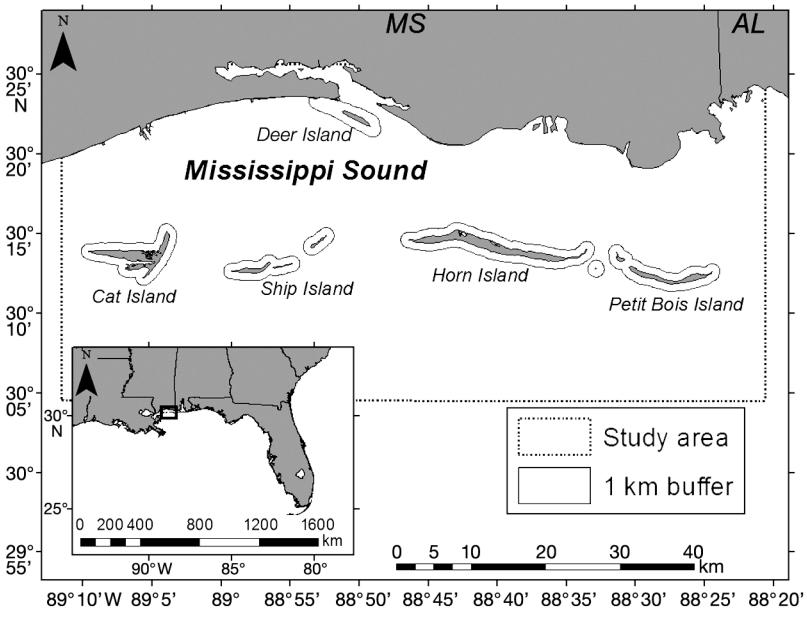

Fig. 1. Map of study area. Surveys were conducted on a random rotation around Cat, Ship, Horn and Deer Islands over a 6 yr study period. The 1 km buffer surrounding the islands represents the area targeted during surveys

the Sound, which during the course of the study ranged from 6 to 41 ppt (mean = 23 ppt). Sea surface temperatures during the current study ranged from a low of 5°C in the winter to a high of 33°C in the summer, averaging an annual mean of 23°C. The average depth during each encounter in the current study ranged from 0.60 to 18 m, with a mean depth of 4.85 m.

Data collection

Data were collected during directed, non-transect surveys targeting the Mississippi coast barrier islands from September 2003 through September 2009. Surveys were alternated randomly between select islands, but under the condition that each island was surveyed at least once each month and an equal number of times each season. Early surveys conducted from September 2003 to June 2005 rotated between Cat (30° 13′ N, 89° 06′ W) and Ship Islands (30° 12′ N, 88° 56′ W). Horn Island (30° 14′ N, 88° 42′ W) was incorporated into the study area in July 2006, but was later replaced by Deer Island (30° 22′ N, 88° 50′ W) in June 2009.[1] Surveys were conducted at least 4 times a month, weather permitting, from one of the following platforms: a 7 to 10 m vessel powered by a 225 Ram injection Evinrude outboard motor, or a center console Nautica rigid inflatable catamaran with twin 150-horsepower Evinrude engines. Surveys originated from either Gulfport Harbor or the Back Bay of Biloxi, beginning at ~08:30 h and continued until the scheduled island had been surveyed completely or until weather conditions deteriorated (e.g. Beaufort sea state >3). During each survey, a minimum of 3 observers continuously scanned for dolphins while the research vessel traveled at a speed of 16 to 20 km h^{-1}. The vessel circumnavigated each respective island at a distance of 1 to 1.5 km from shore. When a group of dolphins was spotted, the research vessel maneuvered toward the group and data collection began. A group of dolphins was defined as individuals within 100 m of each other and engaged in similar activities (Irvine et al. 1981). At the beginning of a dolphin encounter, the time and location were determined using a Garmin GPSMap 76 global positioning device, and environmental conditions (e.g. weather, Beaufort sea state, depth, salinity, glare, and water and air temperature) were recorded. Behavioral data were collected throughout the duration of the encounter following an ethogram derived from Shane (1990; also see Miller et al. 2010b; Table 1).

From September 2003 to June 2006, behavioral data were collected using all-occurrence sampling (Altmann 1974) for behavioral events, while behavioral states were rank-ordered based on amount of occurrence during the observation period (determined once the encounter ended). From July 2006 through September 2009, behavioral data were collected using a combination of instantaneous sampling for behavioral states and all-occurrence sampling for behavioral events (Altmann 1974). The behavioral state of the group (based on the activity of the majority of group members) was recorded at 1 min intervals. If the majority of the group was underwater at the interval, the behavioral state was recorded as the same as the state prior to submerging if it was the same upon the next surfacing (Mann 1999). If the state differed upon the next surfacing, the behavioral state was recorded as 'Not Found'. Interobserver reliability was determined using previously recorded video footage of bottlenose dolphin behaviors observed in Mississippi Sound, which involved coding behavioral states, events, and group size estimates; interobserver reliability was held constant at $r > 0.80$ throughout the study period.

[1]Deer Island was once an extension of the mainland and is not considered a barrier island

Table 1. *Tursiops truncatus.* Operational definitions of behavioral states and events used to determine foraging encounters. See Miller et al. (2010b) for full ethogram used in surveys

Foraging behavior	Operational definition
Behavioral states	
Feed	Group of dolphins is engaged in foraging behaviors such as repeated fluke-in/out dives in one location, feeding circles, lunge feeds, fish kicks, fish tosses, etc.
Probable feed	Indications of feeding such as group of dolphins following shrimp boat or birds diving in the immediate vicinity of the group.
Behavioral events	
Chase fish	A rapid increase in speed; observed in dolphins swimming in normal orientation or side-swim; fish must be observed to record this event.
Fish in mouth	Dolphin surfaces with fish visible between jaws.
Fish kick	Dolphin uses fluke or peduncle to knock a fish into the air.
Fish toss	Fish is thrown into the air by a dolphin using its melon, rostrum, or teeth.
Lunge feed	An accelerated forward motion at the surface that creates a wake moving the distance of approximately one body length.

A given group was followed until (1) a minimum of 15 min of behavioral data was collected, (2) the dolphins disappeared from view and were not located again, (3) weather conditions deteriorated, or (4) the dolphins showed signs of disturbance. Upon ending an encounter, the time, location, group composition (presence/absence of calves), and group size were recorded. Group size included the minimum, maximum, and best estimate of the number of dolphins present with the consensus of the observers.

Data analysis

Ethogram data were reviewed for recordings of dolphin foraging behavior over the study period. To control for biases against longer encounters (i.e. greater opportunity to observe foraging) we only reviewed ethogram data from the first 15 min of each encounter. Due to the methodological changes in behavioral data collection, only presence/absence information were retained and used for analyses. An encounter was considered a foraging encounter and included in the analysis if 'Feed' or 'Probable Feed' were recorded as a behavioral state or if any other foraging events were recorded during the encounter (Table 1). Of the total 266 survey days with 354 foraging encounters, 26 days (with 19 foraging encounters) were eliminated from the analyses due to incomplete data for survey effort calculations, the lack of encounters of any kind, or because of extremely short surveys (outliers). Analyses included the remaining 240 total survey days with 1049 encounters, 335 of which were considered foraging encounters (see Appendix 2 for survey effort). To have comparable time periods, our 72 mo study period was divided into 3 hurricane phases of 24 mo each: Pre-Katrina (Pre-Kat; September 2003–August 2005), Post-Katrina 1 (Post-Kat 1; October 2005–September 2007), and Post-Katrina 2 (Post-Kat 2; October 2007–September 2009). No surveys were conducted in September 2005 due to post-hurricane debris and coastal damage. In order to account for natural seasonal variation in foraging behavior, data were further analyzed across the summer (May–October) and winter (November–April) months as determined by mean sea surface temperature.

Frequency of foraging encounters

Survey effort was accounted for by creating a foraging index for each survey day based on the proportion of foraging encounters to total encounters recorded relative to distance surveyed each day:

$$\text{Foraging index} = \frac{\text{\# Foraging encounters : \# Total encounters}}{\text{Survey effort (km)}}$$

SPSS was used to conduct a Kruskal-Wallis test on ranked data to examine significant differences in the frequency of foraging encounters (using the foraging index) between hurricane phases and several control survey variables: survey effort distance, average group size, and number of overall encounters per kilometers surveyed. Mann-Whitney *U*-tests, with a Bonferroni correction ($\alpha = 0.02$; 2-tailed), were used for follow-up comparisons. Effect sizes (r) were calculated for significant comparisons. A Mann-Whitney *U*-test was also used to examine foraging behavior between seasons ($\alpha = 0.05$; 2-tailed).

The reported decline in annual commercial fisheries landings in Gulfport-Biloxi in the year of hurricane Katrina (National Marine Fisheries Service

2007) would be expected to positively influence prey abundance, suggesting an inverse relationship between reported fisheries landing and the frequency of foraging encounters. To test this, monthly foraging indices were also calculated and compared with monthly fisheries landings data (only available statewide, instead of specific to Gulfport-Biloxi; National Marine Fisheries Service 2012a) for the same period using a Pearson's correlation (1-tailed, $\alpha = 0.05$).

Getis-Ord Gi* hot spot analysis

ArcGIS version 10.0 provides a statistically powerful hot spot analysis using the Getis-Ord Gi* statistic (Getis & Ord 1992). The Gi* analysis calculates a *Z*-score for each feature in a set of weighted features (in the case of this analysis the weighted features were effort-corrected grid cells of 1 km^2 resolution). This *Z*-score (the Gi* statistic) indicates whether features with high or low values tend to cluster in a given area. Specifically, each feature is compared with neighboring features, and then by local summation compared to a global sum (all features in the study area); when this local sum is different from the expected local sum, and that difference is too large to be the result of random chance, a statistically significant *Z*-score is the result. If a feature's value is high and the values for all neighboring features are also high, it is part of a hot spot. Hot spots are defined as areas with statistically significant high *Z*-scores ($p < 0.05$), and conversely cold spots are areas of statistically significant low *Z*-scores ($p < 0.05$, ESRI ArcGIS Resource Center 2011a).

Effort-corrected survey data were parsed into multiple temporal splits to highlight any clustering patterns by season, year, and whether the data were temporally before or after Hurricane Katrina (see Appendix 1). Grid cells (1 km^2) were chosen based on encounters coded as foraging encounters following the methods previously mentioned. Encounters were recorded with a start and end latitude and longitude, thus allowing for centroid calculations for each encounter. The average length value of foraging encounters during surveys was 1014 m (or ~1 km).

Foraging sightings per unit effort (sightings km^{-1}) for each grid cell were then produced by dividing the number of foraging encounters in each grid cell by the length (km) of trackline surveyed in that same grid cell. From these, the closest (by distance) 95% of sightings were retained. The farthest (by distance) 5% were dropped to minimize the impact of outlying areas that were rarely surveyed, preserving the integrity of the hot spot analyses given that the survey design was opportunistic. Incremental Spatial Autocorrelation (utilizing iteration of the Global Moran's I function) tools for all files were first seeded with the output of a preliminary Average Nearest Neighbor analysis (ESRI ArcGIS Resource Center 2011b), and then performed on all files in order to find distances at which, if present, autocorrelation is maximized (in this case, clustered foraging events). These distances were then included in custom Spatial Weights Matrices (again for each respective file). Spatial Weights Matrices allow for a tighter control over how the groupings of cells interact. For this analysis, a minimum of 8 neighbors for each cell were required (ESRI ArcGIS Resource Center 2011c), as well as a threshold distance (as determined with the Incremental Spatial Autocorrelation analysis) beyond which outer cells' influence decreased rapidly (inverse distance squared). If, however, 8 neighbors could not be found within the given threshold distance, the distance was temporarily extended in order to satisfy this rule. After these preparatory analyses were completed, the final Spatial Weights Matrix of each respective file was then used as the customized input parameter for the Getis-Ord Gi* analysis.

Mitchell (2009) points out that the independence of tests is inherently violated during the Getis-Ord Gi* (e.g. each cell's local calculations rely on other local cells), thus producing Type I errors. The Bonferroni correction (Quinn & Keough 2002) was employed in order to mitigate the chances of this happening. While the correction is somewhat conservative, the opportunistic nature of the data used in the analysis warranted conservative estimations. Finally, to be included in the results, a hot spot must have been surveyed in the Pre-Kat phase, as well as at least one Post-Kat phase to ensure that those particular cells that appeared as hot spots in one phase were surveyed again to allow for a fair comparison.

RESULTS

Frequency of foraging encounters

There was a significant difference in foraging between the 3 hurricane phases ($H = 12.379$, df = 2, $p = 0.002$, $\eta^2 = 0.052$) with a mean rank of 112.18, 141.29, and 106.42 for Pre-Kat, Post-Kat 1, and Post-Kat 2, respectively. The proportion of foraging encounters to total encounters for each of the Pre-Kat and Post-Kat 2 phases was ~25%, which is consistent with past

evaluations of dolphin foraging behavior within the Sound (Mullin 1988). However, this proportion was 40% in the phase immediately following Hurricane Katrina (Post-Kat 1), representing a ~15% increase in the proportion of foraging encounters (accounting for effort) compared to Pre-Kat (Table 2; Pre-Kat vs. Post-Kat 1) and Post-Kat 2 (Table 2; Post-Kat 1 vs. Post-Kat 2). There was no significant difference between Pre-Kat and Post-Kat 2 (Table 2, Fig. 2). Additionally, there was no significant difference in foraging between seasons (U = 6760.50, Z = −0.753, p = 0.451).

Table 2. *Tursiops truncatus.* Post hoc results (Mann-Whitney *U*-test with a Bonferroni correction [α = 0.02; 2-tailed]) for variables with significant differences (Kruskal-Wallis, p < 0.05) among hurricane phases. Effect size (*r*) was only calculated for significant (*) Mann-Whitney *U*-test results

Variable	Hurricane phase comparison	Mean ranks	*U*	*Z*	p	*r*
Frequency of foraging encounters	Pre-Kat vs. Post-Kat 1	68.33, 88.04	2292.0	−2.728	0.006*	0.22
	Pre-Kat vs. Post-Kat 2	80.35, 75.96	2819.0	−0.617	0.537	
	Post-Kat 1 vs. Post-Kat 2	96.26, 72.46	2528.0	−3.211	0.001*	0.25
Total encounters	Pre-Kat vs. Post-Kat 1	70.44, 86.25	2443.5	−2.170	0.030	
	Pre-Kat vs. Post-Kat 2	81.45, 75.01	2755.5	−0.834	0.404	
	Post-Kat 1 vs. Post-Kat 2	95.26, 73.48	2613.0	−2.901	0.004*	0.02

Considering our control survey variables, there were no significant differences in survey effort distance (H = 0.557, df = 2, p = 0.757) or average group size (H = 4.482, df = 2, p = 0.106) between each hurricane phase. However, the total number of encounters, accounting for effort, differed significantly across hurricane phases (H = 9.435, df = 2, p = 0.009, η^2 = 0.04). There were fewer total encounters in Post-Kat 2 than in Post-Kat 1 (Table 2), but no differences between Pre-Kat and Post-Kat 1, or Pre-Kat and Post-Kat 2 hurricane phases (Table 2). Finally, although the effect was small, a significant correlation was found between the fisheries landings data and the foraging indices (r = −0.217, p = 0.035, n = 70; e.g. Fig. 3).

Getis-Ord Gi* hot spot analysis

Cells were retained for analysis if they contained at least one foraging event. In all, 335 foraging events were identified within 233 cells: 65 in the Pre-Kat phase, 106 in Post-Kat 1, and 62 in Post-Kat 2 (Fig. 4). After applying the Bonferroni correction, however, only 3 significant hot spots remained (Fig. 5). Two hot spots occurred in the Pre-Kat phase (Bonferroni corrected p-value < 0.001), a single hot spot was identified in the Post-Kat 1 phase (Bonferroni corrected p-value < 0.0005), and no hot spots were found during the Post-Kat 2 phase (Bonferroni corrected p-value < 0.001). No seasonal hot spots were found within the seasonal split analysis. Though only 3 cells are identified as hot spots, each cell uses other cells within the foraging dataset to be calculated and so these hot spots are derived from information inherent within many cells. While the results only highlight 3 hot spot cells, the opportunistic survey design we used warranted a highly parsimonious approach to analysis.

DISCUSSION

Dolphin foraging activity increased significantly following the passage of Hurricane Katrina and remained elevated throughout the Post-Kat 1 phase (Fig. 6). These results suggest that there may have been an increase in feeding opportunity, prey abundance, and/or a need for increased food consumption

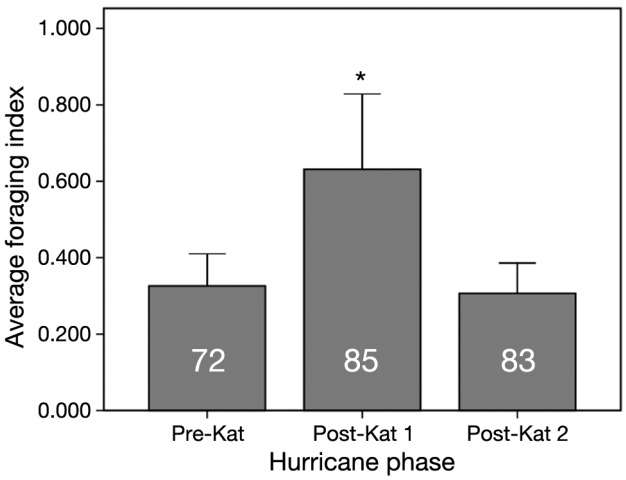

Fig. 2. *Tursiops truncatus.* Average frequency (± SE) of foraging encounters across hurricane phases, using the foraging index (proportion of foraging to non-foraging encounters km^{-1} survey effort). Asterisk indicates significant differences (*p < 0.01) as determined by Mann-Whitney *U* post hoc tests (adjusted α = 0.02). Numbers inside the bars show the total number of surveys conducted during that phase. Pre-Kat: September 2003–August 2005; Post-Kat 1: October 2005–September 2007; Post-Kat 2: October 2007–September 2009 (N = 240 surveys)

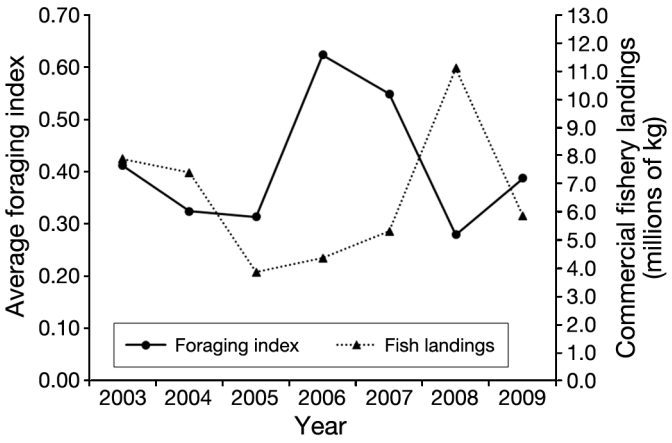

Fig. 3. *Tursiops truncatus.* Relationship between annual commercial fisheries landings for Gulfport-Biloxi (National Marine Fisheries Service 2012b) (▲) and the average foraging index (●) for each year of the study period. Foraging index is the proportion of foraging to non-foraging encounters km^{-1} survey effort

following the hurricane; however, it is difficult to determine the mechanisms that resulted in increased foraging. Our results offer indirect evidence of the intermediate disturbance theory; hurricanes and other acute catastrophic events may create levels of disturbance that can maximize species diversity (Connell 1978). It is likely, however, that there are multiple factors interacting and influencing the observed patterns.

A number of studies have reported that the presence of vessels leads to decreases in cetacean foraging behavior (Aguilar Soto et al. 2006, Miller et al. 2008, Lusseau et al. 2009). The reduction in vessel traffic following the storm may have given bottlenose dolphins in the Sound more time and/or space to forage. Moreover, commercial and recreational fishing within the Sound targets many of the same fish species utilized as prey by bottlenose dolphins (Leatherwood 1975, Benson 1982, Barros & Odell 1990, Barros & Wells 1998, Berens McCabe et al. 2010): striped mullet *Mugil cephalus*, pinfish *Lagodon rhomboids*, Gulf menhaden *Brevoortia patronus*, jack *Caranx hippos*, and spot *Leiostomus xanthurus*. A decrease in fisheries targeting these species for a period after

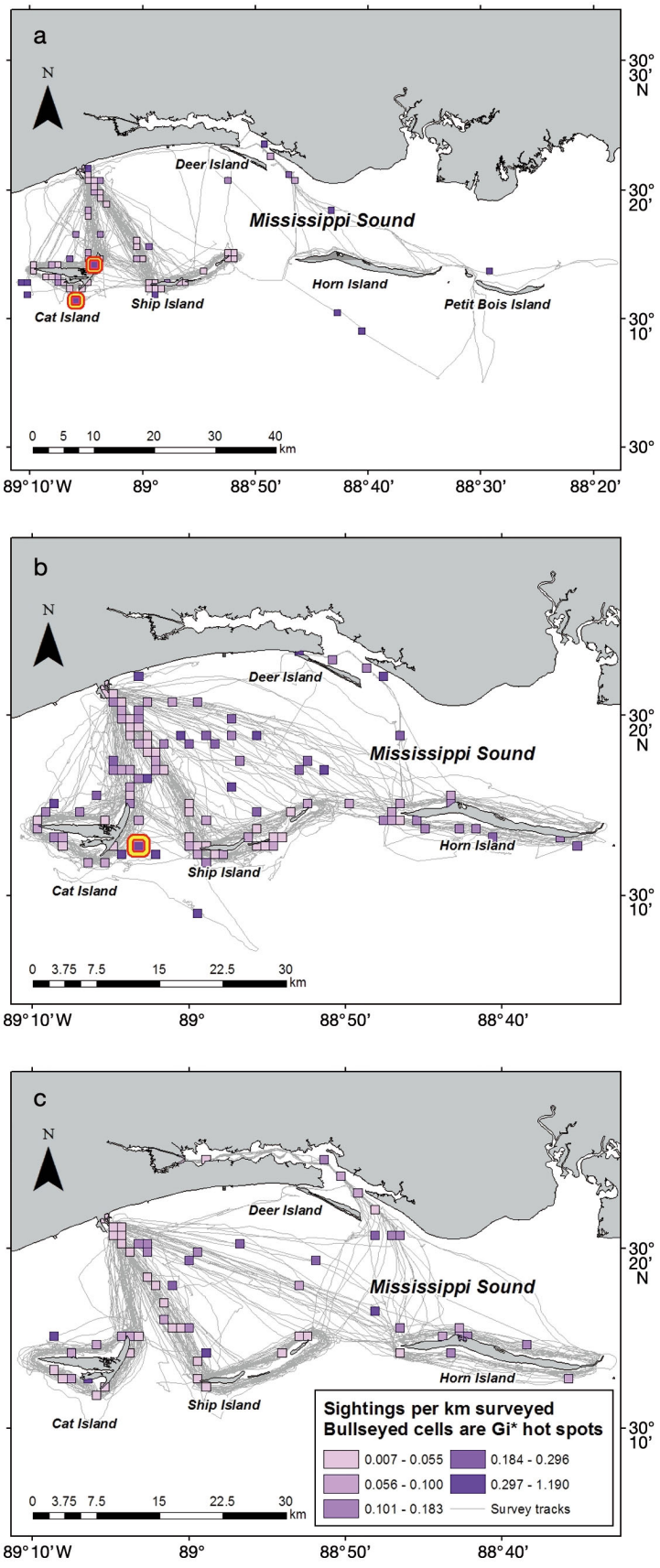

Fig. 4. *Tursiops truncatus.* Survey effort and resulting foraging hot spots in the Mississippi Sound region, by hurricane phase: (a) Pre-Kat, (b) Post-Kat 1, and (c) Post-Kat 2. Significant hot spots following Bonferroni correction are bullseyed. Note: Petit Bois Island was opportunistically surveyed during 2 Horn Island surveys in the Pre-Kat phase, but was not surveyed the remainder of the study (see Appendix 2 for effort)

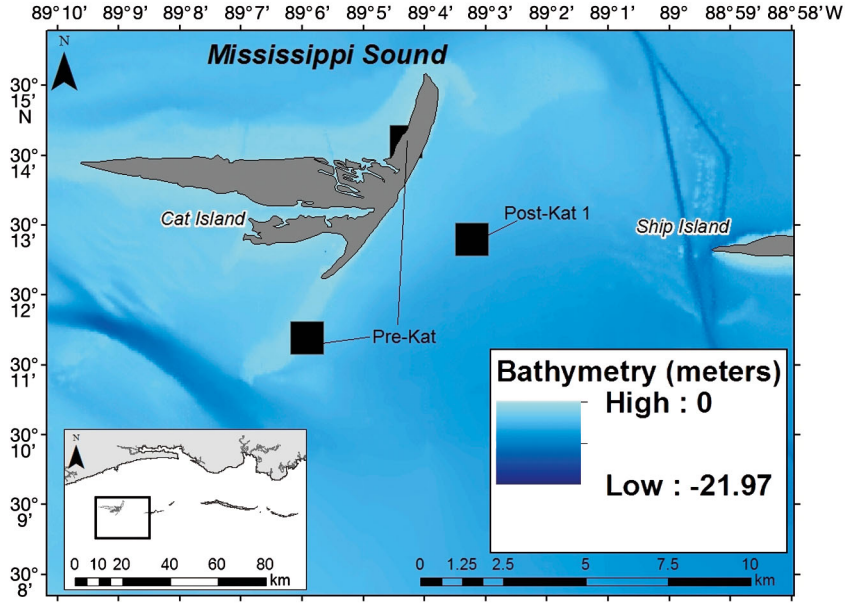

Fig. 5. *Tursiops truncatus*. Foraging hot spots as identified by the Getis-Ord Gi* statistic (bathymetry from Love et al. 2012). Two hot spots were identified during the Pre-Kat phase in shallow waters (westerly black squares) while the Post-Kat 1 hot spot was in deeper waters (single easterly black square as indicated)

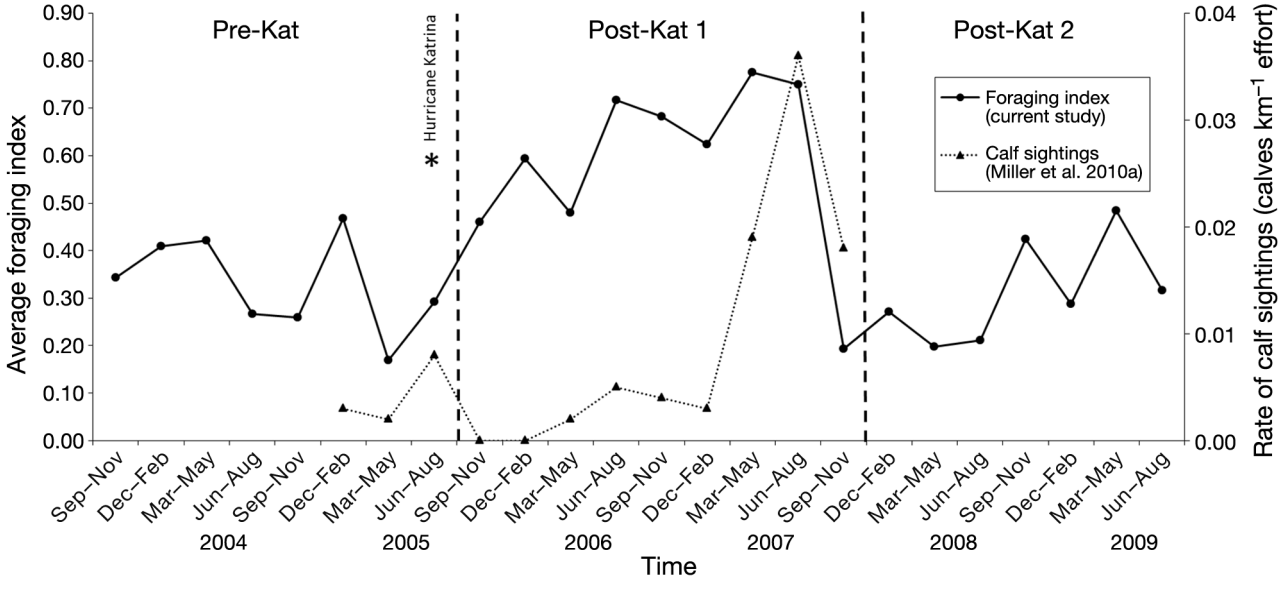

Fig. 6. *Tursiops truncatus*. Changes in average foraging index (●) throughout the study period. Foraging index is the proportion of foraging to non-foraging encounters km^{-1} survey effort. Data from Miller et al. (2010a) (▲) shows increase in dolphin reproductive activity during the increased foraging activity observed in the current study. Dashed vertical lines indicate hurricane phases: Pre-Kat: September 2003–August 2005; Post-Kat 1: October 2005–September 2007; Post-Kat 2: October 2007–September 2009. Note: foraging index data were averaged over 3 mo periods to correspond with the seasons analyzed in Miller et al. (2010a)

the storm likely resulted in increases in abundance of prey. This is supported by the significant negative correlation between foraging indices and the fisheries landings data over the course of the study (see Fig. 3). Furthermore, there was a documented decrease in both the purchase of statewide commercial and residential fishing licenses and in annual fisheries landings specific to Gulfport and Biloxi (National Marine Fisheries Service 2007, Miller et al. 2010a), suggesting a potentially prominent influence on prey availability and/or feeding opportunity in the study area following the hurricane.

Similar effects were seen in Boca Ciega Bay, Florida, where sightings of bottlenose dolphins and calves significantly increased following the 1995 Florida net ban (Eide 1998). Likewise, the observed increase in foraging activity (and decrease in fisheries effort) corresponds to a reported overall increase in dolphin fecundity within the Sound (Miller et al. 2010a; our Fig. 6) following the hurricane, indicating there may have also been an increased need for food consumption. Females in the late stages of pregnancy and lactating females require much higher energy levels for milk production than non-reproductively active adults (Reddy et al. 1991) and therefore consume higher quantities of food during this time (Kastelein et al. 2002). It is unknown whether calf survivorship and/or overall reproductive success of females in the Sound also increased but evidence suggests that there was enough food to at least support a temporary increase in feeding needs. While an increase in observed foraging activities is not always indicative of an increase in prey consumption, there is enough evidence to suggest that this was the case following the hurricane (Post-Kat 1 phase).

In addition to the observed changes in the frequency of foraging encounters following Hurricane Katrina, each of the significant foraging hot spots were concentrated near Cat Island suggesting this area might be a preferred foraging habitat for dolphins. Cetacean distribution patterns are at least partially dependent on habitat features (Gowans & Whitehead 1995, Baumgartner 1997, Davis et al. 1998, Redfern et al. 2006), and these features seem to be clear mechanisms in shaping preferred foraging habitat. For example, bottlenose dolphins near San Diego, California forage in nearshore reefs and kelp beds in a manner that reflects known prey distribution (Hanson & Defran 1993). Likewise, bottlenose dolphins within the Moray Firth, Scotland have displayed seasonal variation for preferred foraging habitat, feeding over deep water and steep seabeds in summer months and moving to more shallow foraging areas during the winter (Hastie et al. 2004). For dolphins in the southeastern United States, most of the literature reports foraging activity that is directly associated with seagrass habitat (see Shane 1990, Waples 1995, Scott et al. 1996, Barros & Wells 1998).

The northern shores of the Mississippi barrier islands were once prevalent with seagrass, with Cat Island having the greatest seagrass coverage and potential seagrass habitat of all the barrier islands within the Sound (Moncreiff 2007). However, seagrasses within the Sound have declined nearly 50% over the last 5 decades due to declining water quality and an increase in turbidity, rather than storm impacts (Moncreiff et al. 1998). In fact, recent evidence suggests that Hurricane Katrina had variable effects on seagrass beds in this region (Anton et al. 2009, Carter et al. 2011). For example, from 2003 through 2007, Cat Island seagrass habitat more than tripled in size, growing from 22 ha to 71 ha (Carter et al. 2011). This growth seems to correspond with the shifts in foraging hot spots we observed at Cat Island; as seagrass extent increased, dolphins shifted their preferred foraging habitats to deeper waters (see Fig. 5). While these results contradict what historic literature reports with respect to preferred seagrass foraging habitat, more recent studies support this suggestion. For example, a fine-scale analysis of foraging habitat near Clearwater, Florida showed coastal bottlenose dolphins not only preferred foraging in natural and dredged channels rather than seagrass habitats, but that these areas had larger and more abundant amounts of pinfish *Lagodon rhomboids*, a preferred prey item (Allen et al. 2001). A similar study also incorporating stomach content data showed that dolphins in Sarasota Bay, Florida also target soniferous prey species that prefer deep water areas as opposed to seagrass habitat (Berens McCabe et al. 2010). Carbon isotope values taken from stranded dolphins in Sarasota Bay following the 1995 Florida net ban had shifted in a manner that was consistent with a decreased use of seagrass habitat; that is, when not in competition with commercial fisheries, coastal bottlenose dolphins exploited prey that were not as dependent on seagrass derived carbon (Rossman et al. 2011).

Similar influences may have been at play in the current study. The increase in foraging behavior following the hurricane also corresponds with the slight shift in foraging hot spots from known seagrass habitat during Pre-Kat (~0.30 to 1.0 m in depth) to a deeper area (~5.0 m in depth) during Post-Kat 1 (Fig. 5). Seagrass habitats can significantly alter the transmission of bioacoustic signals and can provide an acoustic refuge for many smaller and juvenile soniferous prey species (Wilson et al. 2013). Given that bottlenose dolphins use both active and passive acoustic means of locating prey, it may be more energetically costly to target the smaller species inhabiting these areas than the larger prey found in alternative habitats (Gannon et al. 2005, Nowacek 2005). These combined factors may support the growing notion that bottlenose dolphins are selective feeders, rather than opportunistic, preferring a foraging habitat known for larger, soniferous fish species when

prey are likely more abundant (Barros & Wells 1998, Gannon et al. 2005, Berens McCabe et al. 2010, Rossman et al. 2011).

The lack of foraging hot spots and overall decrease in both the total encounters and number of foraging encounters during Post-Kat 2 could be related to several factors. For example, seagrass habitat is indirectly linked to the health of coastal dolphin populations and the degradation of these areas likely elicits shifts in bottlenose dolphin foraging strategies. Recent dredging activities in the main shipping channel between Cat and Ship Islands is thought to have caused substantial erosion along the southern spit and eastern shoreline of Cat Island — which was weakened significantly following Hurricane Katrina — leading to a clockwise rotation of the island's perimeter (the sediments were transported by currents and deposited along the northern and western shorelines of the island; Fritz et al. 2007, Morton 2008) and a potential loss in seagrass habitat. This, combined with increased competition with commercial fisheries — annual landings for Gulfport-Biloxi more than doubled from 2007 to 2008 (National Marine Fisheries Service 2012b) — could explain the overall decrease in foraging encounters and complete lack of foraging hot spots during Post-Kat 2. Furthermore, the later end of the Post-Kat 2 phase is only a few months prior to the start of a widespread and ongoing (as of June 2013) unusual mortality event (UME) for Northern Gulf of Mexico cetaceans, which began in February of 2010 (NOAA Fisheries 2013). Between 1 February and 29 April 2010, 114 cetaceans stranded, a vast majority of which were bottlenose dolphins. Since these strandings took place prior to the response phase for the Deepwater Horizon oil spill, there is evidence suggesting many stressors may have already been acting on Northern Gulf of Mexico dolphin populations prior to the spill. For example, physiological stress from an unusually cold winter in 2010 combined with bacterial infection and depleted food resources are all thought to be responsible for the weakened body condition and poor overall health of stranded bottlenose dolphins during the said UME (Carmichael et al. 2012). The observed decrease in foraging (compared to Post-Kat 1) and lack of hot spots found in the Post-Kat 2 phase may be related and have carried over into the 2010–2012 cetacean UME. Furthermore, one year after the Post-Kat 2 phase (during summer and fall 2010), there were reports of genetic and physiological damage in nearshore fishes and declines in planktivorous fishes, suggesting a reduction in the dolphin prey base following this study (Whitehead et al. 2011, Patterson unpul. data as cited by Carmichael et al. 2012). As such, the present study provides an important baseline to examine how foraging patterns and behavior may have been modified with the UME and Deepwater Horizon oil spill.

Evidence was provided earlier that dolphins may be selective feeders, but little is known about how this may vary between different geographical or behavioral stocks that utilize the study area and subsequently how these interactions might relate to this hot spot analysis. The study area includes 2 of the 6 bay, sound, and estuary management stocks in the Sound and likely overlap with the northern coastal stocks.[2] Inshore and coastal animals may be expected to target different kinds of prey in the same area. For example, Gannon & Waples (2004) found marked differences in the diets of bottlenose dolphins that stranded in estuarine (croaker *Micropogonias undulatus* dominated diets) versus oceanic waters (weakfish *Cynosicon regalis* and squid *Loligo* sp. dominated diets) in North Carolina. Likewise, marked differences in carbon, nitrogen and sulfur isotopic signatures were found between animals stranded in bay, nearshore and offshore waters surrounding Sarasota Bay, Florida (Barros et al. 2010), suggesting differences in targeted trophic levels of prey and in the degree of seagrass dominated habitats utilized between inshore and coastal communities. Similar to other areas in the Gulf (Florida: Irvine et al. 1981, Wells et al. 1987, Barros & Wells 1998, Balmer et al. 2008; Texas: Fertl 1994, Maze & Würsig 1999), a portion of the dolphin population uses the study area on a regular basis, both year-round and seasonally (data from 2004–2007; Mackey 2010). However, it has been estimated that a majority (73.5%) of individuals identified within the study area are transients (Mackey 2010), suggesting this location may be more of a transit area rather than a residential habitat for a closed or semi-closed dolphin population (e.g. Sarasota Bay, Florida: Irvine et al. 1981, Wells et al. 1987). As such, it is possible the Sound may be used as a foraging stopover for migratory and/or seasonal animals, particularly for pregnant or lactating females. More research is needed to examine dynamics between seasonal, resident and transient groups to determine if similar patterns emerged between inshore and coastal communities in the Sound compared to other areas. Stable isotope analyses are becoming more commonly used to dif-

[2]Bottlenose dolphin stock subunits are based largely on geographic features rather than empirical studies (Blaylock & Hoggard 1994, Wade & Angliss 1997)

ferentiate foraging preferences (Walker et al. 1999, Worthy et al. 2011) as well as stock structure (Born et al. 2003, Witteveen et al. 2009) and could be utilized to greatly improve understanding of these dynamics in this area and how they relate to foraging hot spots.

Hurricane Katrina occurred at a time of year when dolphin abundance in the Sound is at its peak and when many coastal animals are expected to be closer inshore (Hubard et al. 2004, Miller et al. 2012). Combined with the subsequent decline in fisheries and vessel activities, there may have been a large disruption in the local group structure and social patterns during that time (e.g. Ansmann et al. 2012). Regardless of any potential short-term impacts on local group dynamics immediately following the hurricane, long-term impacts may be less adverse. For example, dolphin populations utilizing Charlotte Harbor, Florida demonstrated surprising resilience with few long-term changes in population dynamics 2 years following a major hurricane (Bassos-Hull & Wells 2007). Additionally, if dolphins from neighboring areas immigrated into the study area following the hurricane (e.g. Elliser & Herzing 2011), we may have observed an artificial increase in foraging activity. A population increase, however, would likely have been reflected in an increase in group size and/or number of encounters per survey—neither of which were observed in the current study. Moreover, there was no significant increase in the number of new dolphin identifications following the storm (Mackey 2010) and abundance and density estimates in 2007–2008 (Miller et al. 2012) were similar to those many years prior to the storm (Hubard et al. 2004).

We cannot eliminate the possibility of hot spots existing mid-Sound or near Deer or Horn Islands. Survey effort was not evenly distributed throughout the study area since the research focus was on the nearshore waters bordering the barrier islands. Additionally, the survey area was not of consistent size throughout the study given the rotation of Deer and Horn Islands toward the end of the study period. Although the lack of historic seagrass coverage mid-Sound (Moncreiff 2007) makes hot spots in these areas unlikely, Horn Island once had comparable seagrass coverage to that of Cat Island (Moncreiff 2007, Peneva et al. 2008); it is possible that preferred foraging habitat shifted from Cat Island to Horn Island, since Horn Island was surveyed only 3 months during the Post-Kat 2 phase, explaining why we observed fewer overall encounters during Post-Kat 2 than during the Post-Kat 1 phase. To eliminate this possibility in future studies, dedicated mark-recapture surveys should be conducted using transects across the entire Sound—rather than just targeting the barrier islands—ensuring equal effort across the study area.

Bottlenose dolphin foraging habits are dynamic over time, often with changes in both the frequency and distribution of foraging activities likely driven by cumulative effects derived from natural and anthropogenic factors. The temporary cessation of commercial fishing activities as a result of hurricane related damage and debris led to an increase in prey abundance, as evidenced by the increase in foraging encounters. Additionally, the spatial shifts in preferred foraging areas during this time support the growing theory that bottlenose dolphins are selective feeders. The data and subsequent results presented here were derived from surveys that were not designed with the objectives of the current study in mind, and although the post-hoc nature of the study warranted relatively high conservative thresholds for hot spot identification, this method should be considered by future researchers when identifying areas of concentrated usage by marine mammals. Furthermore, few published data regarding past environmental variables relative to the Mississippi Sound ecology were available during the course of the study. Future surveys that incorporate systematic prey sampling, bathymetry, hypoxia conditions and seagrass extents, as well as better knowledge of bottlenose dolphin stock structures in the area, can close past data gaps and better address the conclusions presented here. Finally, this study presents important baseline information on the foraging behavior of bottlenose dolphins within Mississippi Sound that can be applied to future studies on the effects of the Deepwater Horizon oil spill. This event, contrary to Hurricane Katrina, likely caused long-term adverse effects within Mississippi Sound, and should galvanize future research examining the impacts of both natural and anthropogenic catastrophic events, as well as those cumulative factors discussed here and their role in impacts on marine mammal populations.

Acknowledgements. We thank the students, interns, and volunteers at the Marine Mammal Behavior and Cognition Laboratory at the University of Southern Mississippi and personnel of the Institute for Marine Mammal Studies for their assistance in data collection. A. Azzara, K. Goetz, B. Kar, and S. McBride, as well as 3 anonymous reviewers offered helpful comments and insight in developing this manuscript. Funding for this project was supported in part by the Dolphin Communication Fund at the University of Southern Mississippi and by grants from the Department of Commerce and the Institute for Marine Mammal Studies. All research efforts were conducted under permit #1041-1701 through the National Marine Fisheries Service.

LITERATURE CITED

Aguilar Soto NA, Johnson M, Madsen PT, Tyack PL, Bocconcelli A, Borsani JF (2006) Does intense ship noise disrupt foraging in deep-diving Cuvier's beaked whales (*Ziphius cavirostris*)? Mar Mamm Sci 22:690–699

Allen MC, Read AJ, Gaudet J, Sayigh LS (2001) Fine-scale habitat selection of foraging bottlenose dolphins *Tursiops truncatus* near Clearwater, Florida. Mar Ecol Prog Ser 222:253–264

Allison MA, Sheremet A, Goni MA, Stone GW (2005) Storm layer deposition on the Mississippi-Atchafalaya subaqueous delta generated by Hurricane Lili in 2002. Cont Shelf Res 25:2213–2232

Altmann J (1974) Observational study of behavior: sampling methods. Behaviour 49:227–267

Ansmann IC, Parra GJ, Chilvers BL, Lanyon JM (2012) Dolphins restructure social system after reduction of commercial fisheries. Anim Behav 84:575–581

Anton A, Cebrian J, Duarte CM, Heck KL Jr, Goff J (2009) Low impact of Hurricane Katrina on seagrass community structure and functioning in the northern Gulf of Mexico. Bull Mar Sci 85:45–59

Ashe E, Noren DP, Williams R (2010) Animal behaviour and marine protected areas: incorporating behavioural data into the selection of marine protected areas for an endangered killer whale population. Anim Conserv 13:196–203

Balmer BC, Wells RS, Nowacek SM, Nowacek DP, Schwacke LH, McLellan WA, Scharf FS (2008) Seasonal abundance and distribution patterns of common bottlenose dolphins (*Tursiops truncatus*) near St. Joseph Bay, Florida, USA. J Cetacean Res Manag 10:157–167

Barros NB, Odell DK (1990) Food habits of bottlenose dolphins in the southeastern United States. In: Leatherwood S, Reeves RR (eds) The bottlenose dolphin. Academic Press, San Diego, CA, p 309–328

Barros N, Wells R (1998) Prey and feeding patterns of resident bottlenose dolphins (*Tursiops truncatus*) in Sarasota Bay, Florida. J Mammal 79:1045–1059

Barros NB, Ostrom PH, Stricker CA, Wells RS (2010) Stable isotopes differentiate bottlenose dolphins off west-central Florida. Mar Mamm Sci 26:324–336

Bassos-Hull K, Wells R (2007) Investigating potential hurricane and red tide related impacts on bottlenose dolphin (*Tursiops truncatus*) abundance, reproductive rates, distribution, and site fidelity in Charlotte Harbor and Pine Island Sound, Florida. Mote Marine Laboratory Tech Rep #1231, Sarasota, FL

Baumgartner MF (1997) The distribution of Risso's dolphin (*Grampus griseus*) with respect to the physiography of the northern Gulf of Mexico. Mar Mamm Sci 13:614–638

Benson NG (1982) Life history requirements of selected finfish and shellfish in Mississippi Sound and adjacent areas. FWS/OBS-81/51, US Fish & Wildlife Service, Washington, DC

Berens McCabe EJ, Gannon DP, Barros NB, Wells RS (2010) Prey selection in a resident common bottlenose dolphin (*Tursiops truncatus*) community in Sarasota Bay, Florida. Mar Biol 157:931–942

Blake ES, Rappaport EN, Landsea CW (2007) The deadliest, costliest, and most intense United States tropical cyclones from 1851 to 2006 (and other frequently requested hurricane facts). NOAA Tech Mem NWS TPC-5

Blaylock RA, Hoggard W (1994) Preliminary estimates of bottlenose dolphin abundance in southern US Atlantic and Gulf of Mexico continental shelf waters. NOAA Tech Mem NMFS-SEFSC-356

Born EW, Outridge P, Riget FF, Hobson KA, Dietz R, Øien N, Haug T (2003) Population substructure of North Atlantic minke whales (*Balaenoptera acutorostrata*) inferred from regional variation of elemental and stable isotopic signatures in tissues. J Mar Syst 43:1–17

Burkholder J, Eggleston D, Glasgow H, Brownie C and others (2004) Comparative impacts of two major hurricane seasons on the Neuse River and western Pamlico Sound ecosystems. Proc Natl Acad Sci USA 101:9291–9296

Carmichael RH, Graham WM, Aven A, Worthy G, Howden S (2012) Were multiple stressors a 'perfect storm' for Northern Gulf of Mexico bottlenose dolphins (*Tursiops truncatus*) in 2011? PLoS ONE 7:e41155

Carter GA, Lucas KL, Biber PD, Criss GA, Blossom GA (2011) Historical changes in seagrass coverage on the Mississippi barrier islands, northern Gulf of Mexico, determined from vertical aerial imagery (1940-2007). Geocarto Int 26:663–673

Connell JH (1978) Diversity in tropical rain forests and coral reefs. Science 199:1302–1310

Davis RW, Fargion GS, May N, Leming TD and others (1998) Physical habitat of cetaceans along the continental slope in the north central and western Gulf of Mexico. Mar Mamm Sci 14:490–507

Dreyer J, Bailey-Brock JH, McCarthy SA (2005) The immediate effects of Hurricane Iniki on intertidal fauna on the south shore of O'ahu. Mar Environ Res 59:367–380

Eide SD (1998) Correlations between bottlenose dolphin (*Tursiops truncatus*) distribution and presence of calves in Boca Ciega Bay, Florida and the Florida state ban on commercial netting. BSc thesis, Eckerd College, St. Petersburg, FL

Elliser CR, Herzing DL (2011) Replacement dolphins? Social restructuring of a resident pod of Atlantic bottlenose dolphins, *Tursiops truncatus*, after two major hurricanes. Mar Mamm Sci 27:39–59

ESRI ArcGIS Resource Center (2011a) Hot spot analysis (Getis-Ord Gi*) (spatial statistics). Available at: http://help.arcgis.com/en/arcgisdesktop/10.0/help/index.html#/Hot_Spot_Analysis_Getis_Ord_Gi/005p00000010000000/ (accessed 6 June 2011)

ESRI ArcGIS Resource Center (2011b) Supplementary spatial statistics toolbox for ArcGIS 10. Available at: http://resources.arcgis.com/gallery/file/geoprocessing/details?entryID=8E548CF9-1422-2418-8855-2ED418793771 (accessed 5 October 2011)

ESRI ArcGIS Resource Center (2011c) Generate spatial weights matrix (spatial statistics). Available at: http://help.arcgis.com/en/arcgisdesktop/10.0/help/index.html#//005p00000020000000 (accessed 13 October 2011)

Fertl D (1994) Occurrence patterns and behavior of bottlenose dolphins (*Tursiops truncatus*) in the Galveston ship channel, Texas. Tex J Sci 46:299–318

Fritz HM, Blount C, Sokoloski R, Singleton J and others (2007) Hurricane Katrina storm surge distribution and field observations on the Mississippi barrier islands. Estuar Coast Shelf Sci 74:12–20

Gannon DP, Waples DM (2004) Diets of coastal bottlenose dolphins from the US mid-Atlantic coast differ by habitat. Mar Mamm Sci 20:527–545

Gannon DP, Barros NB, Nowacek DP, Read AJ, Waples DM, Wells RS (2005) Prey detection by bottlenose dolphins (*Tursiops truncatus*): an experimental test of the passive listening hypothesis. Anim Behav 69: 709–720

Getis A, Ord JK (1992) The analysis of spatial association by use of distance statistics. Geogr Anal 24:189–206

Gowans S, Whitehead H (1995) Distribution and habitat partitioning by small odontocetes in the Gully, a submarine canyon on the Scotian shelf. Can J Zool 73:1599–1608

Hanson MT, Defran RH (1993) The behaviour and feeding ecology of the Pacific coast bottlenose dolphin, *Tursiops truncatus.* Aquat Mamm 19:127–142

Hastie GD, Wilson B, Wilson LJ, Parsons KM, Thompson PM (2004) Functional mechanisms underlying cetacean distribution patterns: hot spots for bottlenose dolphins are linked to foraging. Mar Biol 144:397–403

Heinsohn GE, Spain AV (1974) Effects of a tropical cyclone on littoral and sub-littoral biotic communities and on a population of dugongs (*Dugong dugon* (Müller)). Biol Conserv 6:143–152

Hubard C, Maze-Foley K, Mullin K, Schroeder W (2004) Seasonal abundance and site fidelity of bottlenose dolphins (*Tursiops truncatus*) in Mississippi Sound. Aquat Mamm 30:299–310

Irvine AB, Scott MD, Wells RS, Kaufmann JH (1981) Movements and activities of the Atlantic bottlenose dolphin, *Tursiops truncatus*, near Sarasota, Florida. Fish Bull 79: 671–688

Kastelein RA, Vaughan N, Walton S, Wiepkema PR (2002) Food intake and body measurements of Atlantic bottlenose dolphins (*Tursiops truncates*) in captivity. Mar Environ Res 53:199–218

Langtimm CA, Krohn MD, Reid JP, Stith BM, Beck CA (2006) Possible effects of the 2004 and 2005 hurricanes on manatee survival rates and movement. Estuaries Coasts 29:1026–1032

Leatherwood S (1975) Some observations of feeding behavior of bottlenosed dolphins (*Tursiops truncatus*) in the northern Gulf of Mexico and (*Tursiops* cf. *T. gilli*) off southern California, Baja California, and Nayarit, Mexico. Mar Fish Rev 37:10–16

Love MR, Amante CJ, Eakins BW, Taylor LA (2012) Digital elevation models of the northern Gulf coast: procedures, data sources and analysis. NOAA Tech Mem NESDIS NGDC-59

Lusseau D, Bain DE, Williams R, Smith JC (2009) Vessel traffic disrupts the foraging behavior of southern resident killer whales *Orcinus orca.* Endang Species Res 6:211–221

Mackey AD (2010) Site fidelity and association patterns of bottlenose dolphins (*Tursiops truncatus*) in the Mississippi Sound. MA thesis, University of Southern Mississippi, Hattiesburg, MS

Mann J (1999) Behavioral sampling methods for cetaceans: a review and critique. Mar Mamm Sci 15:102–122

Marsh H (1989) Mass stranding of dugongs by a tropical cyclone in northern Australia. Mar Mamm Sci 5:78–84

Maze KS, Würsig B (1999) Bottlenose dolphins of San Luis Pass, Texas: occurrence patterns, site-fidelity, and habitat use. Aquat Mamm 25:91–104

Mignucci-Giannoni AA, Toyos-González GM, Pérez-Padilla J, Rodríguez-López MA, Overing J (1999) Mass stranding of pygmy killer whales (*Feresa attenuata*) in the British Virgin Islands. J Mar Biol Assoc UK 79:383–384

Miller LJ, Solangi M, Kuczaj SA (2008) Immediate response of Atlantic bottlenose dolphins to high-speed personal watercraft in the Mississippi Sound. J Mar Biol Assoc UK 88:1139–1143

Miller LJ, Mackey AD, Hoffland T, Solangi M, Kuczaj SA II (2010a) Potential effects of a major hurricane on Atlantic bottlenose dolphin (*Tursiops truncatus*) reproduction in the Mississippi Sound. Mar Mamm Sci 26:707–715

Miller LJ, Solangi M, Kuczaj SA II (2010b) Seasonal and diurnal patterns of behavior exhibited by Atlantic bottlenose dolphins (*Tursiops truncatus*) in the Mississippi Sound. Ethology 116:1127–1137

Miller LJ, Mackey AD, Solangi M, Kuczaj SA II (2012) Population abundance and habitat utilization of bottlenose dolphins in the Mississippi Sound. Aquat Conserv, doi: 10.1002/aqc.2278

Mitchell A (2009) The ESRI guide to GIS analysis, Vol 2: spatial measurements and statistics. ESRI Press, Redlands, CA

Moncreiff CA (2007) Mississippi Sound and the Gulf Islands. In: Handley L, Altsman D, DeMay R (eds) Seagrass status and trends in the northern Gulf of Mexico: 1940-2002. USGS Scientific Investigations Report 2006–5287, p 76–85

Moncreiff CA, Randall TA, Caldwell JD (1998) Mapping of seagrass resources in Mississippi Sound: final report. Dept Mar Res, Gulf Coast Res Lab Project #BY3-156-3238, Biloxi, MS

Morton RA (2008) Historical changes in the Mississippi-Alabama barrier-island chain and the roles of extreme storms, sea level, and human activities. J Coast Res 24: 1587–1600

Mullin KD (1988) Comparative seasonal abundance and ecology of bottlenose dolphins (*Tursiops truncatus*) in three habitats of the North-Central Gulf of Mexico. PhD dissertation, Mississippi State University, Starkville, MS

National Marine Fisheries Service (2007) Report to Congress on the impacts of Hurricanes Katrina, Rita, and Wilma on Alabama, Louisiana, Florida, Mississippi, and Texas Fisheries. NOAA, Silver Spring, MD

National Marine Fisheries Service (2012a) Monthly commercial landing statistics. Available at: www.st.nmfs.noaa.gov/commercial-fisheries/commercial-landings/monthly-landings/index (accessed 29 December 2012)

National Marine Fisheries Service (2012b) Total commercial fishery landings at an individual US port for all years after 1980. Available at www.st.nmfs.noaa.gov/st1/commercial/landings/lport_hist.html (accessed 14 April 2012)

NOAA Fisheries (2013) 2010-2013 cetacean unusual mortality event in northern Gulf of Mexico. Available at www.nmfs.noaa.gov/pr/health/mmume/cetacean_gulfofmexico2010.htm (accessed 27 June 2013)

Nowacek DP (2005) Acoustic ecology of foraging bottlenose dolphins (*Tursiops truncatus*), habitat-specific use of three sound types. Mar Mamm Sci 21:587–602

Peneva E, Griffith JA, Carter GA (2008) Seagrass mapping in the northern Gulf of Mexico using airborne hyperspectral imagery: a comparison of classification methods. J Coast Res 24:850–856

Preen AR, Marsh H (1995) Response of dugongs to large-scale loss of seagrass from Hervey Bay, Queensland, Australia. Wildl Res 22:507–519

Quinn GP, Keough MJ (2002) Experimental design and data analysis for biologists. Cambridge University Press, Cambridge

Reddy M, Kamolnik T, Skaar D, Curry C, Ridgway S (1991) Bottlenose dolphins: energy consumption during pregnancy, lactation, and growth. Proc 1991 Int Mar Anim Trainers Assoc Conf, Vallejo, CA, p 30–37

Redfern JV, Ferguson MC, Becker EA, Hyrenbach KD and others (2006) Techniques for cetacean–habitat modeling. Mar Ecol Prog Ser 310:271–295

Rosel PE, Watts H (2008) Hurricane impacts on bottlenose dolphins in the northern Gulf of Mexico. Gulf Mex Sci 1: 88–94

Rossman S, Barros NB, Stricker CA, Gandhi H, Ostrom PH, Wells RS (2011) Foraging ecology of bottlenose dolphins: a stable isotopic reconstruction over six decades docu-

ments anthropogenic disturbance. 19th Bienn Conf Biol Mar Mamm. Society for Marine Mammalogy, Tampa, FL, p 258 (Abstract)
Scott MD, Wells RS, Irvine AB (1996) Long-term studies of bottlenose dolphins in Florida. IBI Rep 6:73–81
Shane SH (1990) Behavior and ecology of the bottlenose dolphin at Sanibel Island, Florida. In: Leatherwood S, Reeves RR (eds) The bottlenose dolphin. Academic Press, San Diego, CA, p 245–265
Stevens PW, Blewett DA, Casey JP (2006) Short-term effects of a low dissolved oxygen event on estuarine fish assemblages following the passage of Hurricane Charley. Estuaries Coasts 29:997–1003
Tomasko DA, Anastasiou C, Kovach C (2006) Dissolved oxygen dynamics in Charlotte Harbor and its contributing watershed, in response to hurricanes Charley, Frances, and Jeanne—impacts and recovery. Estuaries Coasts 29: 932–938
Wade PR, Angliss RP (1997) Guidelines for assessing marine mammal stocks: Report of the GAMMS workshop, April 3-5, 1996, Seattle, WA. NOAA Tech Mem NMFS-OPR-12
Walker JL, Potter CW, Macko SA (1999) The diets of modern and historic bottlenose dolphin populations reflected through stable isotopes. Mar Mamm Sci 15:335–350
Waples DM (1995) Activity budgets of free-ranging bottlenose dolphins (*Tursiops truncatus*) in Sarasota Bay, Florida. MSc thesis, University of California, Santa Cruz, CA
Wells RS, Scott MD, Irvine BA (1987) The social structure of free-ranging bottlenose dolphins. In: Genoways H (ed) Current mammalogy, Vol 1. Plenum Press, New York, NY, p 247–305
Whitehead A, Dubansky B, Bodinier C, Garcia TI and others (2011) Genomic and physiological footprint of the Deepwater Horizon oil spill on resident marsh fishes. Proc Natl Acad Sci USA 108:6193–6198
Wilson CJ, Wilson PS, Greene CA, Dunton KH (2013) Seagrass meadows provide an acoustic refuge for estuarine fish. Mar Ecol Prog Ser 472:117–127
Witteveen BH, Worthy GAJ, Wynne KM, Roth JD (2009) Population structure of North Pacific humpback whales on their feeding grounds revealed by stable carbon and nitrogen isotope ratios. Mar Ecol Prog Ser 379:299–310
Worthy GAJ, Worthy TAM, Browning N (2011) Seasonal variability in the trophic ecology of bottlenose dolphins and their potential prey in the Indian River Lagoon, FL. Final Report to Harbor Branch Oceanographic Institute for Project Number HBOI PO 0012407
Würsig B (1986) Delphinid foraging strategies. In: Schusterman R, Thomas J, Wood FG (eds) Dolphin cognition and behavior: a comparative approach. Lawrence Erlbaum Associates, Hillsdale, NJ, p 347–359

Appendix 1. Sightings km^{-1} effort analyzed: temporal splits used in spatial analysis

Temporal split	Example	Number of files analyzed
All data	All data files (no splits)	1
Overall by year	2003 (all data), 2004 (all data), etc.	7
Overall by month	January all years, February all years, etc.	12
Overall by season	Summer (all years), winter (all years)	2
Overall by season year	Summer 2003, summer 2004, etc.	14
Overall pre-Kat	All data pre-Katrina	1
Overall post-Kat	All data post-Katrina	1
Pre-Kat by month	'January' for all years before Katrina	12
Post-Kat by month	'January' for all years post-Katrina	12
Pre-Kat by season	Winter for all files before Katrina	2
Post-Kat by season	Winter for all files post-Katrina	2

Appendix 2. Survey effort (km) for each of the islands, calculated within the 1 km buffer zone (see Fig. 1). Note: tracks also occurred outside of the buffer zone

Island	Pre-Kat	Post-Kat 1	Post-Kat 2	Total
Cat	1515.92	784.66	637.13	2937.71
Ship	1174.56	882.04	782.31	2838.91
Horn	122.56	545.27	716.02	1383.85
Deer	14.44	12.60	27.31	54.35
Petit Bois	35.96	0	0	35.96
Total	2863.44	2224.57	2162.77	

Submitted: July 2, 2012; Accepted: April 12, 2013 *Proofs received from author(s): June 30, 2013*

Vol. 487: 245–260, 2013
doi: 10.3354/meps10217

MARINE ECOLOGY PROGRESS SERIES
Mar Ecol Prog Ser

Published July 30

Contribution to the Theme Section 'Biophysical coupling of marine hotspots'

FREE ACCESS

Role of environmental seasonality in the turnover of a cetacean community in the southwestern Gulf of California

Mario A. Pardo[1,5,*], Norman Silverberg[1], Diane Gendron[1], Emilio Beier[2], Daniel M. Palacios[3,4]

[1]Centro Interdisciplinario de Ciencias Marinas, Instituto Politécnico Nacional, La Paz, Baja California Sur 23096, Mexico

[2]Centro de Investigación Científica y de Educación Superior de Ensenada - Unidad La Paz, La Paz, Baja California Sur 23050, Mexico

[3]Cooperative Institute for Marine Ecosystems and Climate, Institute of Marine Sciences, Division of Physical and Biological Sciences, University of California, Santa Cruz, California 95060, USA

[4]NOAA, NMFS, Southwest Fisheries Science Center, Environmental Research Division, Pacific Grove, California 93950-2097, USA

[5]*Present address:* Posgrado en Ciencias del Mar y Limnología, Universidad Nacional Autónoma de México, Distrito Federal 04510, Mexico

ABSTRACT: La Paz Bay is a distinct region within the Gulf of California whose rich cetacean community exhibits an intense annual overturn. We studied the environmental conditions that could drive this change over the course of a year. Cetacean biomass was estimated from monthly surveys, with concurrent collection of water-column measurements of temperature, salinity, nutrients, chlorophyll *a* (chl *a*), and biogenic matter fluxes. The water-column structure showed 3 major conditions: deep mixing during winter, stratified isopycnal shoaling in spring and early summer, and deep stratification during late summer and autumn. Chl *a* and relative fluxes of biogenic silica and calcium carbonate indicated a seasonal succession of primary producers in response to the observed evolution of hydrography. During the periods of mixing and isopycnal shoaling, the bay provided suitable habitat for blue whales, bottlenose dolphins, and common dolphins, while fin whales, Bryde's whales, and short-finned pilot whales were numerically dominant during the period of stratification. To provide a regional context to the observed seasonality, we fitted temporal least-squares to an 11 yr monthly time series of satellite-derived wind, sea surface temperature (SST), and chlorophyll concentration (CHL). Within the bay, the SST followed the annual monsoonal shift in the wind, whereas CHL showed a bi-modal pattern, with a main peak occurring under mixing conditions in winter and a second peak under isopycnal shoaling in spring/early summer. The regional fitting suggested that the latter period was driven by a localized intra-seasonal phenomenon that could be responsible for the higher biological richness of the bay compared to the surrounding gulf.

KEY WORDS: Ecological succession · Seasonal variability · Nutrient supply · Stratification · Biogenic matter fluxes · Trophic levels · Marine hotspots

INTRODUCTION

Biological hotspots in the epipelagic zone have been described as areas where dynamic processes in the physical environment lead to enhanced productivity and aggregation of consumers relative to their surroundings (Palacios et al. 2006). In these areas, upwelling, mesoscale eddies, and fronts may act in concert with the local geomorphology to generate conditions that greatly promote the availability of

*Email: m.pardo@comunidad.unam.mx

prey for large fauna (e.g. Wingfield et al. 2011). Although these hotspots are often detectable through remote sensing of the ocean's surface, other areas that appear oligotrophic and devoid of dynamic features at the surface may also attract large feeding predators and even influence their migration patterns (e.g. Domeier et al. 2012). In such areas, the biological production maxima may be in the subsurface in the presence of a deep/sharp thermocline, underscoring the importance of measuring hydrographic and biological parameters, both at the surface and in the water column, for the characterization of biological hotspots.

The most productive areas of the Gulf of California (hereafter 'the gulf'; Fig. 1) are located along its eastern (continental) side and in the northern region due to winter upwelling and tidal mixing, respectively (Lluch-Cota 2000). The southwestern gulf (peninsular side) is comparatively less productive, except for La Paz Bay (hereafter 'the bay'), whose photosynthetic pigment concentrations remain high year-round compared to its surroundings, constituting an isolated spot of high phytoplankton biomass (Santamaria-del-Angel et al. 1994, Luch-Cota & Teniza-Guillén 2000, Kahru et al. 2004). The bay sustains a diverse megafauna that includes at least 16 cetacean species of temperate, tropical, and subtropical affinities (Flores-Ramírez et al. 1996, Salvadeo et al. 2009). It also hosts a growing colony of California sea lions *Zalophus californianus* (Szteren et al. 2006) and is visited by whale sharks *Rhincodon typus* and spinetail devil rays *Mobula japanica*, which arrive in winter, spring, and early summer to feed on zooplankton (Clark & Nelson 1997, Ketchum-Mejía 2003, Croll et al. 2012). The rich cetacean community exhibits a strong annual overturn, with migratory species such as blue whales *Balaenoptera musculus* and humpback whales *Megaptera novaeangliae* occurring in winter and spring, whereas species with more tropical affinities, like Bryde's whales *Balaenoptera edeni*, bottlenose dolphins *Tursiops truncatus*, and short-finned pilot whales *Globicephala macrorhynchus*, occur mostly during the summer and autumn. Fin whales *Balaenoptera physalus* are resident in the gulf and, together with the common dolphins *Delphinus* spp. occur year-round (Flores-Ramírez et al. 1996, Salvadeo et al. 2009). The hydrographic conditions that support this cetacean diversity and underlie the species' replacement have not been studied.

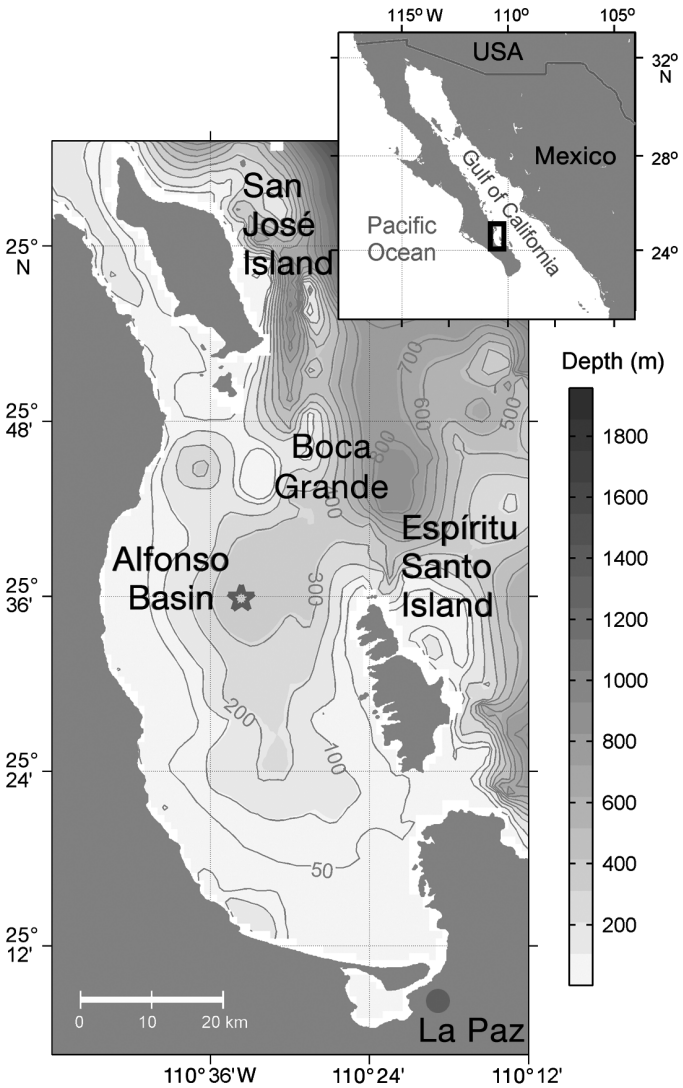

Fig. 1. La Paz Bay, in the southwestern Gulf of California (inset). The gray star in the main panel indicates the position of the oceanographic station and the site of the sediment trap in the deepest part of the bay (~410 m)

In the present study, we posit that seasonal forcing of oceanographic conditions in the bay, including surface mixing driven by northwesterly winds in winter (Badan-Dangon et al. 1991) and cyclonic circulation in summer (Monreal-Gómez et al. 2001, Sánchez-Velasco et al. 2006), lead to enhanced nutrient supply to the base of the food web, attracting low trophic level prey for planktivorous and piscivorous cetaceans. Warmer conditions in summer would, in turn, be favorable for the aggregation of higher trophic level prey looking for a suitable habitat to spawn near the coast (e.g. Staaf et al. 2008), attracting teutophagous cetaceans. To assess the specific hydrographic and biological conditions underlying species' replacement in the cetacean community of the bay, we make use of water-column data collected as part of a multidisciplinary time-series investigation, aimed at examining monthly changes in physical structure, nutrient and chlorophyll *a* (chl *a*) con-

centrations, vertical fluxes of biogenic matter, and cetacean biomasses over the course of a year. The results are put in a regional context (i.e. the southwestern gulf) using time series of remotely sensed (satellite) measurements of surface wind, temperature (SST), and chlorophyll concentration (CHL).

Although direct measurements of the prey field would have probably enhanced our understanding of the relationships between cetaceans and the dynamics of their physical habitat in the bay, collection of such data was not possible due to logistical and financial constraints. Indeed, quantitative and comprehensive assessments of the intermediate trophic levels in the southwestern gulf are lacking. However, considering that most cetacean species must constantly search for food due to their high energetic needs (Trites et al. 1997, Barlow et al. 2008), we interpret their occurrence in the bay, at least in part, as a response to the prey availability, which is in turn aggregated by suitable physical and biological mechanisms. Further, the evolutionary and ecological adaptations of cetaceans to exploit specific types of prey, such as zooplankton, small pelagic fish, or squid (Pauly et al. 1998), facilitate such interpretation. This argument has been widely used to characterize cetacean habitats (e.g. Au & Perryman 1985, Hamazaki 2002, Doniol-Valcroze et al. 2007, Praca et al. 2009) as well as to model cetacean abundance as a function of predominant environmental conditions (e.g. Becker et al. 2010, 2012, Gerrodette & Eguchi 2011, Forney et al. 2012), even when there is no direct measurement of the potential prey.

MATERIALS AND METHODS

Study area

La Paz Bay is the largest and deepest embayment in the Gulf of California (Fig. 1), with an area of ~2160 km^2 and a maximum depth of ~410 m. Water exchange with the surrounding gulf occurs mainly through the northern channel, called Boca Grande (Salinas-González et al. 2003, Obeso-Nieblas et al. 2004). The bay lies within a tropical-subtropical transition zone that seasonally alternates between 2 well-defined periods as a result of the monsoonal regime that dominates the entire gulf. The temperate season, from November to April (winter to spring), is dominated by strong northwesterly winds that enhance evaporation and increase the surface salinity, which induces deep vertical convection (i.e. sinking). More moderate southwesterly winds blow during the warm season, from May to October (summer to autumn). During this period, the water column receives the influence of tropical waters, the thermocline deepens, and the upper layer stratifies (Badan-Dangon et al. 1991, Adams & Comrie 1997, Bordoni et al. 2004).

Hydrographic and biological conditions

The changes in the physical structure of the water column and their influence on the base of the food web, through nutrient supply, help us to identify the predominant ecological conditions that attract different cetacean species at different times of the year. A number of physical, chemical, and biological variables were measured at an oceanographic station located over the deepest part of the bay (~410 m; Fig. 1). Between 17 February 2007 and 18 February 2008, 13 CTD profiles were taken to depths ranging from 50 to 340 m. Temperature, salinity, and density data were standardized to 1 m depth means. From these values, we computed the Brunt-Väisälä frequency (cycles h^{-1}; also known as buoyancy frequency), a measure of the degree of stratification (Wahl & Teague 1983). The depth of maximum buoyancy frequency in a profile corresponds to the depth of the pycnocline. At the same site, 13 profiles of Niskin-bottle samples were taken at discrete depths according to 6 levels of light penetration (0.1, 1, 10, 33, 55, and 100%) estimated from Secchi disc measurements following the Beer-Bourguer-Lambert law (Walker 1982, Bustillos-Guzmán & Lechuga-Devéze 1989). Concentrations of dissolved silica (H_2SiO_4), phosphate (PO_4^{-3}), and total dissolved inorganic nitrogen (NO_2^-+NO_3^-+NH_4^-) were measured from these samples (Strickland & Parsons 1972), as well as the concentration of chl *a* (Ritchie 2008). Since measurements were taken at different times and in some cases different depth levels, we performed an objective interpolation of these variables using a Gaussian weighting function (Jalickee & Hamilton 1977, Boyer et al. 2005) with 30 d horizontal and 1 m vertical scales to represent the temporal evolution. All data were truncated below 100 m depth since preliminary evaluation of the results showed that most of the variability was concentrated above that level.

Biogenic matter fluxes

The sinking particulate matter is indicative of the nature of biogenic components and thus the ecological succession taking place in the upper layers

(Bishop 1988, Silver & Gowing 1991, Silverberg et al. 2006), which could trigger the incursion of different cetacean species according to their feeding requirements. We analyzed samples from a Technicap® PPS 3/3 trap of 0.125 m^2 aperture, which was anchored and suspended at ~310 m depth at the same site as the oceanographic measurements (Fig. 1). The sinking matter was collected in separate bottles during 7 to 15 d periods each and then fixed with a preservative solution of 4% buffered formaldehyde saturated with sodium tetraborate. The total mass flux, in g m^{-2} d^{-1}, was estimated from 4 sub-samples, which were centrifuged for 25 min at 3000 rpm (~1600 × *g*), decanted, and washed with distilled water. The collected material was weighed after a 72 h drying period at ~50°C. The lithogenic fraction of the total flux was subtracted since our interest was only related to the biological processes. From the total biogenic fractions, we analyzed the proportions of biogenic silica, or opal ($SiO_2 \cdot nH_2O$), and calcium carbonate ($CaCO_3$).

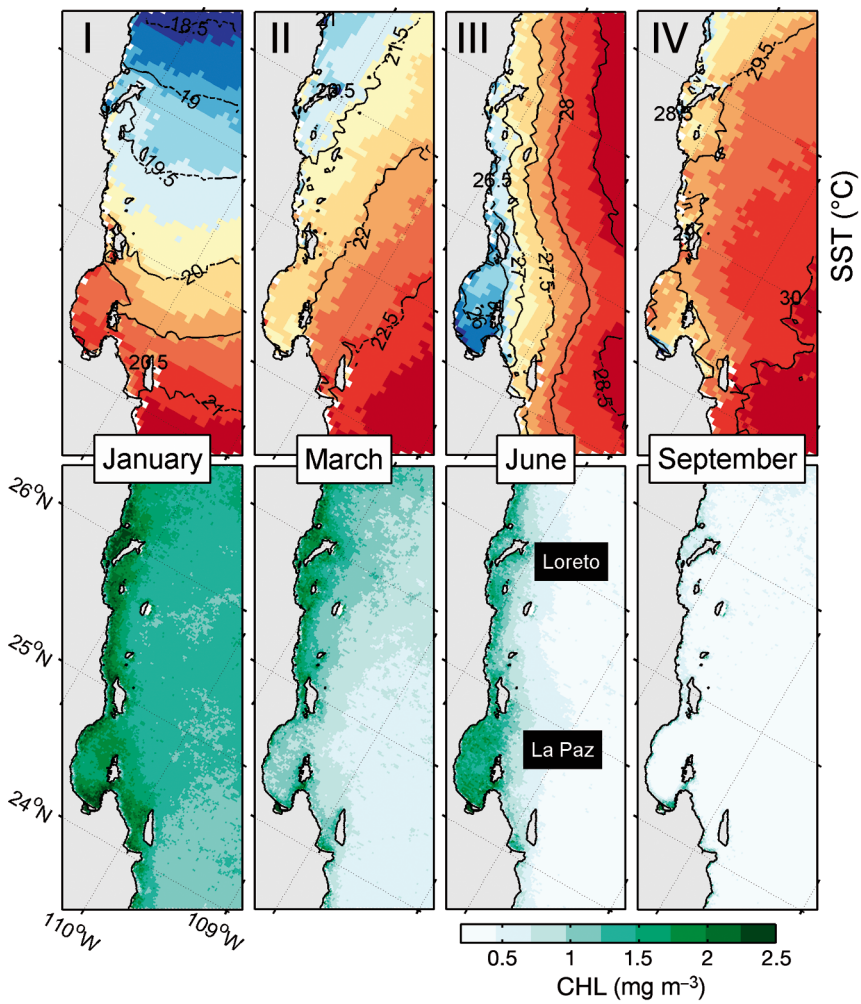

Fig. 2. Spatial representation of the 11 yr seasonal least-squares fits of sea surface temperature (SST; upper panels; in a variable color scale to highlight spatial gradients) and chlorophyll concentration (CHL; lower panels; same color scale among panels) for the southwestern Gulf of California. The periods shown were chosen following the maximum and minimum CHL values of the seasonal least-squares fit within La Paz Bay, which are denoted here and in Fig. 7 as I, II, III, and IV

Local and regional seasonality

Because of their great mobility, the incursions of different cetacean species into the bay could be the result of both local and/or regional conditions. Therefore, it was important to address the larger spatial context in which the hydrographic and biological conditions within the bay occur. Also, since the small sample sizes yielded by the present study (14 monthly data points) prevented us from quantitatively correlating cetacean densities to the monthly evolution of the water column within the bay, it was important to compare those conditions to longer time series of surface variables and put them in the spatial context of the southwestern gulf. We therefore characterized the seasonality of the entire region, from north of Loreto Bay to south of La Paz Bay (Fig. 2), using an 11 yr time series of remotely sensed SST and CHL as proxies for the physical and biological environment. The monthly CHL data came from the Sea-viewing Wide Field-of-view Sensor (SeaWiFS) aboard the satellite Orbview-2 (O'Reilly et al. 1998, 2000, Hooker & McClain 2000), with a pixel resolution of 1.39 km. The monthly SST data came from the Advanced Very High Resolution Radiometer (AVHRR) aboard NOAA satellites (Program Pathfinder 5.0; Walton et al. 1998, Casey & Cornillon 1999, Kilpatrick et al. 2001), with a spatial resolution of 4.89 km. Additionally, we used the monthly wind velocity data from the SeaWinds sensor aboard the NASA satellite QuikSCAT (Freilich 2000). Due to the coarser spatial resolution of this product (13.9 km), only the measurement point closest to the bay was used to compute the local seasonality since the other available nearby points were on land or too far from the bay. All remotely sensed vari-

ables were obtained through the Environmental Research Division's Data Access Program of NOAA, NMFS, Southwest Fisheries Science Center (http://coastwatch.pfeg.noaa.gov/erddap/index.html). A spatially explicit characterization of the seasonal cycle of the southwestern gulf (Fig. 2) was done by fitting temporal least-squares with annual and semi-annual harmonics (Emery & Thomson 1998, Ripa 2002) to the remotely sensed variables. Within the polygon of the bay (see map in Fig. 3), the temporal behavior of each variable was calculated using the same analyses, applied to the mean of all monthly values. The periods of maxima and minima resulting from the local (i.e. within the bay) CHL seasonal analysis were chosen to portray the results of the regional (i.e. southwestern gulf) analysis of SST and CHL (Fig. 2).

Cetacean population density

We conducted monthly visual surveys within the bay over a systematic zig-zag arrangement of transects (Fig. 3) aboard the 28 ft (8.5 m) RV 'CICIMAR XV' at ~18 km h^{-1} between 6 February 2007 and 23 March 2008. Two trained observers simultaneously searched for cetaceans with the aid of 7 × 50 hand-held binoculars (Fujinon®FMTRC-SX) equipped with compass and vertical reticles, independently covering both sides of the transect line, from the front of the vessel to an angle of 90°. A team of 4 observers rotated every 40 min. Observations were made from a platform at 5.09 m effective visual height. The perpendicular distance (x) from the transect line to the sighting was calculated following Lerczak & Hobbs (1998). The animals were approached to confirm species identification only when they were within ~1.5 km of the transect line (i.e. closing mode technique; Dawson et al. 2008). Most of the large species were easily identified beyond this distance, whereas some dolphin schools remained unidentified as well as some whales recorded too far from the transect line. Search effort was suspended during the approach and the time spent with the animals as well as when the Beaufort sea-state was higher than 3.

Monthly population densities (individuals km^{-2}) were estimated using distance sampling line-transect techniques (Buckland et al. 2001) by modeling a detection probability function $g(x)$, based on the distribution of all perpendicular distances from the transect line to the groups sighted of each species. Since the cetacean surveys have continued within and outside the bay after the completion of the present study, we used all of the perpendicular distances available through April 2012 to improve the modeling of the detection functions (Fig. 4). We established *a priori* truncation points (w) based on the frequency distribution of distances. The effective half-strip width (μ) was estimated from the detection function to convert the linear effort into an effectively sampled area (Thomas et al. 2002). Several mathematical functions (uniform, half-normal, and hazard-rate) and expansion series (cosine, sine, simple polynomial, and hermit polynomial) were tested, and Akaike's information criterion (Burnham & Anderson 2002) was used to choose the best fit (Table 1). This function, evaluated at zero perpendicular distance, represents the detection probability $\hat{f}(0)$. Mean group sizes $\hat{E}(s)$ were estimated for the odontocetes and the fin whale, whereas for the blue and the Bryde's whale, the few sightings of >1 animal were split into individual detections to avoid the increase of the variance due to the indeterminacy of the expected group size. For all species, we assumed that all animals located directly on the track-line were detected and counted (i.e. $g(0) = 1$). Finally, $\hat{f}(0)$ was used, together with the number of counted groups (n) and the total transect

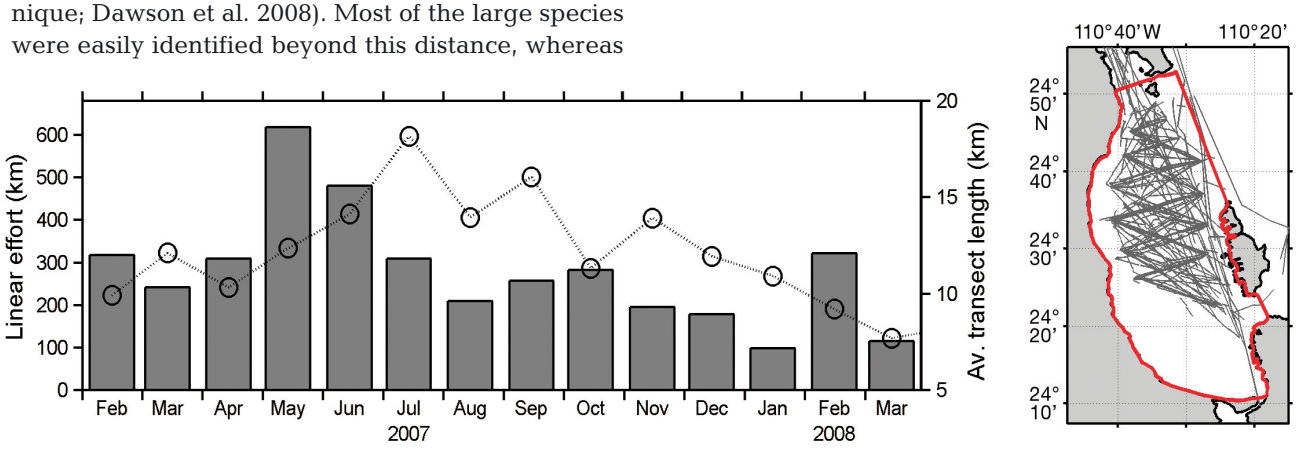

Fig. 3. Total survey effort by month (bars) and the average length of transects in each month (dotted line with circles). Map shows the polygon of La Paz Bay (red line) and the transect track lines (dark grey lines)

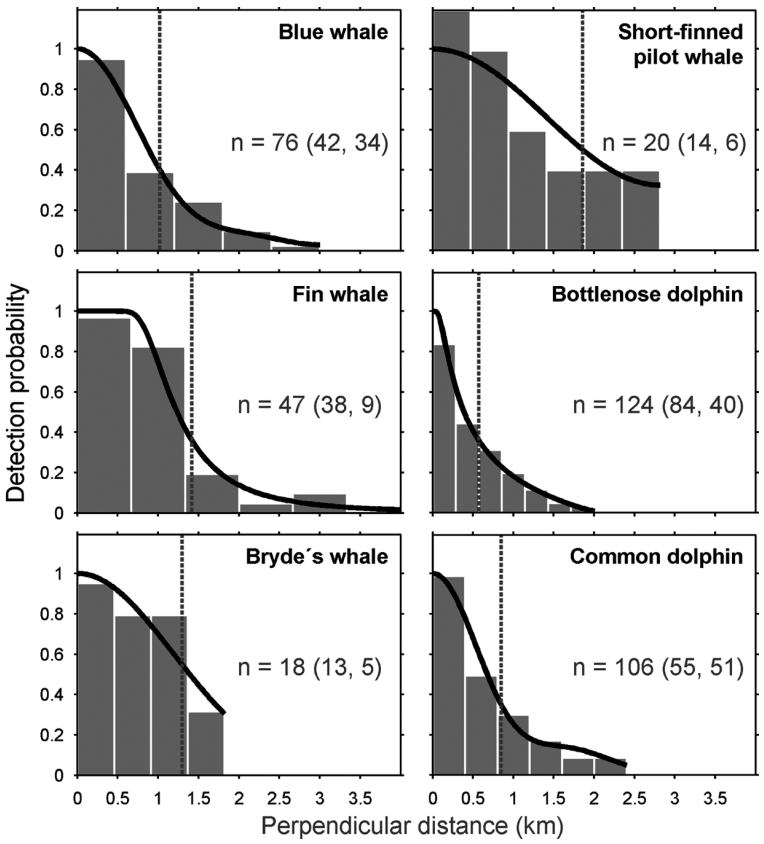

Fig. 4. Detection probability function ($g(x)$; black line), estimated from the distribution of perpendicular sighting distances (gray bars). The estimated effective half-strip width (μ) is shown as a dashed vertical line. The total number of distances used (n) is presented, specifying the number of distances from the study period and area (first value within parentheses) and the distances taken from subsequent years and/or areas aboard the same platform (second value within the parentheses)

length (L), to estimate a point density value ($\hat{D}$) for each month (Thomas et al. 2002). The variance $\widehat{\mathrm{var}}(D)$ and the lower and upper limits of the 95% confidence intervals (D/C, $D \cdot C$) were estimated by a 999 iteration bootstrap analysis of samples (i.e. transects) at each stratum (i.e. month). For the less-frequent species, we only calculated the encounter rate of groups as the number of sightings recorded in the total linear effort in each survey. Although both the short-beaked common dolphin *Delphinus delphis* and the long-beaked common dolphin *Delphinus capensis* occur in the Gulf of California, we treated them at the genus level, given the difficulty in identifying them to species level in most sightings.

Cetacean biomass

The population density estimates (individuals km^{-2}) were converted into values of biomass (t km^{-2}) to make the species comparable. This was done by multiplying the estimated density by the mean species-specific body mass values previously reported for the California Current (Barlow et al. 2008 and references therein). These values come from both direct measurements and regression models of body mass as a function of the mean body length (Table 2).

RESULTS

Hydrographic and biological conditions

Temperature dominated the density structure in the water column (Fig. 5). Cold water (<18°C) occurred throughout the first 100 m during the winter (February 2007 and January to February 2008). During March 2007, the upper 75 m were above 20°C. From April to July, a doming of the isotherms took place, and water below 17°C penetrated the surface layer up to 10 m. From June to November, the upper 25 m warmed above 25°C. December was a transition period in which the temperature in the upper 55 m cooled below 21°C. The Brunt-Väisälä frequency (Fig. 6a) showed 3 major conditions over the year, defined by the depth and degree of stratification. High values indicate a strong stratification, whereas low values mean strong mixing. The low buoyancy contours in February to March 2007 and January to February 2008 indicated deep mixing in the upper water column. During these winter periods, the pycnocline (i.e. the maximum buoyancy frequency along the profile) deepened to at least 100 m. Then, during the spring and early summer, the buoyancies in the upper 25 m marked a period of isopycnal shoaling, when the pycnocline almost reached the surface. This doming of isopycnals lasted 4 mo, until early August, and it was followed by a thickening of the stratified upper layer in the late summer and autumn, marking conditions of deep stratification, with the pycnocline around 40 m depth. These conditions prevailed until December 2007, when a mixed period developed again.

For nutrients, we only show the concentration (μM) of the sum of all components (Fig. 6b) since concentrations of dissolved silica, phosphate, and total dissolved inorganic nitrogen followed similar patterns over the course of the year. Relatively high concen-

Table 1. Parameter results from the distance sampling analyses. Point estimates are provided, followed by the 95% confidence interval in parentheses and the percentage of the coefficient of variation (%CV) in a separate column to the right. From left to right: the mean population density ($\hat{D}$), the mean total abundance ($\hat{N}$), the estimated group size ($\hat{E}$(s)), the detection probability ($\hat{f}$(0)), the effective half-strip width (μ), the mathematical function and the expansion series used in the model chosen, and the *a priori* truncation point (*w*). (–) not available

Species	Mean $\hat{D}$ (ind. km^{-2})	Mean $\hat{N}$ (ind.)	%CV $\hat{D}$, $\hat{N}$	Group size $\hat{E}$(s)	%CV $\hat{E}$(s)	$\hat{f}$(0)	%CV $\hat{f}$(0)	Function	Expansion series	μ (km)	%CV μ	*w* (km)
Bryde's whale	0.0007 (0.0003, 0.0016)	1 (1, 4)	45.0	–	–	0.77 (0.48, 1.23)	22.4	Half-normal	Hermite polynomial	1.30 (0.81, 2.07)	22.4	–
Fin whale	0.0022 (0.0012, 0.0034)	4.7 (3, 7)	32.2	1.3 (1.1, 1.6)	9.51	0.75 (0.56, 1.05)	23.1	Hazard rate	Cosine	1.42 (1.08, 1.86)	13.5	4
Blue whale	0.0034 (0.0019, 0.0058)	7 (4, 13)	38.9	–	–	0.98 (0.80, 1.19)	9.7	Uniform	Cosine	1.02 (0.84, 1.24)	9.7	3
Bottlenose dolphin	0.1911 (0.0950, 0.3842)	412 (205, 828)	36.3	18 (13.6, 24)	14.52	1.76 (1.18, 2.62)	20.3	Hazard rate	Hermite polynomial	0.57 (0.38, 0.84)	20.3	2
Common dolphin	0.3943 (0.2140, 0.7263)	850 (461, 1566)	31.6	85.1 (60.4, 119.9)	17.41	1.18 (0.98, 1.41)	9.3	Half-normal	Cosine	0.85 (0.71, 1.02)	9.3	2.4
Short-finned pilot whale	0.0154 (0.0044, 0.0454)	33.2 (9, 98)	70.3	27.7 (15.8, 48.8)	27.32	0.53 (0.35, 0.90)	30.1	Uniform	Cosine	1.86 (1.32, 2.64)	16.6	–

trations of nutrients were found in the water column during the mixing conditions in the winter, but there was an evident depletion in the upper 50 m during February and March 2007. The pycnocline shoaling of the spring and early summer brought higher sub-surface concentrations of nutrients to just below the thermocline, reaching up to 50 μM in the top 100 m. The surface and sub-surface concentration of nutrients decreased in the late summer and autumn.

Two different types of chl *a* concentration peaks occurred (Fig. 6c): during the winters of 2007 and 2008, high concentrations (~1.5 mg m^{-3}) were recorded above the pycnocline in the upper 40 m and upper 70 m, respectively, whereas under conditions of shallow stratification, higher values (~2.5 mg m^{-3}) occurred as 2 sub-surface maxima in May and August, just below the pycnocline. Low chl *a* concentrations (<0.5 mg m^{-3}) in the upper 100 m characterized the deep stratified conditions of the late summer (September to November). Biogenic silica contributed strongly to the total biogenic flux from winter to early summer, reaching a maximum of 60% in April 2007, whereas carbonate ($CaCO_3$) components dominated during the late summer and autumn, reaching 48% in October 2007 (Fig. 6d). The 2 components showed completely opposite seasonal patterns. A Pearson's test resulted in a correlation of –0.7032 (p = 0.002, 95% CI = [–0.8324, –0.5016], n = 40, effective degrees of freedom (N_{eff}) = 17 following Davis 1978).

Local and regional seasonality

The seasonal cycle of surface wind, SST, and CHL showed different patterns within the bay. The wind followed the monsoonal cycle (Fig. 7a). The annual pattern of the temperature was unimodal, with a

Table 2. Values of body mass used to standardize the density estimates of the dominant species (after Barlow et al. 2008)

Species	Common name	Mean body mass (t)
Mysticetes		
Balaenoptera edeni	Bryde's whale	16.477
Balaenoptera physalus	Fin whale	42.150
Balaenoptera musculus	Blue whale	57. 230
Odontocetes		
Tursiops truncatus	Bottlenose dolphin (offshore)	0.188
Delphinus spp.	Common dolphins	0.080
Globicephala macrorhynchus	Short-finned pilot whale	0.608

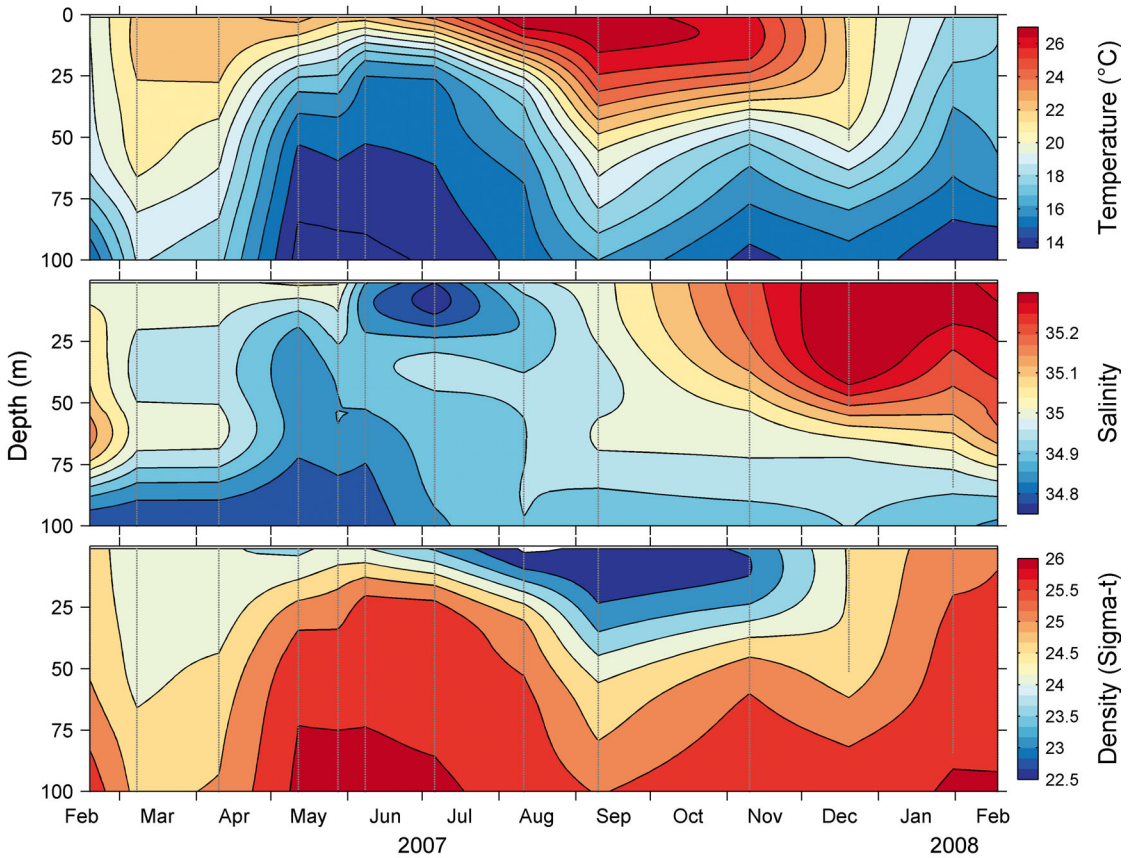

Fig. 5. Monthly progression of hydrographic variables in La Paz Bay (from objective interpolations using a Gaussian weighting function). Each cast is shown as a vertical gray line

maximum in September and a minimum in January (Fig. 7b). In contrast, the CHL pattern was bimodal, with a maximum in January (I in Fig. 7c), a decrease in March (II in Fig. 7c), a secondary peak at the end of May (III in Fig. 7c), and the main minimum in September (IV in Fig. 7c). Note that, except for the very warm September period when CHL values were lowest throughout the region (IV in Fig. 2), the values within the bay tended to be higher than in the gulf waters offshore. These values were similar to adjacent coastal areas in January (I in Fig. 2), lower than offshore and coastal areas in March (II in Fig. 2), and significantly higher than anywhere else in June (III in Fig. 2). The least-squares SST values within the bay were slightly warmer than elsewhere in January and cooler the rest of the year, considerably so in June.

Cetacean population density

Altogether, the effective search effort within the bay during the 14 mo totaled 3937 km (mean ± SD = 281 ± 137 km; Fig. 3). Four mysticete and 6 odontocete species were identified from 276 sightings. The blue whale, fin whale, Bryde's whale, common dolphin, bottlenose dolphin, and short-finned pilot whale were the most frequent species observed (Table 1, Fig. 8). The humpback whale, sperm whale *Physeter macrocephalus*, dwarf sperm whale *Kogia sima*, and killer whale *Orcinus orca* were only sporadically recorded (Fig. 8). Differences in the estimated effective half-strip widths (μ in Fig. 4) between species typically suggest interspecific variations that determine their detectability, such as their body sizes, grouping behavior, and/or level of surface activity (e.g. Barlow & Forney 2007, Williams & Thomas 2007). Mysticetes in general had the widest effective half-strip widths due to their larger body sizes and taller blows. Among the odontocetes, the short-finned pilot whales had the largest effective half-strip width, probably because of the combination of large groups and large body sizes. They were followed by the common dolphins, whose high level of surface activity and tendency to aggregate in very large groups make them detectable at large distances. Bottlenose dolphins had the shortest distance range, which could be attributed to their tendency to approach the vessel and to the small group sizes recorded within the bay.

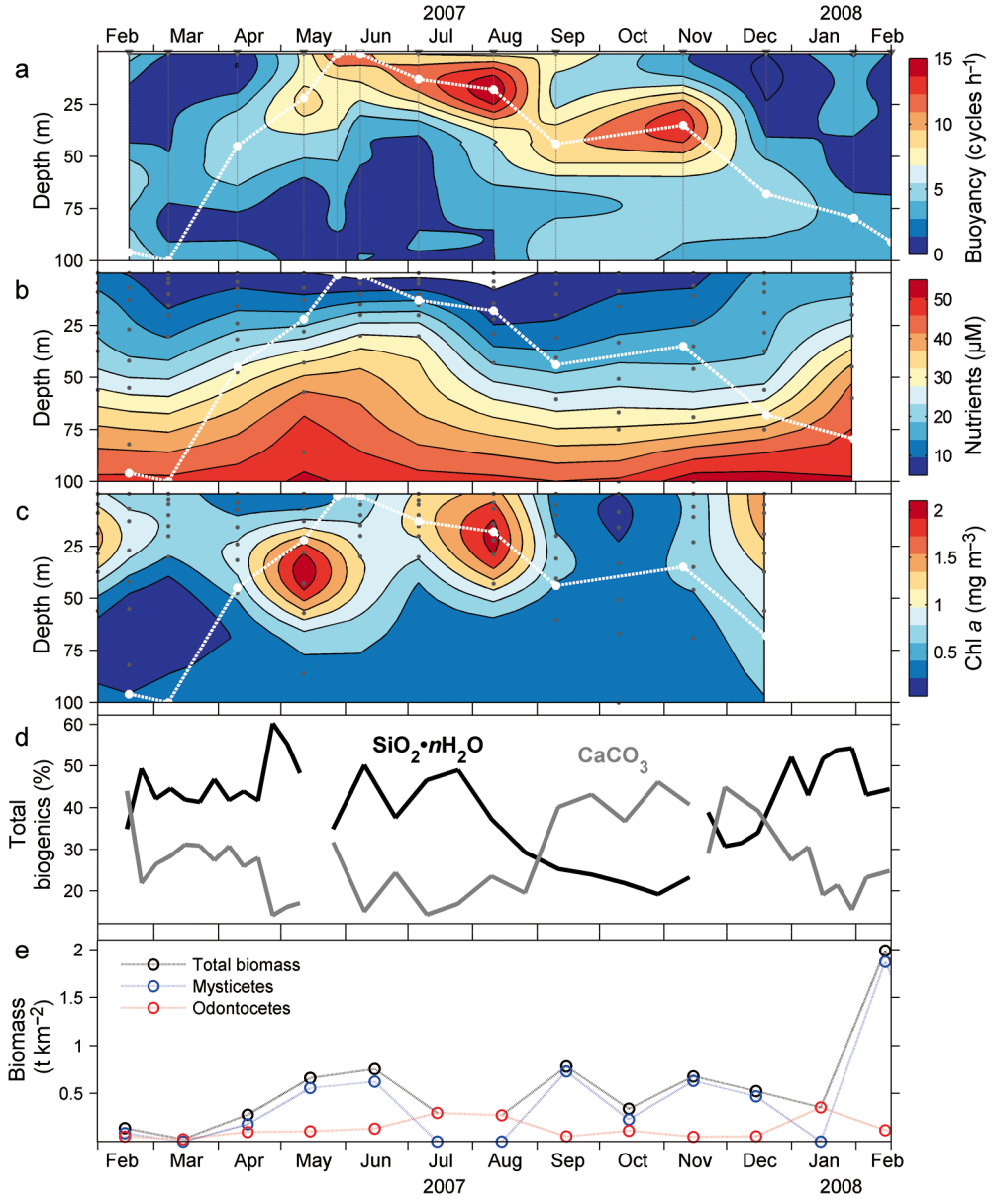

Fig. 6. Physical and biological context underlying variations in cetacean biomass in La Paz Bay. (a) Buoyancy frequency, with the dashed white line representing the depth of the pycnocline (i.e. maximum buoyancy frequency at each profile). Gray dots show the depth of the Niskin-bottle samples for (b) nutrients and (c) chl *a*. (d) The contributions of biogenic silica ($SiO_2 \cdot nH_2O$) and calcium carbonate ($CaCO_3$) to the total biogenic sinking matter, shown as 7 to 15 d absolute values. (e) Monthly cetacean biomass

Cetacean biomass

Overall cetacean biomass was dominated by the mysticetes and displayed 3 major peaks (Figs. 6e & 8). The first occurred in spring, from May to June 2007, the second covered late summer and autumn (September to December), and the third and highest was in February 2008 (Fig. 6e). The odontocetes showed an opposite pattern from the mysticetes (Fig. 6e): They increased in biomass when mysticetes decreased, showing 2 main peaks during July to August 2007 and in January 2008. The first mysticete peak of the spring (0.62 t km^{-2}) resulted from the co-occurrence of the 3 most frequent species but was dominated by the blue whale (Fig. 8). In contrast, the peaks of the late summer and autumn (0.73 and 0.63 t km^{-2}, respectively) were dominated by the fin whale in the absence of the blue whale and the occurrence of the Bryde's whale, the latter always in low biomasses. Finally, the highest peak of mysticete bio-

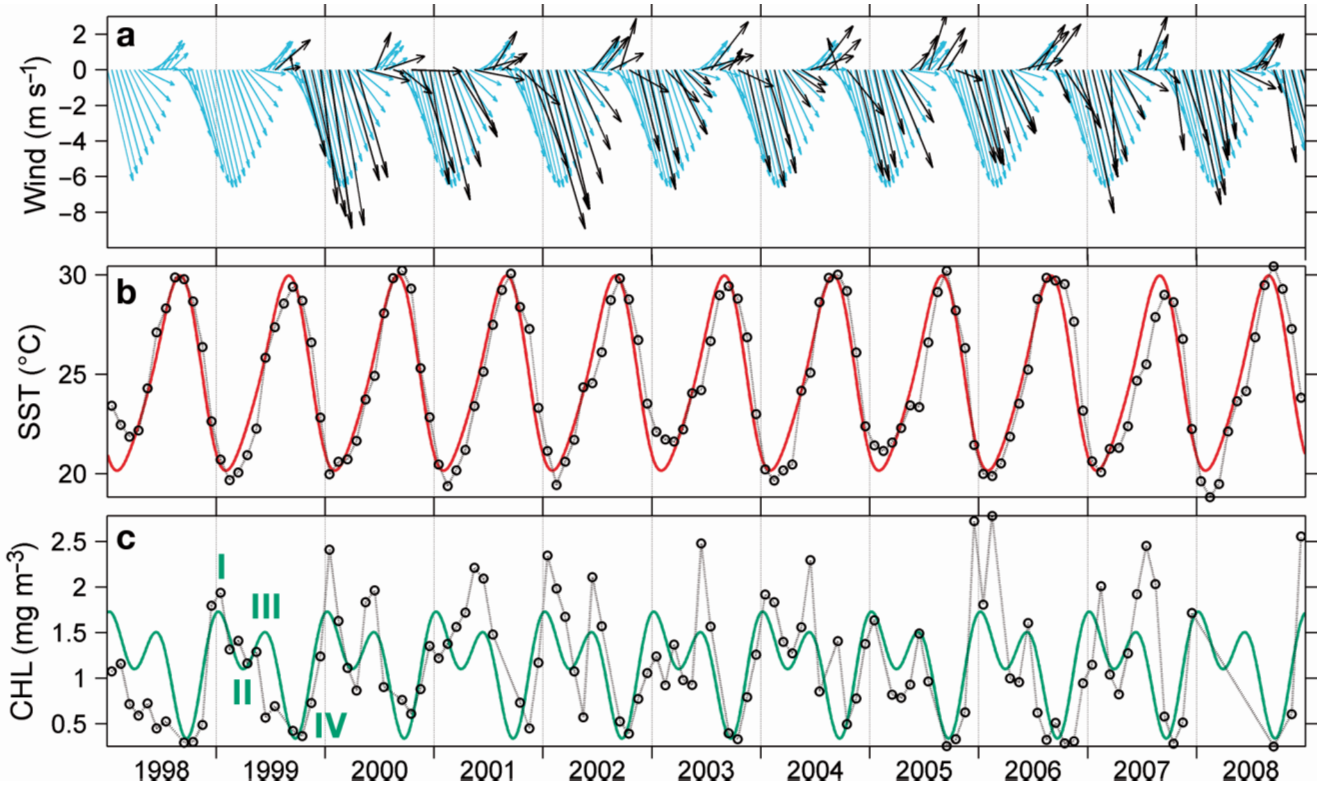

Fig. 7. Seasonal pattern of wind, sea surface temperature (SST), and chlorophyll concentration (CHL) in La Paz Bay. The black arrows (a) and circles (b,c) represent the original monthly values. The seasonal fits of wind, SST, and CHL are drawn as blue arrows and red and green lines, respectively. The seasonally adjusted maxima and minima of CHL are labeled as I, II, III, and IV, which are the periods chosen to portrait the regional (i.e. the entire southwestern gulf) spatial-temporal fit of SST and CHL in Fig. 2

mass (1.87 t km^{-2}) occurred during February 2008 and was also dominated by blue whales but in the presence of fin and Bryde's whales (Fig. 8). The first peak of odontocetes biomass (0.30 to 0.27 t km^{-2}, July to August 2007) resulted from the increase in bottlenose dolphins and from the incursion of short-finned pilot whales, whereas the second peak (0.35 t km^{-2}) was dominated by the common dolphins, with a moderate increase of bottlenose dolphins, which dominated the odontocete biomass during the rest of the year (Fig. 8).

DISCUSSION

The strong mixing in winter and the isopycnal shoaling in spring and early summer produced peaks in surface and subsurface chl *a* concentrations, respectively (Fig. 6c). The high proportion of opal in the biogenic sinking matter (Fig. 6d) suggests that these peaks were dominated by diatoms and silicoflagellates, whose blooms result from the input of new nutrients into the euphotic zone (Egge & Aksnes 1992) and typically favor the aggregation of krill and planktivorous fish (Kudela et al. 2008). Silicoflagellates and diatoms have been previously found as dominant among the micro- and nano-phytoplankton within the bay (Verdugo-Díaz 2003). The former have been associated with peaks of primary production in winter and early summer (Villegas-Aguilera 2009, Martínez-López et al. 2012) and are abundant in the siliceous fraction of the sediment trap samples (Álvarez-Gómez 2010). These 2 chl *a* peaks observed in the water column are in agreement with the remotely sensed CHL peaks of the seasonal analysis derived from the 11 yr least-squares regression (Fig. 7). This constitutes evidence that the isopycnal shoaling within the bay and its influence on phytoplankton is not a phenomenon particular only to the sampled year cycle but a recurring intraseasonal event of local nature. While the first CHL peak within the bay corresponds to a general pattern of high CHL values along the entire region of the southwestern gulf (I in Fig. 2), especially near the coast, the second corresponds to a local phenomenon, in which the bay gets colder and CHL-richer than the surrounding

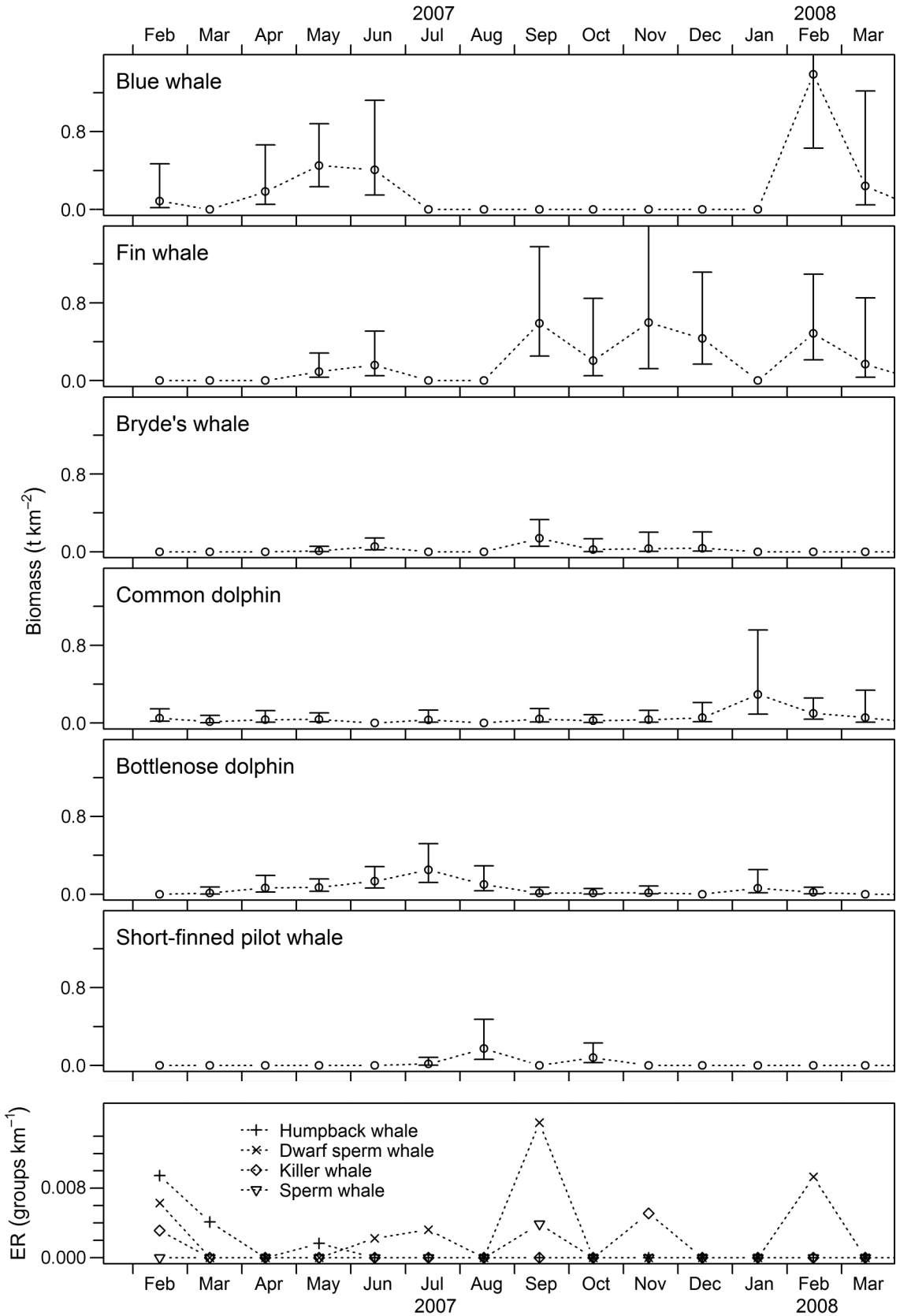

Fig. 8. Monthly estimates of cetacean biomass (±95% confidence intervals) for the dominant species and encounter rates (ER) for the less-frequent species (bottom panel)

gulf (III in Fig. 2). Note that even when the cold water is at subsurface during the period of isopycnal shoaling (Fig. 5), its influence on SST is also noticeable, with the surface remaining ~1.5°C cooler than the surrounding gulf.

The blue whale specializes on krill and dominated the cetacean biomass during these 2 periods of surface and subsurface chl *a* peaks, suggesting those were suitable conditions for low trophic level prey. It is also the only migratory cetacean among all of the species recorded that feeds actively during its wintering period in the gulf (Del-Ángel-Rodríguez 1997, Gendron 2002, Bailey et al. 2009). Variations of its seasonal migration may be responses to a larger scale of interannual oceanic conditions in a manner that is still unstudied. At the seasonal and intraseasonal scales, however, it seems that the distribution of the species within the gulf is guided by the persistence of local pulses of biological production (Pardo et al. 2011) that aggregate krill (Gendron 1992). In one of its major feeding grounds off California, the blue whale abundance also increases in response to the aggregation of krill resulting from the upwelling pulses of the California Current (Croll et al. 2005). In contrast, the migratory humpback whale has been recorded only sporadically feeding on krill within the gulf (Gendron & Urbán 1993), and its occurrence is more associated with breeding activities during winter. Although krill may also serve as prey for fin and Bryde's whales during the winter and spring within the bay, these species can also exploit juvenile stages of Pacific sardine that aggregate along the western coast of the gulf during this period (Hammann et al. 1988, Tershy 1992, Tershy et al. 1993, Gendron et al. 2001, Jaume-Schinkel 2004) and thus reduce competition with blue whales. Small pelagic fish are also the most likely prey for common dolphins (Gallo-Reynoso 1991, Niño-Torres et al. 2006), which exploit the bay in large numbers during winter. The higher biomasses of bottlenose dolphins over the entire isopycnal shoaling period (May to August) may reflect the availability of mesopelagic fish and/or squid, which are likely prey for this opportunistic species (Pauly et al. 1998, Díaz-Gamboa 2009).

In contrast, the deep stratification of the late summer and autumn was not conducive to high near-surface nutrient or chl *a* concentrations. The increase in the proportion of calcareous content in the settling biogenic particles (Fig. 6d) suggests the presence of coccolithophorids, foraminifera, and/or pteropods (Romero et al. 2002). Coccolithophorids are better adapted than silicoflagellates and diatoms to growth at limiting nutrient levels and tend to dominate under oligotrophic conditions (Iglesias-Rodríguez et al. 2002). Nevertheless, despite their dominance, the total flux of coccolithophorids does not increase at all during the late summer in the bay (Rochín-Bañaga 2012), and values of primary production drop (Reyes-Salinas et al. 2003, Cervantes-Duarte et al. 2005). How then might one explain the high peaks of fin and Bryde's whales at this time? The period of high surface water temperatures near the coast frequently marks the spawning season for several pelagic fish species in the southwestern gulf (Moser et al. 1973), including a 'warm stock' of Pacific sardine that enters the gulf (Félix-Uraga et al. 2004). These are likely the main prey for rorqual whales during the deep stratification period, as has been suggested from the $\delta^{15}N$ ratios between fin whales and sardines (Jaume-Schinkel 2004). Similarly, the short-finned pilot whale, along with the other teutophagous odontocetes, such as the dwarf sperm whale and the sperm whale (Clarke 1996, Pauly et al. 1998), were in the bay predominately during summer. The maximum biomass peaks of the short-finned pilot whale (August and October 2007; Fig. 8) occurred just when the surface temperature within the bay was the warmest (Fig. 5). Squid searching for warm waters near the coast to spawn typically aggregate under such conditions (Staaf et al. 2008). Thus, we surmise that spawning prey, at least the squid and the Pacific sardine, could sustain the biomass of teutophagous odontocetes and fin whales, respectively, during the deeply stratified summer conditions.

The physical origin of some of the observed water-column conditions in the bay is still not fully understood. During winter, Ekman upwelling occurs along the eastern coast of the gulf (Lluch-Cota 2000, Lavín & Marinone 2003), but most blue whale sightings (Gendron 2002) and large krill aggregations (Brinton & Townsend 1980) occur on the western side during this period. It is not clear if the series of eddies that form regularly along the gulf (Pegau et al. 2002) could be responsible for cross-gulf transport of nutrients and plankton from east to west, where the material could be retained. Nevertheless, since blooms of siliceous phytoplankton typically occur in response to new nutrient input, it is more likely that the phytoplankton biomass of the southwestern gulf is generated locally due to the strong vertical mixing (Fig. 6a) produced by the northwesterly winds blowing during winter (Fig. 7a). The high surface salinity (>35) observed during this period (Fig. 5) reinforces the hypothesis that strong northwesterly winds lead to a high rate of evaporation, which in turn enhances

vertical mixing. The causes of the intraseasonal isopycnal shoaling, associated with the second peak in CHL within the bay, are also poorly known. Previous studies have described cyclonic circulation (Monreal-Gómez et al. 2001, Sánchez-Velasco et al. 2006) and proposed that it could be related to the wind curl and the overall seasonal circulation of the gulf (Beier 1997). This CHL peak occurs at a time when the southwesterly wind maximum takes place (Fig. 7a), which could also force the cyclonic circulation and resulting Ekman pumping, but the subject has not been investigated in detail due to the lack of high-resolution data.

Nevertheless, it is clear that the isopycnal shoaling enhances subsurface phytoplankton aggregations within the bay at a time when the rest of the southwestern gulf remains oligotrophic. Therefore, it may also be responsible for the higher annual values of CHL previously described for the bay (Santamaria-del-Angel et al. 1994, Luch-Cota & Teniza-Guillén 2000, Kahru et al. 2004). This phenomenon extends the period of phytoplankton blooms that normally would be associated only with the winter mixing. Recent results of a long-term analysis of blue whale density, comparing La Paz Bay to Loreto Bay, showed that blue whales leave Loreto in April, earlier than their departure from La Paz, where they can be seen as late as June (Pardo et al. 2011). This pattern suggests the importance of the intraseasonal isopycnal shoaling within the bay as a potential driver of krill aggregation in the southwestern gulf at a time when the surroundings are comparatively warmer and oligotrophic (III in Fig. 2).

The presence of cetaceans with different requirements over the course of the year in the bay suggests a sustained availability of prey, aggregated by high biological production or suitable physical conditions. Recent measurements of the proportion of particulate organic carbon in the sinking matter and the monthly fluxes (export production) in the bay (Silverberg 2009, Silverberg et al. 2009) show that these do not vary much seasonally, indicating that biological production extends throughout the year regardless of the type of physical forcing. The export production of the bay is more than double that of Guaymas Basin, often considered a particularly high production area in the gulf (García-Pámanes et al. 2011). All of these characteristics lead us to propose that La Paz Bay constitutes a biological hotspot in the southwestern Gulf of California, driven by the seasonal evolution of regional surface mixing conditions in winter, local isopycnal shoaling in spring and early summer, and deep stratification in late summer and autumn. This physical contrast attracts a wide variety of cetaceans foraging at different trophic levels at different times of the year and probably also favors the incursion of other species of marine megafauna.

Future work should focus on addressing the inferences drawn in the present study regarding the physical and biological mechanisms that drive cetacean occurrence in the bay. Such work would require a sampling grid aimed at resolving spatial patterns in environmental variables concurrently with measurements of the low, mid, and high trophic levels. Testing these mechanistic linkages would require a numerical modeling approach. Two species that would be particularly amenable for such work are the blue whale and the short-finned pilot whale because of their specialist diet and because they showed the most evident relationships with the environment, with blue whales using the bay during periods of cool temperature, high CHL, and a primary producer community dominated by siliceous phytoplankton, while short-finned pilot whales occurred during warm, oligotrophic periods dominated by calcareous phytoplankton. The physical mechanisms driving isopycnal shoaling in the bay during spring and early summer, which make this area biologically richer than the surrounding gulf, should be investigated through a study of the effects of the wind field in combination with the local physiography (as shown by Wingfield et al. 2011). The role of the northwesterly winds in the evaporation and subsequent mixing of the surface layer during winter should be studied to understand the reasons for the aggregation of krill and blue whales along the western coast of the gulf rather than along the upwelling-influenced eastern coast.

Acknowledgements. The present study received financial support from the Consejo Nacional de Ciencia y Tecnología (CONACyT) through the projects Monitoreo ecológico contínuo de la Bahía de La Paz: Serie de tiempo (47310-F; PI: N.S.) and Investigaciones Oceanográficas del Sistema Frontal de Baja California (SEP-2008-103898; PI: E.B.), as well as MSc and PhD scholarships to M.A.P. The Instituto Politécnico Nacional (IPN) funded part of the field work through the projects Monitoreo Ecológico Continuo en Bahía de La Paz (SIP 20040095, 2005-0274, 20060199, 20070664, 20080650, 20090523; PI: N.S.) and Estructura poblacional y movimiento de algunos cetáceos del Golfo de California (SIP 20070803; PI: D.G.). D.M.P. was supported by funding from the NASA Applied Sciences Program, Earth Science Division, through a grant provided by Research Announcement NNH07ZDA001N, Research Opportunities in Space and Earth Sciences (ROSES-2007), Program Element A.20: Decision Support through Earth Science Research Results. M.A.P. also received funding from the IPN (PIFI grant), Centro Interdisciplinario de Ciencias Marinas (CICIMAR-IPN; M.Sc. Recovery Funds), The Society for

Marine Mammalogy (Grants in Aid of Research 2009), Cetacean Society International, American Cetacean Society (Monterey Bay Grant 2008), and The Ocean Foundation. We are grateful to all of the personnel from Laboratorio de Ecología de Cetáceos y Quelonios and Departamento de Oceanología at CICIMAR-IPN for their support during environmental and cetacean sampling. We also thank NOAA CoastWatch Program, NASA's Goddard Space Flight Center, and GeoEye for making the satellite data products readily available. Valuable comments during the study were provided by R. Palomares, G. De-La-Cruz-Agüero, O. Victorivich, R. Díaz-Gamboa, G. Busquets-Vass, and A. Martínez-López from CICIMAR-IPN.

LITERATURE CITED

Adams DK, Comrie AC (1997) The North American monsoon. Bull Am Meteorol Soc 78:2197–2213

Álvarez-Gómez IG (2010) Reconstrucción de la variabilidad del clima a través de los silicoflagelados conservados en los sedimentos laminados de Cuenca Alfonso. MSc thesis, Instituto Politécnico Nacional, La Paz, available at www.biblioteca.cicimar.ipn.mx/oacis/tesisdesplegardetalles.php?id=577

Au DWK, Perryman WL (1985) Dolphin habitats in the eastern tropical Pacific. Fish Bull 83:623–643

Badan-Dangon A, Dorman CE, Merrifield MA, Winant CD (1991) The lower atmosphere over the Gulf of California. J Geophys Res 96:16877–16896

Bailey H, Mate BR, Palacios DM, Irvine L, Bograd SJ, Costa DP (2009) Behavioural estimation of blue whale movements in the Northeast Pacific from state-space model analysis of satellite tracks. Endang Species Res 10:93–106

Barlow J, Forney KA (2007) Abundance and population density of cetaceans in the California Current ecosystem. Fish Bull 105:509–526

Barlow J, Kahru M, Mitchell BG (2008) Cetacean biomass, prey consumption, and primary production requirements in the California Current ecosystem. Mar Ecol Prog Ser 371:285–295

Becker EA, Forney KA, Ferguson MC, Foley DG, Smith RC, Barlow J, Redfern JV (2010) Comparing California Current cetacean–habitat models developed using *in situ* and remotely sensed sea surface temperature data. Mar Ecol Prog Ser 413:163–183

Becker EA, Foley DG, Forney KA, Barlow J, Redfern JV, Gentemann CL (2012) Forecasting cetacean abundance patterns to enhance management decisions. Endang Species Res 16:97–112

Beier E (1997) A numerical investigation of the annual variability in the Gulf of California. J Phys Oceanogr 27: 615–632

Bishop JKB (1988) The barite-opal-organic carbon association in oceanic particulate matter. Nature 332:341–343

Bordoni S, Ciesielski PE, Johnson RH, McNoldy BD, Stevens B (2004) The low-level circulation of the North American Monsoon as revealed by QuikSCAT. Geophys Res Lett 31:L10109, doi:10.1029/2004GL020009

Boyer T, Levitus S, Garcia H, Locarnini RA, Stephens C, Antonov J (2005) Objective analyses of annual, seasonal, and monthly temperature and salinity for the World Ocean on a 0.25° grid. Int J Climatol 25:931–945

Brinton E, Townsend AW (1980) Euphausiids in the Gulf of California: the 1957 cruises. Calif Coop Ocean Fish Invest Rep 21:211–236

Buckland ST, Anderson DR, Burnham KP, Laake JL, Borchers DL, Thomas L (2001) Introduction to distance sampling. Oxford University Press, Oxford

Burnham KP, Anderson DR (2002) Model selection and multimodel inference, 2nd edn. Springer, New York, NY

Bustillos-Guzmán J, Lechuga-Devéze CH (1989) Secchi disk lectures and scalar quanta irradiance relationships in the Pacific coast off Baja California and Gulf of California. Cienc Mar 15:39–45

Casey KS, Cornillon P (1999) A comparison of satellite and in situ-based sea surface temperature climatologies. J Clim 12:1848–1863

Cervantes-Duarte R, Verdugo-Díaz G, Váldez-Holguín JE (2005) Modelo estacional de producción primaria estimada mediante fluorescencia natural en una región costera del Golfo de California, México. Hidrobiológica 15:79–87

Clark E, Nelson DR (1997) Young whale sharks, *Rhincodon typus*, feeding on a copepod bloom near La Paz, Mexico. Environ Biol Fishes 50:63–73

Clarke MR (1996) Cephalopods as prey. III. Cetaceans. Philos Trans R Soc Lond B 351:1053–1065

Croll DA, Marinovic B, Benson S, Chavez FP, Black N, Ternullo R, Tershy BR (2005) From wind to whales: trophic links in a coastal upwelling system. Mar Ecol Prog Ser 289:117–130

Croll DA, Newton KM, Weng K, Galván-Magaña F, O'Sullivan J, Dewar H (2012) Movement and habitat use by the spine-tail devil ray in the Eastern Pacific Ocean. Mar Ecol Prog Ser 465:193–200

Davis RE (1978) Predictability of sea level pressure anomalies over the North Pacific Ocean. J Phys Oceanogr 8: 233–246

Dawson S, Wade P, Slooten E, Barlow J (2008) Design and field methods for sighting surveys of cetaceans in coastal and riverine habitats. Mammal Rev 38:19–49

Del-Ángel-Rodríguez JA (1997) Hábitos alimentarios y distribución espacio-temporal de los rorcuales común (*Balaenoptera physalus*) y azul (*Balaenoptera musculus*) en la Bahía de La Paz, B.C.S., México. MSc thesis, Instituto Politécnico Nacional, La Paz, available at www.cicimar.ipn.mx/oacis/productividad.php?id=1621&anio=1997&tipo=5&encabezado=Tesis%20dirigidas

Díaz-Gamboa RE (2009) Relaciones tróficas de los cetáceos teutófagos con el calamar gigante *Dosidicus gigas* en el Golfo de California. PhD thesis, Instituto Politécnico Nacional, La Paz, available at www.cicimar.ipn.mx/oacis/productividad.php?id=3100&anio=2009&tipo=5&encabezado=Tesis%20dirigidas

Domeier ML, Nasby-Lucas N, Palacios DM (2012) The northeastern Pacific white shark shared offshore foraging area (SOFA): a first examination and description from ship observations and remote sensing. In: Domeier ML (ed) Global perspectives on the biology and life history of the white shark. CRC Press, Boca Raton, FL, p 147–158

Doniol-Valcroze T, Berteaux D, Larouche P, Sears R (2007) Influence of thermal fronts on habitat selection by four rorqual whale species in the Gulf of St. Lawrence. Mar Ecol Prog Ser 335:207–216

Egge JK, Aksnes DL (1992) Silicate as regulating nutrient in phytoplankton competition. Mar Ecol Prog Ser 83:281–289

Emery WJ, Thomson E (1998) Data analysis methods in physical oceanography. Elsevier, Amsterdam

Félix-Uraga R, Gómez-Muñoz VM, Quiñonez-Velázquez C, Melo-Barrera FN, García-Franco W (2004) On the existence of Pacific sardine groups off the west coast of Baja California and southern California. Calif Coop Ocean Fish Invest Rep 45:146–151

Flores-Ramírez S, Urbán RJ, Villarreal-Chávez G, Valles-Jiménez R (1996) Spatial and temporal changes in the cetacean community structure at Bahía de La Paz, B.C.S., Mexico (1988-1991). Cienc Mar 22:151–173

Forney KA, Ferguson MC, Becker EA, Fiedler PC and others (2012) Habitat-based spatial models of cetacean density in the eastern Pacific Ocean. Endang Species Res 16: 113–133

Freilich MH (2000) SeaWinds: algorithm theoretical basis document. NASA, Washington, DC, available at http://eospso.gsfc.nasa.gov/eos_homepage/for_scientists/atbd/viewInstrument.php?instrument=15

Gallo-Reynoso JP (1991) Group behavior of common dolphins (*Delphinus delphis*) during prey capture. An Inst Biol Univ Nac Auton Mex Zool 62:253–262

García-Pámanes J, Trasviña-Castro A, Lara-Lara JR, Bazán-Guzmán C (2011) Seasonal variability of the particulate organic matter vertical flux in the central region of the Gulf of California. Cienc Mar 37:33–49

Gendron D (1992) Population structure of daytime surface swarms of *Nyctiphanes simplex* (Crustacea: Euphausiacea) in the Gulf of California, Mexico. Mar Ecol Prog Ser 87:1–6

Gendron D (2002) Ecología poblacional de la ballena azul *Balaenoptera musculus* de la Península de Baja California. PhD thesis, Centro de Investigación Científica y de Educación Superior de Ensenada, Ensenada, available at http://biblioteca.cicese.mx/catalogo/tesis/ficha.php?id=15272

Gendron D, Urbán J (1993) Evidence of feeding by humpback whales (*Megaptera novaeangliae*) in the Baja California breeding ground, Mexico. Mar Mamm Sci 9:76–81

Gendron D, Aguíñiga S, Carriquiry JD (2001) $\delta^{15}N$ and $\delta^{13}C$ in skin biopsy samples: a note on their applicability for examining the relative trophic level in three rorqual species. J Cetacean Res Manag 3:41–44

Gerrodette T, Eguchi T (2011) Precautionary design of a marine protected area based on a habitat model. Endang Species Res 15:159–166

Hamazaki T (2002) Spatiotemporal prediction models of cetacean habitats in the mid-western North Atlantic Ocean (from Cape Hatteras, North Carolina, U.S.A. to Nova Scotia, Canada). Mar Mamm Sci 18:920–939

Hammann MG, Baumgartner TR, Badan-Dangon A (1988) Coupling of the Pacific sardine (*Sardinops sagax caeruleus*) life cycle with the Gulf of California pelagic environment. Calif Coop Ocean Fish Invest Rep 29:102–109

Hooker SB, McClain CR (2000) The calibration and validation of SeaWiFS data. Prog Oceanogr 45:427–465

Iglesias-Rodríguez MD, Brown CW, Doney SC, Kleypas J and others (2002) Representing key phytoplankton functional groups in ocean carbon cycle models: coccolithophorids. Global Biogeochem Cycles 16:1100, doi:10.1029/2001GB001454

Jalickee JB, Hamilton DR (1977) Objective analysis and classification of oceanographic data. Tellus 29:545–560

Jaume-Schinkel MS (2004) Hábitos alimentarios del rorcual común *Balaenoptera physalus* en el Golfo de California mediante el uso de isótopos estables de nitrógeno y carbono. MSc thesis, Instituto Politécnico Nacional, La Paz, available at www.cicimar.ipn.mx/oacis/productividad.php?id=1729&anio=2004&tipo=5&encabezado=Tesis%20dirigidas

Kahru M, Marinone SG, Lluch-Cota SE, Parés-Sierra A, Greg Mitchell B (2004) Ocean-color variability in the Gulf of California: scales from days to ENSO. Deep-Sea Res II 51:139–146

Ketchum-Mejía JT (2003) Distribución espacio-temporal y ecología alimentaria del tiburón ballena (*Rhincodon typus*) en la Bahía de La Paz y zonas adyacentes en el suroeste del Golfo de California. MSc thesis, Instituto Politécnico Nacional, La Paz, available at www.cicimar.ipn.mx/oacis/productividad.php?id=1734&anio=2003&tipo=5&encabezado=Tesis%20dirigidas

Kilpatrick KA, Podestá GP, Evans R (2001) Overview of the NOAA/NASA advanced very high resolution radiometer Pathfinder algorithm for sea surface temperature and associated matchup database. J Geophys Res 106: 9179–9197

Kudela RM, Banas NS, Barth JA, Frame ER and others (2008) New insights into the controls and mechanisms of plankton productivity in coastal upwelling waters of the northern California Current System. Oceanography (Wash DC) 21:46–59

Lavín MF, Marinone SG (2003) An overview of the physical oceanography of the Gulf of California. In: Velasco-Fuentes OU, Sheinbaum J, Ochoa J (eds) Nonlinear processes in geophysical fluid dynamics. Kluwer, Dordrecht, p 173–204

Lerczak JA, Hobbs RC (1998) Calculating sighting distances from angular readings during shipboard, aerial, and shore-based marine mammal surveys. Mar Mamm Sci 14:590–599

Lluch-Cota SE (2000) Coastal upwelling in the eastern Gulf of California. Oceanol Acta 23:731–740

Luch-Cota DB, Teniza-Guillén G (2000) BAC versus áreas adyacentes de la variabilidad interanual de pigmentos fotosintéticos a partir del Coastal Zone Color Scanner (CZCS). In: Lluch-Belda D, Elorduy-Garay J, Lluch-Cota SE, Ponce-Díaz G (eds) BAC, centros de actividad biológica del Pacífico mexicano, 1st edn. Centro de investigaciones Biológicas del Noroeste, S.C., La Paz, p 198–218

Martínez-López A, Álvarez-Gómez IG, Durazo R (2012) Climate variability and silicoflagellate fluxes in Alfonso Basin (southern Gulf of California). Bot Mar 55:1–9

Monreal-Gómez MA, Molina-Cruz A, Salas-de-León DA (2001) Water masses and cyclonic circulation in Bay of La Paz, Gulf of California, during June 1998. J Mar Syst 30:305–315

Moser HG, Ahlstrom EH, Kramer D, Stevens EG (1973) Distribution and abundance of fish eggs and larvae in the Gulf of California. Calif Coop Ocean Fish Invest Rep XVII:112–128

Niño-Torres CA, Gallo-Reynoso JP, Galván-Magaña F, Escobar-Briones E, Macko SA (2006) Isotopic analysis of $\delta^{13}C$, $\delta^{15}N$, and $\delta^{34}S$ 'A feeding tale' in teeth of the longbeaked common dolphin, *Delphinus capensis.* Mar Mamm Sci 22:831–846

O'Reilly JE, Maritorena S, Mitchell BG, Siegel DA and others (1998) Ocean color chlorophyll algorithms for SeaWiFS. J Geophys Res 103:24937–24953

O'Reilly JE, Maritorena S, Siegel DA, O'Brien MC and others (2000) Ocean color chlorophyll *a* algorithms for SeaWiFS, OC2 and OC4: version 4. In: Hooker SB, Firestone ER (eds) SeaWiFS postlaunch calibration and validation analyses, Part 3. NASA Tech Memo 206892, Vol 11, p 9–23

Obeso-Nieblas M, Shirasago B, Sanchez-Velasco L, Gaviño-Rodriguez JH (2004) Hydrographic variability in Bahia De La Paz, B.C.S., Mexico, during the 1997–1998 El Niño. Deep-Sea Res II 51:689–710

Palacios DM, Bograd SJ, Foley DG, Schwing FB (2006) Oceanographic characteristics of biological hot spots in

the North Pacific: a remote sensing perspective. Deep-Sea Res II 53:250–269

Pardo MA, Gendron D, Beier E (2011) Seasonal habitat variability for the blue whale in the southwestern Gulf of California: implications for the species' conservation. Conservation Science Symposium, Species of Concern, Loreto, 25–27 May 2011, p 8–9, available at http://conservationscience.com.mx/abstracts.html (Abstract)

Pauly D, Trites AW, Capuli E, Christensen V (1998) Diet composition and trophic levels of marine mammals. ICES J Mar Sci 55:467–481

Pegau WS, Boss E, Martínez A (2002) Ocean color observations of eddies during the summer in the Gulf of California. Geophys Res Lett 29, doi:10.1029/2001GL014076

Praca E, Gannier A, Das K, Laran S (2009) Modelling the habitat suitability of cetaceans: example of the sperm whale in the northwestern Mediterranean Sea. Deep-Sea Res I 56:648–657

Reyes-Salinas A, Cervantes-Duarte R, Morales-Pérez RA, Valdez-Holguín JE (2003) Variabilidad estacional de la productividad primaria y su relación con la estratificación vertical en la Bahía de la Paz, B.C.S. Hidrobiológica 13:103–110

Ripa P (2002) Least squares data fitting. Cienc Mar 28: 79–105

Ritchie RJ (2008) Universal chlorophyll equations for estimating chlorophylls *a*, *b*, *c*, and *d* and total chlorophylls in natural assemblages of photosynthetic organisms using acetone, methanol, or ethanol solvents. Photosynthetica 46:115–126

Rochín-Bañaga H (2012) Aporte de carbonato de calcio en Cuenca Alfonso mediante el flujo de nanoplánctón calcáreo. BSc thesis, Universidad Autónoma de Baja California Sur, La Paz

Romero O, Boeckel B, Donner B, Lavik G, Fischer G, Wefer G (2002) Seasonal productivity dynamics in the pelagic central Benguela System inferred from the flux of carbonate and silicate organisms. J Mar Syst 37:259–278

Salinas-González F, Zaytsev O, Makarov V (2003) Formation of the thermohaline structure of water in the Bahía de La Paz from summer to autumn. Cienc Mar 29:51–65

Salvadeo CJ, Gómez-Gallardo A, Lluch-Belda D, Urbán RJ (2009) The odontocete community and its environment in the southwestern Gulf of California. Lat Am J Aquat Mamm 7:23–32

Sánchez-Velasco L, Beier E, Avalos-García C, Lavín MF (2006) Larval fish assemblages and geostrophic circulation in Bahía de La Paz and the surrounding southwestern region of the Gulf of California. J Plankton Res 28: 1081–1098

Santamaria-del-Angel E, Alvarez-Borrego S, Muller-Karger FE (1994) Gulf of California biogeographic regions based on coastal zone color scanner imagery. J Geophys Res 99: 7411–7421

Silver MW, Gowing MM (1991) The 'particle' flux: origins and biological components. Prog Oceanogr 26:75–113

Silverberg N (2009) Vistazo sobre la producción exportada de carbono orgánico particulado en las áreas marinas de México. In: Primer Simposio Internacional del Carbono en Mexico. INE - PMC, Ensenada

Silverberg N, Aguirre F, Aguíñiga S, Romero N (2006) Vertical flux of particulate matter in Alfonso Basin, La Paz Bay, during 2002. Cienc Mar 32:73–82

Silverberg N, Aguirre-Bahena F, Zaytsev O (2009) Últimos resultados sobre la materia en hundimiento en Cuenca Alfonso, Bahía de La Paz: Serie de tiempo 2002-2009. In: Reunión Anual de la Unión Geofísica Mexicana - Sesión Especial: Acoplamiento bio-oceanográfico en la Bahía de La Paz y región sur del Golfo de California. Unión Geofísica Mexicana, Puerto Vallarta, p 122, available at www.ugm.org.mx/publicaciones/geos/index.php?page=publicaciones-2009-i

Staaf DJ, Camarillo-Coop S, Haddock SHD, Nyack AC and others (2008) Natural egg mass deposition by the Humboldt squid (*Dosidicus gigas*) in the Gulf of California and characteristics of hatchlings and paralarvae. J Mar Biol Assoc UK 88:759–770

Strickland JDH, Parsons TR (1972) A practical handbook of seawater analysis, 2nd edn. Bull Fish Res Board Can 167: 1–310

Szteren D, Aurioles D, Gerber LR (2006) Population status and trends of the California sea lion (*Zalophus californianus californianus*) in the Gulf of California, Mexico. In: Trites A, Atkinson S, DeMaster D, Fritz L, Gelatt T, Rea L, Wynne K (eds) Sea lions of the world. Alaska Sea Grant College Program/University of Alaska Fairbanks, Fairbanks, AK, p 369–384

Tershy BR (1992) Body size, diet, habitat use, and social behavior of *Balaenoptera* whales in the Gulf of California. J Mammal 73:477–486

Tershy BR, Acevedo-G A, Breese D, Strong CS (1993) Diet and feeding behavior of fin and Bryde's whales in the central Gulf of California, Mexico. Rev Invest Cient Univ Auton Baja Calif Sur 1:1–4 (Ser Cienc Mar)

Thomas L, Buckland ST, Burnham KP, Anderson DR, Laake JL, Borchers DL, Strindberg S (2002) Distance sampling. In: El-Shaarawi AH, Piegorsch WW (eds) Encyclopedia of environmetrics. John Wiley & Sons, Chichester, p 544–552

Trites AW, Christensen V, Pauly D (1997) Competition between fisheries and marine mammals for prey and primary production in the Pacific Ocean. J Northwest Atl Fish Sci 22:173–187

Verdugo-Díaz G (2003) Respuesta ecofisiológica del fitoplancton ante la variabilidad ambiental en una laguna costera sub-tropical de Baja California Sur, México. PhD thesis, Instituto Politécnico Nacional, La Paz

Villegas-Aguilera MM (2009) Fitoplancton silíceo de la zona eufótica, como señal de la productividad primaria en Cuenca Alfonso, Golfo de California. MSc thesis, Instituto Politécnico Nacional, La Paz, available at www.cicimar.ipn.mx/oacis/productividad.php?id=3155&anio=2009&tipo=5&encabezado=Tesis%20dirigidas

Wahl RJ, Teague WJ (1983) Estimation of Brunt-Väisälä frequency from temperature profiles. J Phys Oceanogr 13: 2236–2240

Walker TA (1982) Use of a Secchi disc to measure attenuation of underwater light for photosynthesis. J Appl Ecol 19:539–544

Walton CC, Pichel WG, Sapper JF, May DA (1998) The development and operational application of nonlinear algorithms for the measurement of sea surface temperatures with the NOAA polar-orbiting environmental satellites. J Geophys Res 103:27999–28012

Williams R, Thomas L (2007) Distribution and abundance of marine mammals in the coastal waters of British Columbia, Canada. J Cetacean Res Manag 9:15–28

Wingfield DK, Peckham SH, Foley DG, Palacios DM and others (2011) The making of a productivity hotspot in the coastal ocean. PLoS ONE 6:e27874

Submitted: July 9, 2012; Accepted: December 6, 2012

Proofs received from author(s): April 1, 2013

Vol. 487: 261–273, 2013
doi: 10.3354/meps10384

MARINE ECOLOGY PROGRESS SERIES
Mar Ecol Prog Ser

Published July 30

Contribution to the Theme Section 'Biophysical coupling of marine hotspots'

FREE ACCESS

Fine-scale biophysical interactions drive prey availability at a migratory stopover site for *Phalaropus* spp. in the Bay of Fundy, Canada

L. H. Thorne[1,2,*], A. J. Read[2]

[1]School of Marine and Atmospheric Sciences, Stony Brook University, Stony Brook, New York 11794, USA
[2]Division of Marine Science and Conservation, Duke University, 135 Duke Marine Lab Road, Beaufort, North Carolina 28516, USA

ABSTRACT: We examined the role of biophysical interactions in structuring the foraging habitat of phalaropes *Phalaropus* spp. at an important migratory stopover site in the Bay of Fundy. We sampled both biological and physical aspects of the environment and integrated these observations into generalized additive models (GAMs). Strong tidal currents interact with steep bathymetric gradients at the Brier Island ledges to enhance vertical mixing, creating dense surface aggregations of *Calanus finmarchicus* copepods at fine temporal and spatial scales. The resulting spatial variation in copepod density in near-surface waters creates a highly heterogeneous foraging environment for phalaropes, which are obligate surface feeders. Models of phalarope abundance over the ledges suggested that phalaropes forage on upwelled zooplankton aggregations as they drifted downstream. Our results highlight the importance of considering underlying physical processes when assessing hotspots of prey aggregations for marine species, particularly within highly dynamic systems such as the Bay of Fundy. This is particularly relevant to considerations of the conservation status of red-necked phalaropes *Phalaropus lobatus*, which have abandoned a long-time migratory stopover area previously used by more than one million birds during the mid-1980s.

KEY WORDS: Upwelling · Zooplankton · *Calanus finmarchicus* · Bay of Fundy · Tidal currents · Phalarope

INTRODUCTION

Biophysical interactions structure habitat patches in marine environments at a variety of spatial and temporal scales (Haury et al. 1978). The importance of fine-scale heterogeneity in marine systems is exemplified by the importance of oceanographic features that create prey patches and aggregate or attract animals from lower to upper trophic levels, thus creating important 'hotspots' of marine life (e.g. Alldredge & Hamner 1980, Hamner & Hauri 1981, Franks 1992, Rodhouse et al. 1996, Griffin 1999, Johnston et al. 2005). In particular, predators that are restricted to feeding at the water's surface, such as many seabird species, often rely on oceanographic features to make prey accessible through upwelling or other mechanisms (e.g. Haney 1986, 1987, Brown & Gaskin 1988, Pakhomov & McQuaid 1996, van Franeker et al. 2002). It is important to understand how such oceanographic processes create foraging opportunities for marine predators and thus structure these hotspots in space and time.

Phalaropes *Phalaropus* spp. offer an interesting opportunity to examine the effects of sub-surface

*Email: lesley.thorne@stonybrook.edu

biophysical processes in structuring foraging habitat at the water's surface. We focus here on red-necked phalaropes *Phalaropus lobatus* because of the importance of our study site for this species, though the results of our work apply equally to red phalaropes *Phalaropus fulicarius*, which are also observed in the area. These small, pelagic shorebirds are obligate surface feeders that consume large zooplankton such as *Calanus finmarchicus* copepods, which have complex life cycles comprised of 6 nauplid stages (NI-NVI) and 5 copepodid stages (CI-CV) in addition to the egg and adult stages. During their autumn southward migration along the Atlantic seaboard, red-necked phalaropes feed on surface aggregations of *C. finmarchicus* (particularly on the lipid-rich CV stage) at several sites in the Bay of Fundy, Canada (Mercier & Gaskin 1985, Brown & Gaskin 1988, 1989, Hirche 1996). These prey aggregations are important to the energetic balance of migrating phalaropes, allowing them to increase their fat reserves by as much as 30% in a 2 wk period prior to their departure for waters further south (Mercier 1985). It is important to understand factors controlling prey abundance of this species because the number of birds observed in the Bay of Fundy declined drastically during the late 1980s and has failed to recover since that time. Surveys during the early 1980s produced estimates of nearly 2 million red-necked phalaropes using a small foraging area in the western Bay of Fundy, but phalaropes have since abandoned this foraging area (Finch 1977, Vickery 1978, Morrison et al. 2001, Brown et al. 2005). Recent observations suggest that red-necked phalaropes currently use the Bay of Fundy in smaller numbers during summer months (aggregations of 20 000–50 000 individuals), and that the largest numbers of red-necked phalaropes typically occur near the Brier Island ledges in the south of the bay (R. Hunnewell pers. comm.). It is unlikely that the observed changes in the abundance of phalaropes using the Bay of Fundy during summer months represents a change in stopover site used by the birds since large aggregations of red-necked phalaropes have not been observed in other locations. Aggregations of the size previously observed in the Bay of Fundy would be easily observable, even from a distance, and the Bay of Fundy still represents the primary staging ground for red-necked phalaropes typically during their southern migration. Declines in surface prey have been suggested to be responsible for the decreased abundance of red-necked phalaropes (Brown et al. 2005), but no published studies have investigated distribution or abundance of prey in foraging areas since the early 1980s.

It has long been suggested that fine-scale oceanographic features are responsible for making *Calanus finmarchicus* available to predators in surface waters, but early studies in the Bay of Fundy did not quantify the occurrence or effects of these features. For example, Brown (1980) and Brown & Gaskin (1988) developed, but did not test, hypotheses regarding the oceanographic processes responsible for patterns in the distribution of phalarope prey.

In the present study, we test the following hypothesis initially proposed by Brown (1980): Phalarope foraging habitat is formed when tidal currents interact with underwater ledges to generate fine-scale regions of upwelling which, in turn, transport dense zooplankton aggregation into surface waters. Our specific objectives were to: (1) determine the abundance, species and stage composition of copepods observed in surface waters, and (2) assess how physical oceanography structures the prey field of phalaropes at fine spatial and temporal scales.

MATERIALS AND METHODS

Study area

The Bay of Fundy hosts some of the largest tides in the world, with spring tidal ranges of up to 16 m in some places. The resulting strong tidal currents can structure the prey distribution and foraging habitat of marine predators at fine temporal and spatial scales (e.g. Brown & Gaskin 1989, Murison & Gaskin 1989, Baumgartner et al. 2003).

The Brier Island ledges are located at the outer reaches of the Bay of Fundy. Northwest Ledge is ~5 km northwest of Brier Island (Fig. 1). Bottom topography around the ledges is steep and irregular; depths increase rapidly from <10 m over Northwest Ledge to >200 m in the Grand Manan Channel, over a horizontal distance of <3 km. Our surveys were primarily conducted in the vicinity of the Northwest Ledge in order to elucidate the effects of the ledges on surface zooplankton concentration.

Oceanographic sampling

We conducted oceanographic sampling on 9 survey days between August and September 2007 during both the ebb and flood tide phases. We designed box transects to cover a variety of habitats over and beyond the ledges (Fig. 1), and repeatedly sampled the same locations through time to evaluate

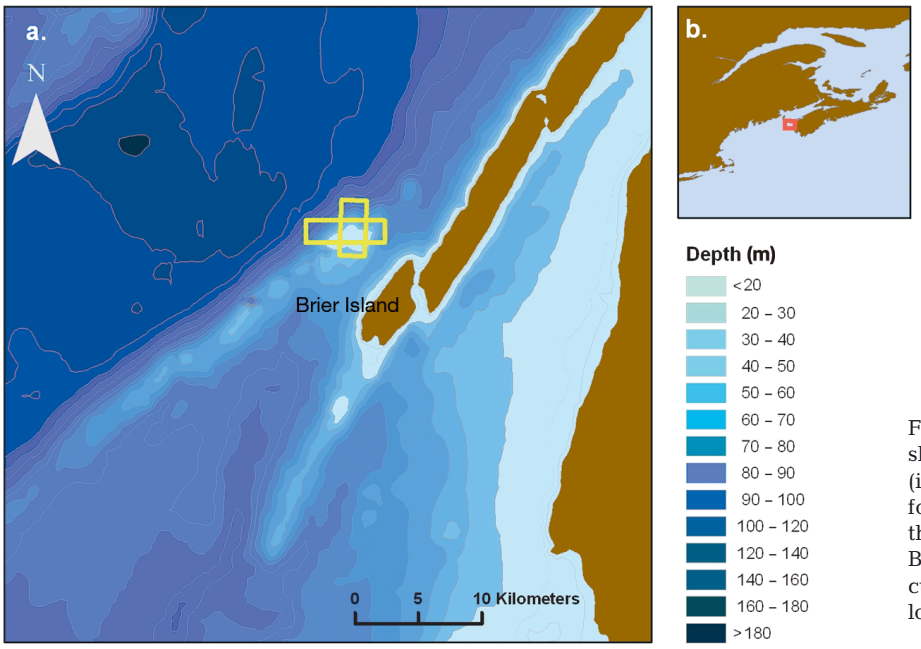

Fig. 1. Study area in Atlantic Canada showing (a) example of box transects (indicated by the yellow boxes) used for oceanographic surveys relative to the bathymetry surrounding the Brier Island ledges (study efforts focused on Northwest Ledge); and (b) location of the study site in the lower Bay of Fundy

physical and biological parameters throughout the tidal cycle (as in Johnston & Read 2007). This allowed us to correlate zooplankton samples (detailed in the next section) with physical parameters relative to tidal cycle and bathymetric relief. We sampled sea surface temperature (SST) and current speeds at depth using a 300 kHz RDI Workhorse Sentinel acoustic Doppler current profiler (ADCP) with bottom tracking capability. The ADCP was deployed over the side of a 12 m boat and the transducer head was positioned 1 m below the water surface. Survey speed did not exceed 2.6 m s^{-1}. The ADCP was set to ping as fast as possible; data were averaged over 1 min intervals and collected in 4 m bins with a maximum of 60 bins, reflecting the deepest regions surveyed. We collected data using VmDas software and visualized the observations in VmDas and WinADCP and imported them into ArcGIS 9.2 to overlay the ADCP data with bathymetry, zooplankton and phalarope data. A new ADCP file was created for each box transect to avoid obtaining multiple measurements from a given location.

Zooplankton sampling

We sampled zooplankton concurrent with ADCP surveys and followed the general sampling design of Brown & Gaskin (1989) to enable us to capture prey items accessible to foraging phalaropes. Zooplankton samples were collected at locations along oceanographic sampling box transects so as to cover a variety of bathymetric regions (over and extending beyond the ledge), and were repeatedly sampled at the same locations at different points in the tidal cycle in order to evaluate changes in surface zooplankton concentrations relative to tidal phase.

We employed a net with a 363 µm mesh size attached to a metal ring with a diameter of 0.33 m. Tows lasted for 5 min at a speed of ~1 m s^{-1}, during which the net was half submerged in the water. The R-ratio of the net, indicating the ratio of open area of net mesh to the area of the mouth opening of the net, was 10:1, which was suggested in Harris et al. (2000) in order to reduce internal water pressure in the net, and to account for flow rates at higher speeds (though our tow speeds were lower than the speeds of >1.5 m s^{-1} indicated in Harris et al. 2000). The net was occasionally lifted to avoid floating rockweed. We preserved samples in buffered formalin and transferred them to 70% ethanol for counting and identification. Zooplankton samples were divided using a Folsom plankton splitter to produce sub-samples of approximately 250 individuals. Zooplankton were counted and identified to species, and *Calanus finmarchicus* were counted, sexed and identified to life stage using a stereo microscope. All species identifications were verified by Dr. Pat Tester at the National Oceanographic and Atmospheric Administration Southeast Fisheries Science Center Laboratory in Beaufort, NC. *C. finmarchicus* density was calculated as the number of *C. finmarchicus* copepods m^{-3} by calculating the volume of water passing through the net as a function of the tow duration, the

net surface area (assuming that half of the cross-sectional surface area of the net was submerged, as described above), and the direction and speed of the boat relative to that of the measured current. After counts and identifications were conducted, we oven-dried the samples and weighed them using a balance with a precision of 0.0001 g.

We could not use ADCP backscatter and upwelling velocities to estimate zooplankton densities or identify regions of local upwelling because of problems associated with assessing zooplankton backscatter while steaming (Heywood et al. 1991) and because of noise produced from pitch and roll during boat-based surveys across the ledges. In addition, we were specifically interested in the abundance and distribution of zooplankton that was available to phalaropes in surface waters, which could not be assessed using a hull-mounted ADCP.

Phalarope observations

Our primary objective was to investigate relationships between oceanographic processes and zooplankton distribution in surface waters, and our box transect surveys were designed to survey a given area repeatedly throughout the tidal cycle. We also collected oceanographic data during boat-based surveys assessing phalarope distribution and abundance on 4 days, and collected 16 zooplankton tows on these survey days. Two observers conducted visual surveys from approximately 6 m above the water in early August and mid-September 2007 to estimate the abundance and species composition of phalaropes. In the Bay of Fundy, phalaropes occur in large, ephemeral feeding flocks, so modified survey methods are required to generate estimates of phalarope abundance and species composition. Tracks were initiated at the north or south end of the ledges, and were conducted across the ledges using a saw-tooth pattern until birds were observed. We decreased speed when flocks of phalaropes were encountered and maneuvered the boat alongside the flocks to obtain accurate counts and to confirm species identification. In late summer, red and red-necked phalaropes occur in large mixed aggregations in non-breeding plumage and can be difficult to distinguish. Surveys on these days yielded 82 sightings of phalaropes, comprising more than 13 000 birds, with concurrent oceanographic data. Survey tracks were divided into 1 km bins in ArcGIS, and phalarope counts in grid cells were analyzed relative to oceanographic predictor variables using multivariate analyses (see next section).

Analysis

We interpolated depth estimates from ADCP surveys to provide a comprehensive bathymetric coverage of the study area. We produced continuous rasters of SST, average current speed and depth by interpolating short-term averaged data (1 min) in ArcGIS 9.2 using ordinary kriging interpolation in the spatial analyst extension. The bathymetric raster was then used to generate a continuous coverage of distance to the 20 m depth contour, which we used as a metric of distance to the Northwest Ledge. We used depth rasters to create grids of depth gradients (percent rise) using the slope function in spatial analyst. All interpolated rasters had a pixel size of 50 m. Before including variables in our statistical analyses, we examined our data for co-linearity. Variables with a significant Pearson's correlation coefficient of 0.5 or greater were not included within the same model.

We used generalized additive models (GAMs) to model zooplankton and phalarope abundance relative to oceanographic parameters. GAMs are non-parametric extensions of linear regression models. These additive models consist of the sum of smooth functions describing the covariates, which replace the linear predictors of covariates used in linear regression models (Hastie & Tibshirani 1990). A link function is used to relate response variables to a smoothed function of the explanatory variables. In comparison to linear models, GAMs allow a wider range of response curves to be modeled and are better suited to evaluate highly non-linear relationships between response and explanatory variables. These attributes are particularly useful in ecological studies (see Yee & Mitchell 1991, Guisan et al. 2002). Selecting an appropriate level of smoothing is an important step in developing a GAM, and can be achieved by using the concept of the effective degrees of freedom (Guisan et al. 2002). We constructed GAMs using cubic spline smoothers with 3 or fewer degrees of freedom to avoid over-fitting the models while assessing relationships between copepod density, total zooplankton biomass or phalarope abundance and the following predictor variables: SST, SST gradient, daily SST anomaly (i.e. deviance of a given SST measurement from the daily mean SST over all tracks lengths), distance to 20 m contour, depth gradient, current speed and time since slack low tide. This analysis was intended to capture the effects of current speed and bathymetry on surface distributions of copepods that are more typically observed at depths of more than 50 m during daylight hours, so we used current speed

throughout the water column in this analysis. We constructed models both for counts and dry mass values of zooplankton tows, as well as the proportion of all copepods comprised of *Calanus finmarchicus*, standardized by the tow volume to account for differences due to increased water flow. We assessed the normality of counts and dry mass values using Q-Q plots and Anderson-Darling normality tests. We employed a Gaussian distribution to evaluate dry mass values, which were log-transformed to meet assumptions of normality. We analyzed copepod and phalarope count data using a quasi-Poisson distribution due to over-dispersion of the data. For all GAM models, we conducted variable selection using backwards stepwise regression model selection and selected the model with the lowest generalized cross-validation (GCV) value as described in Wood & Augustin (2002). We assessed goodness-of-fit using adjusted R^2 values. Non-significant values were removed from the final model. To examine the temporal structure of the copepod data, we assessed the relationship between volume-corrected copepod counts and tidal phase (hours since slack low tide).

We used Moran's *I* correlograms (Legendre & Legendre 1998) to identify potential effects of spatial autocorrelation in model residuals. Moran's *I* indicates the degree of spatial autocorrelation of data from −1 to 1, and can be used to determine whether significant autocorrelation is present. Negative values of Moran's *I* indicate segregation, while positive values indicate aggregation (Fortin et al. 1989). We assessed spatial autocorrelation in model residuals using Moran's *I* correlograms for all zooplankton and phalarope models and assessed significance using 1000 permutations (Bjornstad & Falck 2001). We used lag distances of 500 m for zooplankton models, reflecting the shortest distance travelled between zooplankton tows, and 1000 m for phalarope models, representing the bin size used to assess phalarope counts, up to a distance of 10 km. If significant spatial autocorrelation was observed in model residuals at any distance lag, we fitted generalized additive mixed models (GAMMs) with an AR1 autoregressive correlation structure (Dormann et al. 2007). We then compared GAM and GAMM models to determine whether autocorrelation influenced the model results.

We conducted all statistical analyses in the R statistical package (version 2.9) using the 'mgcv', 'ncf', and 'stats' packages to evaluate GAMs and GAMMs, Moran's *I* correlograms, and Pearson's correlation coefficients, respectively.

RESULTS

We conducted 133 zooplankton tows on the Brier Island ledges, and 117 tows with concurrent oceanographic data (16 tows were conducted during phalarope surveys). On average, *Calanus finmarchicus* made up 54% of the copepod species collected. There was a high degree of variation between samples, with *C. finmarchicus* ranging from 4.5 to 95.5% of copepods and from 0.01 to 200.6 ind. m^{-3}, and dry biomass of zooplankton samples ranging from 0.01 to 13.8 mg m^{-3}. Stages CIV to CVI *C. finmarchicus* dominated zooplankton tows, making up 90.2% of all *C. finmarichus* individuals. The average density of total and stage CV *C. finmarchicus* (ind. m^{-3}) peaked in late August. Due to the large variation in abundance and biomass, we also examined trends in *C. finmarchicus* through time using maximum observed values and found that the maximum density of stage CV *C. finmarchicus* (ind. m^{-3}) also peaked in late August (Fig. 2).

We analyzed separate models using daily SST anomalies and SST values as predictor variables of copepod density and phalarope counts because these terms provided different means of examining the importance of temperature and were highly correlated (Pearson's correlation, $r = 0.74$, $p < 0.001$). Variables included in the optimal model describing total *Calanus finmarchicus* density were current speed, SST, distance to ledge, time since slack low tide, and depth gradient (Table 1). The density of *C. finmarchicus* was strongly and negatively correlated with distance to ledge (20 m contour) and SST, and positively correlated with current speed. The highest densities of *C. finmarchicus* were observed at ~3 h into the flood tide, and at intermediate or high values of depth gradient (Fig. 3). To illustrate tempo-

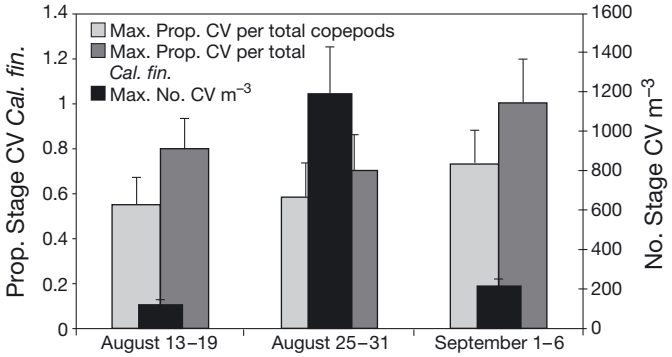

Fig. 2. Maximum proportion and density of stage CV *Calanus finmarchicus* by survey week (±1 SD). Stage CV is shown both as a proportion of total copepods and as a proportion of total *C. finmarchicus* (indicated as *Cal. fin.*)

Table 1. Variables included in best fit models for total *Calanus finmarchicus*, stage CV *C. finmarchicus*, *C. finmarchicus* as a proportion of total copepods, dry zooplankton biomass and phalarope counts. D20 = distance to 20 m contour; SST = sea surface temperature; Δ depth = depth gradient (percent rise)

Dependent variable	Variables used in model	Estimate ± SE	*t*	p	Deviance explained (%)	R^2
C. finmarchicus density (ind. m^{-3})	(intercept)	3.02 ± 0.33	9.15	1.07×10^{-12}	71.0	0.68
	D20			3.59×10^{-5}		
	Current speed			1.65×10^{-2}		
	SST			2.57×10^{-7}		
	Time since low tide			1.14×10^{-2}		
	Δ depth			1.90×10^{-3}		
Stage CV *C. finmarchicus* density (ind. m^{-3})	(intercept)	2.54 ± 0.38	6.78	2.62×10^{-9}	57.3	0.37
	D20			0.031		
	Current speed			0.0012		
	SST			0.0064		
C. finmarchicus as a proportion of total copepods	(intercept)	1.72 ± 0.084	20.54	$<2.00 \times 10^{-16}$	33.3	0.29
	D20			1.27×10^{-3}		
	Current speed			5.95×10^{-2}		
	SST			1.05×10^{-2}		
Dry mass of zooplankton samples (mg m^{-3})	(intercept)	−7.93± 0.14	−57.79	$< 2.00 \times 10^{-16}$	36.6	0.34
	D20			2.39×10^{-5}		
	SST			2.42×10^{-3}		
Phalarope counts	(intercept)	2.74 ± 0.34	8.08	5.07×10^{-13}	51.0	0.30
	Current speed			4.00×10^{-3}		
	SST			9.80×10^{-10}		
	D20			7.61×10^{-4}		

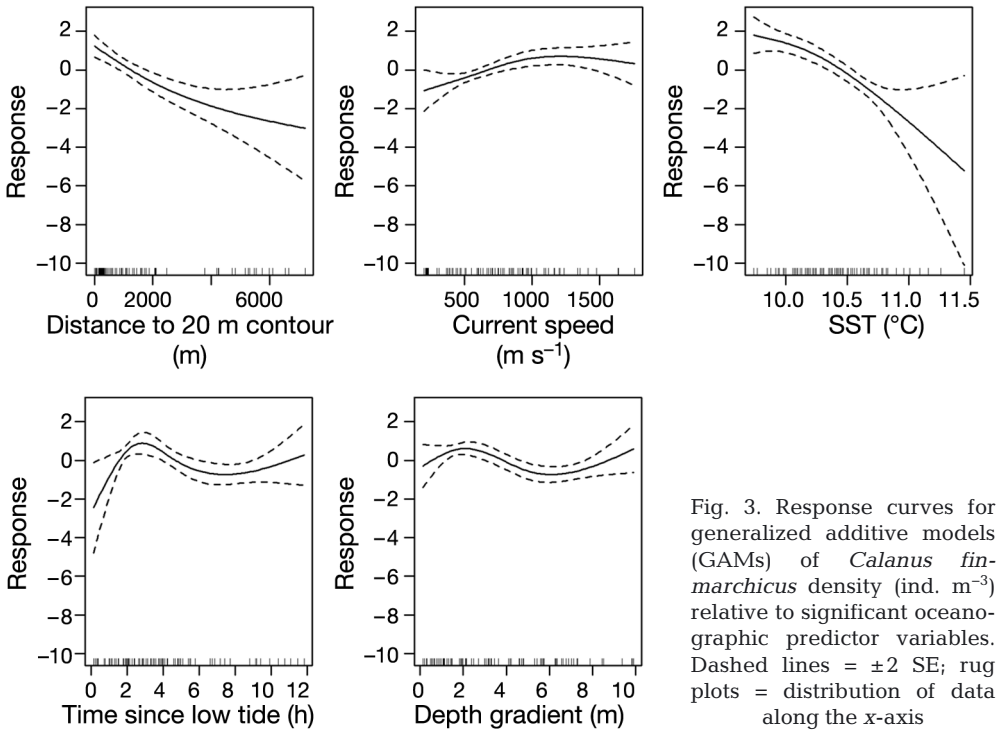

Fig. 3. Response curves for generalized additive models (GAMs) of *Calanus finmarchicus* density (ind. m^{-3}) relative to significant oceanographic predictor variables. Dashed lines = ±2 SE; rug plots = distribution of data along the *x*-axis

ral trends in the abundance of *C. finmarchicus*, fluctuations in total *C. finmarchicus* density at a given location on Northwest Ledge are shown throughout the tidal cycle relative to SST and current speed in Fig. 4.

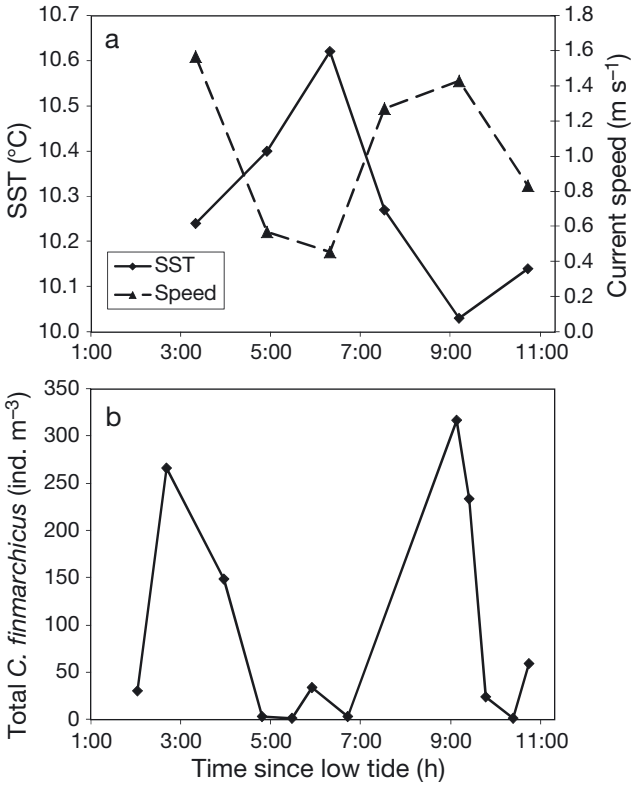

Fig. 4. Example of (a) sea surface temperature (SST) and current speed relative to time of tidal cycle (sampled at a central point on Northwest Ledge with a depth of 30 m on 30 August 2007). Note that current speeds measured at this location during slack high tide were >0.40 m s^{-1}. Current speeds measured in other locations during slack high tide reached approximately 0.05 m s^{-1}. (b) The density of total *Calanus finmarchicus* is shown relative to time since low tide for the same day

For stage CV density and the proportion of *Calinus finmarchicus* in zooplankton tows, distance to ledge, current speed and SST were the best predictors (Table 1). In both models, distance to ledge (20 m depth contour) showed a strong negative relationship with the model response, while the model response differed somewhat for the models evaluating CV density and the proportion of *C. finmarchicus* among copepods. The density of stage CV *C. finmarchicus* increased with current speed and leveled off at current speeds of ~1 m s^{-1}, while the proportion of *C. finmarchicus* increased with current speed throughout the range of current speeds measured. Both stage CV density and the proportion of *C. finmarchicus* among copepods showed a strong negative relationship with SST (Figs. 5 & 6). SST and distance to ledge were the only significant predictors of dry zooplankton biomass (Table 1) and dry zooplankton biomass was negatively correlated with both of these variables (Fig. 7). Adjusted R^2 values for the models ranged from intermediate (0.37 for stage CV *C. finmarchicus* density, 0.29 for the proportion of *C. finmarchicus* among copepods, and 0.30 for dry zooplankton biomass) to high (0.68 for total *C. finmarchicus* density), indicating a good model fit. For all zooplankton models, correlograms indicated no significant spatial autocorrelation in model residuals.

Distance to the 20 m contour was an important predictor value in all of the zooplankton GAM models, so we used this parameter to examine the spatial and temporal extent of the effects of the ledges on surface zooplankton densities. Raw data plots of the number of *Calanus finmarchicus* m^{-3} vs. distance to the 20 m contour suggested that we would expect to observe measurable effects of the physical environment on the abundance of zooplankton at the surface at distances of 1100 m from the ledges (defined by the 20 m contour). To examine whether this distance

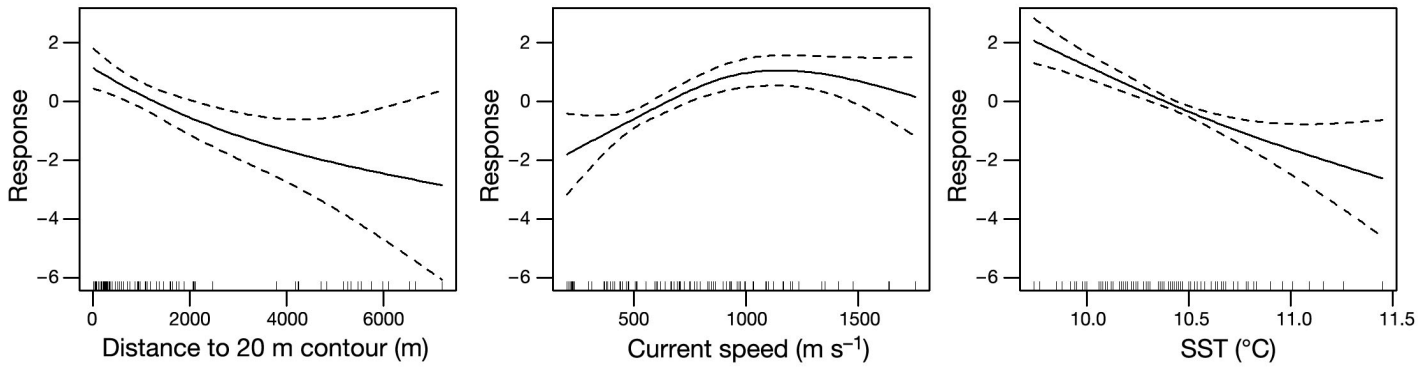

Fig. 5. Response curves for generalized additive models (GAMs) of *Calanus finmarchicus* stage CV density (ind. m^{-3}) relative to significant oceanographic predictor variables. Dashed lines = ±2 SE, rug plots = distribution of data along the *x*-axis

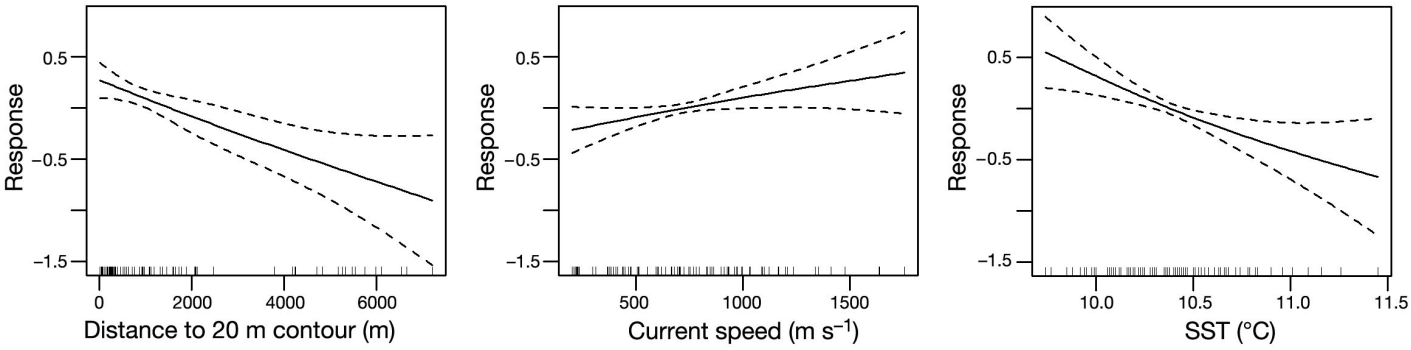

Fig. 6. Response curves for generalized additive models (GAMs) of *Calanus finmarchicus* as a proportion of total copepods relative to significant oceanographic predictor variables

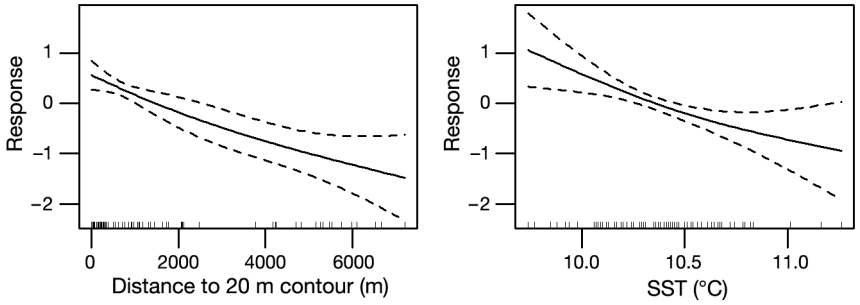

Fig. 7. Response curves for generalized additive models (GAMs) of dry zooplankton biomass (mg m^{-3}) relative to significant oceanographic predictor variables. Dashed lines = ±2 SE; rug plots = distribution of data along the *x*-axis

appropriately captured patterns in the abundance of *C. finmarchicus*, we compared temporal patterns in the abundance of *C. finmarchicus* collected at locations both within and beyond 1100 m of Northwest Ledge (69 samples were collected within this distance, while 48 were collected beyond this distance). Both the average and maximum abundance of *C. finmarchicus* were higher within 1100 m of Northwest Ledge, particularly during the flood tide phase. Due to the high degree of variation between samples as described above, we focused on the maximum abundance of *C. finmarchicus* throughout the tidal phase both within and beyond 1100 m (Fig. 8). Given the observed relationship between current speed and surface densities of *C. finmarchicus* and zooplankton biomass, we expected that broader temporal trends in current speed might also have important effects on the abundance of *C. finmarchicus* in surface waters. Fig. 9 shows the maximum observed abundance of total *C. finamarchicus* and stage CV *C. finmarchicus* relative to the average tidal amplitude at Brier Island (determined from tidal charts for Westport, NS). Maximum tidal amplitude peaked in the week of 25–31 August, as did the maximum abundance of total *C. finamarchicus* and stage CV *C. finmarchicus* in surface waters.

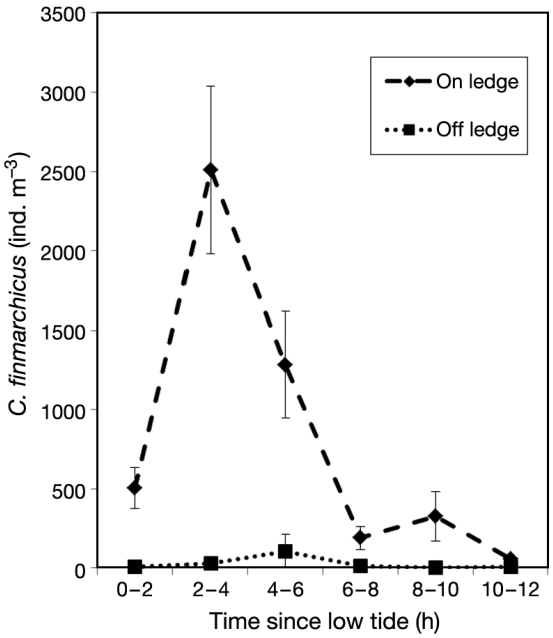

Fig. 8. Maximum *Calanus finmarchicus* density (ind. m^{-3}) by tidal phase on Northwest Ledge (within 1100 m of the 20 m depth contour) and off of Northwest Ledge

The GAM describing phalarope counts performed relatively well (R^2 = 0.30) and indicated that the best model included current speed, SST, SST gradient and distance to ledge. Correlograms indicated significant positive spatial autocorrelation in phalarope model residuals at a distance lag of ~8000 m. Consequently, GAMMs were constructed using an autocorrelated correlation structure, and results indicated

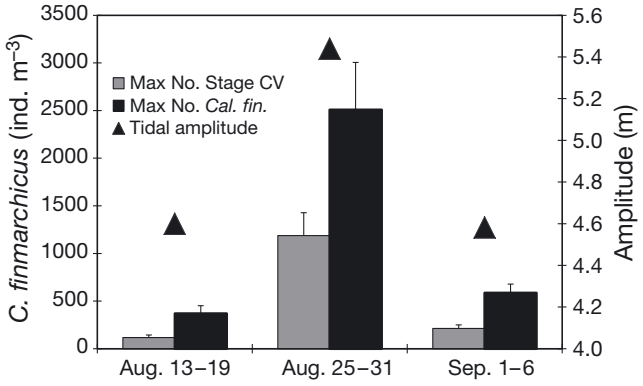

Fig. 9. Maximum density of total *Calanus finmarchicus* and stage CV *C. finmarchicus* (ind. m^{-3}) by survey week relative to tidal amplitude at the Brier Island ledges

that SST gradient was not a significant predictor variable in the mixed model. The full mixed model excluding this variable found no significant residual spatial autocorrelation. The resulting mixed model for phalarope counts is described in Table 1. Phalaropes were most abundant at low to mid values of current speed, and at intermediate values of distance to ledge (Fig. 10), which differed from the zooplankton models. As with surface zooplankton densities, phalaropes were found to be more abundant in regions of low SST, with the highest phalarope aggregations occurring at temperatures of less than 10.5°C (Fig. 10).

DISCUSSION

Calanus finmarchicus and other zooplankton are physically forced into surface waters at the Brier Island ledges due to interactions between strong tidal currents and steep bathymetric gradients. Our findings build on previous studies, which demonstrated high surface densites of *C. finmarchicus* and emphasized the importance of weed slicks in aggregating zooplankton in this region, but did not examine temporal variation in zooplankton densities or zooplankton counts within tidal phases (Brown & Gaskin 1989). Our models highlighted the importance of tidally driven upwelling in structuring zooplankton distributions in surface waters. Both the total density of *C. finmarchicus* and the proportion of this species to total copepods were strongly correlated with SST, distance to the ledge, and current speed. Together, stages CIV to CVI made up 90.2% of the total *C. finmarchicus* in surface zooplankton tows over the Brier Island ledges, although these stages are typically found in much deeper water during daylight hours in the Bay of Fundy (Baumgartner et al. 2003). Stage CV *C. finmarchicus* are a particularly important energy resource for phalaropes, and this stage typically occurs at depths of 50 to >100 m during daylight hours (Baumgartner et al. 2003).

The density of *Calanus finmarchicus* showed a significant negative relationship with SST and a positive relationship with current speed, indicating that local upwelling occurring during periods of high current speed creates aggregations of *C. finmarchicus* in surface waters, particularly on the flood tide. Observations of water temperature at depth in the Bay of Fundy, which typically declines from surface temperatures of 10.5–11°C to 10°C at depths of 40–50 m during August and September, further support the hypothesis that tidal forcing aggregates zooplankton in surface waters. *C. finmarchicus* stages typically found at or below these depths (Baumgartner & Mate 2003) were particularly prevalent in surface waters with temperatures of ~10°C or lower. Total dry zooplankton biomass, representing all zooplankton species observed in surface waters, also showed similar rela-

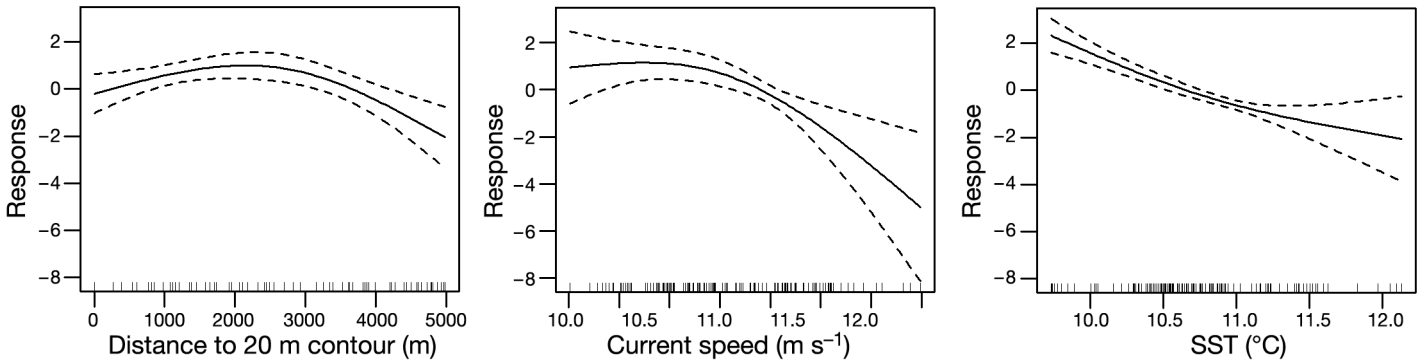

Fig. 10. Response curves for generalized additive models (GAMs) of phalarope counts relative to significant oceanographic predictor variables. Dashed lines = ±2 SE; rug plots = distribution of data along the *x*-axis

tionships with oceanographic processes over the Brier Island ledges. Taken together, therefore, our observations support the original hypothesis proposed by Brown (1980).

Model results and zooplankton measurements on the ledges (Figs. 3 & 8) indicated that the abundance of *Calanus finmarchicus* was highest during the flood tide phase. ADCP data indicated that during this tide phase, the northwestern part of the ledge was dominated by a stronger eastward flow than elsewhere on the ledge; and thus waters in this region pass over a very steep bathymetric gradient, resulting in strong vertical mixing. In addition, this causes a convergence of strong tidal currents on this part of the ledge. Both of these factors likely lead to increased densities of zooplankton in surface waters at this location during the flood tide.

Our models also indicated that both phalaropes and *Calanus finmarchicus* were more abundant in areas of low SST (e.g. Figs. 3, 4b, 5, 6, 7 & 10). Phalaropes are visual predators (Mercier 1983), and it is possible that the birds may be able to identify surface manifestations of upwelling to help locate prey aggregations. Interestingly, phalaropes were associated with regions of lower current speed and intermediate distances from the ledge, but maximum *C. finmarchicus* distributions occurred in close proximity to the ledge and at high current speeds. These findings are consistent with our visual observations of phalaropes near the ledge. When current speeds were highest, the surface waters immediately over the ledge were quite turbulent, and current speeds tended to be higher immediately over the ledges (authors' unpubl. obs.). As visual predators, phalaropes may require relatively calm waters to locate individual zooplankton prey, and thus avoid rough waters immediately over the ledges. In addition, Brown (1980) hypothesized that cool waters upwelled over the ledges drift downstream and create convergence streaks, where zooplankton and flotsam are aggregated at the surface as they sink, and that phalaropes might follow these upwelled patches of water. This hypothesis, along with our observation of rough waters over the ledges when cold water is upwelled, could explain the differences in the oceanographic parameters associated with phalarope and copepod abundance. Studies quantifying the fine-scale movements of phalaropes throughout the tidal cycle are logistically challenging to undertake, particularly due to the small size of the birds (~30 g in mass) but would improve our understanding of phalarope habitat use in this area considerably. In the future, lighter GPS tags sampling at a high spatial resolution may allow us to examine these trends in detail.

If phalaropes avoid rough waters immediately above the ledges or use weed slicks as a visual cue to detect prey aggregations in cool waters that have drifted downstream, one would expect a negative relationship between phalarope abundance and both SST and current speed, as observed. Similarly, one would expect to see maximum values of phalarope abundance to occur at intermediate distances from the ledge, as indicated by our model. Copepod densities would be expected to be high in these downstream regions of upwelled water, although not as high as in upwelling regions immediately above the ledge, as reflected in the copepod GAM models. Future studies following patches of low SST through time, or those incorporating fine-scale optical plankton counter (OPC) surveys with concurrent oceanographic surveys to provide continuous measurements of zooplankton distributions, would allow zooplankton to be evaluated relative to drifting patches of upwelled water. However, OPC measurements would not provide measurements in the upper centimeters of the water column, which are accessible to phalaropes; therefore, surface zooplankton tows should be included when assessing prey availability for this species of concern. Studies linking movements of cool water patches through time with the aggregation of surface zooplankton and formation of weed slicks, though logistically challenging, would be particularly relevant to studies of phalarope foraging.

Our models suggested that proximity to the Brier Island ledges, current speed, SST and tidal state were significant predictors of the abundance of *Calanus finmarchicus.* These findings demonstrate that the ledges affect the abundance of surface *C. finmarchicus* densities at fine spatial and temporal scales. Thus, the location of samples collected relative to the ledge and the timing of the tidal phase are important factors to consider during future efforts seeking to quantify available phalarope prey in this migratory stopover region. This would allow future studies to make comparisons with the results of the present study, and to further sampling efforts in phalarope foraging habitat. The significant effects of oceanographic processes on zooplankton abundance in both space and time highlights that these underlying processes must be considered before patterns in zooplankton or phalarope abundance can be understood over both short and long time scales.

Oceanographic processes in other locations within the Bay of Fundy also create dynamic foraging habi-

tat for phalaropes. Phalaropes likely move between different foraging patches over different tidal phases. For example, we observed phalaropes feeding on weed 'slicks', likely associated with convergence fronts (Brown 1980), south of Brier Island during low tide — when convergence between in- and outflowing tidal currents would be expected. Similarly, observations of foraging phalaropes from aerial survey data suggest that these birds are associated with bathymetric gradients and features in other locations within the Bay of Fundy (R. Hunnewell unpubl. obs.). Evaluating surface zooplankton distributions in these areas would provide a more complete picture of the prey field currently available to foraging phalaropes. Ongoing bay-wide aerial and boat-based surveys in the Bay of Fundy by the Manomet Center for Conservation Science will provide a more comprehensive picture of present-day phalarope habitat use within this region.

We emphasize that the physical mechanism influencing the distribution of *Calanus finmarchicus* is one of direct tidal forcing and physical advection. This differs from the mechanism of prey aggregation in many oceanographic features, in which increases in primary productivity are followed by time-lagged effects at successive trophic levels of the food web (e.g. Croll et al. 2005). The effects of biophysical interactions appeared to be most pronounced within 1100 m of the Brier Island ledges, but continuous sampling would be required to assess the spatial dimensions of zooplankton patches. Again, optical plankton counters would be useful in further assessing fine-scale zooplankton patch dynamics in this area.

In recent research in the Bay of Fundy, maximum depth-integrated densities of stage CV *Calanus finmarchicus* observed by Michaud & Taggart (2007) were similar to those in the present study (~1200 Stage CV *C. finmarchicus* m^{-3} in both cases). However, it is unclear how, or to what extent, the abundance and species composition of zooplankton in the Bay of Fundy may have changed since large phalarope aggregations were observed in the 1980s. Long-term zooplankton sampling studies in the Gulf of Maine have indicated a dramatic change in zooplankton community structure during the late 1980s. *C. finmarchicus* in the Gulf of Maine declined between 1989 and 1991 and remained low throughout the 1990s, likely due to changes in circulation associated with the North Atlantic Oscillation (Pershing et al. 2005). These changes in *C. finmarchicus* are thought to have influenced the abundance of another predator foraging primarily on this zooplankton species, the North Atlantic right whale *Eubalaena glacialis* (Greene & Pershing 2004) and may have played a role in the decline in red-necked phalaropes using the Bay of Fundy as a migratory stopover. Red-necked phalaropes have not been reported in such large aggregations during summer months since studies by Mercier (1983) and Brown & Gaskin (1988, 1989), despite increases in *C. finmarchicus* in the Gulf of Maine in recent years (Pershing et al. 2005). This suggests that the decreases in red-necked phalaropes in the Bay of Fundy may reflect population declines rather than shifts in habitat use.

Several studies have found associations between foraging seabirds and tidally-driven oceanographic features, and some have demonstrated that temporal components of these features were important factors influencing seabird abundance and distribution (Braune & Gaskin 1982, Zamon 2003). However, the mechanism by which these features create regions of increased prey for foraging seabirds was not investigated specifically. Independent of seabird research, many studies have evaluated processes creating aggregations of zooplankton and fish relative to different bathymetric features such as continental shelf breaks, banks, seamounts and canyons (e.g. Werner et al. 1993, Townsend & Pettigrew 1996, Genin 2004). Several studies have suggested that bathymetric features have important effects on seabird foraging habitat (e.g. Coyle et al. 1992, Hunt et al. 1998), though few studies of seabirds in relation to bathymetric features have included surveys of prey distribution. Hunt et al. (1998) demonstrated that crested, least, and parakeet auklets show species-specific patterns, foraging in regions of shallow passes in the Aleutian Islands that are upstream, downstream, and on top of the passes, respectively. Spatial differences in the location of the different prey species of these auklets were found to drive this pattern of differential habitat use, and increased tidal speed was associated with an increase in the number of auklets foraging in the passes. While biological oceanographers have made substantial progress in understanding how biophysical interactions within different oceanographic features structure biological patterns (e.g. Alldredge & Hamner 1980, Wolanski & Hamner 1988, Tremblay & Sinclair 1992, Genin 2004), our understanding of how the effects of these interactions are transferred up the food web to foraging seabirds could be improved by studies such as that of Hunt et al. (1998) which connect physical oceanographic processes with distributions of both foraging seabirds and their prey.

In conclusion, our results support the hypothesis of Brown (1980) and demonstrate that strong tidal cur-

rents generate zooplankton-rich upwelling hotspots above the ledges at fine temporal and spatial scales. We documented the zooplankton prey field available to phalaropes foraging in the Brier Island region of the Bay of Fundy and demonstrated the importance of physical forcing in structuring zooplankton abundance and species composition at fine spatial and temporal scales. At broader scales, we observed high variation in the density of surface zooplankton samples due to the extremely dynamic nature of this area, demonstrating the need for careful survey design and methods in future assessments of zooplankton distributions in this region, particularly in efforts to quantify phalarope prey. It is particularly important to capture this source of variation in the distribution of prey, so that we can accurately assess the potential drivers of the demography of red-necked phalaropes in the Bay of Fundy.

Acknowledgements. We thank R. Hunnewell and the Manomet Center for Conservation Studies for assistance in the field and for providing phalarope data for the 2007 field season. We are grateful to M. O'Brien and E. J. Rayner for their assistance during field studies, and to D. Forward, P. Tester and B. Waggett for providing advice on zooplankton sampling and identification. M. Bowers and J. Moore are thanked for assistance with weighing zooplankton samples and providing statistical advice, respectively. Funding for this project was provided by the National Geographic Society and the Oak Foundation.

LITERATURE CITED

Alldredge AL, Hamner WM (1980) Recurring aggregation of zooplankton by a tidal current. Estuar Coast Mar Sci 10: 31–37

Baumgartner MF, Mate BR (2003) Summertime foraging ecology of North Atlantic right whales. Mar Ecol Prog Ser 264:123–135

Baumgartner MF, Cole TVN, Clapham PJ, Mate BR (2003) North Atlantic right whale habitat in the lower Bay of Fundy and on the SW Scotian Shelf during 1999–2001. Mar Ecol Prog Ser 264:137–154

Bjornstad ON, Falck W (2001) Nonparametric spatial covariance functions: estimation and testing. Environ Ecol Stat 8:53–70

Braune BM, Gaskin DE (1982) Feeding ecology of nonbreeding populations of Larids off Deer Island, New Brunswick. Auk 99:67–76

Brown RGB (1980) Seabirds as marine animals. In: Winn HE, Burger J, Olla BL (eds) Behaviour of marine animals: marine birds. Plenum Press, New York, NY

Brown RGB, Gaskin DE (1988) The pelagic ecology of the grey and red-necked phalaropes *Phalaropus fulicarius* and *P. lobatus* in the Bay of Fundy, eastern Canada. Ibis 130:230–250

Brown RGB, Gaskin DE (1989) Summer zooplankton distributions at the surface of the outer Bay of Fundy, eastern Canada. Can J Zool 67:2725–2730

Brown S, Duncan C, Chardine J, Howe M (2005) Red-necked phalarope research, monitoring, and conservation plan for the Northeastern US and Maritimes Canada (version 1.0). Manomet Center for Conservation Sciences, Manomet, MA

Coyle KO, Hunt GL Jr, Decker MB, Weingartner TJ (1992) Murre foraging, epibenthic sound scattering and tidal advection over a shoal near St. George Island, Bering Sea. Mar Ecol Prog Ser 83:1–14

Croll DA, Marinovic B, Benson S, Chavez FP, Black N, Ternullo R, Tershy BR (2005) From wind to whales: trophic links in a coastal upwelling system. Mar Ecol Prog Ser 289:117–130

Dormann CF, McPherson JM, Araújo MB, Bivand R and others (2007) Methods to account for spatial autocorrelation in the analysis of species distributional data: a review. Ecography 30:609–628

Finch EW (1977) Northeastern maritime region. Am Birds 31:225–231

Fortin MJ, Drapeau P, Legendre P (1989) Spatial autocorrelation and sampling design in plant ecology. Plant Ecol 83:209–222

Franks PJS (1992) Sink or swim: accumulation of biomass at fronts. Mar Ecol Prog Ser 82:1–12

Genin A (2004) Bio-physical coupling in the formation of zooplankton and fish aggregations over abrupt topographies. J Mar Syst 50:3–20

Greene CH, Pershing AJ (2004) Climate and the conservation biology of North Atlantic right whales: the right whale at the wrong time? Front Ecol Environ 2:29–34

Griffin RB (1999) Sperm whale distributions and community ecology associated with a warm-core ring off Georges Bank. Mar Mamm Sci 15:33–51

Guisan A, Edwards TC, Hastie T (2002) Generalized linear and generalized additive models in studies of species distributions: setting the scene. Ecol Model 157:89–100

Hamner WM, Hauri IR (1981) Effects of island mass: water flow and plankton pattern around a reef in the Great Barrier Reef Lagoon, Australia. Limnol Oceanogr 26: 1084–1102

Haney JC (1986) Seabird segregation at Gulf Stream frontal eddies. Mar Ecol Prog Ser 28:279–285

Haney JC (1987) Aspects of the pelagic ecology and behavior of the black-capped petrel (*Pterodrama hasitata*). Wilson Bull 99:153–168

Harris RP, Wiebe PH, Lenz J, Skjoldal HR, Huntley M (2000) Zooplankton methodology manual. Academic Press, San Diego, CA

Hastie T, Tibshirani R (1990) Generalized additive models. Chapman & Hall, New York, NY

Haury LR, McGowan JA, Weibe P (1978) Patterns and processes in the time-space scales of plankton distributions. In: Steele JH (ed) Spatial pattern in plankton communities. Plenum Press, New York, NY

Heywood KJ, Scrope-Howe S, Barter ED (1991) Estimation of zooplankton abundance from shipborne ADCP backscatter. Deep-Sea Res 38:677–691

Hirche HJ (1996) Diapause in the marine copepod, *Calanus finmarchicus* — a review. Ophelia 44:129–143

Hunt GL Jr, Russell RW, Coyle KO, Weingartner TJ (1998) Comparative foraging ecology of planktivorous auklets in relation to ocean physics and prey availability. Mar Ecol Prog Ser 167:241–259

Johnston DW, Read AJ (2007) Flow-field observations of a tidally driven island wake used by marine mammals in the Bay of Fundy, Canada. Fish Oceanogr 16:422–435

Johnston DW, Thorne LH, Read AJ (2005) Fin whales *Balaenoptera physalus* and minke whales *Balaenoptera acutorostrata* exploit a tidally driven island wake ecosystem in the Bay of Fundy. Mar Ecol Prog Ser 305:287–295

Legendre P, Legendre L (1998) Numerical ecology. Elsevier, Amsterdam

Mercier F (1983) Feeding ecology and lipid deposition in migrating northern phalaropes in the Head Harbour region, New Brunswick. M.Sc. thesis, University of Guelph

Mercier F (1985) Fat reserves and migration of red-necked phalaropes (*Phalaropus lobatus*) in the Quoddy region, New Brunswick, Canada. Can J Zool 63:2810–2816

Mercier F, Gaskin DE (1985) Feeding ecology of migrating red-necked phalaropes (*Phalaropus lobatus*) in the Quoddy region, New Brunswick, Canada. Can J Zool 63: 1062–1067

Michaud J, Taggart C (2007) Lipid and gross energy content of North Atlantic right whale food, *Calanus finmarchicus*, in the Bay of Fundy. Endang Species Res 3:77–94

Morrison G, Gill RE, Harrington BA, Skagen S, Page GW, Gratto-Trevor CL, Haig SM (2001) Estimates of shorebird populations in North America. Occasional Paper No. 104. Canadian Wildlife Service, Ottawa

Murison LD, Gaskin DE (1989) The distribution of right whales and Zooplankton in the Bay of Fundy, Canada. Can J Zool 67:1411–1420

Pakhomov EA, McQuaid CD (1996) Distribution of surface zooplankton and seabirds across the Southern Ocean. Polar Biol 16:271–286

Pershing AJ, Greene CH, Jossi JW, O'Brien L, Brodziak JKT, Bailey BA (2005) Interdecadal variability in the Gulf of Maine zooplankton community, with potential impacts on fish recruitment. ICES J Mar Sci 62:1511–1523

Rodhouse PG, Prince PA, Trathan PN, Hatfield EMC and others (1996) Cephalopods and mesoscale oceanography at the Antarctic Polar Front: satellite tracked predators locate pelagic trophic interactions. Mar Ecol Prog Ser 136:37–50

Townsend DW, Pettigrew NR (1996) The role of frontal currents in larval fish transport on Georges Bank. Deep-Sea Res II 43:1773–1792

Tremblay MJ, Sinclair MM (1992) Planktonic sea scallop larvae (*Placopecten magellanicus*) in the Georges Bank Region: broadscale distribution in relation to physical oceanography. Can J Fish Aquat Sci 49:1597–1615

van Franeker JA, van den Brink NW, Bathmann UV, Pollard RT, de Baar HJW, Wolff WJ (2002) Responses of seabirds, in particular prions (*Pachyptila* sp.), to small-scale processes in the Antarctic Polar Front. Deep-Sea Res II 49: 3931–3950

Vickery PD (1978) Northeastern maritime region. Am Birds 32:174–180

Werner FE, Page FH, Lynch DR, Loder JW and others (1993) Influences of mean advection and simple behavior on the distribution of cod and haddock early life stages on Georges Bank. Fish Oceanogr 2:43–64

Wolanski E, Hamner WM (1988) Topographically controlled fronts in the ocean and their biological influence. Science 241:177–181

Wood SN, Augustin NH (2002) GAMs with integrated model selection using penalized regression splines and applications to environmental modelling. Ecol Model 157: 157–177

Yee TW, Mitchell ND (1991) Generalized additive models in plant ecology. J Veg Sci 2:587–602

Zamon JE (2003) Mixed species aggregations feeding upon herring and sandlance schools in a nearshore archipelago depend on flooding tidal currents. Mar Ecol Prog Ser 261:243–255

Submitted: November 13, 2012; Accepted: April 22, 2013

Proofs received from author(s): July 9, 2013

Vol. 487: 275–286, 2013
doi: 10.3354/meps10304

MARINE ECOLOGY PROGRESS SERIES
Mar Ecol Prog Ser

Published July 30

Contribution to the Theme Section 'Biophysical coupling of marine hotspots'

FREE ACCESS

Effects of currents and tides on fine-scale use of marine bird habitats in a Southeast Alaska hotspot

Gary S. Drew[1,*], John F. Piatt[1], David F. Hill[2]

[1]US Geological Survey, Alaska Science Center, 4210 University Drive, Anchorage, Alaska 99508, USA
[2]Oregon State University, 207 Owen Hall, Corvallis, Oregon 97331, USA

ABSTRACT: Areas with high species richness have become focal points in the establishment of marine protected areas, but an understanding of the factors that support this diversity is still incomplete. In coastal areas, tidal currents—modulated by bathymetry and manifested in variable speeds—are a dominant physical feature of the environment. However, difficulties resolving tidally affected currents and depths at fine spatial-temporal scales have limited our ability to understand their influence on the distribution of marine birds. We used a hydrographic model of the water mass in Glacier Bay, Alaska, USA, to link depths and current velocities with the locations of 15 common marine bird species observed during fine-scale boat-based surveys of the bay conducted during June of 4 consecutive years (2000 to 2003). Marine birds that forage on the bottom tended to occupy shallow habitats with slow-moving currents; mid-water foragers used habitats with intermediate depths and current speeds; and surface-foraging species tended to use habitats with fast-moving, deep waters. Within foraging groups there was variability among species in their use of habitats. While species obligated to foraging near bottom were constrained to use similar types of habitat, species in the mid-water foraging group were associated with a wider range of marine habitat characteristics. Species also showed varying levels of site use depending on tide stage. The dramatic variability in bottom topography—especially the presence of numerous sills, islands, headlands and channels—and large tidal ranges in Glacier Bay create a wide range of current-affected, fine-scale foraging habitats that may contribute to the high diversity of marine bird species found there.

KEY WORDS: Current velocity · Tides · Bathymetry · Seabirds · Glacier Bay

INTRODUCTION

As resource exploitation and anthropogenic disturbance of marine ecosystems have increased, there has been a commensurate increase in the effort to identify and protect biodiversity (Boersma & Parrish 1999, Hyrenbach et al. 2000, Yen et al. 2006, Nur et al. 2011). Marine birds represent the most visible component of these systems, yet our understanding of the factors that affect their habitat use and local diversity are limited.

At coarse scales (100 to 1000 km), increased numbers and species of marine birds have been associated with large oceanographic features such as fronts and upwellings (Hunt & Schneider 1987, Hunt et al. 1998, Spear et al. 2001, Piatt et al. 2006, Suryan et al. 2006, Weimerskirch 2007). However, at finer scales, associations between oceanographic features and marine bird distributions have been more difficult to quantify (Schneider & Piatt 1986, Hunt & Schneider 1987, Fauchald et al. 2000). This difficulty has been attributed to the imperfect knowledge of predators regarding where and when prey are available (Schneider & Piatt 1986), the mismatch between ecosystem components (Francis et al. 1998) and the patchy and ephemeral nature of the prey concentra-

*Email: gdrew@usgs.gov

tions (Hunt & Schneider 1987). One factor that has not been well studied is the role of fine-scale spatial and temporal variability of environmental factors affecting the distribution of marine birds. In part, this has been due to a lack of high-resolution environmental data.

The issue of fine-scale habitat use is of particular importance for understanding the distribution of marine birds in coastal areas, where tidally affected currents and water depths provide high levels of spatial and temporal habitat heterogeneity. Bottom depth directly affects accessibility to prey, especially for obligate bottom-feeding species, while current speed affects prey encounter rates (Sims et al. 2008) and may contribute to the concentration or dispersion of prey aggregations (Alldredge & Hamner 1980). In Alaska, tide-related changes in depth are not insignificant, as tides routinely range in height between 3 and 5 m, with extremes of up to 13 m. In coastal areas, tidal regimes should provide marine birds with predictable foraging conditions due to diurnal and monthly cycles (Holm & Burger 2002).

Until recently, the difficulties of acquiring high-resolution (100 m) data on constantly changing physical factors such as tidal currents have limited our ability to test for associations at these scales. Recent advances in high-resolution hydrographic models make it possible to model fine-scale current speeds and depths over time and, therefore, to directly assess tidal effects on habitat use by different marine species (Etherington et al. 2007, Chenoweth et al. 2011). In addition to current strength and depth, tidal current direction (ebb or flood) may also be important. Black-legged kittiwakes *Rissa tridactyla* in Prince William Sound were found to concentrate their foraging efforts during ebbing tides (Irons 1998), and, in the Bering Sea, murre *Uria* spp. foraging has been linked to tidal ebbs (Coyle et al. 1992).

Glacier Bay, a glacially affected fjord in southeast Alaska, is known to have high primary productivity (Etherington et al. 2007), diverse fish communities (Arimitsu et al. 2003) and a diverse assemblage of marine top-predators (Drew et al. 2008). Species-richness data from the North Pacific Pelagic Seabird Database (NPPSD) (USGS 2012) indicate that Glacier Bay is a regional marine bird hotspot (Fig. 1). Species that comprise the diverse Glacier Bay marine bird community (Drew et al. 2008) employ a wide variety of foraging strategies and food types. As such, physical factors such as current speed and bottom depth should influence the choice of habitats used by each species in the bay. Our objectives were to investigate the use of habitats created by basic tidal forces, i.e. speed, direction and bottom topography on the distribution of 15 common marine birds in Glacier Bay. From this, we hope to improve our understanding of coastal habitat use and species richness of marine birds in southeast Alaska.

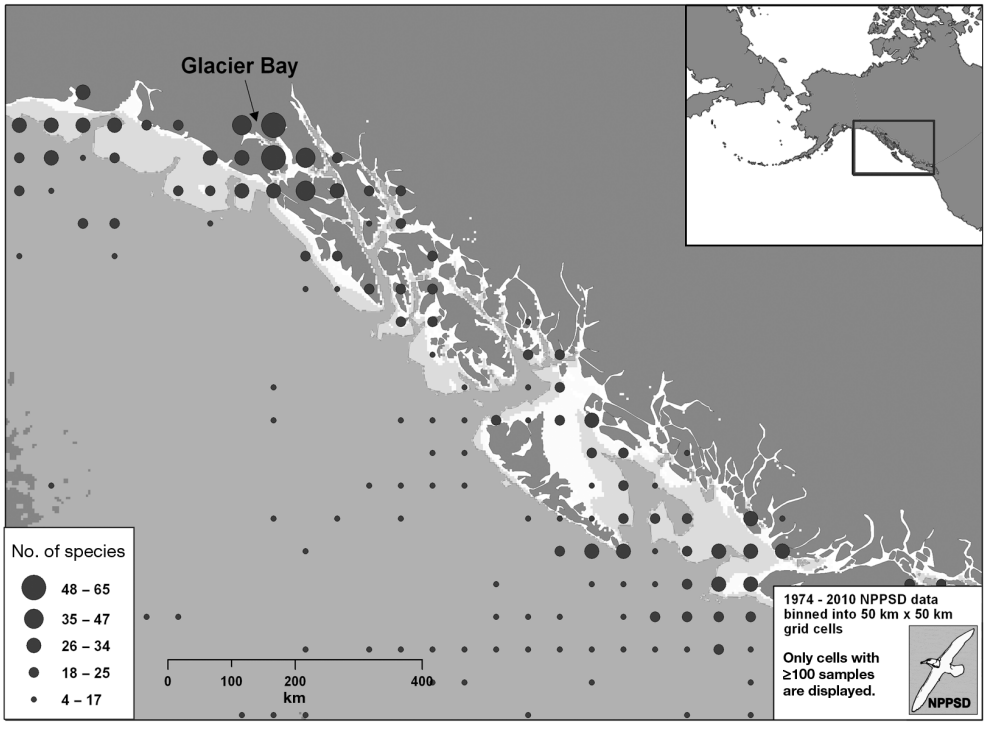

Fig. 1. Species richness across Southeast Alaska, USA, and western British Columbia, Canada. Data were obtained from the North Pacific Seabird Database and binned into 50 × 50 km cells

METHODS

Study area

Glacier Bay is a 100 km long Y-shaped glacial fjord in southeast Alaska, with a complex shoreline that includes several constrictions (Fig. 2). The bathymetry of the bay includes numerous sills and basins up to 457 m deep (Fig. 2). Tides in the bay range from an average of 3.7 m at Bartlett Cove to 4.2 m in the upper part of the bay. The hydrographic interactions of this complex marine area result in a wide range of tidal effects including extreme current speeds and complete mixing in shallow narrow sections such as Sitakaday Narrows (Etherington et al. 2007, Hill et al. 2009). Glacier Bay supports large concentrations of zooplankton and forage fish (Abookire et al. 2002, Robards et al. 2003, Arimitsu et al. 2008), as well as abundant benthic invertebrates (Bodkin et al. 2007). In turn, these forage resources support a large number and variety of marine bird species (Robards et al. 2003, Bodkin et al. 2007).

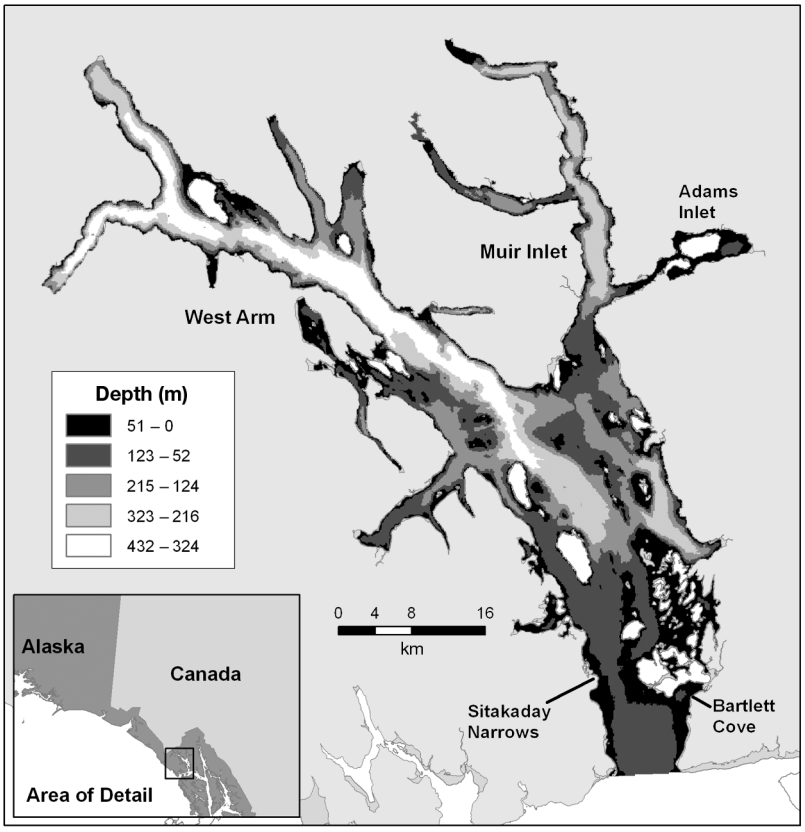

Fig. 2. Glacier Bay study area, associated bathymetry and place names

Bird survey design

We conducted surveys for marine birds and mammals in Glacier Bay, Alaska, during the summers of 2000 to 2003 using a systematic design to sample all areas of the bay. The entire coastline of Glacier Bay was surveyed, and offshore areas were sampled with a series of transects perpendicular to the shore spaced 2.5 km apart. We used strip-transect protocols established by the US Fish and Wildlife Service (USFWS) for census of marine bird and mammal communities (Gould & Forsell 1989). All marine birds observed within the 300 m wide strip-transect were recorded continuously. Because surveys were conducted during the reproductive season when energetic needs peak, we expected that this would also be the period with the strongest correlation between the availability of prey and the distribution of top predators. We included all observations of surface-foraging birds, due to our inability to distinguish active searching from transiting. For all other species only those on the water were used for analysis. Detailed descriptions of the survey tracks and methodology can be found in Drew et al. (2008).

Current modeling

To investigate correlations between bird observation locations and tidal conditions, 2 different measures of tidal velocity were computed. The first was the root-mean-square (RMS) value of the velocity. Mean values of tidal velocity are generally very close to zero, when averaged over many tidal cycles; therefore, the RMS value is a much more useful indicator of tidal strength and potential mixing of the water column. The second measure of interest was simply the modeled instantaneous depth-averaged (barotropic) velocity at each bird observation site, at the time of observation.

To obtain both of these measures of tidal velocity, the tidal model ADCIRC (Luettich & Westerink 1991) was applied to the Glacier Bay region. ADCIRC uses an unstructured finite-element mesh in the horizontal plane and can be run in 3-dimensional or 2-dimensional

depth-averaged modes. The model can be forced with open boundary tides, freshwater runoff, and surface wind stress and pressure fields. ADCIRC outputs time series of elevation and velocity and (optionally) harmonic analysis results. Previous application of the model to Glacier Bay revealed the rich spatial structure of tidal amplitudes and barotropic velocity circulation patterns (Hill et al. 2009). The computational extent of both that and the present modeling effort included all of Glacier Bay proper, as well as the outlying waters of Icy Strait and Cross Sound. Tidal parameters predicted by computational runs with this mesh were validated by demonstrating excellent agreement with values accepted and distributed by the National Oceanographic and Atmospheric Association (NOAA) (Hill et al. 2009).

For our study, estimates of RMS tidal velocity were derived from simulating 90 d of tidal motion. The open boundaries were forced with 10 tidal constituents drawn from the ENPAC database (Spargo et al. 2004). After 30 d of ramp-up, to help suppress initial transients, harmonic analysis was applied to the remaining 60 d of model output to determine the amplitudes and phases of the primary tidal constituents for both water surface elevation and water velocity. RMS velocities were obtained from these constituents.

To estimate instantaneous tidal velocity, a total of 4 computational runs were conducted, 1 for each summer survey (2000 to 2003). Each model run began with a ramp-up before the first bird observation and lasted until the last bird observation. As with the RMS runs, the model was forced by tides at the 2 open boundaries (Spargo et al. 2004). No meteorological or river forcing was used. Figs. 9 & 10 of Hill et al. (2009) demonstrate that the depth-averaged velocity is strongly dominated by tidal forcing, as opposed to the freshwater runoff, justifying this choice. The nodal factors and equilibrium arguments, which are used to set the 'starting time' for each simulation, were obtained from the T_TIDE Matlab package (Pawlowicz 2002).

For each model run, time series of water surface elevation and velocity were computed and recorded in 30 min intervals, at every location reporting a bird observation for that particular year. As a final step, the output data were temporally interpolated to the exact observation times, thereby providing an 'instantaneous' calculation of tidal elevation and velocity at each observation location (latitude, longitude) at the time of observation.

Data analysis

To examine the differential use of habitats by marine birds in relation to the physical factors that define them, we used the ADCIRC model to identify depth and current values associated with each observation time and location collected during boat surveys. Tidal stage was determined by extracting tidal information using the NOAA Tide/Current Predictor (www.tidesandcurrents.noaa.gov). Although there is some variation in tides across the length of Glacier Bay, we were restricted to the only tide station in Bartlett Cove, which had a range of 3.7 m (Fig. 2). The extracted data had a resolution of 1 min and were assigned as either ebb or flood. We used time to match the tidal stage with the ADCIRC output for each bird observation. Due to the variability in group size and the affinity for grouping among some species, we treated all observations, whether of groups or single birds, as a single observation. We classified the 15 species into 3 groups, surface feeders, midwater feeders and bottom feeders, based on their foraging habits within the water column.

Logistic regression was used to test the presence or absence of each species or foraging group for associations, when birds were observed, with 3 variables: (1) instantaneous depth, hereafter referred to as used depth; (2) instantaneous current speed, hereafter referred to as used current; and (3) tidal direction (ebb or flood). Although wind has long been identified as an important factor in coastal upwelling (Smith 1968, Small & Menzies 1981), previous research on the oceanographic patterns in Glacier Bay suggested that wind was not a major factor influencing the stability of the water column in the bay (Etherington et al. 2007); therefore, we did not include it in our analysis.

While the logistic regressions indicate which of the environmental factors are influencing the use of sites by species, marine habitats are temporally variable. Species may select locations during periods when currents or depths are higher or lower than expected based on the RMS currents or mean sea level (MSL). These patterns of use may provide a form of resource partitioning between species. For example, some species may use habitats with high RMS currents, but only when currents are below the RMS value. The logistic regressions could identify the use of high or low current speeds, but not whether currents or depths were higher or lower than expected based on average values. Use of sites during periods with specific current or depth conditions could provide

insights regarding results of our logistic regressions. Fortunately, the ADCIRC model provided both instantaneous and RMS current speeds, as well as instantaneous and MSL depths. We used paired *t*-tests to compare used versus RMS current speeds and used versus MSL depths for all species. A significant result in the paired *t*-test would suggest that a species was using areas at current flows different from the RMS values. We used 95% CI plots of the difference between used and expected currents and depths to identify whether species were using sites under specific conditions. If a species focused their use on an area regardless of instantaneous current and depth factors, we would expect the mean use to be zero.

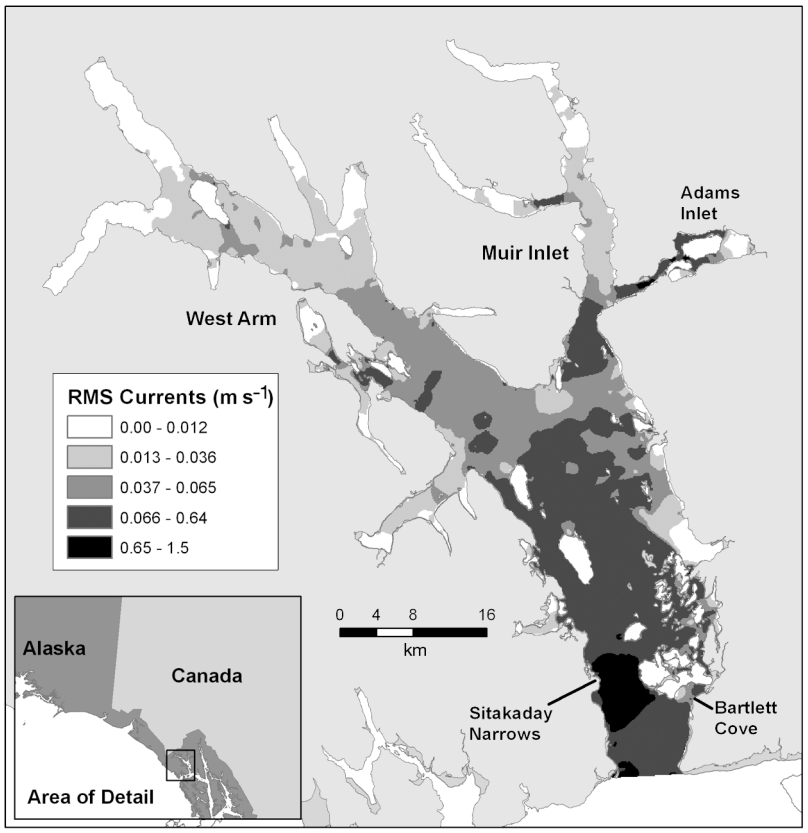

Fig. 3. Tidal currents in Glacier Bay, Alaska. Root-mean-square (RMS) current flow from the ADCIRIC model. Light areas: low currents, dark areas: high currents (see key)

RESULTS

There is a general increase in RMS current speeds moving from the head of Glacier Bay to the mouth (Hill et al. 2009). Areas of physiographic constriction, such as those found at Sitakaday Narrows and in Adams inlet (Fig. 2) were characterized by particularly high RMS values (Fig. 3). Although there was a correlation between bottom depth and current speed ($n = 12\,995$, $p < 0.001$), depth explained <1.3% of the variation in current speeds, so we treated these 2 factors as independent.

Habitat associations of foraging groups

Logistic regressions conducted on the 3 foraging groups indicated differences in the use of sites by depth and current speed (Table 1). Bottom foragers used shallow habitats (Fig. 4) with slow average current speeds (Fig. 5). Surface foragers used habitats with deeper water (Fig. 4) and the fastest current speeds (Fig. 5). Mid-water foraging birds used habitats that fell between the other 2 groups in terms of both depth and current speed. None of the 3 foraging groups showed any preference for tidal direction (Table 1).

Habitat associations by species

Depth was a significant factor in the use of sites by the majority of species. Of the 15 species tested, 11 had an association with depth (Table 1; see also for scientific names and codes). Glaucous-winged gulls, black-legged kittiwakes, marbled murrelets and Kittlitz's murrelets used sites with depths greater than the average for other species (Fig. 6). Conversely, mew gulls, common loons, pelagic cormorants, common mergansers, pigeon guillemots, harlequin ducks and white-winged scoters used habitats that were shallower than the average for other species (Fig. 6). In addition to species-specific differences in selected depths, there was considerable variation within all foraging groups. These differences were most pronounced in the mid-water group which contained the species using the shallowest depths (common merganser) and the deepest depths (Kittlitz's murrelet).

Significant associations were identified between current speeds and 10 of the 15 species tested (Table 1). Glaucous-winged gulls, black-legged kittiwakes,

Table 1. Logistic regressions on 15 species and 3 foraging groups testing for associations with depth, currents and tidal direction. Marine bird survey data were collected in Glacier Bay, Alaska, USA, during the summers of 2000 to 2003. ns: not significant; *: $p < 0.05$; **: $p < 0.01$; ***: $p < 0.001$

Species	Code	Foraging group	Observations (n)	Depth (m)	Current (m s^{-1})	Ebb–Flood	Direction
Surface foraging group							
Glaucous-winged gull *Larus glaucescens*	GWGU	Surface	1626	*	***	**	Ebb
Herring gull *Larus argentatus*	HEGU	Surface	160	ns	ns	ns	–
Mew gull *Larus canus*	MEGU	Surface	673	***	ns	**	Ebb
Black-legged kittiwake *Rissa tridactyla*	BLKI	Surface	1590	***	***	**	Flood
Arctic tern *Sterna paradisaea*	ARTE	Surface	534	ns	***	*	Flood
Overall surface foragers		Surface	3722	***	***	ns	–
Mid-water foraging group							
Common loon *Gavia immer*	COLO	Mid-water	96	***	ns	ns	–
Pacific loon *Gavia pacifica*	PALO	Mid-water	83	ns	ns	ns	–
Pelagic cormorant *Phalacrocorax pelagicus*	PECO	Mid-water	97	*	*	*	Flood
Common merganser *Mergus merganser*	COME	Mid-water	299	***	***	ns	–
Marbled murrelet *Brachyramphus marmoratus*	MAMU	Mid-water	3265	***	***	ns	–
Kittlitz's murrelet *Brachyramphus brevirostris*	KIMU	Mid-water	752	***	ns	ns	–
Pigeon guillemot *Cepphus columba*	PIGU	Mid-water	3136	***	***	*	Ebb
Overall mid-water foragers		Mid-water	7620	***	***	ns	–
Bottom foraging group							
Harlequin duck *Histrionicus histrionicus*	HADU	Bottom	279	***	**	ns	–
White-winged scoter *Melanitta fusca*	WWSC	Bottom	246	***	*	ns	–
Surf scoter *Melanitta perspicillata*	SUSC	Bottom	194	ns	**	ns	–
Overall bottom foragers		Bottom	719	***	***	ns	–

Arctic terns, common mergansers, pigeon guillemots and marbled murrelets were associated with faster currents (Fig. 7). Pelagic cormorants, harlequin ducks, white-winged scoters and surf scoters were associated with slower currents (Fig. 7). There was considerable variation in used current speeds among species in the surface foraging and mid-water foraging groups. However, bottom foraging species were more uniform, with all being associated with slower than expected current speeds.

Tidal direction was significantly associated with the use of areas by glaucous-winged gulls, mew gulls, black-legged kittiwakes, Arctic terns, pelagic cormorants and pigeon guillemots (Table 1). Tidal direction was identified as significant for 4 of the 5 surface foragers and 2 of the 7 mid-water foragers. None of the 3 bottom foragers displayed any association with tidal direction. Herring gulls *Larus argentatus* were the only surface foraging species that was not associated with tidal direction, but were also

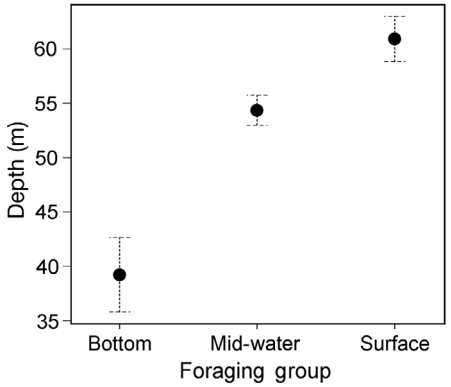

Fig. 4. Depths at marine bird observation sites within Glacier Bay (2000 to 2003) grouped into 3 foraging classes: bottom, (n = 719), mid-water (n = 7620) and surface (n = 3722). Means ± 95% CI

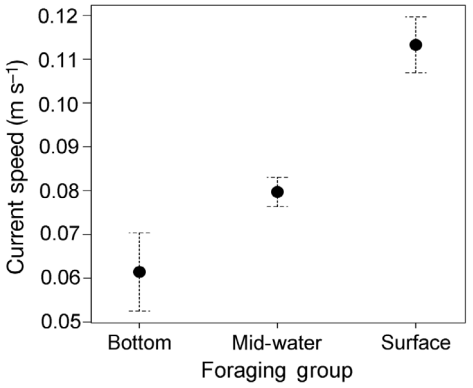

Fig. 5. Current speed at marine bird observation sites within Glacier Bay (2000 to 2003) grouped into 3 foraging classes: bottom (n = 719), mid-water (n = 7620) and surface (n = 3722). Means ± 95% CI

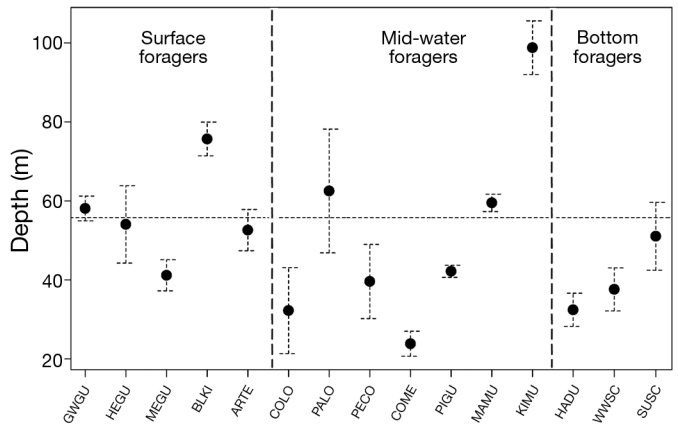

Fig. 6. Depths at observation sites for 15 species in Glacier Bay. Means ± 95% CI. Dashed horizontal line: overall mean depth for all observed birds. Vertical dashed lines separate foraging groups. Species codes see Table 1

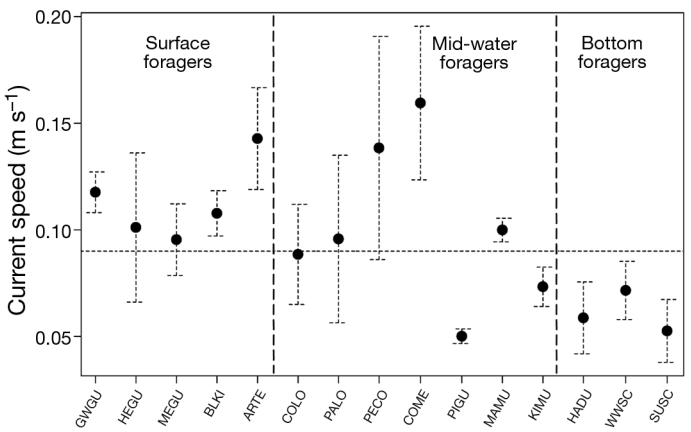

Fig. 7. Current speeds at observation sites for 15 species in Glacier Bay. Means ± 95% CI. Dashed horizontal line: overall mean depth for all observed birds. Vertical dashed lines separate foraging groups. Species codes see Table 1

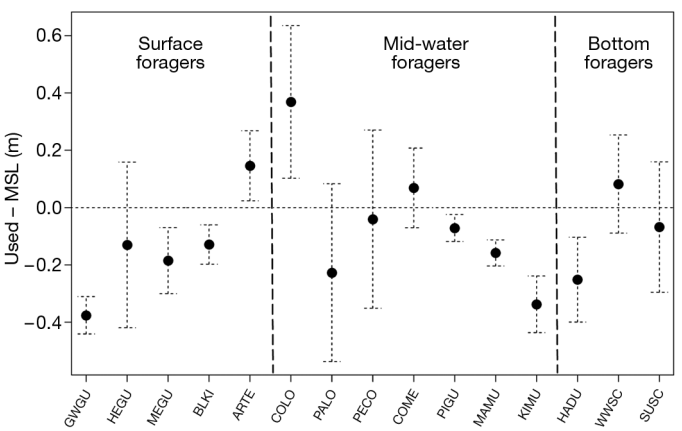

Fig. 8. Deviations from mean sea level (MSL) at observation sites for 15 species in Glacier Bay. Means ± 95% CI. Dashed horizontal line: no difference between used depths and MSL. Vertical dashed lines separate foraging groups. Species codes are given in Table 1

the least common species (Table 1). Among the mid-water foraging species that exhibited a preference for tidal direction, 4 most commonly used floods and 3 most commonly used ebbs. Within groups there was no consistency in the choice of tidal direction.

Paired comparisons between instantaneous depths and MSL indicated that 9 of the 15 species used sites when depths were significantly different than the average (Table 2). Plots of used versus MSL depths indicated that Arctic terns and common loons used sites when depths were greater than expected (Fig. 8). Conversely, glaucous-winged gulls, mew gulls, black-legged kittiwakes, pigeon guillemots, marbled murrelets, Kittlitz's murrelets and harlequin ducks used sites when depths were less than expected for used locations (Fig. 8).

Paired comparisons between instantaneous currents and RMS (average) currents for these same locations indicated that 7 of the 15 species used sites when currents were significantly different than the RMS currents. Glaucous-winged gulls, black-legged kittiwakes, Pacific loons *Gavia pacifica*, pigeon guillemots, marbled murrelets, Kittlitz's murrelets and white-winged scoters used sites based on relative current speed (Table 2). Plots of used versus RMS currents indicated that all of these 7 species tended to use habitats when current speeds at the time of observation were lower than the RMS average at that location (Fig. 9). No species tended to use habitats when instantaneous speeds were greater than the RMS speeds.

Table 2. Paired *t*-tests comparing used currents and depths versus the root-mean-square currents and mean sea level values for each observed species location. Foraging group: S = surface, M = mid-water, B = bottom. *: $p < 0.05$; **: $p < 0.01$; ***: $p < 0.001$. Species codes see Table 1

Species code	Foraging group	df	*t*-test	
			Speed	Depth
GWGU	S	1507	−9.075***	−11.310***
HEGU	S	116	−1.131	−0.893
MEGU	S	542	1.023	−3.155**
BLKI	S	1475	−4.231***	−3.685***
ARTE	S	501	0.677	2.343*
COLO	M	85	−1.381	2.749**
PALO	M	72	−2.000*	−1.460
PECO	M	85	−0.544	−0.258
COME	M	262	0.733	0.972
PIGU	M	2803	−6.898***	−2.970**
MAMU	M	3085	−15.001***	−6.788***
KIMU	M	717	−5.653***	−6.709***
HADU	B	221	−0.267	−3.345***
WWSC	B	220	−3.446***	0.944
SUSC	B	163	−1.968	−0.591

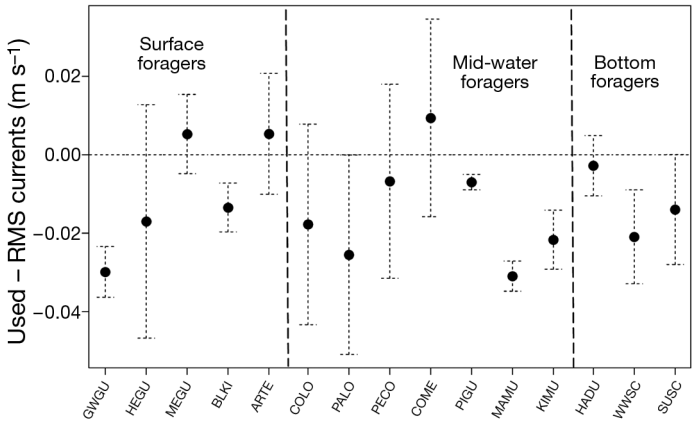

Fig. 9. Deviations from the root-mean-square (RMS) current speeds at observation sites for 15 species in Glacier Bay. Mean ± 95% CI. Dashed horizontal line represents no difference between used current speeds and RMS values. Vertical dashed lines separate foraging groups. Species codes see Table 1

DISCUSSION

Habitat associations of bottom foraging species

The use of shallow areas by bottom foragers was both expected and understandable given their foraging constraints. These species must be able to reach bottom and forage efficiently in the substrate (Wilson & Wilson 1988, Vermeer et al. 1993, Lewis et al. 2008). Bottom foraging species usually feed on sessile prey and only infrequently benefit from concentrations of free-swimming prey in the water column. Access to prey by bottom foragers may be inhibited by high currents due to increased foraging effort (Lovvorn & Gillingham 1996, Heath & Gilchrist 2010). Accordingly, bottom foraging species were observed using the lowest absolute and relative current speeds. Our findings are consistent with observations of diving ducks off the coast of British Columbia (Holm & Burger 2002). Tidal direction was not found to be significant for any bottom foragers.

The use of relatively shallow depths by 2 of the 3 bottom foraging species was expected due to their requirement for access to benthic substrate. Similarly, all 3 bottom foraging species used sites with lower current speeds (but note that pigeon guillemots, from the mid-water foraging group, selected the slowest currents). For species foraging in benthic substrate, costs should increase both with increasing depths and current speed. The prey items for bottom foragers are largely filter-feeding sessile organisms that rely on actively moving water for their food supply (Strathmann 1985). Paradoxically, bottom foraging birds forage most efficiently where currents are low, due to energetic costs, but many of their prey may be most common in areas with moderately high currents (Wells 1957, Mileikovsky 1971). Harlequin ducks appear to be particularly sensitive to depth as they used shallow habitats and tended to use them when tides were below MSL. Although bottom foraging species generally favored lower current speeds, white-winged scoters were particularly sensitive to current speeds, using sites when currents were lower than the RMS current. This suggests that white-winged scoters may be adjusting their forging times to minimize their exposure to the higher currents and presumably higher foraging costs.

Habitat associations of mid-water foraging species

The disproportionate use of intermediate depths by mid-water foragers may reflect the use of these habitats by their primary prey, schooling fish, while limiting the water column to depths within the dive range of these birds (Coyle et al. 1992, Maniscalco et al. 1998). In general, mid-water foragers were associated with moderate current speeds. Despite the potential benefits of prey being driven closer to the surface with tidal mixing (Begg & Reid 1997) and increased encounter rates (Sims et al. 2008), high current speeds can also increase the energetic costs of swimming (Lovvorn et al. 2001), and fish schools may be disrupted by high current speeds (Pitcher 1973). Previous research had found associations between mid-water foraging birds during both ebbs (Coyle et al. 1992, Irons 1998, Thompson & Price 2006) and floods (Zamon 2001); however, this is the first study where a range of species was simultaneously tested. The wide variation in habitat use by mid-water foraging species suggests that this group employs the most diverse set of foraging strategies. In turn, this makes it more difficult to make general conclusions about habitat quality based on physical forces.

Pigeon guillemots used shallow habitats with the slowest currents. While we binned them with the mid-water foragers, and they often feed on pelagic schooling fish, they also are known to forage extensively on epi-benthic fishes (Duffy et al. 1987, Vermeer et al. 1993, Litzow et al. 2004). Indeed, their choice of habitat factors more closely resembled that of the diving ducks rather than other mid-water foraging birds and suggests they employ more of a benthic-feeding strategy in Glacier Bay. The disproportionate use of habitats when tides are below

MSL depths and currents are below RMS speeds supported our speculation that pigeon guillemots are searching more intensively along the bottom and thus benefit from slower currents and greater access afforded by decreased depths. Alternatively, pelagic cormorants, another species that has been known to forage on epi-benthic fish (Ainley et al. 1981), tended to use high-current habitats. Clearly, these 2 species were using very different strategies despite having similar food habits (Drent 1965, Robertson 1974, Kotzerka et al. 2011). A possible explanation for this difference may be related to different body forms. Research has shown that the longer neck of pelagic cormorants provides them with an energetic advantage over alcids at faster current speeds, but a disadvantage at lower speeds (Lovvorn et al. 2001). Tidal direction was a significant factor for both of these species, but differed in direction, with pelagic cormorants using floods more than expected and pigeon guillemots using ebbs more than expected. It is notable that common mergansers, a mid-water forager similar in size to pelagic cormorants, also used habitats with similar depths and current speeds, suggesting that these species may share similar foraging strategies.

The mid-water foraging group in Glacier Bay contained 2 groups of closely related species, murrelets *Brachyramphus* spp. and loons *Gavia* spp. This allowed us to compare habitat use for each of these congeneric pairs. Competition theory suggests that we should expect resource partitioning along important physical gradients. If currents and depths were important in this partitioning we should be able to detect differences in the use of these features. The 2 loon species used similar current speeds and neither showed a preference for tidal direction, but common loons tended to use shallower habitats than Pacific loons. The loons also showed differences in relative habitat use, with common loons using sites when depths were greater than MSL while Pacific loons used habitats when current speeds were less than RMS.

The murrelets also displayed differences in habitat use. Kittlitz's murrelets used deep habitats, but did not show any preference for current speed. Conversely marbled murrelets used faster than expected currents and shallower than expected habitats. This is consistent with frequent observations of marbled murrelets in shallow channels between islands where tide rips are commonly observed (Day et al. 2003). It has been proposed that the larger eye of the Kittlitz's murrelet allows them to forage under low-light conditions (Day et al. 2003). This hypothesis has been tested in relation to highly turbid glacially affected waters (Day et al. 2003); however, we lacked the data necessary to assess the light attenuation in areas where Kittlitz's murrelets were foraging. The ability to forage at relatively greater depths could also explain the use of Kittlitz's murrelet of habitats with lower current speeds. Both murrelet species were associated with sites where depths and current speeds were less than expected, and this pattern was true of all of the small alcids in our study.

Habitat associations of surface foraging species

Glaucous-winged gulls and black-legged kittiwakes used deeper habitats, whereas mew gulls and Arctic terns tended to disproportionately use shallower habitats. Glaucous-winged gulls, black-legged kittiwakes and Arctic terns all used habitats with higher than expected current speeds. This was predictable because previous studies have shown an association between elevated current speeds and concentrations of nekton closer to the surface, thereby making them available to surface foragers (Brown & Gaskin 1988, Hunt et al. 1990, Coyle et al. 1992). We speculate that Arctic terns were taking advantage of foraging opportunities associated with fast currents in Adams Inlet (Fig. 2), which has a very narrow entrance. Of the 5 surface foraging species, 4 were significantly associated with a tidal direction, 2 with ebbs and 2 with floods. This range of associations may be related to differences in foraging strategies. Despite their association with shallow depths, mew gulls used sites when depths were shallower than MSL. This suggests that mew gulls, which commonly forage along the shoreline, are temporally adjusting their habitat use to gain a foraging advantage.

Although black-legged kittiwakes in Prince William Sound, Alaska, have previously been found to forage primarily during ebb tides (Irons 1998), we found black-legged kittiwakes in Glacier Bay to use flood tides more than expected. These results suggest that, at least for black-legged kittiwakes, tidal direction does not impart any general advantage. Interactions between flow direction and other physical factors, including currents and bathymetry, may not be easily generalized. An ebb tide may produce conditions that increase foraging efficiency, e.g. concentration of prey, but the shape of submarine features, strength of current, depth and prey type appear to be more critical than tidal direction.

The disproportionate use of flood tides by Arctic terns may be related to their use of spatially

restricted areas such as Adam's Inlet where they rely on the tidal floods to bring prey into the inlet or closer to the surface. Because Adam's Inlet also contains an Arctic tern colony site, we cannot discount the influence of proximity to nesting area; however, data available on their foraging range suggest that this should not be a restriction (Pearson 1968, Hatch 2002).

Implications for species richness

In this paper, we examined the influence of tidally driven currents on the fine-scale habitat use of marine birds in Glacier Bay, Alaska. Our study was unique because we were able to link bird observations to instantaneous environmental factors, including depths and currents at fine spatial-temporal scales. Our results indicate that foraging groups displayed clear differences in habitat use based on current, water depth and tidal direction. Within these groups we also found considerable between-species variation in habitat use, suggesting varying levels of resource partitioning. Owing to dramatic variability in bottom topography—especially the presence of numerous sills, islands, headlands and channels—and large tidal ranges, we suspect that Glacier Bay offers a greater-than-average range of fine-scale foraging habitats. This temporally sensitive habitat diversity may explain the high marine bird diversity in the bay. Although this work was conducted in a topographically complex fjord ecosystem, the concepts of resource partitioning based on tidally driven depth and current associations should be applicable to other coastal areas. As fine- or meso-scale current modeling becomes more available in other areas, it would be instructive to examine the role of current speed and tides on the spatial-temporal availability of habitats and its role in determining the local diversity of marine birds.

Acknowledgements. We thank the US National Park Service and the US Geological Survey (USGS) for providing the funding for this research. In addition to funding, park personnel provided invaluable logistical support. Marine surveys were conducted by employees of the USGS, US Fish and Wildlife Service and the National Park Service. Special thanks to Captains Jim de La Bruere of the USGS vessel RV 'Alaskan Gyre' and Greg Snedgen of the USGS vessel RV 'David Grey' for their capable assistance on surveys. We thank K. Oakley and R. Taylor for comments on the manuscript. Any mention of trade names is for descriptive purposes only and does not reflect endorsement by the federal government.

LITERATURE CITED

Abookire AA, Piatt JF, Speckman S (2002) A near-surface, daytime occurrence of two mesopelagic fish species (*Stenobrachius leucopsarus* and *Leuroglossus schmidti*) in a glacial fjord. Fish Bull 100:376–380

Ainley DG, Anderson DW, Kelly PR (1981) Feeding ecology of marine cormorants in southwestern North America. Condor 83:120–131

Alldredge AL, Hamner WM (1980) Recurring aggregation of zooplankton by a tidal current. Estuar Coast Mar Sci 10: 31–33

Arimitsu ML, Litzow MA, Piatt JF, Robards MD, Abookire AA, Drew GS (2003) Inventory of marine and estuarine fishes in southeast and central Alaska national parks. Final Rep. for Glacier Bay National Park, US Geological Survey, Anchorage, AK

Begg GS, Reid JB (1997) Spatial variation in seabird density at a shallow sea tidal mixing front in the Irish Sea. J Mar Sci 54:552–565

Bodkin JL, Ballachey BE, Esslinger GG, Kloecker KA, Monson DH, Coletti HA (2007) Perspectives on an invading predator—Sea otters in Glacier Bay. In: Piatt JF, Gende SM (eds) Proc 4th Glacier Bay Sci Symp. US Geol Surv Sci Invest Rep 2007 5047:133–136

Boersma PD, Parrish JK (1999) Limiting abuse: marine protected areas, a limited solution. Ecol Econ 31:287–304

Brown RGB, Gaskin DE (1988) The pelagic ecology of grey and red-necked phalaropes *Phalaropus fulicarius* and *P. lobatus* in the Bay of Fundy, eastern Canada. Ibis 130: 234–250

Chenoweth EM, Gabriele CM, Hill D (2011) Tidal influences on humpback whale habitat selection near headlands. Mar Ecol Prog Ser 423:279–289

Coyle KO, Hunt GL Jr, Decker MB, Weingartner TJ (1992) Murre foraging, epibenthic sound scattering, and tidal advection over a shoal near St. George Island, Bering Sea. Mar Ecol Prog Ser 83:1–14

Day RH, Prichard AK, Nigro DA (2003) Ecological specialization and overlap of *Brachyramphus* murrelets in Prince William Sound, Alaska. Auk 120:680–699

Drent RH (1965) Breeding biology of the pigeon guillemot, *Cepphus columba.* Ardea 53:99–160

Drew GS, Speckman S, Piatt JF, Burgos JM, Bodkin JL (2008) Survey design considerations for monitoring marine predator populations in Glacier Bay, Alaska: results and post-hoc analyses of surveys conducted in 1999–2003. USGS administrative report, US Geological Survey, Reston, VA

Duffy DC, Todd FS, Siegfried WR (1987) Submarine foraging behavior of alcids in an artificial environment. Zoo Biol 6:373–378

Etherington LL, Hooge PN, Hooge ER, Hill DF (2007) Oceanography of Glacier Bay, Alaska: implications for biological patterns in a glacial fjord estuary. Estuaries Coasts 30:927–944

Fauchald P, Erikstad KE, Skarsfjord H (2000) Scale-dependent predator–prey interactions: the hierarchical spatial distribution of seabirds and prey. Ecology 81: 773–783

Francis RC, Hare SR, Hollowed AB, Wooster WS (1998) Effects of interdecadal climate variability on the oceanic ecosystems of the NE Pacific. Fish Oceanogr 7: 1–21

Gould PJ, Forsell DJ (1989) Techniques for shipboard surveys of marine birds. Tech Rep 25, US Fish & Wildlife Service, Washington, DC

Hatch JJ (2002) Arctic tern (*Sterna paradisaea*). In: Poole A, Gill F (eds) The birds of North America, No. 707. The Birds of North America, Philadelphia, PA

Heath JP, Gilchrist HG (2010) When foraging becomes unprofitable: energetics of diving in tidal currents by common eiders wintering in the Arctic. Mar Ecol Prog Ser 403:279–290

Hill DF, Ciavola SJ, Etherington L, Klaar MJ (2009) Estimation of freshwater runoff into Glacier Bay, Alaska and incorporation into a tidal circulation model. Estuar Coast Shelf Sci 82:95–107

Holm KJ, Burger AE (2002) Foraging behavior and resource partitioning by diving birds during winter in areas of strong tidal currents. Waterbirds 25:312–325

Hunt GL, Schneider D (1987) Scale dependent processes in the physical and biological environment of marine birds. In: Croxall J (ed) Seabirds: feeding biology and role in marine ecosystems. Cambridge University Press, Cambridge, p 7–41

Hunt GL Jr, Harrison NM, Cooney RT (1990) The influence of hydrographic structure and prey abundance on foraging of least auklets. Stud Avian Biol 14:7–22

Hunt GL Jr, Russell RW, Coyle KO, Weingartner T (1998) Comparative foraging ecology of planktivorous auklets in relation to ocean physics and prey availability. Mar Ecol Prog Ser 167:241–259

Hyrenbach KD, Forney KA, Dayton PK (2000) Marine protected areas and ocean basin management. Aquat Conserv 10:437–458

Irons DB (1998) Foraging area fidelity of individual seabirds in relation to tidal cycles and flock feeding. Ecology 79: 647–655

Kotzerka J, Hatch SA, Garthe S (2011) Evidence for foraging-site fidelity and individual foraging behavior of pelagic cormorants rearing chicks in the Gulf of Alaska. Condor 113:80–88

Lewis TL, Esler D, Boyd WS (2008) Foraging behavior of surf scoters and white-winged scoters in relation to clam density: inferring food availability and habitat quality. Auk 125:149–157

Litzow MA, Piatt JF, Abookire AA, Speckman SG, Arimitsu ML, Figurski JD (2004) Spatiotemporal predictability of schooling and non-schooling prey of pigeon guillemots. Condor 106:410–414

Lovvorn JR, Gillingham MP (1996) Food dispersion and foraging energetics: a mechanistic synthesis for field studies of avian benthivores. Ecology 77:435–451

Lovvorn JR, Liggins GA, Borstad MH, Calisal SM, Mikkelsen J (2001) Hydrodynamic drag of diving birds: effects of body size, body shape and feathers at steady speeds. J Exp Biol 204:1547–1557

Luettich R, Westerink J (1991) A solution for the vertical variation of stress, rather than velocity, in a three-dimensional circulation model. Int J Numer Methods Fluids 12:911–928

Maniscalco JM, Ostrand WD, Coyle KO (1998) Selection of fish schools by flocking seabirds in Prince William Sound, Alaska. Colon Waterbirds 21:314–322

Mileikovsky SA (1971) Types of larval development in marine bottom invertebrates, their distribution and ecological significance: a re-evaluation. Mar Biol 10: 193–213

Nur N, Jahncke J, Herzog JP, Howar J and others (2011) Where the wild things are: predicting hotspots of seabird aggregations in the California Current System. Ecol Appl 21:2241–2257

Pawlowicz R (2002) Classical tidal harmonic analysis including error estimates in MATLAB using T_TIDE. Comput Geosci 28:929–937

Pearson TH (1968) The feeding biology of sea-bird species breeding on the Farne Islands, Northumberland. J Anim Ecol 37:521–552

Piatt JF, Wetzel J, Bell K, DeGange AR and others (2006) Predictable hotspots and foraging habitat of the endangered short-tailed albatross (*Phoebastria albatrus*) in the North Pacific: implications for conservation. Deep-Sea Res II 53:387–398

Pitcher TJ (1973) The three-dimensional structure of schools in the minnow, *Phoxinus phoxinus.* Anim Behav 21: 673–686

Robards M, Drew G, Piatt J, Anson JM and others (2003) Ecology of selected marine communities in Glacier Bay: zooplankton, forage fish, seabirds and marine mammals. Final Rep for Glacier Bay National Park, US Geological Survey, Anchorage, AK

Robertson I (1974) The food and nesting of double-crested and pelagic cormorants at Mandarte Island, British Columbia, with notes on feeding ecology. Condor 76: 346–348

Schneider DC, Piatt JP (1986) Scale-dependent correlation of seabirds with schooling fish in a coastal ecosystem. Mar Ecol Prog Ser 32:237–246

Schneider DC, Harrison NM, Hunt GL Jr (1987) Variation in the occurrence of marine birds at fronts in the Bering Sea. Estuar Coast Shelf Sci 25:135–141

Sims DW, Southall EJ, Humphries NE, Hays GC and others (2008) Scaling laws of marine predator search behavior. Nature 451:1098–1102

Small LF, Menzies DW (1981) Patterns of primary productivity and biomass in the coastal upwelling region. Deep-Sea Res 28:123–149

Smith RL (1968) Upwelling. Oceanogr Mar Biol Annu Rev 6: 11–46

Spargo E, Westerink J, Luettich R, Mark D (2004) ENPAC 2003: a tidal constituent database for the eastern North Pacific Ocean. Report ERDC/CHL TR-04-12 191, United States Army Corps of Engineers, Washington, DC

Spear LB, Ballance LT, Ainley DG (2001) Responses of seabirds to thermal boundaries in the tropical Pacific: the thermocline versus the Equatorial Front. Mar Ecol Prog Ser 219:275–289

Strathmann RR (1985) Feeding and nonfeeding larval development and life-history evolution in marine invertebrates. Annu Rev Ecol Syst 16:339–361

Suryan RM, Sato F, Balogh GR, Hyrenbach KD, Sievert PR, Ozaki K (2006) Foraging destinations and marine habitat use of short-tailed albatrosses: a multi-scale approach using first-passage time analysis. Deep-Sea Res II 53: 370–386

Thompson SA, Price JJ (2006) Water clarity and diving behavior in wintering common loons. Waterbirds 29: 169–175

US Geological Survey (2012) North Pacific pelagic seabird database. Alaska Science Center, Anchorage, AK

Vermeer K, Morgan KH, Smith GEJ (1993) Nesting bio-

logy and predation of pigeon guillemots in the Queen Charlotte Islands, British Columbia. Colon Waterbirds 16:119–129

Weimerskirch H (2007) Are seabirds foraging for unpredictable resources? Deep-Sea Res II 54:211–223

Wells HW (1957) Abundance of the hard clam *Mercenaria mercenaria* in relation to environmental factors. Ecology 38:123–128

Wilson RP, Wilson MPT (1988) Foraging behaviour in four sympatric cormorants. J Anim Ecol 57:943–955

Yen PPW, Sydeman WJ, Bograd SJ, Hyrenbach KD (2006) Spring-time distributions of migratory marine birds in the southern California Current: oceanic eddy associations and coastal habitat hotspots over 17 years. Deep-Sea Res II 53:399–418

Zamon JE (2001) Seal predation on salmon and forage fish schools as a function of tidal currents in the San Juan Islands, Washington, USA. Fish Oceanogr 10:353–366

Submitted: July 3, 2012; Accepted: February 6, 2013

Proofs received from author(s): March 28, 2013

Vol. 487: 287–304, 2013
doi: 10.3354/meps10350

MARINE ECOLOGY PROGRESS SERIES
Mar Ecol Prog Ser

Published July 30

Contribution to the Theme Section 'Biophysical coupling of marine hotspots'

FREE ACCESS

Spatio-temporal persistence of top predator hotspots near the Antarctic Peninsula

Jarrod A. Santora[1,2,3,*], Richard R. Veit[4]

[1]Antarctic Ecosystem Research Division, Southwest Fisheries Science Center, National Marine Fisheries Service, NOAA, La Jolla, California 92037, USA

[2]Farallon Institute for Advanced Ecosystem Research, 101 H Street, Suite Q, Petaluma, California 94952, USA

[3]Center for Stock Assessment Research, University of California, Santa Cruz, 110 Shaffer Road, Santa Cruz, California 95060, USA

[3]Biology Department, College of Staten Island, City University of New York, 2800 Victory Boulevard, Staten Island, New York 10314, USA

ABSTRACT: We quantified species richness and abundance of seabirds and marine mammals in order to identify marine areas that are persistently attractive to top predators. Shipboard surveys across a 150 000 km^2 grid off the Antarctic Peninsula were conducted once or twice each year from 2003 to 2011 during which the distribution and abundance of top predators were mapped. We hypothesized that spatial organization of species richness and abundance hotspots reflect persistent habitat use and are regionalized according to distance from land and oceanographic boundaries. To test this, we used a new hotspot variance metric based on the percentage of time that the species richness or abundance estimate at any one location is greater than 1 standard deviation above the long term means for the entire survey grid. Species richness hotspots were based on all species sighted, while abundance hotspots were based on concentrations of 16 species: 13 seabirds (penguins, petrels and albatrosses), 1 pinniped and 2 baleen whales. Species abundance hotspots reflected 2 major groupings—those with oceanic and coastal origins. We identified 15 richness hotspots, 9 of which were in proximity to the southern Antarctic Circumpolar Current front; the 6 others were associated with major breeding colonies and the location of 2 submarine canyon systems. Our approach integrates temporal and spatial variances over 14 individual surveys and provides useful reference points for identifying ecologically important areas, refining food web models and developing spatial management of and conservation strategies for marine ecosystems.

KEY WORDS: Abundance · Antarctic · Conservation · Hotspot · Persistence · Richness · Seabirds · Marine mammals · Marine spatial management

INTRODUCTION

Inhabiting the largest ecosystem on earth, seabirds and marine mammals are truly global organisms and sentinels of ocean ecosystem state (Tittensor et al. 2010, Sydeman et al. 2012). With conservation of seabirds and marine mammals becoming increasingly urgent, there is a need for the quantitative designation of hotspots—areas characterized by persistent, elevated abundance and species richness (Piatt et al. 2006, Sydeman et al. 2006, Davoren 2007, Santora et al. 2010, Nur et al. 2011, Suryan et al. 2012). Top predator hotspots can be identified either by tracking individuals and quantifying how much time they spend in each encountered habitat (Block et al. 2011), or alternatively, via shipboard surveys documenting the abundance and species richness of predators measured in each habitat (Yen et al. 2006, Santora et al. 2010, Nur et al. 2011, Suryan et al. 2012). However, persistence of hotspots is rarely quantified. Using a shipboard approach, we present information on the persistence of predator hotspots near the

*Email: jasantora@gmail.com

Antarctic Peninsula based on data collected during 14 shipboard surveys between 2003 and 2011. This is a region of rapid climate change (Meredith & King 2005) that has experienced serial depletion of marine mammals (Fraser et al. 1992, Ballance et al. 2006), and is becoming a growing ecotourism destination (Tin et al. 2008, Lynch et al. 2010) and a commercial krill fishery (Kawaguchi et al. 2006, Nicol et al. 2012). Therefore, we need to know where top predators and their prey are persistently concentrated to benefit marine spatial management and conservation (Reid et al. 2004, Santora et al. 2012a,b, Sigler et al. 2012).

The hotspot concept is useful in studies of highly mobile organisms such as seabirds and mammals, because the extreme variability characteristic of the distributions of marine organisms makes it highly unlikely that any single mapping would be truly representative. As a consequence, one needs repeated standardized surveys to determine those areas that persist in their attractiveness to top predators. However, the hotspot concept applied to top predators in marine ecosystems has received somewhat mixed definitions. According to Sydeman et al. (2006), marine hotspots are defined as 'sites of critical ecosystem linkages between trophic levels'. Piatt et al. (2006) defined hotspots as a 'relatively small area in which we expect to find animal aggregations repeatedly'. Davoren (2007) defined hotspots as 'areas where high abundance of species overlap in space and time'. Indeed, there have been many uses of the term hotspot, but the commonality of these definitions is some aspect of spatio-temporal persistence (Gende & Sigler 2006, Sigler et al. 2012, Suryan et al. 2012). We decided to quantify both abundance hotspots for individual species, and richness hotspots for the entire community. We calculated these from a suite of highly replicated shipboard surveys sampled over many years (Santora et al. 2010, 2012a). Using a grid-based approach, we define hotspots of species richness and abundance as locations with anomalies that exceed the mean for the entire study region by 1 standard deviation in a given survey, and define their frequency of occurrence by estimating the percentage of time a hotspot occurs over many surveys (Suryan et al. 2012).

Motivation for this study was based on the following: (1) the Antarctic Peninsula marine ecosystem has been impacted by human disturbances over the past 2 centuries (e.g. commercial whaling; krill fishing; Fraser et al. 1992, Trivelpiece et al. 2011, Nicol et al. 2012) and is experiencing rapid climate change (Meredith & King, 2005); (2) krill stocks have declined and gelatinous salps are increasing (Atkinson et al. 2004); (3) ecosystem-based management of the Southern Ocean krill fishery will benefit from the delineation of top predator hotspots so that overlap between fishing vessels and predators is minimized (Reid et al. 2004, Santora et al. 2010, 2012a) and; (4) the likelihood of seabirds and marine mammals exhibiting extremely dense aggregations at sea is high and leads to difficulties in modeling their spatial distribution that is not yet resolved (Oppel et al. 2012, Sigler et al. 2012). Our overarching objective was to quantify the location of persistent species richness and abundance hotspots. We applied a new variance-based metric to identify hotspots by accounting for their persistence (consistent or frequent occurrence) of anomalies through time (Suryan et al. 2012). We tested the hypothesis that the geospatial variability of species richness and abundance hotspots relates to distance from land and oceanographic boundaries.

METHODS

Study area

The US Antarctic Marine Living Resources (AMLR) program conducts surveys on a fixed grid along north-south transects with stations spaced at ~55 km intervals across a 150 000 km^2 area surrounding the South Shetland Islands at the northern tip of the Antarctic Peninsula (Fig. 1). The study area is located within the narrowest latitudinal stretch of the Southern Ocean (closest point between South America and Antarctica). The hydrography and circulation of this region is complex and variable and reflects inputs and mixing of waters from the Antarctic Circumpolar Current (ACC) within Drake Passage, the western portion of the Weddell gyre, and upstream regions along the western Antarctic Peninsula that enter through Gerlache Strait and western Bransfield Strait (Amos 2001, Thompson et al. 2009). The rugged bathymetry of the region (which includes the continental shelf around the islands, deep basins of Bransfield Strait, and the South Shetland Trench and Shackleton Fracture Zone ridge in Drake Passage) provides additional hydrographic and circulation variability (Orsi et al. 1995; Fig. 1). Physical oceanographic conditions around the South Shetland Islands exhibit a broad range of water mass characteristics because of the mixing of the ACC, Scotia Sea, Antarctic coastal current and the higher latitude waters of the Weddell Sea (Orsi et al. 1995, Amos 2001, Thompson et al. 2009). Relevant to this study, the southern Antarctic

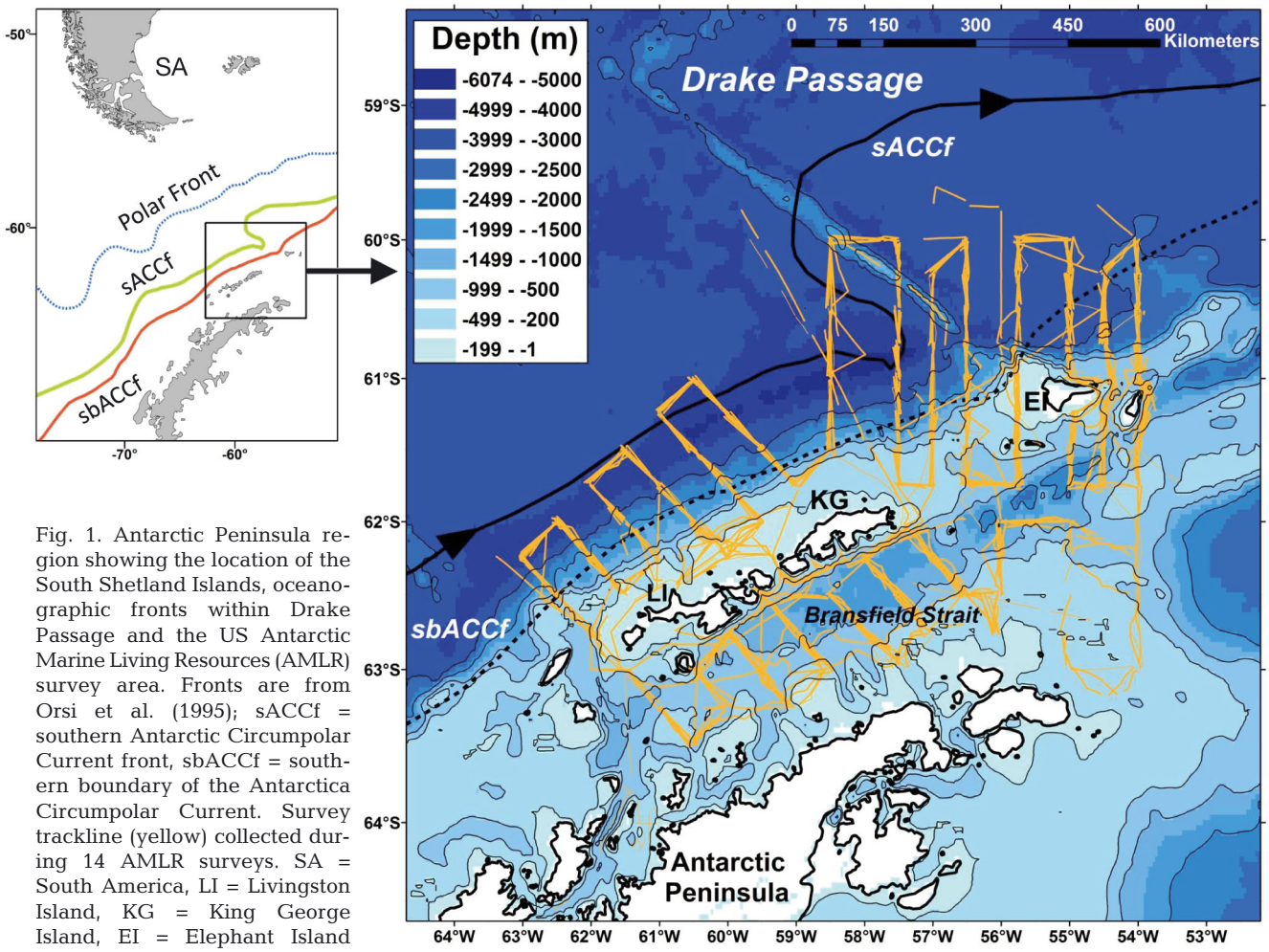

Fig. 1. Antarctic Peninsula region showing the location of the South Shetland Islands, oceanographic fronts within Drake Passage and the US Antarctic Marine Living Resources (AMLR) survey area. Fronts are from Orsi et al. (1995); sACCf = southern Antarctic Circumpolar Current front, sbACCf = southern boundary of the Antarctica Circumpolar Current. Survey trackline (yellow) collected during 14 AMLR surveys. SA = South America, LI = Livingston Island, KG = King George Island, EI = Elephant Island

Circumpolar Current front (sACCf) and its southern boundary (sbACCf) (Fig. 1) is an ecologically important oceanographic frontal zone for whales and krill (Tynan 1998, Atkinson et al. 2008).

During January–March 2003 to 2011, we conducted 14 surveys to map the distribution and relative abundance of seabirds, pinnipeds and cetaceans (Table 1, Fig. 1). Our coverage of transects was replicated annually and within the summer season; occasionally there were 2 surveys per year (Table 1, Fig. 1). The grid design enabled sampling of a variety of habitats, including the extensive insular shelf systems around the archipelago, submarine canyons, shelf-break regions, deep basins of Bransfield Strait and the oceanic waters of southern Drake Passage; see Fig. 2 for a summary of survey effort

Table 1. Summary of survey effort for predator observations conducted on 14 Antarctic Marine Living Resource (AMLR) program surveys. Only survey effort that falls within the 54 regularly sampled grid cells is presented

Year	Survey	Days	Survey dates	Survey hours	Distance (km)
2003	1	16	16 January – 28 January	129.27	2394.1
	2	16	10 February – 25 February	113.73	2106.7
2004	1	17	13 January – 31 January	126.60	2344.6
2005	1	15	15 January – 30 January	121.02	2241.3
	2	16	22 February – 9 March	107.03	1982.2
2006	1	16	16 January – 31 January	114.07	2112.6
2007	1	18	8 January – 26 January	148.10	2742.8
2008	1	23	13 January – 5 February	154.47	2860.8
	2	17	16 February – 5 March	128.93	2387.8
2009	1	18	12 January – 29 January	165.12	3058.0
2010	1	13	25 January – 9 February	84.88	1571.9
	2	14	19 February – 6 March	90.30	1666.8
2011	1	21	14 January – 4 February	188.22	3481.7
	2	15	17 February – 5 March	98.48	1823.8

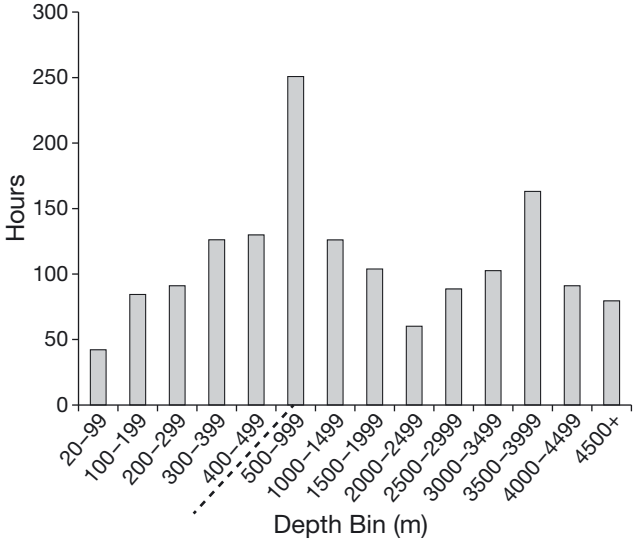

Fig. 2. Summary of survey effort in relation to bathymetry; dashed line indicates change from 100 m to 500 m depth bin size, due to sampling of shelf-break and slope regions

according to different sea depth bins. Previously, a subset of this dataset was used to identify the location and spatial association of baleen whale and krill demographic hotspots (Santora et al. 2010). Moreover, the grid design has permitted the description of habitat use for poorly known cetaceans (Santora & Brown 2010, Santora 2012) as well as modeling mesoscale structure and spatial organization of krill hotspots (Santora et al. 2012a).

Predator surveys

Sighting data on predator abundance and distribution were continuously collected during daylight hours between sampling stations along fixed transects (Fig. 1). Additional survey methods are described in Santora et al. (2009, 2010) and Santora & Reiss (2011). Ship speed during transits was generally 10 knots (~18.6 km h^{-1}), and observers used hand-held binoculars to scan for predators from a height of ~13 m above sea level. Each sighting was assigned a time and a spatial position from the ship's global positioning system. Sea surface state (Beaufort scale) and visibility (e.g. fog, glare) were continuously monitored and effort during unfavorable conditions (e.g. Beaufort >5, heavy fog) was excluded prior to analysis. Counts of seabirds were made within a 90° arc from 300 m ahead of the ship to one side while underway (Camphuysen & Garthe 2004). Ship-following birds were recorded when first encountered and ignored thereafter. Surveys of whales were conducted using standard line transects by trained observers each year. All recorded cetacean sightings were observed in a 180° arc forward of the vessel and up to 3 km away. For each whale sighting, a best-estimate spatial position, bearing and a perpendicular distance estimate to the ship's trackline were logged (Buckland et al. 1993). Observations of seals were collected in a 180° arc forward of the vessel and included position and group size (Santora 2013). True to all shipboard surveys of air-breathing marine animals, there is an inherent issue of detectability associated with the animal's behavior and sea state conditions (Southwell et al. 2008). Although line-transect (distance) sampling was not used to estimate absolute marine mammal density, sightings were collected consistently across all 14 surveys to estimate a standardized relative abundance index.

We selected the 16 most numerous and frequently sighted top predator species for quantifying abundance hotspots (Table 2, Appendix 1; Hunt et al. 1990). Three species of marine mammals (2 baleen whales, 1 pinniped) and 13 species of seabirds were selected based on their overall abundance, representing a variety of different foraging behaviors and life histories. All of the species examined in this study feed on small zooplankton and nekton (e.g. krill, copepods, mesopelagic fish, squid), but differ in their feeding behavior due to locomotion and body size (Croxall & Prince 1980, Laws 1985). Baleen whales predominantly feed on krill and exploit dense patches of krill throughout the water column (Laws 1977). Penguins and pinnipeds are pursuit diving predators and select a variety of krill and fish species (Croxall & Prince 1980, Reid et al. 2006). The flying seabirds examined in this study are restricted to feeding near the sub-surface and select a variety of prey (Croxall & Prince 1980). For comparative purposes, we focused on 2 species each of baleen whales (*Balaenopteridae*), penguins (*Spheniscidae*), albatross (*Diomedeidae*), storm petrels (*Hydrobatidae*) and 6 species of petrels (*Procellaridae*). Because of the difficulty identifying prions (*Pachyptila* spp.) at sea, counts of unidentified prion, Antarctic prion (*P. desolata*) and thin-billed prion (*P. belcheri*) were pooled into 'prion species'. Our analysis of species richness hotspots were based on all species observed (Appendix 1).

Analysis

All shipboard trackline and predator sightings were combined in a geographic information system. The shipboard trackline was extensive and covered open

Table 2. Summary of species, total sightings (S), total individuals (Ind.) and individuals per unit effort (*IPUE*) observed at sea for 14 US Antarctic Marine Living Resources (AMLR) surveys (January – March, 2003 to 2011). SE = standard error, SD = standard deviation, CV = coefficient of variation, *Species that breed at the South Shetland Islands or Antarctic Peninsula

Common name	Scientific name	S	Ind.	*IPUE* (No. h^{-1} $cell^{-1}$ $survey^{-1}$)			
				Mean	SE	SD	CV
Cape petrel*	*Daption capense*	8523	70703	42.85	6.56	22.75	0.53
Antarctic fulmar*	*Fulmarus glacialoides*	5955	34700	22.79	5.54	19.19	0.84
Black-browed albatross	*Thalassarche melanophrys*	2966	5003	3.51	0.84	2.92	0.83
Grey-headed albatross	*Thalassarche chrysostoma*	844	966	0.64	0.14	0.49	0.76
Southern giant petrel*	*Macronectes giganteus*	1628	2334	1.43	0.21	0.74	0.51
White-chinned petrel	*Procellaria aequinoctialis*	1468	2085	1.18	0.46	1.62	1.37
Blue petrel	*Halobaena caerulea*	1154	2159	1.04	0.34	1.19	1.15
Prion	*Pachyptila* spp.	2736	5108	2.11	0.71	2.45	1.16
Wilson's storm petrel*	*Oceanites oceanicus*	5169	7646	5.04	0.74	2.59	0.51
Black-bellied storm petrel*	*Fregetta tropica*	6046	8165	4.48	0.84	3.22	0.72
Chinstrap penguin*	*Pygoscelis antarctica*	4877	28066	17.09	2.12	7.35	0.43
Gentoo penguin*	*Pygoscelis papua*	275	1612	1.16	0.46	1.61	1.38
South polar skua*	*Catharacta maccormicki*	531	579	0.38	0.05	0.18	0.47
Humpback whale	*Megaptera novaeangliae*	767	1346	0.92	0.14	0.48	0.53
Fin whale	*Balaenoptera physalus*	543	1084	0.76	0.33	1.16	1.51
Antarctic fur seal*	*Arctocephalus gazella*	1517	2261	1.46	0.30	1.05	0.72

water (there was no pack ice present), bays, inlets and passages between islands. Survey effort was binned into 54 cells, each 0.5° latitude × 1° longitude in dimension (~2860 km^2). The ship's trackline (at 1 min intervals) was plotted to determine the number of hours sampled per cell and survey, as an index of effort (Table 1, Fig. 1). Only cells that were sampled during at least 7 surveys and for at least 1.5 h (~27.78 km) were used in subsequent analyses. Using these criteria, a total of 546 cells and 1684 h were sampled over 14 surveys for a mean ± SD of 38 ± 11 cells $survey^{-1}$ and 3 ± 0.3 h $cell^{-1}$ $survey^{-1}$, respectively (Table 1). This cell size has been used extensively in this region to examine net-based spatial distribution and abundance patterns of Antarctic krill (Atkinson et al. 2004, 2008), associations between hotspots of baleen whales and krill (Santora et al. 2010), and mesoscale structure of krill hotspots (Santora et al. 2012a).

A 3-step process, similar to that of Suryan et al. (2012), was used to quantify temporal and spatial variance and anomaly persistence of a cell's value of species per unit effort (*SPUE*) and individuals per unit effort (*IPUE*). This procedure integrates variability and anomaly persistence into a metric that, when mapped, produces a seascape of resolved peak species richness and abundance values (hotspots). First, for each survey, rates of *SPUE* and *IPUE* are calculated (1) by dividing the total number of species (out of 54 species; see Appendix 1) or individuals of a given species (Table 2) by the amount of hours surveyed per cell and then subtracting the survey mean and dividing by the survey standard deviation to normalize each survey (e.g. z-score; Table 2):

$$SPUE_{i,j} \text{ or } IPUE_{i,j,z} = [(N_{i,j}/E_{i,j}) - S_j x] / S_j sd \quad (1)$$

where $N_{i,j}$ is the number of species sighted (or relative species abundance; z refers to the species under consideration in $IPUE_{i,j,z}$) in cell i during survey j, $E_{i,j}$ is the number of hours sampled per cell, $S_j x$ and $S_j sd$ are the survey mean and standard deviation of species richness and abundance in a given survey. Second, the grand mean and standard deviation of $SPUE_{i,j}$ and $IPUE_{i,j,z}$ is estimated for each cell over all surveys. Within a given survey, hotspots are cells with species richness or abundance anomalies that exceed the grand survey mean by >1 SD. Third, the percentage of time a cell displayed an anomaly >1 SD above the grand mean is tabulated. This threshold of >1 SD is a common measure for variance of anomalies in space-time series analysis and has previously been used to map persistence of remotely-sensed chlorophyll *a* (chl *a*) (Suryan et al. 2012) as well as krill and whale hotspots (Santora et al. 2010, 2012a). Cells with higher percentages reflect locations where species richness or species abundance is persistently higher than the baseline standardized anomaly. For mapping purposes, persistence is classified to permit comparison of hotspot spatial distribution patterns. Classes, based on percentage of surveys, are 0–15%, 15–30%, 30–45% and >45%.

Our first objective was to examine whether groups of species exhibit similar spatial persistence based on the distribution of their abundance hotspots. We used 2 complementary multivariate statistical procedures to address this objective regarding species abundance hotspots: hierarchical cluster analysis and

principal component analysis (PCA; Legendre & Legendre 1998). Estimates of species hotspot persistence (per cell, based on percentage of surveys) were approximately normally distributed (Kolmogorov-Smirnov test, $p > 0.05$) and were inputted into PCA and cluster analysis as a Pearson correlation matrix. Meaningful principal components were determined by inspecting eigenvalues (e.g. Scree plot) and percent variance explained (Legendre & Legendre 1998). Cluster analysis (Ward's method with Euclidean distance metric and standard deviation scaling) was used to produce a dendrogram indicating groups of species sharing similar hotspot persistence.

Our second objective was to determine how the persistence of species richness and abundance hotspots varied relative to distance to land and the hydrographic boundaries. Tynan (1998) suggested that the southern boundary of the ACC front has ecological significance for whales throughout the Southern Ocean, and Bost et al. (2009) discussed how fronts are likely regions of elevated trophic transfer and therefore important foraging areas for both seabirds and mammals. Therefore, we tested the hypothesis that the persistence of species richness and abundance hotspots are spatially associated with the ACC front and its southern boundary, and inversely related to distance from land. To test this hypothesis, we correlated a cell's persistence value (percentage of surveys with an anomaly >1 SD) with distance to land and hydrographic features. We calculated the nearest distance (km) from each cell centroid to the position of the southern ACC front and its southern boundary (Orsi et al. 1995) and nearest land. For perspective, the mean distance from land across all cells is 112.2 ± 90.4 km, and the mean distance to the southern ACC front and its southern boundary is 222.9 ± 140.5 and 134.1 ± 100.8 km, respectively. We used a randomization procedure (bootstrap and Monte Carlo analysis; 10 000 randomizations) to calculate Spearman rank correlations and probabilities, with an emphasis on significant negative correlations as indicators of association (i.e. less distance between hotspot and feature).

RESULTS

Species richness hotspots

The mean (± SD) number of species sighted per cell was 12.1 ± 2.3 and ranged from 5.4 to 18.9 for all 14 surveys. All richness hotspots exhibited persistence values >50%, indicating that species richness within these locations was generally high on nearly half of total surveys (Fig. 3). Species richness hotspots were located throughout the study area (n = 15), but were generally more common north of the South Shetland Islands in association with the southern ACC front and its southern boundary (Fig. 3). There were 3 richness hotspots associated with the location of 2 submarine canyon systems; cells C5 and C6 near Livingston Island and cell F7 in Bransfield Strait adjacent to the northwestern tip of the Antarctic Peninsula (see bathymetry in Fig. 1). There were 3 species richness hotspots (cells E5, F4 and F5) located to the east, north, and south of King George Island (Admiralty and Maxwell Bays). In addition, there were 2 adjacent richness hotspots at the southern edge of the study area near a confluence formed by the mixing of waters from Bransfield and Gerlache Straits (cells C8 and D8; Fig. 3).

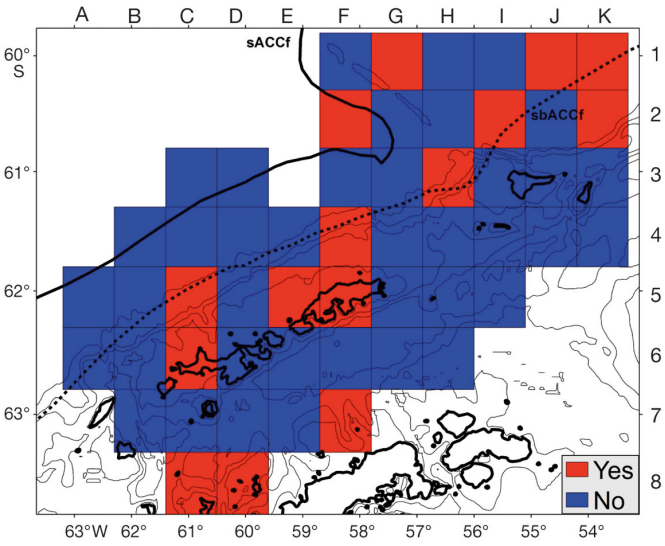

Fig. 3. Location of species richness hotspots. All richness hotspots were persistent for >50% of all surveys; red square (Yes) indicates richness hotspots

Table 3. Principal component analysis (PCA) for the persistence of abundance for 16 species; eigenvalues and total variance for PCA factors

PCA factor	Eigenvalue	% Total variance
1	5.24	32.72
2	2.39	14.91
3	1.54	9.60
4	1.42	8.89
5	1.04	6.47
6	0.89	5.57

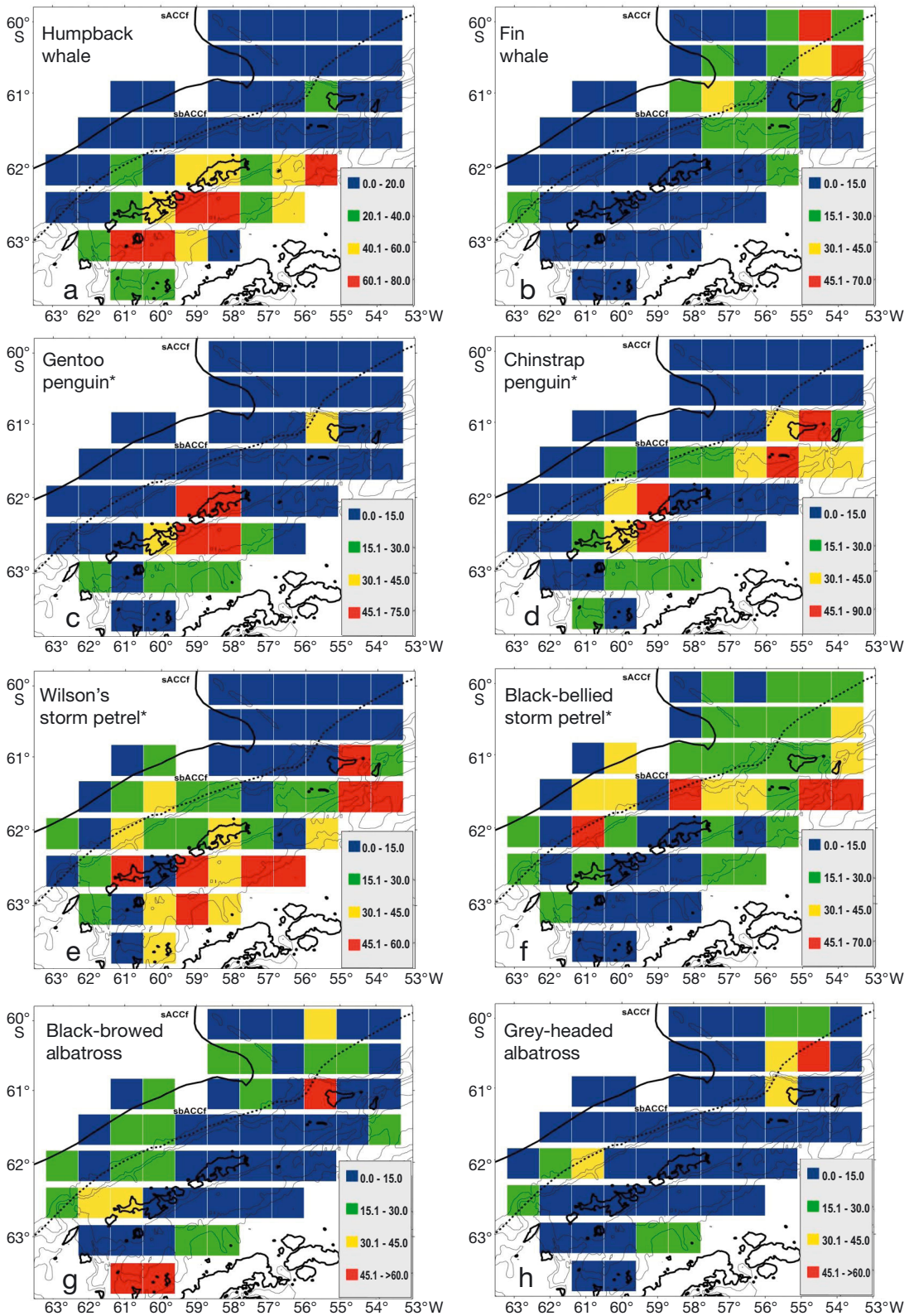

Fig. 4. Classified persistent abundance hotspots (percentage of time cell anomaly exceeds 1 standard deviation above the mean) of (a) humpback whale, (b) fin whale, (c) gentoo penguin, (d) chinstrap penguin, (e) Wilson's storm petrel, (f) black-bellied storm petrel, (g) black-browed albatross, (h) grey-headed albatross, (i) cape petrel, (j) Antarctic fulmar, (k) Antarctic fur seal, (l) south polar skua, (m) blue petrel, (n) prions (o) white-chinned petrel and (p) southern giant petrel. *Species breeds in study region and therefore some hotspot locations may represent land-based breeding colonies

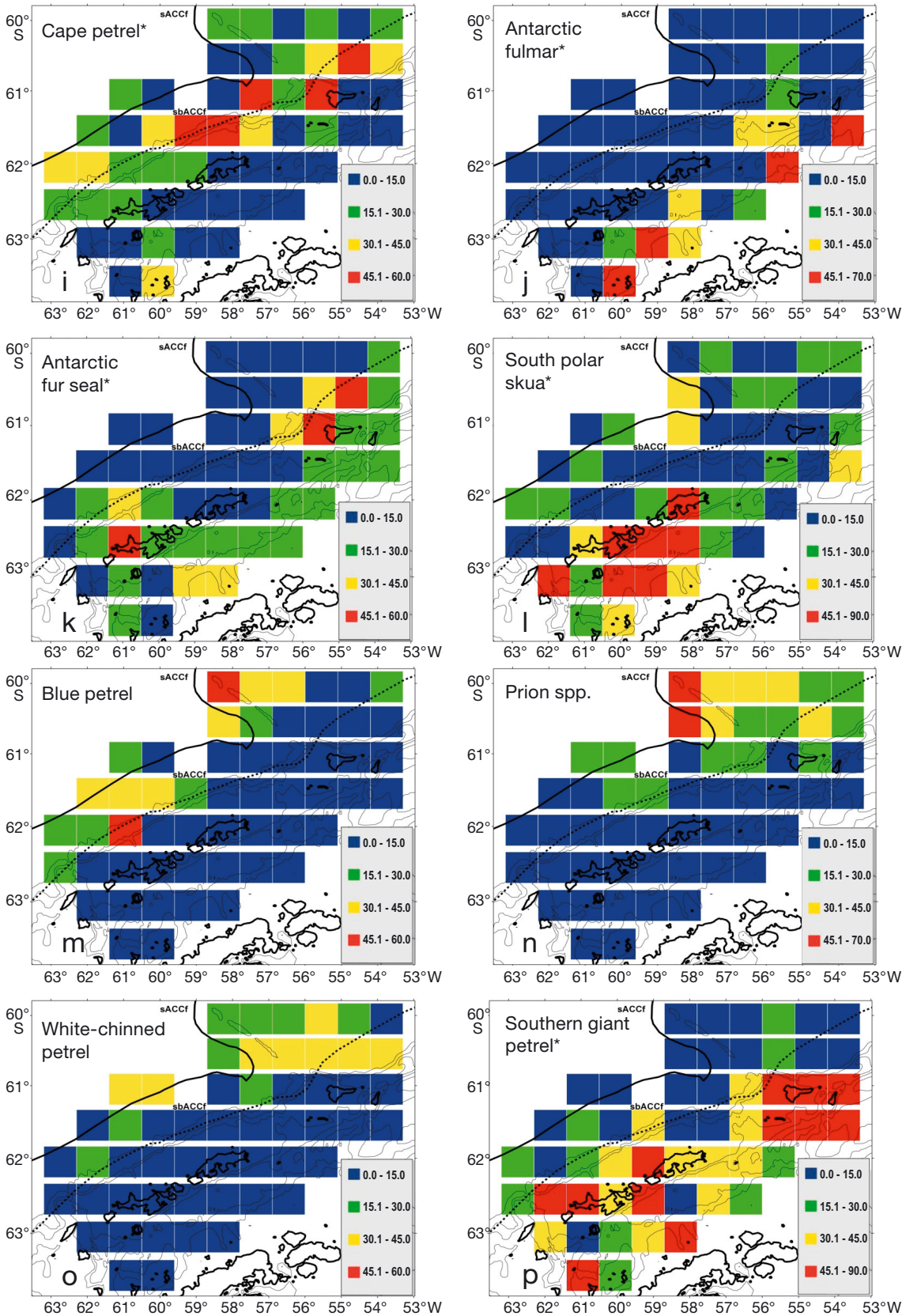

Fig. 4 (continued)

Species abundance hotspots

We identified abundance hotspots as those areas that consistently displayed abundance anomalies exceeding 1 standard deviation above the long term spatial mean >45% of the times surveyed. We identified abundance hotspots for 16 top predators and generally showed 2 areas of concentration related to coastal and oceanic habitats (Figs. 4a–p & 5). Cluster analysis and PCA of species abundance hotspots revealed 2 groupings that reflect their preferred foraging habitats and for some species, probable land-based breeding locations (Table 3, Fig. 5). There is an 'Oceanic Drake Passage' group, including fin whale, black-bellied storm petrel, prions, white-chinned petrel, blue petrel, Antarctic fur seal, grey-headed albatross, cape petrel and black-browed albatross; and a 'Coastal Bransfield Strait' group, including humpback whale, gentoo penguin, chinstrap penguin, south polar skua, Antarctic fulmar, Wilson's storm petrel and southern giant petrel (Fig. 5). In addition, cell loadings of PC1 and PC2 dichotomized by positive and negative values illustrate this apparent spatial segregation (Fig. 6).

We found that closely related species, such as gentoo and chinstrap penguins and black-browed and grey-headed albatrosses, aggregated together in the same hotspots (Fig 4c,d,g,h). By contrast, other

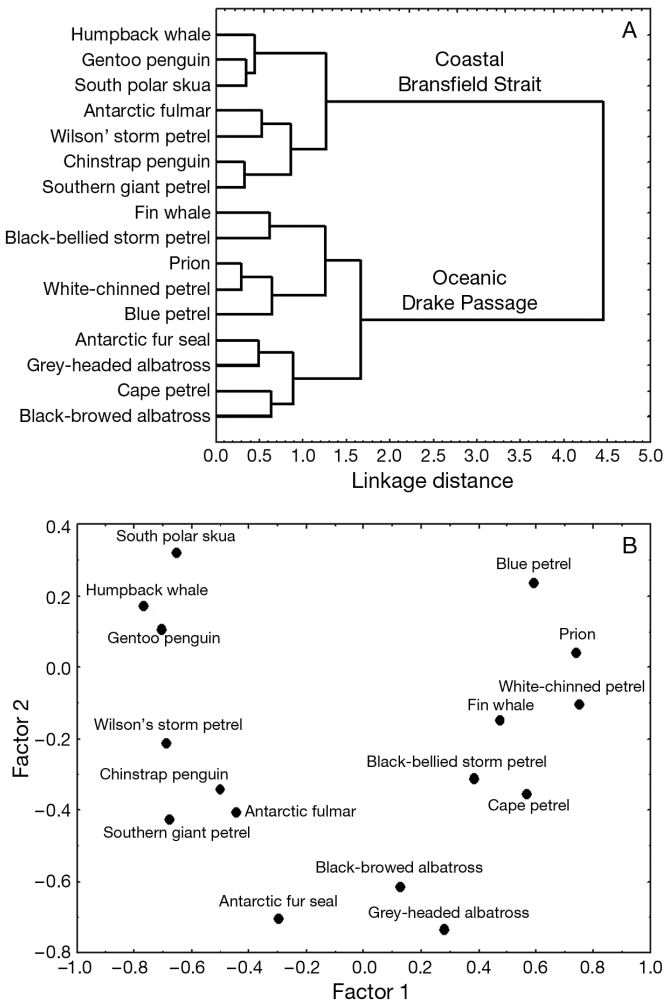

Fig. 5. Species assemblages defined based on their persistence of abundance as determined by (A) hierarchical cluster analysis and (B) ordination of factors from principal component analysis

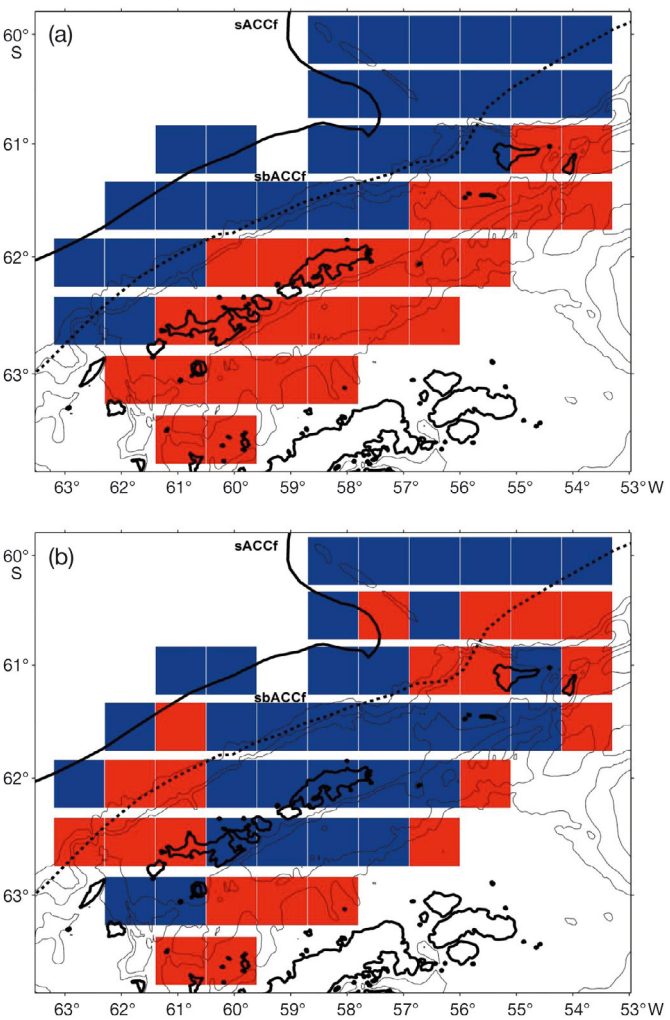

Fig. 6. Plot of principal component analysis (PCA) factor loadings per cell (grouped by positive [red] and negative [blue] values) for (a) PC1, illustrating species assemblages based on abundance hotspots and showing a separation of the 'Oceanic Drake Passage' from 'Coastal Bransfield Strait' (see Fig. 1) and (b) PC2, showing regionally specific areas to the spatial persistence of top-predators due to island locations and unique circulation or water mixing/retention

species pairs appeared to segregate into different hotspots. This apparent segregation seemed to be based on oceanographic habitats. For example, hotspots of humpback whales and Wilson's storm petrels were concentrated within Bransfield Strait, whereas hotspots of fin whales and black-bellied storm petrels were concentrated in southern Drake Passage (Fig. 4a,b,e,f). The closely related and similarly sized cape petrel and Antarctic fulmar are frequently observed in aggregations numbering in the thousands, yet their hotspot locations were separated according to oceanic and coastal origins. Abundance hotspots of cape petrels occurred mainly within the southern ACC frontal zone (Fig. 4i), whereas abundance hotspots of Antarctic fulmars were chiefly in southern Bransfield Strait (Fig. 4j).

We found that some species exhibited more hotspots than other species (Fig. 7). For example, black-bellied storm petrels, southern giant petrels, Antarctic fur seals and humpback whales showed more hotspots, while species such as grey-headed albatross, gentoo and chinstrap penguins, and Antarctic fulmar had fewer (Fig. 7). The medium and high persistence species abundance hotspots (yellow and red cells) were summed across all 16 species per cell to reveal the importance of a cell (Fig. 8). Several cells proved attractive to multiple species. For example, the cell that includes the western half of Elephant Island (I3) includes hotspots for 6 species (grey-headed albatross, black-browed albatross, cape petrel, fur seal, southern giant petrel, gentoo and chinstrap penguins) and the one that includes the eastern portion of Livingston Island (C6) includes hotspots for 6 species (humpback whale, gentoo and chinstrap

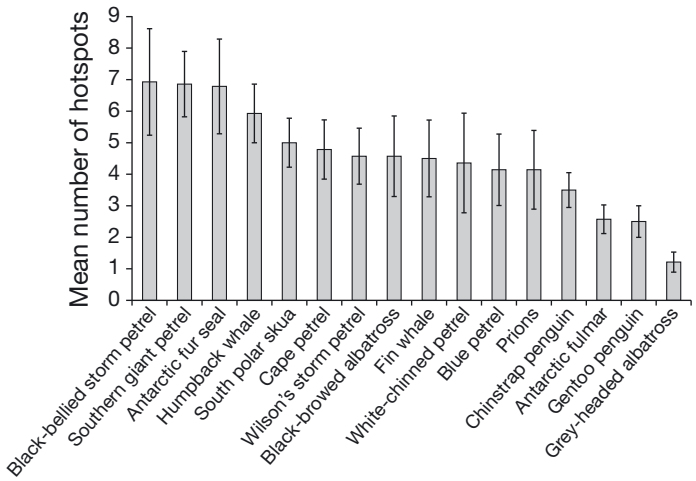

Fig. 7. Mean number (±SD) of species abundance hotspots over 14 surveys. Species are sorted relative to frequency of hotspots

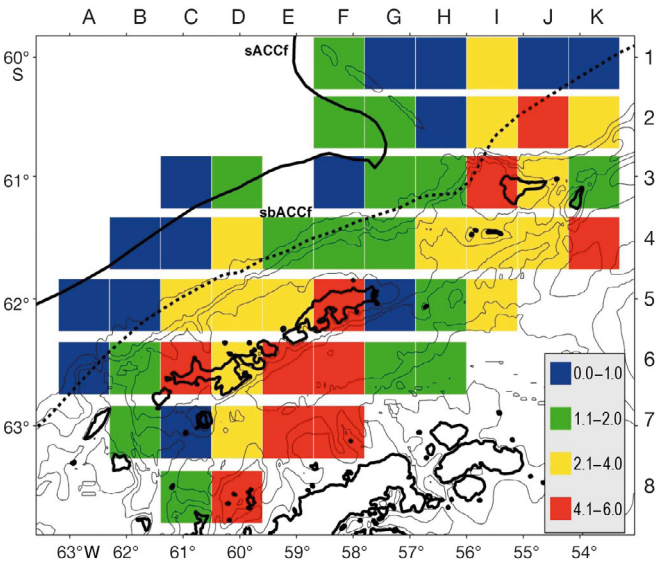

Fig. 8. Summary of the number of species (n = 16) abundance hotspots determined by summing the number of species hotspots per cell (see Fig. 4)

penguins, Wilson's storm petrel, south polar skua and southern giant petrel). The highest concentration of neighboring cells with multiple species abundance hotspots (cells D6, E6–7, and F5–7) are located in Bransfield Strait.

Oceanographic determinants of hotspots

The last application of the hotspot variance metric investigated the relationship between hotspot persistence and distance to land and 2 hydrographic boundaries (Table 4). Several species belonging to the 'Coastal Bransfield Strait' group (Fig. 5) exhibited significant associations (negative) between their spatial persistence and distance to land: humpback whale, Antarctic fur seal, Antarctic fulmar, chinstrap and gentoo penguins, southern giant petrel and south polar skua. None of these species displayed persistent hotspots that were associated with the position of hydrographic boundaries. On the other hand, species from the 'Oceanic Drake Passage' group displayed persistent hotspots that were closely associated with the position of the 2 hydrographic boundaries: fin whale, cape petrel, black-bellied storm petrel, prions, blue petrel, and white-chinned petrel. Interestingly, some species within this group exhibited higher correlation with one oceanographic boundary over the other, suggesting even further niche separation in the oceanic domain. For example, persistent hotspot of prions, blue petrel and white-chinned

Table 4. Spearman rank correlations for persistence of species abundance and richness relative to distance to land and the southern Antarctic Circumpolar Current front (sACCf) and the southern boundary (sbACCf). Bold values indicate significant association. *Significant negative association. Confidence limits (L95% and U95%) are based on a randomization test

Variable	Distance land			Distance sACCf			Distance sbACCf		
	Rho, p	L95%, U95%	R^2	Rho, p	L95%, U95%	R^2	Rho, p	L95%, U95%	R^2
Humpback whale	**−0.57, <0.01***	−0.36, −0.73	0.24	**0.59, <0.01**	0.38, 0.74	0.33	**0.51, <0.01**	0.28, 0.69	0.26
Fin whale	**0.30, 0.02**	0.04, 0.53	0.04	−0.16, 0.25	0.11, −0.41	0.007	**−0.33, 0.01***	−0.07, −0.55	0.11
Antarctic fur seal	**−0.48, <0.01***	−0.24, −0.66	0.25	**0.55, <0.01**	0.33, 0.71	0.21	0.02, 0.88	−0.25, 0.29	0
Cape petrel	0.24, 0.08	−0.03, 0.47	0.02	**−0.46, <0.01***	−0.22, −0.65	0.15	**−0.63, <0.01***	−0.43, −0.77	0.31
Antarctic fulmar	**−0.32, 0.02***	−0.06, −0.54	0.10	**0.49, <0.01**	0.26, 0.67	0.30	0.24, 0.08	−0.03, 0.48	0.20
Black-browed albatross	0.07, 0.62	−0.20, 0.33	0.004	−0.17, 0.22	0.10, −0.42	0.003	−0.11, 0.42	0.16, −0.37	0.003
Grey-headed albatross	0.13, 0.46	−0.17, 0.36	0.0002	0.12, 0.40	−0.16, 0.37	0.02	−0.11, 0.85	0.15, −0.37	0.02
Wilson's storm petrel	**−0.47, <0.01***	−0.23, −0.65	0.21	**0.46, <0.01**	0.22, 0.65	0.25	**0.37, <0.01**	0.12, 0.58	0.16
Black-bellied storm petrel	0.17, 0.21	−0.09, 0.42	0.007	−0.21, 0.13	0.06, −0.45	0.05	**−0.38, <0.01***	−0.12, −0.59	0.15
Prion spp.	**0.65, <0.01**	0.46, 0.78	0.54	**−0.50, <0.01***	−0.26, −0.68	0.22	**−0.30, 0.03***	−0.04, −0.53	0.03
Blue petrel	**0.68, <0.01**	0.49, 0.79	0.51	**−0.76, <0.01***	−0.62, −0.85	0.45	**−0.30, 0.03***	−0.04, −0.53	0.04
Chinstrap penguin	**−0.51, <0.01***	−0.27, −0.68	0.24	**0.28, 0.03**	0.02, 0.51	0.09	0.14, 0.32	−0.14, 0.39	0.005
Gentoo penguin	**−0.54, <0.01***	−0.32, −0.71	0.18	**0.48, <0.01**	0.25, 0.66	0.13	**0.32, 0.02**	0.06, 0.54	0.04
White-chinned petrel	**0.60, <0.01**	0.39, 0.75	0.38	**−0.57, <0.01***	−0.36, −0.73	0.26	**−0.29, 0.03***	−0.03, −0.52	0.07
Southern giant petrel	**−0.73, <0.01***	−0.58, −0.84	0.45	**0.52, <0.01**	0.29, 0.69	0.25	0.25, 0.07	−0.02, 0.48	0.04
South polar skua	**−0.27, 0.04***	−0.001, −0.51	0.07	**0.33, 0.01**	0.07, 0.55	0.15	**0.41, <0.01**	0.16, 0.61	0.17
Species richness	−0.09, 0.52	0.18, −0.35	0.003	0.07, 0.58	−0.19, 0.33	0.02	−0.12, 0.39	0.15, −0.37	0

petrel displayed higher correlation with the location of the southern ACC front than the southern boundary of the ACC front (Table 4, Fig. 4), whereas hotspots of fin whale, cape petrel and black-bellied storm petrel displayed higher association with the southern boundary. Species richness hotspots (Fig. 3) were not significantly associated with distance to land or hydrographic boundaries (Table 4), possibly indicating that persistence of these areas may be attributed to unique biological conditions and complex habitat heterogeneity.

DISCUSSION

Through years of replicated shipboard surveys and use of a variance-based hotspot metric, this study provides an atlas of persistent species richness and abundance hotspots. Unlike other recent efforts (Nur et al. 2011, Oppel et al. 2012), we used only actual observations and did not include estimated presence based on habitat models. That is, our quantification was based on places where we actually observed aggregations of seabirds and marine mammals, and we did not include those areas predicted to have aggregations on the basis of their habitat characteristics (which confuses what is observed and what is modeled). The quantification of hotspots is important from 2 different perspectives. First, identifying foraging hotspots is important for the conservation of top predators. Because marine ecosystems are highly variable, quantifying persistence of hotspots will benefit development of Marine Protected Areas to effectively conserve top predator species (Hyrenbach et al. 2000, Hooker & Gerber 2004, Hooker et al. 2011). For example, near the Antarctic Peninsula, knowledge of hotspot locations could be used to minimize conflict between top predators and humans; in particular, spatial allocation of krill fishing activity and vessel traffic patterns (Reid et al. 2004, Hill et al. 2009). Second, it is of interest from a perspective of foraging theory to identify how top predators find prey (Ainley et al. 1992, 2009, Veit 1999, Davoren et al. 2003, Silverman et al. 2004). If top predators memorize the locations of productive feeding areas, then areas we have identified as hotspots are likely to be among those locations memorized. How long individuals spend at such hotspots (Block et al. 2011) and the characteristics of prey aggregations, namely krill within hotspots (Santora et al. 2010, 2012a), remains to be quantified. In the future, blending shipboard surveys and satellite telemetry studies of top predators offers a promising way forward to accomplish estimates of population- and individual-level use of hotspots.

The novelty of the method we used is twofold. Most importantly, it was based on actual observations of species richness and abundance rather than modeled richness and abundance. The issue here is that top predators only aggregate in a small proportion of the habitats that are actually suitable to them, so that

regression-style habitat models may overpredict hotspots. Part of the reason for this is that top predators are tracking highly mobile and patchy prey (Davoren et al. 2003). Second, the analysis was not contingent upon knowing any particular statistical distribution of top predator richness or abundance, and in that sense it was a nonparametric analysis. Also, most habitat models predict seabird and mammal abundance based on averages of satellite-based data (e.g. chl *a*, sea-surface temperature) that often lack the components that were likely attractive to the birds and mammals that were aggregated at the time of sampling (Block et al. 2011, Nur et al. 2011, Oppel et al. 2012). This study differs from others because top predator hotspots were defined based on their persistence; specifically accounting for the frequency of surveys that a particular location exhibited an anomaly richness or abundance value exceeding the long-term spatial mean by 1 SD. Using a similar approach, Suryan et al. (2012) defined persistence of remotely-sensed surface chl *a* areas (a widely used index of ocean productivity), revealing that the persistence metric explained more variance of seabird density than did mean chl *a*. This study builds on the work of Suryan et al. (2012), but differs because the persistence metric is applied directly to standardized rates of species richness and abundance of seabirds and marine mammals. We advocate the use of this method because it is straightforward and can be easily applied to shipboard surveys of top predators, their prey, and productivity.

Drivers of hotspots

We did not examine environmental predictors of hotspot occurrence, but rather focused on identifying their location and persistence so they could be examined in future studies combining information on oceanographic features and micronekton collectively to understand trophic transfer in marine environments (Santora et al. 2012b). Potential drivers of persistent top predator hotspots may include features such as abrupt topographies, hydrographic boundaries (Genin 2004), persistent chl *a* concentration (Suryan et al. 2012) and prey aggregations (Gende & Sigler 2006, Sigler et al. 2012). However, some environmental features are likely more persistent than others. For example, seamounts and submarine canyons are fixed locations, whereas locations of hydrographic fronts and prey aggregations may move (Hyrenbach et al. 2000, Morato et al. 2010). Future studies ought to apply dynamic habitat models to the hotspot persistence metric to determine what environmental predictors (e.g. bathymetry, sea surface temperature, ch *a* persistence) explain the spatial distribution and persistence of hotspots (Zydelis et al. 2011, Santora et al. 2012a, 2013). Importantly, hotspots identified in this study reflect summertime conditions when many species are using the area for breeding (e.g. penguins, fur seals) or replenishing energy reserves depleted during migration from wintering grounds (e.g. humpback and fin whales). The persistence of hotspots outside of the summer season remains unknown.

Although krill hotspots are an important predictor of baleen whale hotspots near the Antarctic Peninsula (Santora et al. 2010), future work should assess spatial relationships among krill and top predator hotspots and physical forces simultaneously (Hunt et al. 1998, Santora et al. 2012b, Sigler et al. 2012). Temporal and spatial scales of atmospheric and oceanographic process should be considered when weighing their predictive capabilities on the formation and persistence of biological hotspots (Palacios et al. 2006). For example, eddies are important sources of biological production that may contain high concentrations of chl *a* and krill (Kahru et al. 2007, Santora et al. 2012a,b), and likely affect spatial and temporal variation in top predator hotspots (Gende & Sigler 2006, Block et al. 2011). Bathymetry derived circulation patterns and coastal transport processes (e.g. Ekman transport) are likely important for understanding persistence and connectivity of top predator hotspots. Piñones et al. (2011) investigated transport pathways and residence times of water using a regional ocean modeling system (ROMS) to track simulated particles throughout the Antarctic Peninsula, revealing that biological hotspots were sites with the longest particle residence times (~30 d). If areas with long residence times contain predictable krill concentrations (Hofmann et al. 2004), then ROMS is an important tool for understanding mesoscale transport patterns of krill and connectivity among top predator hotspots among seasonal and inter-annual time scales (Santora et al. 2013).

Spatial organization of hotspots

Some areas clearly emerge as abundance hotspots because they are located close to large breeding colonies (AMLR 2007, Harris et al. 2011, Santora 2013). Others are nowhere near any known nesting locations (such as for the albatrosses and whales) and are therefore clearly attractive due to their potential

food resources (e.g. submarine canyons north of Livingston Island; Santora & Reiss 2011). Our results indicate there are species abundance hotspots that are related to distance to land, in contrast to those related to the position of hydrographic boundaries. This gradient analysis is important for summarizing spatial organization of hotspots relative to the mesoscale structure of the marine environment (Santora et al. 2012a,b). For example, hotspots of fin whales, black-bellied storm petrels and cape petrels are associated with the southern boundary of the ACC, an ecologically important productivity zone throughout the Southern Ocean (Orsi et al. 1995, Tynan 1998). Species hotspots that were associated with the ACC were not associated with distance to land, indicating their affinity for oceanic waters. Distribution of hotspots of seabirds, such as blue petrel, prion species, and white-chinned petrel that do not breed in the study region but hail from colonies originating in sub-Antarctic latitudes, are not associated with islands and are concentrated in the oceanic domain (Hunt et al. 1990, Ainley et al. 1994). Exceptions to this are the black-browed and grey-headed albatross, which also breed on sub-Antarctic islands, and exhibit hotspots near Livingston and Elephant Islands. By contrast, species hotspots identified for chinstrap penguin, gentoo penguin, Antarctic fur seal, south polar skua, southern giant petrel and Wilson's storm petrel were closely associated with distance to land and may indicate probable breeding colony locations (Harris et al. 2011, Santora 2013).

Interestingly, all species richness hotspots displayed persistence values equal to or greater than 50% of the total time surveyed. This is in contrast to the species abundance hotspots identified, which showed a range of persistence values. In total, 15 species richness hotspots were identified, 9 of which occured near the southern Antarctic Circumpolar Current front, while others were located in proximity to the South Shetland Islands and the location of 2 submarine canyon systems. However, collectively the 15 species richness hotspots were not statistically associated with distance to the ACC or land. The consistently higher level of persistence exhibited by species richness hotspots may indicate there are likely unique physical and biological features specific to each of these locations, and therefore widely attractive to multiple top predator species. For example, krill hotspots located within the ACC, principally composed of large sexually mature krill, are distributed along the shelf-slope coinciding with moderate levels of eddy kinetic energy (Santora et al. 2010, 2012a); areas that attract diverse species groups including procellariid seabirds, toothed cetaceans and mesopelagic fishes (Appendix 1; Barrera-Oro 2002, Santora & Brown 2010, Santora 2012). Richness hotspots located near land may indicate higher numbers of species that either breed there, or are attracted to the complex bathymetric irregularities (such as submarine canyons) that foster predictable concentrations of krill (Santora & Reiss 2011); such bathymetric features are typical of the nearshore environment throughout the South Shetland Islands and Antarctic Peninsula region. Future studies should examine each species richness hotspot in greater detail, especially their scale-dependent responses to physical and biological drivers (Hurlbert & Jetz 2007) to determine if generalities can be made and applied throughout the Southern Ocean.

Hotspots and species interactions

Formation and maintenance of hotspots are also likely influenced by interactions such as competition and mutualism or facilitation (Reed & Dobson 1993, Camphuysen & Webb 1999, Ainley et al. 2006, 2009). Spatial segregation of species abundance hotspots may in fact indicate niche partitioning among species, and relate to difference in prey density and spatial organization (Piatt 1990, Piatt & Methven 1992, Santora et al. 2010, 2011). We found that several closely related species displayed strikingly different hotspot distribution patterns reflecting oceanic and coastal origins. For example, hotspots of humpback and fin whales—both major krill consumers requiring extremely dense krill patches—displayed virtually no spatial overlap (Santora et al. 2010, Sigler et al. 2012). Hotspots of similar sized cape petrel and Antarctic fulmar also exhibited non-overlapping hotspot patterns. Moreover, Wilson's and black-bellied storm petrel, 2 seemingly identical small petrel species, exhibited hotspots that overlapped very little. Additional characterization of physical and biological features of hotspots could be used to examine potential mechanisms of spatial segregation among sympatric species (Ainley et al. 2009, Santora et al. 2012b).

Species that benefit from one another (e.g. local enhancement; Grünbaum & Veit 2003) may exhibit higher levels of spatial persistence, having overlapping aggregations within profitable foraging areas. For example, albatross and petrels often aggregate together with pursuit-diving penguins and seals, which are able to exploit a larger portion of the water column, and whose foraging behavior may drive prey

close to the surface in reach of the flying seabirds (Harrison et al. 1991, Silverman et al. 2004). Our results show that hotspots for black-browed and grey-headed albatrosses also contained fur seal hotspots, and were located near known major fur seal breeding colonies (e.g. Livingston and Seal Islets; cells C5–6 and H3–I2; Fig. 3). Thus, the location of fur seal colonies may be important to albatross conservation because of their facilitatory role in providing access to prey through the action of the seals. Moreover, the abundance hotspots described here may serve as a basis for examining potential competition among seabirds, seals and baleen whales, especially as whale populations continue to rebuild from commercial whaling (Fraser et al. 1992, Ainley et al. 2006, Trivelpiece et al. 2011). For example, hotspots of humpback whales were also closely associated with coastal areas, likely placing them in competition with neighboring seabird and seal colonies (Santora & Reiss 2011, Santora 2013). Such critically important interspecific interactions need to be taken into account in the implementation of effective conservation measures, as nonlinear impacts of the decline of a single predator can have disproportionate effects (Berec 2010).

Implications for marine spatial management and conservation

The hotspot patterns presented in this study have implications for marine spatial management in the Southern Ocean. The majority of krill-predator and commercial fishing demand for krill in the Antarctic Peninsula region occurs within 150 to 200 km from land (Croll & Tershy 1998, Jones & Ramm 2004, Reid et al. 2004), coinciding with many of the hotspots identified in this study located near islands. Additionally, the commercial krill catch has increased in recent years, coinciding with new developments in fishing methods enabling nets to remain submerged for weeks and continuously pump krill to factory ships; some estimates suggest krill catches may be as high as 800 t per vessel per day (Nicol et al. 2012). To advance spatial management of krill and krill-predators the Commission for the Conservation of Antarctic Marine Living Resources (CCAMLR) developed small-scale management units (SSMUs) to manage catch allocations of krill in small areas ensuring additional protection of important predator foraging areas where fishing vessels may pose potential competition (Constable et al. 2000, Hewitt et al. 2004, Hill et al. 2009). Near the Antarctic Peninsula region, there are 8 SSMUs whose boundaries were established in part due to the foraging range of land-based breeding penguins and seals. The SSMUs did not necessarily take into account the marine distribution of cetaceans, male fur seals, aerial seabirds (e.g. cape petrels, fulmars) and sub-Antarctic breeding seabirds that concentrate in the region. Moreover, potential overlap between krill-predators and fishing vessels was derived from a single shipboard survey spanning a week of survey effort near the Antarctic Peninsula (CCAMLR 2000 Survey; Reid et al. 2004). Due to the high level of temporal and spatial variance in the distribution of seabirds and marine mammals, using shipboard surveys to inform marine spatial management decisions for marine predators should require integration of multiple surveys replicated over many years to quantify mesoscale structure and oceanographic determinants of krill and predator hotspots (Santora et al. 2010, 2012a). Therefore, persistent top predator hotspots identified here should be compared to fluxes in krill abundance (Reiss et al. 2008), fishing pressure (Jones & Ramm 2004, Nicol et al. 2012), boundaries of existing SSMUs (Hewitt et al. 2004) as well as commercial shipping traffic patterns, which have steadily increased during the past few decades (i.e. tourist ships; Tin et al. 2008, Lynch et al. 2010).

The term hotspot is important for generating awareness and particular attention to species of conservation concern (Myers et al. 2000, Worm et al. 2003, Rodrigues et al. 2006). CCAMLR and BirdLife International are interested in the status of seabird and marine mammal predator populations of ecological and conservation value in the Antarctic Peninsula region. The frequency of occurrence and International Union for Conservation of Nature (IUCN; Rodrigues et al. 2006) status for all 54 taxa recorded during our surveys is presented in Appendix 1. In summary, there were 3 endangered species (hotspots identified for black-browed albatross and fin whale), 4 near threatened (hotspots identified for gentoo penguin) and 5 vulnerable (hotspots identified for grey-headed albatross and white-chinned petrel) species recorded during our surveys. Due to their frequency of occurrence and overall abundance, we were only able to apply the hotspot persistent metric to the 16 most common species inhabiting the study region, some of which may not be candidates for conservation. Species richness hotspots were identified based on sighting rates of all species, keeping in line with the classical concept of a biological hotspot (Myers et al. 2000, Hurlbert & Jetz 2007). Although some species were sighted less frequently than others

(Appendix 1), they collectively contributed to our identification of persistent species richness hotspots, indicating the ecology of these areas is likely unique. Therefore, the species richness hotspots we identified are obvious candidates for further evaluation of their vulnerability to anthropogenic disturbance and climate change. Future research ought to characterize and compare these richness hotspots in terms of their oceanography, habitat quality and the prey concentrations they may foster (Worm et al. 2003, Sydeman et al. 2006, Palacios et al. 2006).

In recognition of their vulnerability to human disturbances and climate change, an atlas of Important Bird Areas (IBA) based on breeding bird colonies in the Antarctic Peninsula region highlights many locations throughout South Shetland Island archipelago (Harris et al. 2011). Although identifying land-based IBA is valuable, it does not ensure protection of marine environments where seabirds concentrate their foraging effort and spend the majority of their time (Hooker & Gerber 2004, Hooker et al. 2011). Generally, foraging seabirds are found in proximity to their breeding colonies, suggesting an inverse function between their at sea abundance and distance to land (Croll & Tershy 1998). However, non-breeding species of seabirds are not tied to land for provisioning offspring, and some species traveling afar from breeding grounds to distant foraging grounds (e.g. albatross species in this study) indicate that land-based IBA alone will not ensure protection of habitats critical for sustaining seabird populations. The persistent hotspots presented in this study have important implications for designation of marine IBA and should be considered along with land-based IBA for developing Marine Protected Areas in the future. Therefore, future management, conservation and marine spatial planning near the Antarctic Peninsula should benefit from the baseline distribution of persistent multispecies hotspots quantified in this study.

Acknowledgements. We greatly appreciate the dedication of the many US Antarctic Marine Living Resources (AMLR) program field workers for their support over the years. J.A.S. is especially grateful to M. P. Force for his dedication to the observer team. Thanks also to following observers: S. Mitra, A. J. Bernick, D. J. Futuyma, R. Heil, B. Nikula, T. P. White, E. T. Brown and K. Ampela. We thank R. Hewitt, A. Jenkins, C. S. Reiss and G. Watters for their support of the seabird and marine mammal survey team within the AMLR program. The manuscript was improved by comments and feedback from 3 anonymous reviewers, M. F. Sigler, W. J. Sydeman, R. Suryan and V. J Loeb. This study was funded and supported by AMLR contracts to J.A.S. and NSF-OPP grants (9983751, 0337648) to R.R.V.

LITERATURE CITED

Ainley DG, Ribic CA, Fraser WR (1992) Does prey preference affect habitat choice in Antarctic seabirds? Mar Ecol Prog Ser 90:207–221

Ainley DG, Ribic CA, Fraser WR (1994) Ecological structure among migrant and resident seabirds of the Scotia-Weddell Confluence region. J Anim Ecol 63:347–364

Ainley DG, Ballard G, Dugger KM (2006) Competition among penguins and cetaceans reveals trophic cascades in the western Ross Sea, Antarctica. Ecology 87:2080–2093

Ainley DG, Dugger KD, Ford RG, Pierce SD and others (2009) Association of predators and prey at frontal features in the California Current: competition, facilitation and co-occurrence. Mar Ecol Prog Ser 389:271–295

AMLR (2007) United States Antarctic Marine Living Resources Program 2006/2007 field season report: objectives, accomplishments and tentative conclusions. Lipsky JD (ed) NOAA Southwest Fisheries Science Center, Antarctic Ecosystem Research Group, La Jolla. Available at swfsc.noaa.gov/uploadedFiles/Divisions/AERD/Publications/FSR%202006-07p.pdf

Amos A (2001) A decade of oceanographic variability in summertime near Elephant Island, Antarctica. J Geophys Res 106:22401–22423, doi:10.1029/2000JC000315

Atkinson A, Siegel V, Pakhomov E, Rothery P (2004) Long-term decline in krill stock and increase in salps within the Southern Ocean. Nature 432:100–103

Atkinson A, Siegel V, Pakhomov EA, Rothery P and others (2008) Oceanic circumpolar habitats of Antarctic krill. Mar Ecol Prog Ser 362:1–23

Ballance L, Pitman RL, Hewitt RP, Siniff DB, Trivelpiece WZ, Clapman PJ, Brownell RL Jr (2006) The removal of large whales from the Southern Ocean: evidence for long-term ecosystem effect? In Estes JA, DeMaster DP, Doak DF, Williams TE, Brownell RL Jr (eds) Whales, whaling and ocean ecosystems. University of California Press, Berkeley, p 215–130

Barrera-Oro E (2002) The role of fish in the Antarctic marine food web: differences between inshore and offshore waters in the southern Scotia Arc and west Antarctic Peninsula. Antarct Sci 14:293–309

Berec L (2010) Impacts of foraging facilitation among predators on predator-prey dynamics. Bull Math Biol 72: 94–121

Block BA, Jonsen ID, Jorgensen SJ, Winship AJ and others (2011) Tracking apex marine predator movements in a dynamic ocean. Nature 475:86–90

Bost CA, Cotté C, Bailleul F, Cherel Y and others (2009) The importance of oceanographic fronts to marine birds and mammals of the southern oceans. J Mar Res 78:363–376

Buckland ST, Anderson DR, Burnham KP, Laake JL (1993) Distance sampling: estimating abundance of biological populations. Chapman & Hall, London

Camphuysen CJ, Garthe S (2004) Recording foraging seabirds at sea: standardised recording and coding of foraging behavior and multi-species foraging associations. Atlantic Seabirds 6:1–32

Camphuysen CJ, Webb A (1999) Multi-species feeding associations in north sea seabirds: jointly exploiting a patchy environment. Ardea 87:177–198

Constable AJ, de la Mare WK, Agnew DJ, Everson I, Miller D (2000) Managing fisheries to conserve the Antarctic marine ecosystem: practical implementation of the Convention on the Conservation of Antarctic Marine Living

Resources (CCAMLR). ICES J Mar Sci 57:778–791
Croll DA, Tershy BR (1998) Penguins, fur seals, and fishing: prey requirements and potential competition in the South Shetland Islands, Antarctica. Polar Biol 19:365–374
Croxall JP, Prince PA (1980) Food, feeding ecology and ecological segregation of seabirds at South Georgia. Biol J Linn Soc 14:103–131
Davoren GK (2007) Effects of gill-net fishing on marine birds in a biological hotspot in the Northwest Atlantic. Conserv Biol 21:1032–1045
Davoren GK, Montevecchi WA, Anderson JT (2003) Search strategies of a pursuit-diving marine bird and the persistence of prey patches. Ecol Monogr 73:463–481
Fraser WR, Trivelpiece WZ, Ainley DG, Trivelpiece SG (1992) Increases in Antarctic penguin populations: reduced competition with whales or a loss of sea ice due to environmental warming? Polar Biol 11:525–531
Gende SM, Sigler MF (2006) Persistence of forage fish 'hot spots' and its association with foraging Steller sea lions (*Eumetopias jubatus*) in southeast Alaska. Deep-Sea Res II 53:432–441
Genin A (2004) Bio-physical coupling in the formation of zooplankton and fish aggregations over abrupt topographies. J Mar Syst 50:3–20
Grünbaum D, Veit RR (2003) Foraging behavior of black-browed albatrosses exploiting Antarctic krill: density-dependence through local enhancement. Ecology 84: 3265–3275
Harris CM, Carr R, Lorenz K, Jones S (2011) Important bird areas in Antarctica: Antarctic Peninsula, South Shetland Islands, South Orkney Islands – Final Report. Prepared for BirdLife International and the Polar Regions Unit of the UK Foreign & Commonwealth Office. Environmental Research & Assessment, Cambridge
Harrison NM, Whitehouse MJ, Heinemann D, Prince PA, Hunt GL, Veit RR (1991) Observations of multispecies seabird flocks around South Georgia. Auk 108:801–810
Hewitt RP, Watters G, Trathan PN, Croxall JP and others (2004) Options for allocating the precautionary catch limit of krill among small-scale management units in the Scotia Sea. CCAMLR Sci 11:81–97
Hill SL, Trathan PN, Agnew DJ (2009) The risk to fishery performance associated with spatially resolved management of Antarctic krill (*Euphausia superba*) harvesting. ICES J Mar Sci 66:2148–2154
Hofmann EE, Haskel AGE, Klinck JM, Lascara CM (2004) Lagragian modelling studies of Antarctic krill (*Euphausia superba*) swarm formations. ICES J Mar Sci 61: 617–631
Hooker SK, Gerber LR (2004) Marine reserves as a tool for ecosystem-based management: the potential importance of megafauna. Bioscience 54:27–39
Hooker SK, Cañadas A, Hyrenbach KD, Corrigan C, Polovina JJ, Reeves RR (2011) Making protected area networks effective for marine top-predators. Endang Species Res 13:203–218
Hunt GL, Heinemann D, Veit RR, Heywood RB, Everson I (1990) The distribution, abundance and community structure of marine birds in the southern Drake Passage and Bransfield Strait, Antarctica. Cont Shelf Res 10: 243–257
Hunt GL, Russell RW, Coyle KO, Weingartner T (1998) Comparative foraging ecology of planktivorous auklets in relation to ocean physics and prey availability. Mar Ecol Prog Ser 167:241–259
Hurlbert AH, Jetz W (2007) Species richness, hotspots, and the scale dependence of range maps in ecology and conservation. Proc Natl Acad Sci USA 104:13384–13389
Hyrenbach KD, Forney KA, Dayton PK (2000) Marine protected areas and ocean basin management. Aquatic Conserv: Mar Freshw Ecosyst 10:437–458
Jones CD, Ramm DC (2004) The commercial harvest of krill in the southwest Atlantic before and during the CCAMLR 2000 Survey. Deep-Sea Res II 51:1421–1434
Kahru M, Mitchell BG, Gille ST, Hewes CD, Hom-Hansen O (2007) Eddies enhance biological production in the Weddell-Scotia Confluence of the Southern Ocean. Geophys Res Lett 34:L14603, doi:10.1029/2007GL030430
Kawaguchi S, Nicol S, Takio K, Naganobu M (2006) Fishing ground selection in the Antarctic krill fishery: trends in patterns across years, seasons and nations. CCAMLR Sci 13:117–141
Laws RM (1977) Seals and whales of the Southern Ocean. Philos Trans R Soc Lond B 279:81–96
Laws RM (1985) Ecology of the Southern Ocean. Am Sci 73: 26–40
Legendre P, Legendre L (1998) Numerical ecology. Elsevier, Amsterdam
Lynch HJ, Crosbie K, Fagan WF, Naveen R (2010) Spatial patterns of tour ship traffic in the Antarctic Peninsula region. Antarct Sci 22:123–130
Meredith MP, King JC (2005) Rapid climate change in the ocean west of the Antarctic Peninsula during the second half of the 20th century. Geophys Res Lett 32:L19604, doi:10.1029/2005GL024042
Morato T, Hoyle SD, Allain V, Nicol SJ (2010) Seamounts are hotpots of pelagic diversity in the open ocean. Proc Natl Acad Sci USA 107:9707–9711
Myers N, Mittemeier RA, Mittemeier CG, da Fonseca GAB, Kent J (2000) Biodiversity hotspots for conservation priorities. Nature 403:853–858
Nicol S, Foster J, Kawaguchi S (2012) The fishery for Antarctic krill — recent developments. Fish Fish 13:30–40
Nur N, Jahncke J, Herzog MP, Howar J and others (2011) Where the wild things are: predicting hotspots of seabird aggregations in the California Current System. Ecol Appl 21:2241–2257
Oppel S, Meirinho A, Ramírez I, Gardner B, O'Connell AF, Miller PI, Louzao M (2012) Comparison of five modeling techniques to predict the spatial distribution of seabirds. Biol Conserv 156:94–104
Orsi AH, Whitworth T, Nowlin WD (1995) On the meridional extent and fronts of the Antarctic Circumpolar Current. Deep-Sea Res I 42:641–673
Palacios DM, Bograd SJ, Foley DG, Schwing FB (2006) Oceanographic characteristics of biological hot spots in the North Pacific: a remote sensing perspective. Deep-Sea Res II 53:250–269
Piatt JF (1990) The aggregative response of common murres and Atlantic puffins to schools of capelin. Stud Avian Biol 14:36–51
Piatt JF, Methven DA (1992) Threshold foraging behavior of baleen whales. Mar Ecol Prog Ser 84:205–210
Piatt JF, Wetzel J, Bell K, DeGange AR and others (2006) Predictable hotspots and foraging habitat of the endangered short-tailed albatross (*Phoebastria albatrus*) in the North Pacific: implications for conservation. Deep-Sea Res II 53:387–398
Piñones A, Hofmann EE, Dinniman MS, Klinck JM (2011) Lagragian simulation of transport pathways and resi-

dence times along the western Antarctic Peninsula. Deep-Sea Res II 58:1524–1539

Reed JM, Dobson AP (1993) Behavioral constraints and conservation biology: conspecific attraction and recruitment. Trends Ecol Evol 8:253–256

Reid K, Sims M, White RW, Gillon K (2004) Spatial distribution of predator/prey interactions in the Scotia Sea: implications for measuring predator/fisheries overlap. Deep-Sea Res II 51:1383–1396

Reid K, Davis D, Staniland IJ (2006) Spatial and temporal variability in the fish diet of Antarctic fur seal (*Arctocephalus gazella*) in the Atlantic sector of the Southern Ocean. Can J Zool 84:1025–1037

Reiss CS, Cossio AM, Loeb V, Demer DA (2008) Variations in the biomass of Antarctic krill (*Euphausia superba*) around the South Shetland Islands, 1996–2006. ICES J Mar Sci 65:497–508

Rodrigues ASL, Pilgrim JD, Lamoreaux JF, Hoffman M, Brooks TM (2006) The value of the IUCN Red List for conservation. Trends Ecol Evol 21:71–76

Santora JA (2012) Habitat use of hourglass dolphins near the South Shetland Islands, Antarctica. Polar Biol 35: 801–806

Santora JA (2013) Dynamic intra-seasonal habitat use of Antarctic fur seals suggests migratory hotspots near the Antarctic Peninsula. Mar Biol 160:1383–1393

Santora JA, Brown ET (2010) Spatial distribution patterns of Southern bottlenose whales *Hyperoodron planifrons* near the South Shetland Islands. Mar Mamm Sci 26: 960–968

Santora JA, Reiss CS (2011) Geospatial variability of krill and top-predators within an Antarctic submarine canyon system. Mar Biol 158:2527–2540

Santora JA, Reiss CS, Cossio AC, Veit RR (2009) Interannual spatial variability of Antarctic krill (*Euphausia superba*) influences seabird foraging behavior near Elephant Island, Antarctica. Fish Oceanogr 18:20–35

Santora JA, Reiss CS, Loeb VJ, Veit RR (2010) Spatial association between hotspots of baleen whales and demographic patterns of Antarctic krill *Euphausia superba* suggests size-dependent predation. Mar Ecol Prog Ser 405:255–269

Santora JA, Ralston S, Sydeman WJ (2011) Spatial organization of krill and seabirds in the central California Current. ICES J Mar Sci 68:1391–1402

Santora JA, Sydeman WJ, Schroeder ID, Reiss CS and others (2012a) Krill space: a comparative assessment of mesoscale structuring in polar and temperate marine ecosystems. ICES J Mar Sci 69:1317–1327

Santora JA, Field JC, Schroeder ID, Sakuma KM, Wells BK, Sydeman WJ (2012b) Spatial ecology of krill, micronekton and top predators in the central California Current System: implications for defining ecologically important areas. Prog Oceanogr 106:154–174

Santora JA, Sydeman WJ, Messié M, Chai F and others (2013) Triple check: observations verify structural realism of an ocean ecosystem model. Geophys Res Lett 40: 1367–1372

Sigler MF, Kuletz KJ, Ressler PH, Friday NA, Wilson CD, Zerbini AN (2012) Marine predators and persistent prey in the southeast Bering Sea. Deep-Sea Res II 65–70: 292–303

Silverman ED, Veit RR, Nevitt GA (2004) Nearest neighbors as foraging cues: information transfer in a patchy environment. Mar Ecol Prog Ser 277:25–36

Southwell C, Paxton CGM, Borchers D, Boveng P, De La Mare W (2008) Taking account of dependent species in management of the Southern Ocean krill fishery: estimating crabeater seal abundance off east Antarctica. J Appl Ecol 45:622–631

Suryan RM, Santora JA, Sydeman WJ (2012) New approach for using remotely-sensed chlorophyll *a* to identify seabird hotspots. Mar Ecol Prog Ser 451:213–225

Sydeman WJ, Thompson SA, Kitaysky A (2012) Seabirds and climate change: roadmap for the future. Mar Ecol Prog Ser 454:107–117

Sydeman WJ, Brodeur RD, Grimes CB, Bychkov AS, Mckinnel S (2006) Marine habitat 'hotspots' and their use by migratory species and top predators in the North Pacific Ocean: Introduction. Deep-Sea Res II 53:247–249

Thompson AF, Heywood KJ, Thorpe SE, Renner AHH, Trasvina A (2009) Surface circulation at the tip of the Antarctic Peninsula from drifters. J Phys Oceanogr 39: 3–26

Tin T, Fleming ZL, Hughes KA, Ainley DG and others (2008) Impacts of local human activities on the Antarctic environment. Antarct Sci 21:3–33

Tittensor DP, Mora C, Jetz A, Lotze HK, Ricard D, Vanden Berghe E, Worm B (2010) Global patterns and predictors of marine biodiveristy across taxa. Nature 466: 1098–1101

Trivelpiece WZT, Hinke J, Miller AK, Reiss CS, Trivelpiece SG, Watters GM (2011) Variability in krill biomass links harvesting and climate warning to penguin populations in Antarctica. Proc Natl Acad Sci USA 108: 7625–7628

Tynan CT (1998) Ecological importance of the southern boundary of the Antarctic Circumpolar Current. Nature 392:708–710

Veit RR (1999) Behavioral responses by foraging petrels to swarms of Antarctic krill. Ardea 87:41–50

Worm B, Lotze HK, Myers RA (2003) Predator diversity hotspots in the blue ocean. Proc Natl Acad Sci USA 100: 9884–9888

Yen PPW, Sydeman WJ, Bograd SJ, Hyrenbach KD (2006) Spring-time distributions of migratory marine birds in the southern California Current: oceanic eddy associations and coastal habitat hotspots over 17 years. Deep-Sea Res II 53:399–418

Zydelis R, Lewison RL, Shaffer SA, Moore JE and others (2011) Dynamic habitat models: using telemetry data to project fisheries bycatch. Proc R Soc B 278:3191–3200

Appendix 1. Species observed during 14 US Antarctic Marine Living Resource (AMLR) surveys January – March, 2003–2011 (sorted alphabetically within frequency of surveys). Conservation status is provided by the International Union for Conservation of Nature (IUCN; www.iucnredlist.org); see Rodrigues et al. 2006 for details about the IUCN Red List

Name		Surveys observed	IUCN status
Antarctic fulmar	*Fulmarus glacialoides*	14	Least Concern
Antarctic fur seal	*Arctocephalus gazella*	14	Least Concern
Antarctic minke whale	*Balaenoptera bonaerensis*	14	Data Deficient
Antarctic prion	*Pachyptila desolata*	14	Least Concern
Antarctic tern	*Sterna vittata*	14	Least Concern
Black-browed albatross	*Thalassarche melanophrys*	14	Endangered
Black-bellied storm petrel	*Fregetta tropica*	14	Least Concern
Blue petrel	*Halobaena caerulea*	14	Least Concern
Brown skua	*Catharacta antarctica*	14	Least Concern
Cape petrel	*Daption capense*	14	Least Concern
Chinstrap penguin	*Pygoscelis antarctica*	14	Least Concern
Fin whale	*Balaenoptera physalus*	14	Endangered
Grey-headed albatross	*Thalassarche chrysostoma*	14	Vulnerable
Humpback whale	*Megaptera novaeangliae*	14	Least Concern
Light-mantled albatross	*Phoebetria palpebrata*	14	Near Threatened
Southern giant petrel	*Macronectes giganteus*	14	Least Concern
South polar skua	*Stercorarius maccormicki*	14	Least Concern
Wandering albatross	*Diomedea exulans*	14	Vulnerable
Wilson's storm petrel	*Oceanites oceanicus*	14	Least Concern
Gentoo penguin	*Pygoscelis papua*	13	Near Threatened
Northern giant petrel	*Macronectes halli*	13	Least Concern
White-chinned petrel	*Procellaria aequinoctialis*	13	Vulnerable
Soft-plumaged petrel	*Pterodroma mollis*	12	Least Concern
Kelp gull	*Larus dominicanus*	11	Least Concern
Southern bottlenose whale	*Hyperoodon planifrons*	11	Least Concern
Antarctic petrel	*Thalassoica antarctica*	10	Least Concern
Arctic tern	*Sterna paradisaea*	10	Least Concern
Macaroni penguin	*Eudyptes chrysolophus*	10	Vulnerable
Thin-billed prion	*Pachyptila belcheri*	10	Least Concern
Adelie penguin	*Pygoscelis adeliae*	9	Least Concern
Killer whale	*Orcinus orca*	9	Data Deficient
Snowy sheathbill	*Chionis albus*	8	Least Concern
Snow petrel	*Pagodroma nivea*	8	Least Concern
Antarctic shag	*Phalacrocorax bransfieldensis*	7	Not Evaluated
Common diving petrel	*Pelecanoides urinatrix*	7	Least Concern
Hourglass dolphin	*Lagenorhynchus cruciger*	7	Least Concern
Southern elephant seal	*Mirounga leonina*	7	Least Concern
Southern royal albatross	*Diomedea epomophora*	7	Vulnerable
Weddell seal	*Leptonychotes weddellii*	7	Least Concern
Leopard seal	*Hydrurga leptonyx*	6	Least Concern
Long-finned pilot whale	*Globicephala melas*	6	Data Deficient
Southern right whale	*Eubalaena australis*	5	Least Concern
Crabeater seal	*Lobodon carcinophaga*	4	Least Concern
Sooty shearwater	*Puffinus griseus*	4	Near Threatened
Kerguelen petrel	*Lugensa brevirostris*	3	Least Concern
White-headed petrel	*Pterodroma lessonii*	3	Least Concern
Parasitic jaeger	*Stercorarius parasiticus*	2	Least Concern
Emperor penguin	*Aptenodytes forsteri*	1	Least Concern
Fairy prion	*Pachyptila turtur*	1	Least Concern
Gray's beaked whale	*Mesoplodon grayi*	1	Data Deficient
King penguin	*Aptenodytes patagonicus*	1	Least Concern
Mottled petrel	*Pterodroma inexpectata*	1	Near Threatened
South Georgia diving petrel	*Pelecanoides georgicus*	1	Least Concern
Sooty albatross	*Phoebetria fusca*	1	Endangered

Submitted: November 14, 2012; Accepted: March 24, 2013 *Proofs received from author(s): May 16, 2013*